Size Effect in Shear Critical FRP RC Beams

By:

Szymon Piotr Chołostiakow

MSc, BSc

A thesis submitted for the degree of
Doctor of Philosophy

The University of Sheffield
Department of Civil and Structural Engineering

Sheffield

December 2018

This page intentionally left blank

To my dark side,
always saying no

This page intentionally left blank

ABSTRACT

Owing to its non-corrosive characteristics, Fibre-Reinforced Polymer (FRP) reinforcement can be a promising alternative to conventional steel reinforcement in structural elements exposed to severe environments, such as in bridge girders. However, the use of FRPs in such elements is limited, as their shear behaviour is still very little understood. In fact, only limited number of studies have focused on size effect, which is associated with a reduction of shear strength in larger elements, and how this affects the relative shear contributions of concrete and FRP shear reinforcement. Many design recommendations adopted size effect provisions developed for steel RC beams without investigating the validity of these models in great depth or accounting for the unique mechanical properties of FRP and their effect on overall structural behaviour (e.g. wider cracks and larger strain).

This study aims to advance the understanding of the influence of beam's depth on the shear behaviour and development of shear resisting mechanisms in FRP RC beams, so as to develop more refined and reliable shear predicting models, especially for larger elements.

Based on detailed experimental measurements obtained from three point bending tests carried out on fifteen FRP RC beams with and without external FRP shear links, a decomposition of the basic shear resisting mechanisms is performed to estimate the individual contributions of concrete and shear reinforcement.

The results confirm a considerable size effect for members without shear reinforcement (up to 40 % reduction for larger elements), and indicate that this is strongly related to the maximum strain that can be attained in the flexural reinforcement. The analysis shows that both contributions of concrete and shear reinforcement are variable, and change with increasing strain in the flexural and shear reinforcement. However, even when relatively large strain values are mobilised in the reinforcement, the additive nature of these shear resisting components can be effectively maintained, as long as the individual contributions offered by concrete and shear reinforcement are sufficiently accounted for.

Based on the experimental observations, a unified design model for FRP and steel RC beams is proposed. The model accounts for size effect, increases the safety margins for larger RC beams and reduces the COV in shear predictions by up to 25%.

This page intentionally left blank

ACKNOWLEDGMENTS

This page intentionally left blank

TABLE OF CONTENTS

LIST OF FIGURES

LIST OF TABLES

LIST OF PHOTOGRAPHS

LIST OF SYMBOLS

a = length of the test shear span;

a'= length of the non-test shear span;

a_{max} = maximum aggregate size;

A_{fl} = total area of FRP longitudinal reinforcement;

A_s = total area of steel longitudinal reinforcement;

A_{fv} = total area of the shear reinforcement at given spacing;

b_w = width of the beam;

C_{Rd} = empirical coefficient for steel RC equal to 0.18;

d = effective depth of the beam;

d_v = effective shear depth of the beam;

E_c = modulus of elasticity of the concrete;

E_{fl} = Young's modulus of longitudinal FRP reinforcement;

E_{fv} = Young's modulus of shear FRP reinforcement;

$E_{fw}\rho_{fw}$ = mechanical stiffness ratio of FRP shear reinforcement;

f'_c = concrete cylinder strength;

f_{ck} = characteristic compressive strength of concrete;

f_{fb}= allowable strength of the bent portion of the FRP stirrup;

f_{FRPu} = ultimate strength of the shear link;

f_{fv} = allowable stress in the shear reinforcement;

f_y = yielding strength of steel reinforcement;

$F_{sl,i}$ = experimental force developed in i[th] shear link;

h = overall depth of the beam;

k_1 = ratio between the shear load in the test shear span and applied load;

k_m = coefficient taking into account the effect of moment at section on shear strength;

k_r = coefficient taking into account the effect of reinforcement rigidity on its shear strength;

k_s = coefficient taking into account the effect of member size on its shear strength;

k_ε = parameter accounting for the effect of member's depth on the development of shear resisting mechanisms based on the strain demand on the flexural reinforcement;

L = beam's clear span;

M = applied moment;

M_a = applied moment;

M_{fl} = flexural capacity;

M_u = ultimate bending moment;

P_{ult} = ultimate load applied;

s = spacing of the FRP shear links;

s_{ze} = effective crack spacing;

V = applied shear force;

V_a = applied shear force;

V_c = shear capacity provided by concrete;

V_{con} = estimated experimental contribution of concrete;

V_{exp} = experimental shear capacity;

V_f = calculated shear strength provided by FRP shear links;

V_s = calculated shear strength provided by steel stirrups;

V_{scr} = experimental shear force in tested shear span at diagonal cracking;

$w_{,max,DIC}$ = maximum crack width measured through DIC;

β = factor depending on ability of concrete to transmit tensile stresses;

$\varepsilon_{fl,norm}$ = longitudinal strain in FRP reinforcement;

$\varepsilon_{fl,norm}$ = longitudinal strain in FRP reinforcement normalized by yielding strain of steel;

$\varepsilon_{fw,max}$ = maximum design strain level in FRP shear reinforcement;

$\varepsilon_{ft,exp}$ = experimental maximum strain in FRP shear reinforcement;

$\varepsilon_{l,max}$ = maximum strain in the main longitudinal reinforcement;

$\varepsilon_{t,max}$ = maximum strain in the shear links;

$\varepsilon_{t,max,DIC}$ = maximum strain in the shear links measured through DIC;

ε_{ti} = experimental strain measured in i[th] shear link (measured through DIC or strain gauge);

ε_x = strain at beam mid-depth calculated at the distance d from the loading plate;

θ = angle of inclination of the principal diagonal compressive stresses;

λ = factor accounting for concrete density;

ρ_{fl} = longitudinal FRP reinforcement ratio.

φ_c = resistance factor for concrete;

φ_e = ratio equal to 1.8

φ_f = resistance factor for FRP reinforcement.

LIST OF ACRONYMS

3PB – three-point bending;

4PB – four-point bending;

AASHTO - American Association of State Highway and Transportation Officials;

ACI – American Concrete Institution;

AFRP – aramid fibre reinforced polymers;

ASCE – American Society of Civil Engineers;

BFRP – basalt fibre reinforced polymers;

BISE – British Institution of Structural Engineers;

CFRP – carbon fibre reinforced polymers;

CHBDC – Canadian Highway Bridge Design Code;

COV – coefficient of variance;

CSA – Canadian Standard Association;

DT – diagonal tension;

EC2 – Eurocode 2;

fib – Fédération internationale du béton;

FRP – fibre reinforced polymer;

GFRP – glass fibre reinforced polymers;

JSCE – Japan Society of Civil Engineers;

LVDT – linear variable differential transformer;

MCFT – Modified Compression Field Theory;

NA – neutral axis;

RC – reinforced concrete;

ST – shear test;

ST – standard deviation; and

VAR – variance.

Chapter 1

Introduction

This chapter presents the significance of this study, the main objectives, the layout of the thesis and expected impact.

1.1   Introduction

Many RC bridges built after the war have surpassed their designed lifespan, and the performance of their internal reinforcement or prestressing tendons might have been significantly compromised due to environmental exposure and development of corrosion products. When steel corrodes, the resulting rust accumulates on the reinforcement surface creating tensile stresses in concrete, which can eventually lead to cracking delamination and spalling. Recent report on the condition of the bridges in US, prepared by the American Road and Transportation Builders Association (ARTBA 2018), revealed that 54,259 bridges are structurally deficient and need urgent repair. Corrosion is also believed to be one of the main reasons for the recent collapse of the Morandi Bridge in Genoa, Italy (Figure 1-1), which took the life of 43 people, leaving 16 injured (Winfield 2018; Taylor 2018).

Figure 1-1 Collapse of the Morandi Bridge in Genoa, August 2018

In the past two decades, engineers started to use more advanced materials as reinforcing materials for concrete, such as Fibre Reinforced Polymer (FRP) reinforcement, which is resistant to corrosion and has the potential to significantly prolong the structure's lifespan. Owing to these superior durability characteristics, one of the most promising applications for FRP reinforcement is in bridge construction, for which the use of large structural elements is often required to transfer the high design shear forces.

Due to its complexity, different, and often contrasting theories have been developed over the years to explain the shear behaviour of concrete elements reinforced with steel reinforcement (Mitchell and Collins 1974; Vechhio and Collins 1986; Nielsen 1984; Kotsovos 1988; Reineck 1991). In particular, although it has been shown experimentally that size effect can reduce overall shear strength capacity, the ways in which shear resisting mechanisms are affected is still not fully understood and the behaviour of large RC beams warrants further investigation.

When FRP reinforcement is used, a more brittle behaviour is observed and larger deformations and wider cracks develop in the concrete elements, thus affecting the residual shear resistance that can be mobilized along the cracks (Razaqpur et al. 2006). Therefore, shear resistance of FRP RC beams is expected to be affected by size effect to a higher degree than in equivalent steel RC beams.

1.2   Research significance

Although much experimental work on the shear behaviour of FRP RC beams has been carried out so far, and several shear design-oriented models have been already proposed, research on size effect is still scarce and inconclusive. In addition, most of the available guidelines are based on modifications of standards that were originally developed for conventional steel RC, and still adopt the same size effect provisions, or are calibrated against a fairly limited amount of experimental data. This has resulted in the development of equations that, although generally conservative, can overestimate the strength of large elements and do not provide uniform safety margins. Hence, it is critical to develop more reliable shear design equations capable to account for different types of reinforcing materials and that can provide more uniform margins of safety for the wide range of member depth typically used in construction, including large elements.

1.3   Aims and objectives

The aim of this study is to gain a better understanding on shear behaviour of FRP RC beams in terms of size effect and relative contribution of the shear resisting mechanisms offered by concrete and shear reinforcement, so as to propose more

reliable analytical design approaches. This aim will be achieved by completing the following objectives:

Obj. 1. Create a database of FRP RC beams with/without shear reinforcement.

Obj. 2. Investigate the influence of effective depth on the overall shear resistance and strain distribution in the flexural and shear reinforcement.

Obj. 3. Assess the performance of current FRP shear design provisions in predicting V_c and V_f, for different ranges of effective depths.

Obj. 4. Design and carry out an experimental programme to investigate the shear behaviour of FRP RC beams with and without shear FRP reinforcement, with the overall depth ranging from 260 mm to 460 mm.

Obj. 5. Estimate size effect in FRP RC beams without shear reinforcement and in beams with minimum shear reinforcement.

Obj. 6. Decouple the shear resisting components V_c and V_f, and assess their relative contributions to the overall shear resistance.

Obj. 7. Develop more reliable predictive design models, which more accurately account for size effect, and reflect the contribution of shear reinforcement in a more realistic manner.

1.4   Methodology

The effect of beam depth on shear strength was assessed based on fifteen tests on shear critical FRP RC beams with the overall depth varying from 260 mm to 460 mm. The remaining parameters, such as concrete strength, aggregate size, shear span-to-depth ratio, and longitudinal and shear reinforcement ratios were kept constant throughout all tests. First nine tests were carried out on beams without shear reinforcement. Subsequently, six tests were performed on beams with external FRP shear links, designed to provide minimum shear reinforcement ratio (according to ACI 440 provisions). The instrumentation was designed to measure load, vertical displacement of the beam and strains in the FRP flexural and shear reinforcement. In addition to conventional instrumentation, 3D Digital Image Correlation measurements were employed to precisely monitor development of strain in shear links and crack propagation within the shear span. The measurements were used to

determine the individual shear contributions of FRP shear reinforcement and concrete.

1.5   Thesis layout

This thesis is organised into six chapters and six appendices including the complete sets of data and other relevant information. Chapters 1 and 6 are written following a conventional thesis format, whilst Chapters 2, 3, 4, and 5 present "stand alone" sections, which have been already submitted for publication in peer review journals (Chapters 3 and 4) or are to be submitted (Chapters 2 and 5).

Chapter 2 discusses the main differences in shear behaviour of FRP and steel RC beams and presents the relevant background on size effect. In addition, comprehensive databases of FRP RC beams with and without shear reinforcement are presented and used to evaluate the performance of existing FRP shear predicting models (Obj. 1-3). The data used in this chapter was collected in an open source database and the URL to the online repository is included in Appendices A and B, along with the complete set of results used to assess the shear design models examined as part of this study.

Chapter 3 (Cholostiakow et al. 2018a) describes the experimental programme including the material properties and methodology, and presents the main test results in terms of failure modes, deformations and crack development. The results confirm a considerable size effect for members without shear reinforcement, with an average reduction in normalized shear strength up to 40%. It is also shown that current design provisions are overall conservative, but with non-uniform margins of safety that decrease with increasing member depth (Obj. 4 and 5). Additional information on the experimental programme and test results can be found in Appendices C, D, and F.

Chapter 4 (Cholostiakow et al. 2018b) discusses the development of shear resisting mechanisms in FRP reinforced concrete beams with shear reinforcement on the basis of detailed strain measurements obtained from digital image correlation and strain gauges. The study reveals that the contribution of concrete decreases gradually after diagonal cracking with increasing strain and crack width. The results

of the analysis indicate that the relative shear contributions of shear resisting components should be re-examined in order to provide more reliable shear design equations (Obj. 6). Additional information on the experimental programme and test results can be found in Appendix E.

Chapter 5 presents the development of a shear model based on the current EC2 equation for steel RC. The new approach introduces a new parameter, which accounts for the effect of member's depth on the development of shear resisting mechanisms on the basis of the strain demand on the flexural and shear reinforcement. The proposed model yields more accurate estimates of total shear resistance and can better approximate the individual contributions offered by concrete and shear reinforcement.

1.6   Originality of work

Based on extensive experimental evidence and detailed DIC measurements, the work presented herein leads to a more reliable estimate of the relative contributions of concrete and shear reinforcement to the overall shear capacity of FRP beams varying in depth, and allows a more in-depth understanding of size effect. This work also led to the development of a strain-based unified shear design approach for steel and FRP RC beams.

1.7   Expected impact

The work presented herein offers invaluable insights into the effect of varying depth on the development of shear resisting mechanisms in FRP RC beams. It is anticipated that the experimental data and resulting analysis will support the development of rational and reliable shear design provisions, the application of which will ensure appropriate levels of safety for large FRP RC elements, and increase engineers' confidence in the use of FRP reinforcement.

1.8   Publications resulted from this study

Journal publications

Authors	Title	Journal	Status
Cholostiakow, S., Di Benedetti, E., Pilakoutas, K. and Guadagnini, M.	Shear design for size effect in RC beams	ACI Structural Journal	To be submitted
Cholostiakow, S., Di Benedetti, M., Zappa, E., Pilakoutas, K. and Guadagnini, M. (2018b)	Shear Resisting Mechanisms in FRP RC Beams	Materials and Structures	Submitted
Cholostiakow, S., Di Benedetti, M., Pilakoutas, K. and Guadagnini, M. (2018a)	Effect of Beam Depth on Shear Behaviour of Fibre Reinforced Polymer Reinforced Concrete Beams	Journal of Composites for Construction	Published

Peer reviewed conference publications

Authors	Title	Conference	Date, Location
Di Benedetti, M., Gomez, J., **Cholostiakow**, S., Fergani, H., Barris, C., Guadagnini, M., (2018)	Reliability of DIC Measurements for the Structural Monitoring of FRP RC Elements	Proc. of 9th International Conference on Fibre-Reinforced Polymer (FRP) Composites in Civil Engineering (CICE 2018)	July 17-19, 2018, Paris, France
Cholostiakow, S., Di Benedetti, M., Guadagnini, M., Zappa., E., (2017b)	Size Effect in FRP RC Beams with and without Shear Reinforcement	FRPRCS-13 The 13th International Symposium on Fiber-Reinforced Polymer Reinforcement for Concrete Structures	October 14-15, 2017, Anaheim, California, USA
Cholostiakow, S., Di Benedetti, M., Guadagnini, M., Zappa., E., (2017a)	Shear Behaviour of FRP RC Beams: Does Size Matter?	Advanced Composites in Construction, ACIC2017	September 5-7, 2017, Sheffield, UK
Cholostiakow, S., Di Benedetti, M., Guadagnini, M., Gowda, C., Barros, J., Zappa, E., (2016b)	Experimental and numerical study on the shear behaviour of geometrically similar FRP RC beams	CICE2016 – 8th International Conference on Fibre-Reinforced Polymer (FRP) Composites in Civil Engineering	December 14-16, 2016, Hong-Kong, China
Cholostiakow, S., Di Benedetti, M., Guadagnini, M., (2016a)	Shear Strength and Size Effect in FRP RC Beams	11th fib International Symposium in Civil Engineering	August 23-31, 2016, Tokyo, Japan

1.9   References

- American Road and Transportation Builders Association (ARTBA). 2018 Deficient Bridge Report. Available at: https://www.artbabridgereport.org/

- Kotsovos MD. Compressive force path: Basis for ultimate limit state reinforced concrete design. ACI Struct. *J.* 1988*;* 85(1), pp. 68–75.

- Mitchell D, Collins MP. Diagonal compression field theory - A rational model for structural concrete in pure torsion. ACI J. 1974;71(8), 396–408.

- Nielsen MP. Limit analysis and concrete plasticity. Prentice-Hall Inc., Englewood Cliffs, N.J, 1984.

- Razaqpur, A. G., and Isgor, O. B. (2006). Proposed shear deign method for FRP-reinforced concrete members without stirrups. *ACI Struct. J.*, 103(1), 93–102.

- Reineck KH. Ultimate shear force of structural concrete members without transverse reinforcement derived from a mechanical model. ACI Struct. *J.* 1991; 88, (5), 592-602.

- Taylor M. (2018). Genoa bridge collapse: 'Unusual' span had seen frequent repair work. The Guardian, URL: https://www.theguardian.com/world/2018/aug/14/unusual-span-of-collapsed-genoa-bridge-had-seen-frequent-repair-work
  Last visited: 06.12.2018.

- Vecchio FJ, Collins MP. The modified compression field theory for reinforced concrete elements subjected to shear. ACI J. 1986; 83(2), 219–231.

- Winfield N. (2018). Genoa bridge collapse: Designer warned of corrosion risk nearly 40 years ago. The Independent, URL: https://www.independent.co.uk/news/world/europe/genoa-bridge-collapse-engineer-riccardo-morandi-warning-corrosion-rust-concrete-a8498716.html Last visited: 06.12.2018.

Chapter 2

Review of shear design models for FRP RC beams

This chapter introduces the fundamental approaches that form the basis of current design codes and discusses the main difference in the shear behaviour of concrete elements reinforced with steel and FRP reinforcement. Based on a comprehensive database of FRP RC beams with and without shear reinforcement (appendices A and B), the performance of current design-oriented models is evaluated.

2.1 Introduction

The transfer of shear in RC structures is controlled by a number of internal resisting mechanisms (Figure 2-1). The joint ASCE-ACI Committee 445 (ASCE-ACI 1998) reports that the total shear resistance of steel RC beams consists of the resistance offered by the shear reinforcement, V_s, resistance of concrete in compression, V_c, aggregate interlock, V_a, dowel action of the longitudinal reinforcement, V_d, and also residual tensile stress across cracks and arch action. The same resisting mechanisms develop in elements with FRP reinforcement; however, owing to the different mechanical properties of FRPs, the relative magnitudes of these mechanisms differs from that observed in steel RC.
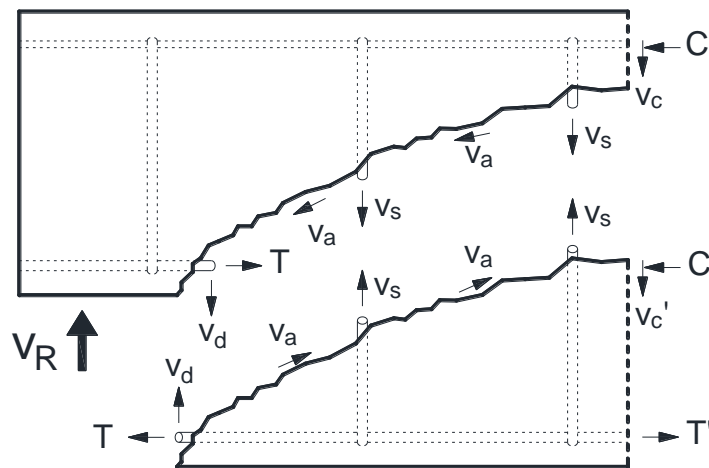
Figure 2-1: Internal shear carrying mechanisms in reinforced concrete beams

The contribution of the shear reinforcement depends on the maximum stress level that can develop in the stirrups. In the case of FRP reinforcement, due to lack of plasticity, the failure of the links occurs always in a brittle manner, near the vicinity of the largest tensile stresses or at the bent portions of the links, where the mechanical properties of the composite are weakened.

A component of shear can be transferred through the non-cracked concrete in the compression zone. This mechanism deteriorates very quickly in steel RC following yielding of the flexural reinforcement. Because of the lower stiffness of the FRP reinforcement and lack of yielding plateau (see also Figure 2-11), a different behaviour is observed. In fact, FRP RC beams with comparable amounts of flexural

reinforcement are characterised by considerably smaller neutral axis depths than equivalent steel RC beams, and in result, less concrete works in compression. Although a smaller shear resistance is observed in FRP RC beams after cracking, a more gradual degradation is expected to occur at higher stain levels (*fib* 2007).

The mechanical interlocking between aggregates (aggregate interlock) has been shown to significantly contribute to the overall shear strength of concrete (Fenwick and Paulay 1968; Walraven 1981). For the beams without shear reinforcement the magnitude of this mechanism is estimated to be between 33 % and 50 % of shear strength of the uncracked concrete (Taylor 1970). The contribution of aggregate interlock decreases with increasing crack widths and depends on the type and size of the coarse aggregates. In elements with FRP reinforcement much larger crack widths are observed and therefore a smaller amount of shear is expected to be transferred through aggregate interlock.

The dowel action of the longitudinal reinforcement is significant in steel RC beams without shear reinforcement having large flexural bar diameters (up to 25 % according to Taylor 1970) or in regions where the development of the horizontal splitting cracks is prevented (e.g. short span beams). In all other cases, however, dowel action has only a minor contribution to shear comparing to other shear resisting mechanisms. In FRP RC elements the contribution of this action is significantly smaller due to low transverse stiffness of the FRP bars (Tottori and Wakui 1993) and some researchers assume that this additional shear resistance can be considered as negligible (Kanakubo and Shindo 1997).

The residual tensile strength of concrete has a minor importance in terms of shear contribution and was found to be ineffective in steel RC above crack width corresponding to about 0.2 mm (Hordijk 1992). In FRP RC elements in general larger and deeper crack widths are observed, thus, the contribution of this mechanism to the overall shear resistance is expected to be marginal (Razaqpur et al. 2006).

Significantly higher shear loads can be developed in beams with shear span-to-depth ratios less than 2.5 through arch action. In such case, shear resistance is dependent on the effective compressive strength rather than the shear strength of

concrete and on the strength and proper anchorage of the tensile reinforcement. If the FRP tensile reinforcement is properly anchored, the arch action can be more efficient than beams with conventional reinforcement as larger tensile stress levels can be attained in the tie (Razaqpur et al. 2006).

2.2 Size effect on shear strength

Kani (1967) was amongst the first to investigate the size effect in steel RC members. In his work, he examined the performance of series of beams with varying effective depth, d, percentage of steel reinforcement, ρ, and shear span-to-depth ratio, a/d. He observed that lower normalised shear strength develops in beams with higher effective depth. It was noted that both M/Vd ratio (which is the same as a/d ratio, given in Figure 2-2) and the longitudinal reinforcement have a significant effect on shear strength.
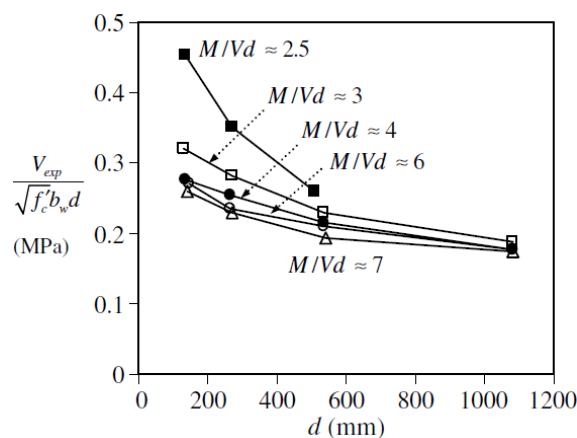
Figure 2-2: Influence of member depth and M/Vd ratio on normalised shear strength (adopted from Kani 1969)

Kani also observed that different failure modes, and thus shear carrying mechanisms, develop and progress for different a/d ratios. Irrespective of member sizes and steel reinforcement ratios, an a/d=2.5 was found to represent a transition point between shear critical beams and flexure-dominated elements. The behaviour of elements with extremely low percentage of steel reinforcement (much lower than minimum recommended values) does not show this transition as the mode of failure is always flexural dominated (Figure 2-3).

12
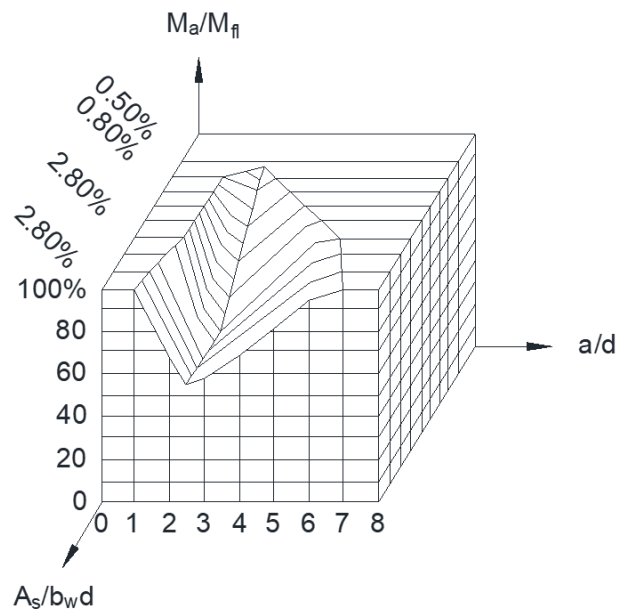
Figure 2-3: Kani's Valley of diagonal failure for mild steel (reproduced from Kani 1966)

Shioya et al. (1989, 1990) conducted an extensive experimental programme on large scale (up to 3000mm depth) RC beams without transverse shear reinforcement, a/d ratio equal to 3.0 and different aggregate size. The authors noticed that shear strength at failure decreased as the member depth increased and as the aggregate size decreased (Figure 2-4).
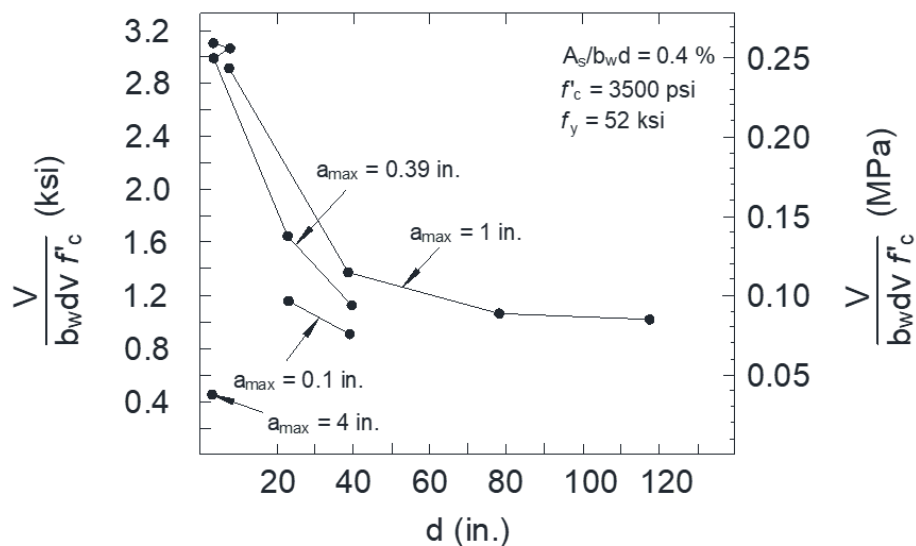
Figure 2-4: Influence of member depth and aggregate size on normalised shear strength at failure (reproduced from Collins and Kuchma 1999)

13

Although the largest reduction in average shear strength was observed for beams with depth between 120mm (5inches) and 500mm (20inches), some reduction in shear strength was also seen for larger beams up to a depth of 3000mm (118').

A different concept based on fracture mechanics and energy release rate at cracking was suggested by Bazant and Kim (1984) and used to develop a simplified design model. The proposed model was calibrated against a large experimental database collected from the literature and accounted for the size of the tested elements as well as their longitudinal steel reinforcement ratio and maximum aggregate size. Bazant's model was improved following further research on size effect in RC beams with shear reinforcement (Bazant and Sun 1987) and in 1:16 scaled RC beams without stirrups (Bazant and Kazemi 1991).

Tests conducted at the University of Toronto (Podgorniak and Stanik 1998; Collins and Kuchma 1999; Yoshida 2000; Shen Cao 2001; Angelakos et al. 2001 and Sherwood 2008) as well as the work of other researchers (Frosch 2000; Lubell et al. 2004;) showed that size effect can result mainly from the reduction of shear stress transferred across the shear crack. The researchers indicated that the larger the elements, the larger crack widths and crack spacing can be observed, which leads to reduction of shear resisting mechanisms.

Although significant research effort has been made to investigate the size effect in RC elements no rational explanation has yet been given. However, the Joint ASCE-ACI Committee on Shear and Torsion (ASCE-ACI 1998) attribute the size effect mainly to the reduction of the aggregate interlock caused by larger crack widths developing in larger elements.

Experimental studies on FRP RC elements varied in overall depth (e.g. Matta et al. 2007; Bentz et al. 2010; Alam and Hussein 2012; Ashour and Kara 2014; Mahmoud and El-Salakawy 2016) show that size effect is significant primarily in beams without web reinforcement and is mitigated by the presence of shear reinforcement (Matta et al. 2013), as the shear cracks are effectively bridged by stirrups/shear links. In particular, test results on large beams having effective depth 880 mm and low longitudinal reinforcement ratios (0.09-0.12 %), report a decrease in nominal

shear strength up to 65 %, when compared to equivalent specimens with the overall depth of 146 mm (e.g. Matta et al. 2013; Massam 2001).

2.3   Experimental database of FRP RC beams

The database presented herein encompasses almost 30 years of research on shear behaviour of FRP RC beams and includes only specimens failed in shear and fully reinforced with FRP reinforcement (aramid, basalt, carbon or glass). The database comprises 326 beams without shear reinforcement (Appendix A) and 152 beams with FRP shear reinforcement (Appendix B). The typical notation for the beams is given in Figure 2-5.
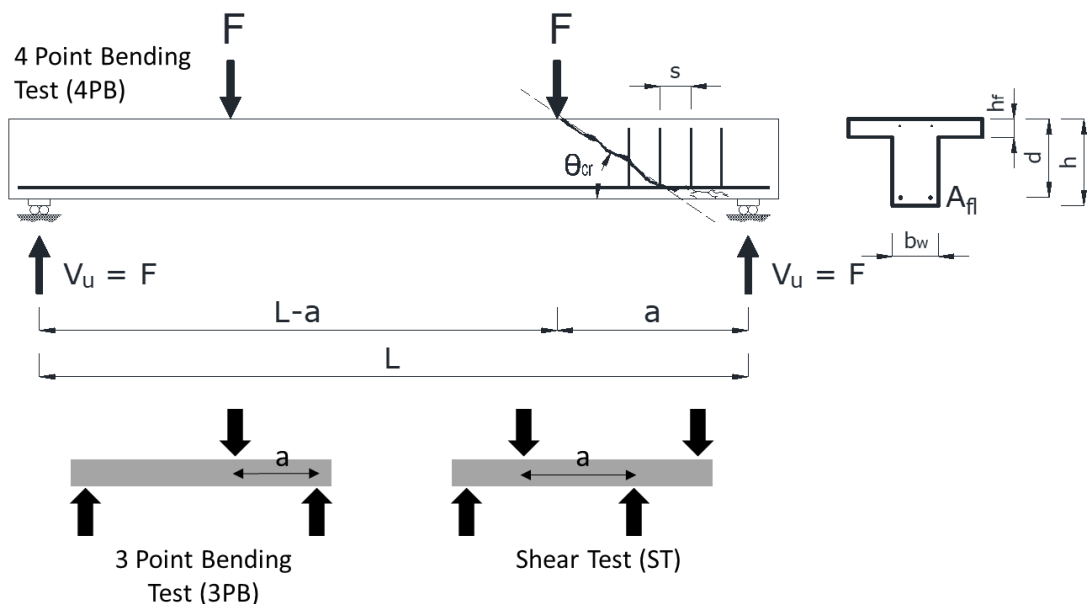
Figure 2-5 Typical notations and load arrangements

2.3.1 Beams without shear reinforcement

The parameters that were collected for the beams without shear reinforcement include: number of specimens (if the number of identical tests was more than one then an average between the tests was taken); width of the beam b_w (measured at the level of tensile reinforcement); effective depth d (measured from the top compression fibre to the centroid of the tensile reinforcement); width of the flange b_f and depth of the flange d_f (apply to T-section beams); mean compressive strength

of concrete f'_c (determined on 100x200 mm cylinders); experimental tensile strength of concrete f_{ct} (determined on 100x200 mm cylinders through tensile splitting test); experimental modulus of elasticity of concrete E_c; maximum aggregate size a_g; area of the flexural reinforcement A_{fl} (taken as an area of all reinforcing FRP bars working in tension); longitudinal reinforcement ratio ρ_{fl} (calculated as $A_{fl}/b_w d$); modulus of elasticity of longitudinal FRP reinforcement E_{fl}; nominal tensile strength of the longitudinal reinforcement f_{fv}; and experimental inclination of the main shear crack θ_{cr} (measured from the beam axis). Table 2-1 shows the distribution of the main shear design parameters.

Table 2-1 Distribution of the main shear design parameters for beams without shear reinforcement

b_w (mm)		d (mm)		f'_c (MPa)		ρ_{fl} (%)		E_f (MPa)	
range	freq.	range	freq.	range	freq.	range	freq.	range	freq.
<150	14	<250	171	<35	119	<0.75	120	<50	176
150-250	216	250-500	133	35-60	167	0.75-1.5	131	500-100	47
>250	96	>500	22	>60	40	>1.5	75	>100	103

Table 2.1 (*Continued.*)

a/d		Type of fibres		Type of test	
range	freq.	type	freq.	test	freq.
<2.5	65	AFRP	12	ST	3
2.5-4.5	216	GFRP	186	3PB	60
		BFRP	15		
>4.5	45	CFRP	113	4PB	263

2.3.2 Beams with FRP shear reinforcement

In addition to the parameters mentioned above, the following parameters are included: shear reinforcement area, A_{fw} (taken as the area of shear reinforcement at a given spacing), shear reinforcement spacing, s, shear reinforcement ratio, ρ_{fw}

(calculated as $A_{fw}/b_w s$), shear reinforcement inclination, α, and modulus of elasticity of shear FRP reinforcement, E_{fw}. Table 2-2 shows the distribution of the main shear design parameters for beams with FRP shear reinforcement.

Table 2-2 Distribution of main shear design parameters for beams with shear reinforcement

b_w (mm)		d (mm)		$f'c$ (MPa)		ρ_{fl} (%)		E_{fl} (MPa)		a/d	
range	freq	range	freq	range	freq	range	freq	range	freq	range	freq
<150	2	<250	31	<35	74	<0.75	27	<50	44	<2.5	45
150-250	133	250-500	114	35-60	74	0.75-1.5	56	50-100	75	2.5-4.5	107
>250	17	>500	7	>60	4	>1.5	69	>100	33	>4.5	0

Table 2.2 (*Continued.*)

Type of fibres		Type of test		ρ_{fw} (%)		E_{fw} (MPa)		Type of links	
type	freq.	test	freq.	range	freq.	range	freq.	type	freq.
AFRP	42	ST	35	<0.1	17	<50	44	AFRP	17
GFRP	57	3PB	14	0.1-0.5	92	500-100	75	GFRP	66
BFRP	6							BFRP	6
CFRP	47	4PB	103	>0.1	43	>100	33	CFRP	63

2.4   Shear carrying mechanisms in FRP RC beams

Figure 2-6 illustrates the effect of shear span-to-depth ratio on the normalized shear strength at failure based on the results from 324 FRP beams without shear reinforcement. Similarly to the case of steel RC (see also section 2.2), this parameter significantly affects the shear strength of shear spans with a/d less than about 2.0. In such spans shear is transferred mostly through arch action and considerably more shear resistance can be developed at ultimate. Failure of such elements is usually by shear compression failure and it is characterised by the development of a diagonal shear crack propagating from the support toward the loading point. In shear critical elements with a/d between 2.0 and 6.0 shear is carried through a truss-like mechanisms and usually occurs as a brittle diagonal tension failure caused by the propagation of an inclined crack towards the loading point, which initiates

from the tip of one of the flexural cracks. For longer shear spans, in which the flexural behaviour dominates, *a/d* has a minor effect on the shear strength and its influence is usually neglected.
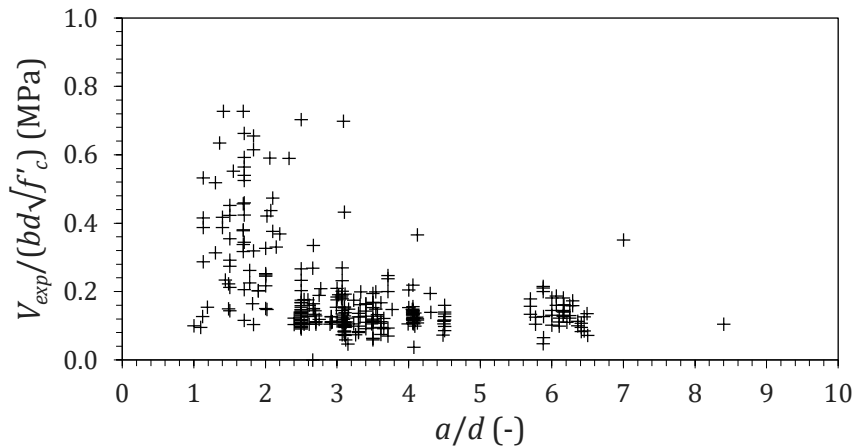
Figure 2-6 The effect of a/d ratio on the shear strength (no shear reinf.)

The effect of beam size on normalised shear strength of 219 FRP RC beams without shear reinforcement is shown in Figure 2-7.

The effect of beam size on normalised shear strength of 219 FRP RC beams without shear reinforcement is shown in Figure 2-6 (black markers). So as to investigate specimens with a comparable shear/bending interaction, only the elements having shear span-to-depth ratio ranging from 2.5 to 4.5 were considered. The shear stress was normalised by the term $\sqrt{f'_c}E_{fl}\rho_{fl}$ to account for the different stiffness of the FRP longitudinal reinforcement and the variability in concrete strength. In general, a similar trend as for steel RC beams (red markers) is observed; however, the beams with FRP reinforcement seem to exhibit a more pronounced reduction in shear strength (see trend lines). A similar behaviour was observed experimentally for steel, CFRP and GFRP RC beams with effective depth varying from 305 mm to 758 mm (Alam and Hussein 2013). Such behaviour may be attributed to a higher degradation rate of the shear resisting mechanisms caused by larger crack widths in FRP RC elements. It is worth noting that, although many tests were performed also on very large beams, the largest reduction in shear strength can be observed already in members with effective depth smaller than 500 mm.

Although the elements investigated in this study do not represent very large beams, Figure 2-7 suggests that size effect is more prominent when comparing relative

strength of small to medium height beams (from about 250 mm to 500 mm). Given also the limitations imposed by the available equipment, the authors targeted this range and comparisons to existing studies on larger elements are taken into account in the discussion.
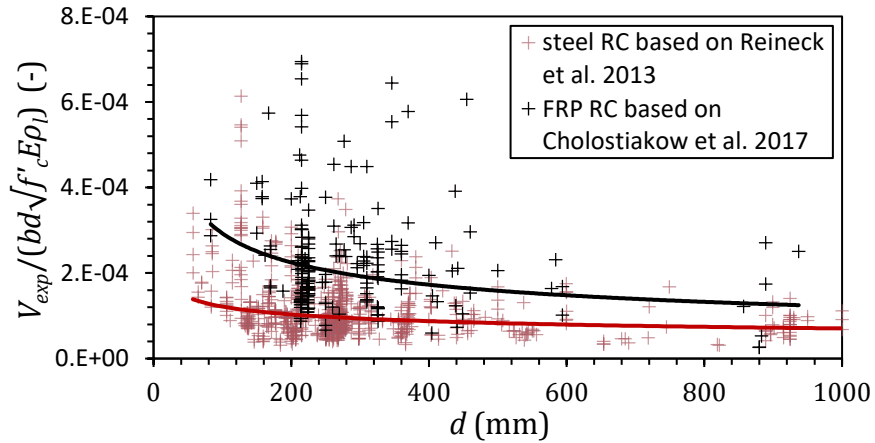
Figure 2-7 Comparison of size effect in steel and FRP RC (no shear reinf.)

The size of coarse aggregates plays an important role in carrying shear stresses along the shear crack and affects aggregate interlock. Experimental evidence shows that larger aggregates can carry more shear and mitigate size effect (e.g. Shioya et al. 1990). Figure 2-8 shows the effect of aggregate size on normalised shear strength of 47 beams without shear reinforcement and comparable a/d.
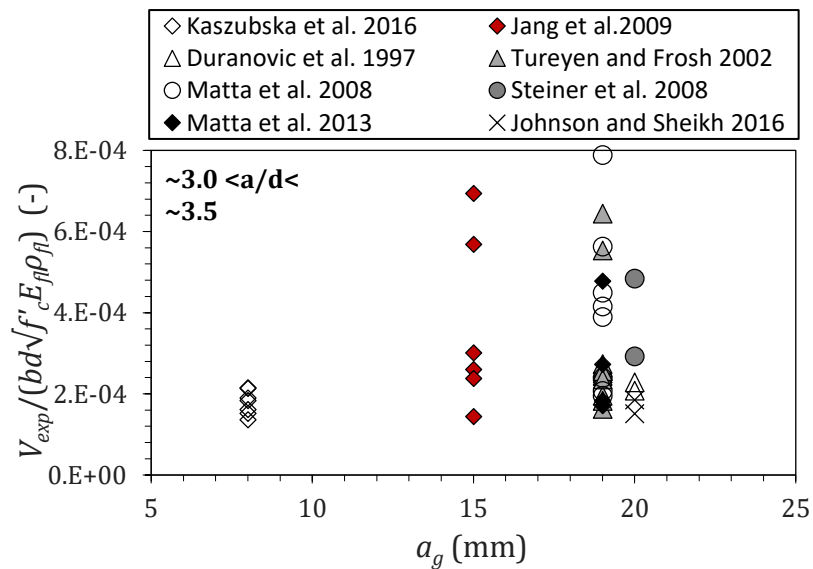
Figure 2-8 The effect of maximum aggregate size on normalised shear strength (no shear reinf.)

An increase in shear strength is observed with increasing aggregate size. In particular, the largest increase is observed between the beams with maximum aggregate size equal to 8 mm and 15 mm.

Figure 2-9 shows the variation in experimental maximum strain at failure with the axial stiffness of the shear reinforcement. A decrease in the strains is observed with increasing stiffness of the shear reinforcement. As can be seen, most of the reported peak strain values exceeded the design limits (horizontal dotted lines) reaching values even up to 4 times higher (e.g. Johnson and Sheikh 2016). The beams with stiffer shear reinforcement (e.g. Lee et al. 2016) exhibited strain levels slightly below 4,000 με and developed the largest shear strength. It is worth noting that the largest and the lowest strains corresponded to the deepest and the shallowest beams, which suggests that effective depth somehow affects the utilization of the shear reinforcement. Figure 2-9 illustrates the maximum strain in the shear reinforcement for different effective depths.

Figure 2-9 Maximum experimental strain values recorded in FRP shear reinforcement with respect to the mechanical stiffness ratio

Figure 2-10 Effect of member's effective depth on the peak strain in FRP reinforcement

It can be observed, that in larger elements, in general, larger strains are attained at failure. The different strain values measured in shear reinforcement of beams having the same effective depth can be attributed to different values of the axial stiffness ratio of shear reinforcement, $E_{fw}\rho_{fw}$. As such, the higher $E_{fw}\rho_{fw}$, the lower the strain attained in the shear reinforcement. However, beams with similar $E_{fw}\rho_{fw}$ values (e.g. triangular markers, Cholostiakow et al. 2018) present a clear relationship between the strain and effective depth, d. This indicates there is a scope for limiting strains in the shear reinforcement based on the effective depth of the member.

2.5   Evaluation of current shear design models

2.5.1   Design concept

The rapid growth of the FRP reinforcement industry at the beginning of the millennium required a fast development of safe design procedures for FRP RC concrete elements. To satisfy this demand the code developers decided to adopt similar design procedures as for steel RC and modify them to account for the different properties of FRP reinforcement. The design concept adopted by various

FRP design models is based on the fundamental principle that, as long as perfect bond between FRP and concrete is maintained, the strain and force developed in the concrete section do not depend on the type of the reinforcement used.

Most of the existing design codes have been modified for the use of FRP internal reinforcement in RC structures using a strain approach (e.g. Guadagnini et al. 2003). This approach is based on an assumption that at the same level of design strains in the longitudinal steel or FRP reinforcement, the same design forces are developed (Eq. 2-1). Hence, a given area of longitudinal FRP reinforcement, A_{FRP}, will provide the same capacity of an equivalent amount of conventional steel reinforcement, A_{eq}, determined using Eq. 2-2.

$$F_s = \varepsilon_s \cdot E_s \cdot A_s = \varepsilon_{FRP} \cdot E_{FRP} \cdot A_{FRP} \qquad \text{(Eq. 2-1)}$$

$$A_{eq} = \frac{E_{FRP}}{E_s} \cdot A_{FRP} \qquad \text{(Eq. 2-2)}$$

As FRP reinforcement is fully elastic, the failure of FRP RC elements is always of a brittle nature and the design concepts based on stress redistribution (de facto occurring in steel RC members) cannot be directly adopted in FRP RC members without affecting safety margins (Stratford and Burgoyne 2003). However, research evidence (Maruyama and Zhao 1994, Nakamura and Higai 1995, Guadagnini et al. 2006) shows that, as long as crack widths are efficiently controlled by the FRP shear reinforcement, the structural integrity is preserved and the total shear capacity can be safely determined by adding the contribution of concrete and shear reinforcement ($V_c + V_f$) as in case of steel RC. V_f depends on the number of stirrups bridging the shear cracks and can be estimated using the well-established truss analogy, while empirical models are generally adopted to determine V_c, which implicitly account for the contribution of several internal shear transfer mechanisms (i.e. concrete in compression, aggregate interlock and dowel action of the flexural reinforcement).

Current design models control the width of the shear cracks by imposing strain limits ($\varepsilon_{fw,\text{lim}}$) in shear reinforcement. The maximum stress that can be developed in the shear links (f_{fw}) is then simply taken as the strain limit $\varepsilon_{fw,\text{lim}}$ multiplied by the modulus of elasticity of the FRP shear reinforcement E_{fw} (Figure 2-11).
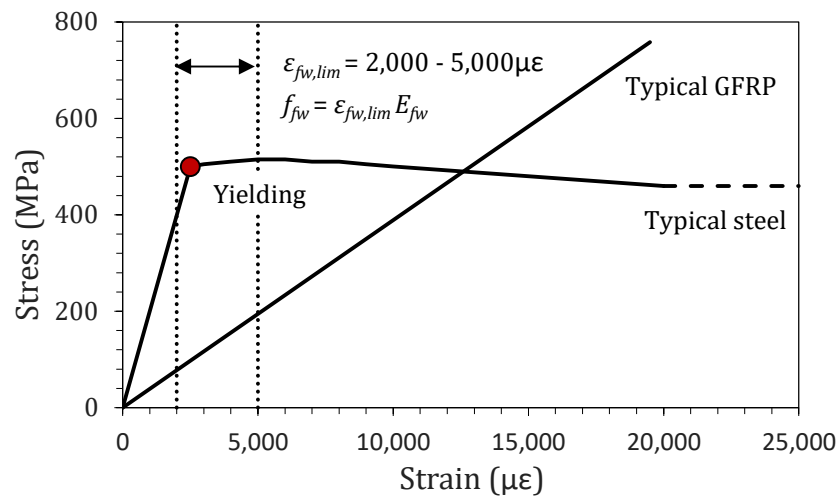
Figure 2-11 Strain limitations adopted by current FRP codes of practice

The shear capacity can be subsequently determined using the well-known truss analogy. A limiting value of strain corresponding to yielding of steel reinforcement was initially proposed (IstructE 1999). However, researchers quickly realised that even at larger strain levels in shear reinforcement shear resisting mechanism can be sufficiently mobilized and the limits were subsequently increased to 4,000 $\mu\varepsilon$ (ACI440 2003). Further investigations showed that these limits can be increased up to 4,500 $\mu\varepsilon$ (*fib* bulletin 40) and recently CSA adopted 5,000 $\mu\varepsilon$ as the maximum allowable strain in the FRP reinforcement.

2.5.2 Shear design provisions

Table 2-3 shows the shear design models proposed by: Japanese Society of Civil Engineers - JSCE (1997); British Institution of Civil Engineers - BISE (1999); Italian National Research Council CNR-DT 203/2006 – CNR (2006); *fib* bulletin 40 – *fib* (2007); Intelligent Sensing for Innovative Structures ISIS M03-07 – ISIS (2007); Hoult et al. (2008); Canadian Standard Association CSA S806-12 (CSA 2012) as well as CSA S6-14 – CSA (2014); and American Concrete Institute ACI440.1R-15 – ACI (2015).

Table 2-3 Current shear design provisions for FRP RC beams

Design code	Contribution of concrete (V_c)	Contribution of shear reinforcement (V_f)
JSCE	$V_c = \sqrt[4]{\dfrac{1000}{d}} \cdot \sqrt[3]{\dfrac{100\rho_{fl}E_f}{E_s}} \cdot 0.2 \cdot \sqrt[3]{f'_c} \cdot b_w d$	$V_f = \dfrac{A_{fw}E_{fw}\varepsilon_{fw}z}{s} / \gamma_b;$ $\varepsilon_{fw} = \sqrt{\left(\dfrac{h}{0.3}\right)^{-1/10} \dfrac{f'c}{\gamma_c}\dfrac{\rho_{fl}E_{fl}}{\rho_{fw}E_{fw}} \cdot 10^{-4}}$
BISE	$V_c = 0.79\left(100\rho_{fl}\dfrac{E_{fl}}{E_s}\right)^{1/3} \cdot \left(\dfrac{400}{d}\right)^{1/4} \cdot \left(\dfrac{f_{cu}}{25}\right)^{1/3} \cdot b_w d$	$V_f = \dfrac{0.0025E_{fw}A_{fw}}{s}d;$
CNR-DT 203	$V_c = 1.3\left(\dfrac{E_f}{E_s}\right)^{1/2} \cdot 0.25f_{ctd}(1.6-d)(1.2+40\rho_{fl})b_w d$	$V_f = \dfrac{A_{fw}f_{fw}d}{s};$ $f_{fw} = f_{fd}/\gamma_{f,\Phi}$
fib bulletin 40	$V_c = [C_{Rd,c} \cdot \left(1+\sqrt{\dfrac{200}{d}}\right) \cdot$ $\left(100 \cdot \dfrac{A_{fl}}{b_w \cdot d} \cdot \dfrac{E_f}{E_s} \cdot \dfrac{0.0045}{0.0025} \cdot f_{ck}\right)^{1/3} + k_1 \cdot \sigma_{cp}] \cdot b_w \cdot d$	$V_f = \dfrac{A_w}{s}0.0045E_{fw}z$
ISIS M03-07	if $d > 300mm \Rightarrow$ $V_c = \left(\dfrac{260}{1000+d}\right)\lambda\phi_c\sqrt{f'_c}b_w d\sqrt{\dfrac{E_{frp}}{E_s}}$ if $d \le 300mm \Rightarrow$ $V_c = 0.2\lambda\phi_c\sqrt{f'_c}b_w d\sqrt{\dfrac{E_{frp}}{E_s}}$	$V_f = \phi_c\dfrac{A_{fw}f_{fw}d_v}{s};$ $f_{fw} = \min\left\{\dfrac{(0.05\dfrac{r_b}{d_s}+0.3)f_{fw}}{1.5}; E_{fw}\varepsilon_{fw}\right\};$ $\varepsilon_{fw} = 0.0001\left(f'_c\dfrac{\rho_{fl}E_{fl}}{\rho_{fw}E_{fw}}\right)^{1/2} \cdot$ $\cdot\left(1+2\left(\dfrac{\sigma_N}{f'_c}\right)\right) \le 0.0025$
Hoult et al. 2008	$V_c = \left(\dfrac{0.3}{0.5+(1000\varepsilon_x+0.15)^{0.7}}\right) \cdot$ $\cdot\left(\dfrac{1300}{1000+s_{ze}}\right)\sqrt{f'_c}bd_v;$ $\varepsilon_x = \dfrac{\dfrac{M_a}{d_v}+V_a}{2(A_{fl}E_{fl})} \le 3,000\mu\varepsilon$	*NA*

CSA S806-12

if $d > 300mm \Rightarrow$

$$V_c = \left(\frac{750}{450+d}\right) \cdot 0.05\lambda\phi_c \sqrt{\frac{V_f d}{M_f}} \left(1 + E_f \rho_{Fw}\right)^{1/3} \cdot$$

$$\cdot \sqrt[3]{f'_c} b_w d \; ;$$

if $d \leq 300mm \Rightarrow$

$$V_c = 0.05\lambda\phi_c \sqrt{\frac{V_f d}{M_f}} \left(1 + E_f \rho_{Fw}\right)^{1/3} \cdot \sqrt[3]{f'_c} b_w d \; ;$$

$$0.11\phi_c \sqrt{f'_c} b_w d \leq V_c \leq 0.22\phi_c \sqrt{f'_c} b_w d$$

$$V_f = \frac{0.4\phi_F A_{Fv} f_{Fu} d_v}{s} \cot\theta;$$

$$30° \leq \theta = 30 + 7000\varepsilon_x \leq 60°;$$

$$\varepsilon_x = \frac{\frac{M_a}{d_v} + V_a}{2(A_{fl} E_{fl})}$$

CSA S6-2014

$$V_c = \beta\phi_C \sqrt{f'_c} b d_v;$$

$$\beta = \left(\frac{0.4}{1+1500\varepsilon_x}\right)\left(\frac{1300}{1000+s_{ze}}\right)$$

$$\varepsilon_x = \frac{\frac{M_a}{d_v} + V_a}{2(A_{fl} E_{fl})} \leq 3,000\mu\varepsilon$$

$$V_f = \frac{\phi_{FRP} E_{fw} 0.004 A_{fw} d_v \cot\theta}{s};$$

$$\theta = (29 + 7000\varepsilon_x)(0.88 + s_{ze}/2500);$$

$$30° \leq \theta \leq 60°;$$

ACI 440-15R

$$V_c = \frac{12}{5}\left(\sqrt{2\rho_f n_f + (p_f n_f)^2} - p_f n_f\right)\frac{1}{6}\sqrt{f'_c} b_w d$$

$$V_f = \frac{A_{fw} f_{fv} d}{s};$$

$$f_{fv} = \min\left\{0.004 E_{fw}; f_{fb}; f_{fd}\right\}$$

The contribution of concrete V_c is usually modelled in an empirical or semi-empirical manner as a function of several parameters, while the contribution of shear reinforcement V_f is always calculated on the basis of the truss analogy with strain limits imposed on the shear reinforcement. All design approaches assume an additive nature of shear resisting components ($V_c + V_f$); however, different codes rely on different shear transfer theories and assumptions. For instance, JSCE (1997), BISE (1999), CNR (2006), *fib* (2007) estimate V_c in an empirical manner, similarly to steel RC, and apply modification factors (E_f/E_s) to account for the different stiffness of FRP reinforcement. Although these models are based on a similar design concept, the effect of critical shear design parameters is modelled in different ways (e.g. the tensile strength of concrete is modelled using a square or a cubic root of f'_c).

Shear provisions according to ISIS (2007) do not include the effect of longitudinal reinforcement in their equations, which may lead to an overly conservative design and large discrepancy in the predicted values. On the other hand, an additional

25

parameter is introduced in CSA (2012) to account for the shear transfer via arch action in members with a/d ratio lesser than 2.5.

More complex models published by CSA based on the Modified Compression Field Theory (MCFT, Vecchio and Collins 1986) assume a variable contribution of concrete and a variable inclination of the concrete compressive strut. This approach has been shown to model the stiffness of steel RC elements between the cracks with a higher level of accuracy, and yields a more precise estimate of the ultimate shear strength. This design model was extended to FRP RC in the Canadian Highway Bridge Design Code (CHBDC) CSA S6-00, considering some modifications to account for the differences between steel and FRP reinforcement. This approached was later revised in two following versions of the code: CSA S6 (2006) and CSA S6 (2014). Hoult et al. (2008) have shown that the accuracy and conservativeness of the Canadian design models can be improved using a "second order" MCFT equation, which reflects better the larger longitudinal strains typically attained in FRP RC beams.

On the other hand, the design recommendations developed by the American Concrete Institute (ACI 2015) use a completely different approach and model the contribution of concrete V_c as a function of the neutral axis depth. In this model V_c is assumed as the shear causing inclined cracking without including any additional contribution from aggregate interlock, dowel action or shear transmitted across the concrete compression zone.

It is worth noting that although some advanced shear-oriented design models for steel RC allow using a variable inclination of the concrete strut (e.g. Model code 2010, Eurocode 2, CSA), most of the FRP design provisions still conservatively recommend to use a fixed inclination of 45° to estimate V_f. The shear provisions for FRP RC given by CSA allow calculating the angle of the average principal compression stress based on a theoretical value of longitudinal strain ε_x and limit it between 30° and 60°.

2.5.3 Modelling of size effect

The effect of member's depth on shear strength is included implicitly in the design equations as a reducing factor for V_c. In general, current FRP shear design provisions

model size effect with an empirically derived function of the effective depth. However, each size effect parameter is calibrated using different datasets, and thus, the magnitude of these factors varies within the different design guidelines (Figure 2-12). For instance, although both CSA (2012) and ISIS reduce the shear strength only for the beams with effective depth greater than 300mm, the reduction in shear strength varies up to 500%.
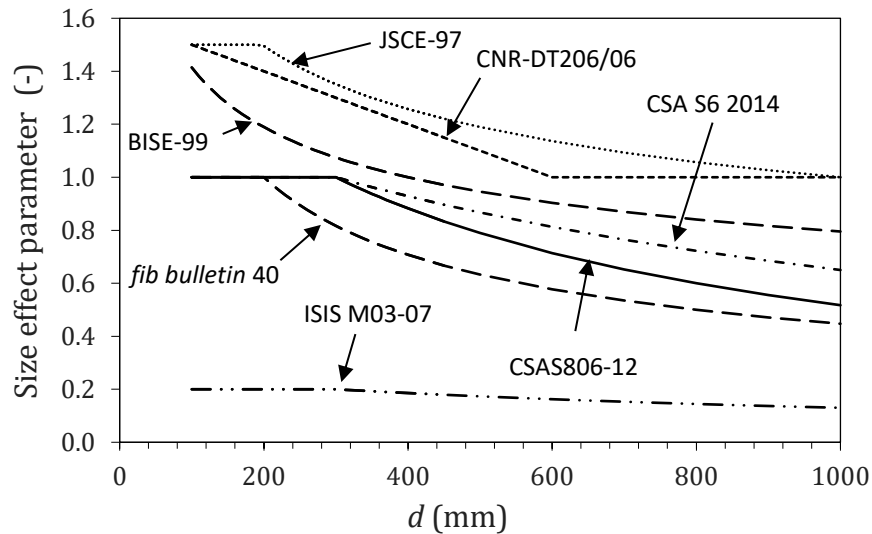
Figure 2-12 Implication of size effect in various shear design models

CNR and BISE recommend the most severe reduction; however, CNR does not show any reduction when the member depth is greater than 600mm. On the other hand, provisions given by ACI (2015) do not consider any size effect, which may potentially lead to a decrease in safety margins for larger FRP RC elements. It should be also noted that some of the size effect provisions for FRP RC remain the same as for conventional steel RC (e.g. BISE, JSCE, *fib*, CSA 2012), and hence, assume the same reduction in shear strength as in steel RC concrete.

The variability in the presented size effect provisions can be attributed to the fact that the respective equations to estimate the concrete contributions have been calibrated using different sets of governing parameters. Most notably, the equation proposed by ISIS does not include the effect of longitudinal reinforcement ratio.

2.5.4 Shear predictions for beams without shear reinforcement

Based on the analysis of a large experimental database (Appendix A) the performance of the shear design formulas discussed above in predicting V_c is assessed (Table 2-3). For the sake of comparison with the experimental results, all partial material factors as well as load and resistance factors were omitted in the calculations. In addition, to avoid considering very deep members or flexure-dominated specimens, the analysis was performed only for the elements having a/d ratio ranging from 2.5 to 4.5 (216 beams).

Figure 2-13 to Figure 2-20 show the performance of the shear design models for the examined range of beam's effective depth. The comparison shows that code provisions and proposed design modifications, in general, yield conservative predictions (green area) for the majority of the specimens (Table 2-4). However, these models exhibit non-uniform margins of safety, which decrease with increasing member's depth. This indicates that not including size effect (or not accounting for it accurately) can lead to overestimation of the concrete shear capacity for larger FRP RC members.

Table 2-4 Statistical coefficients for various shear provisions – beams without shear reinforcement

Design provision	AVERAGE		SD		VAR		COV (%)	
	All	d > 400mm	All	d > 400mm	All	d > 400mm	All	d > 400mm
JSCE-97	1.33	1.33	0.29	0.21	0.08	0.05	21.5	16.0
BISE-99	1.39	1.26	0.30	0.20	0.09	0.04	21.4	16.1
CNR-DT 203/2006	0.90	0.91	0.23	0.22	0.05	0.05	25.6	24.3
fib bulletin 40	0.89	0.86	0.19	0.14	0.04	0.02	21.4	16.2
ISIS M03-07	1.88	1.85	0.57	0.61	0.32	0.38	30.2	33.0
Hoult et al. 2008	0.95	0.84	0.26	0.17	0.07	0.03	27.2	20.2
CSA S806-12	0.93	0.87	0.19	0.16	0.04	0.03	20.3	19.0
CSA S6-2014	1.35	1.14	0.39	0.26	0.15	0.07	28.9	23.2
ACI 440 1R-15	1.83	1.55	0.44	0.32	0.19	0.10	23.9	20.7

ISIS and ACI (2015) (Figure 2-17 and Figure 2-20, respectively) provide the most conservative predictions, underestimating the experimental shear capacity by up to 100% on average and are affected by the largest standard deviation and variance. The most accurate predictions, though slightly unconservative, were achieved using the design formulations proposed by Hoult et al. (2008) and CSA (2012) suggesting that both the refined MCFT model and the semi-empirical CSA model originally proposed by Razaqpur and Isgor (2006) can be successfully used to estimate the concrete shear contribution of FRP RC members. In comparison, the original implementation of the MCFT derived equation in CSA (2014) yields rather conservative predictions of V_c, with an average V_{exp}/V_{pred} ratio equal to 1.35 and COV equal to 28.9%. Slightly more unconservative results were obtained using the *fib* and CNR approaches as evidenced by the mean V_{exp}/V_{pred} values of 0.89 and 0.90, respectively. However, the *fib* model is characterised by the relatively low scatter (COV= 21.4%, see Table 2-4).
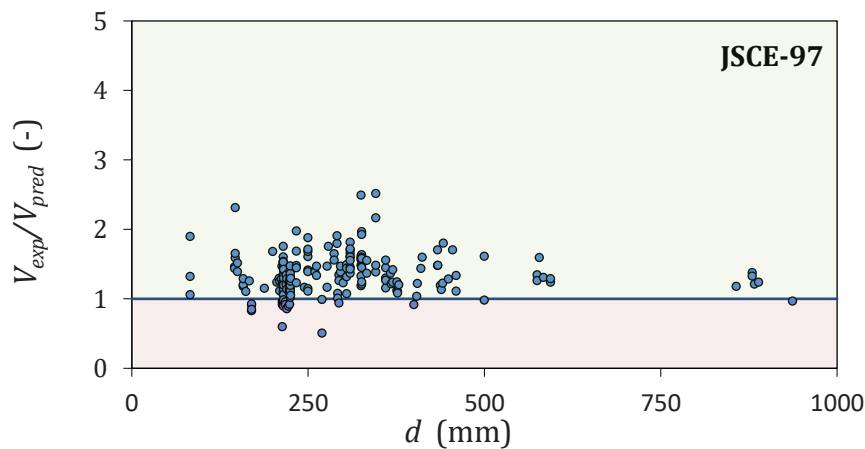
Figure 2-13 Predictions of the experimental values according to JSCE (1997)
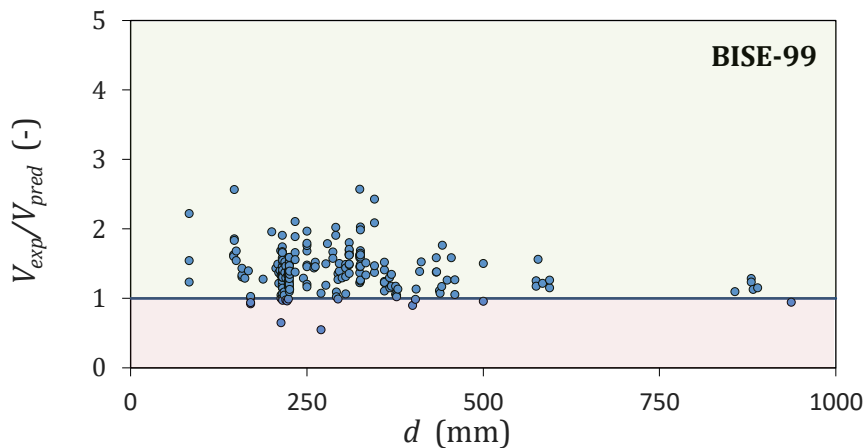
Figure 2-14 Predictions of the experimental values according to BISE (1999)

Figure 2-15 Predictions of the experimental values according to CNR (2006)

Figure 2-16 Predictions of the experimental values according to *fib* (2007)

Figure 2-17 Predictions of the experimental values according to ISIS (2007)

Figure 2-18 Predictions of the experimental values according to Hoult et al. (2008)

Figure 2-19 Predictions of the experimental values according to CSA (2012)

Figure 2-20 Predictions of the experimental values according to CSA (2014)

Figure 2-20 Predictions of the experimental values according to ACI (2015)

2.5.5 Shear predictions for beams with shear reinforcement

Based on the analysis of the experimental database included in Appendix B, the performance of JSCE (1997), CNR (2006), *fib* (2007), ISIS (2007), CSA (2012), CSA (2014) and ACI (2015) in predicting total shear resistance (V_c+V_f) is assessed (Figure 2-21 to Figure 2-27). The statistical summary of the predicted values is presented in Table 2-5. As can be seen, all codes except CNR yield conservative predictions of the total shear resistance. The shear provisions proposed by JSCE (1997) produce the largest V_{exp}/V_{pred} ratios with an average value equal to 2.63 and COV=46.2%. This may be attributed to a very conservative approach for predicting the allowable strain in the shear reinforcement, which ranged from about 350 µε to 3,600 µε.

On the other hand, allowing the development of a relatively high level of stress in the shear reinforcement as proposed by CNR (up to 50% of the design strength) produces on average unsafe predictions (V_{exp}/V_{pred} = 0.89). The *fib* model, which limits the allowable strain in the shear reinforcement to 4,500 με, shows a fairly good performance, with a mean value of V_{exp}/V_{pred} equal to 1.21 and the low scatter (COV=19.7%).

Table 2-5 Statistical coefficients for various shear provisions – beams with shear reinforcement

| Design provision	AVERAGE		SD		VAR		COV (%)	
	All	d > 400mm	All	d > 400mm	All	d > 400mm	All	d > 400mm
JSCE-97	2.63	2.61	1.22	0.87	1.48	0.76	46.2	33.4
CNR-DT 206/2006	0.89	1.06	0.23	0.26	0.05	0.07	25.3	25.0
fib bulletin 40	1.21	1.25	0.24	0.20	0.06	0.04	19.7	15.8
ISIS M03-07	2.50	2.80	0.67	0.62	0.45	0.38	27.0	22.1
CSA S806-12	1.63	1.85	0.42	0.55	0.18	0.30	26.0	29.7
CSA S6-2014	2.21	2.37	0.61	0.38	0.37	0.38	27.5	26.2
ACI 440 1R-15	1.83	1.72	0.35	0.25	0.12	0.06	19.1	14.6

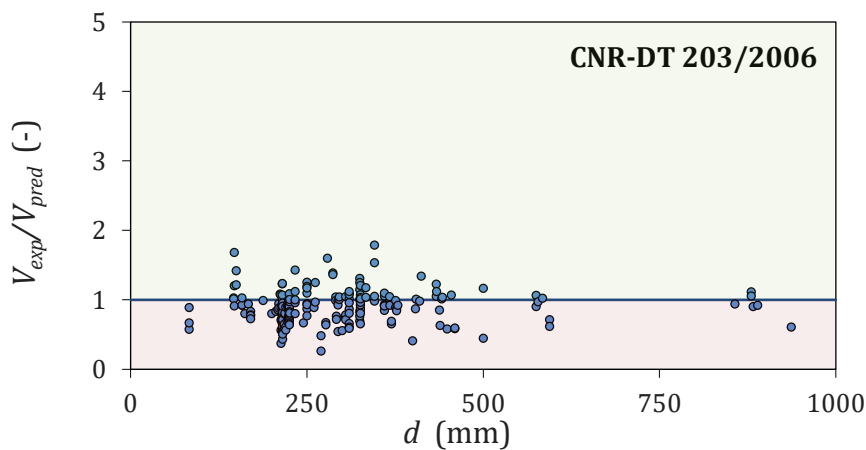**Figure 2-21** Predictions of the experimental values according to JSCE (1997)
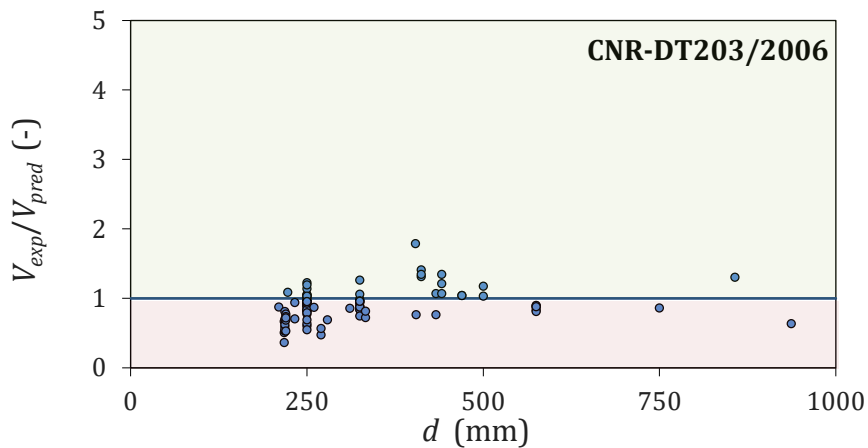
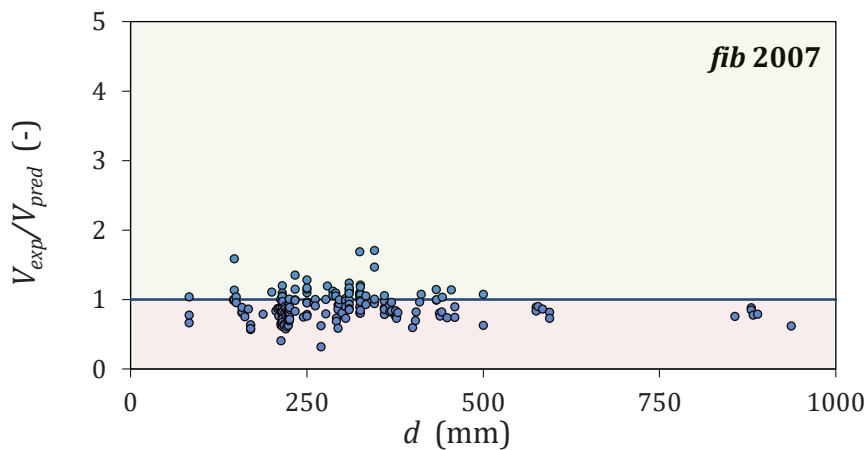**Figure 2-22** Predictions of the experimental values according to CNR (2006)
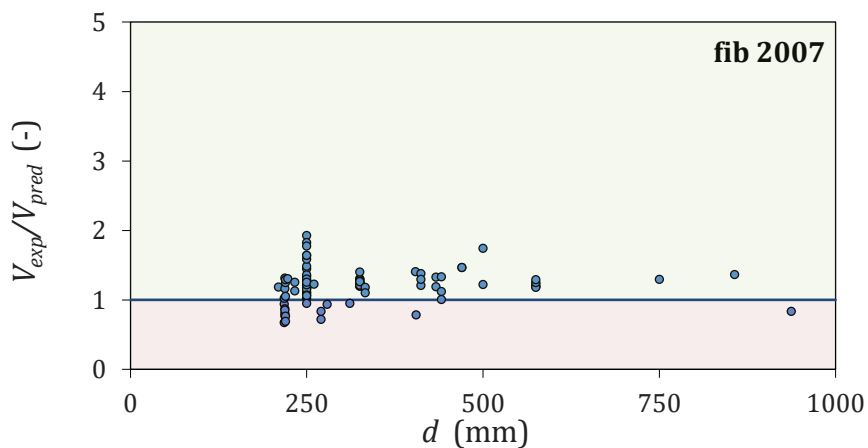
Figure 2-23 Predictions of the experimental values according to *fib* (2007)
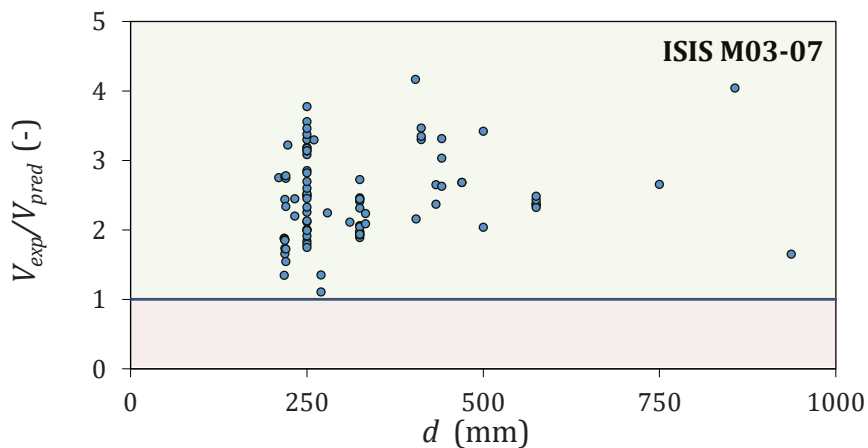
Figure 2-24 Predictions of the experimental values according to ISIS (2007)
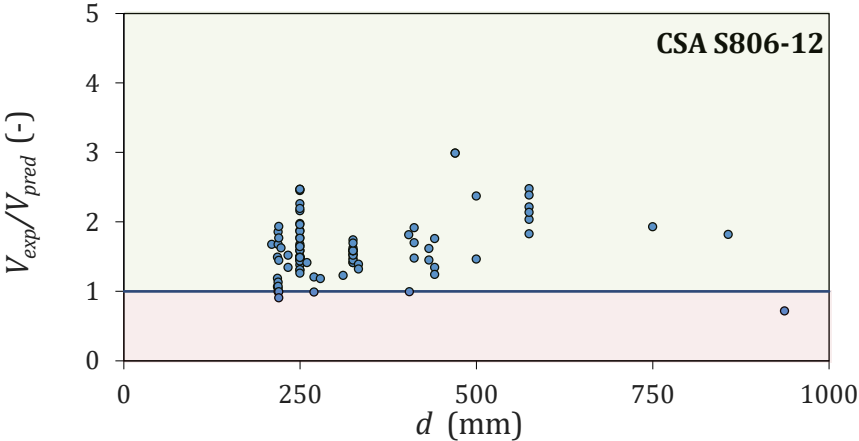
Figure 2-25 Predictions of the experimental values according to CSA (2012)
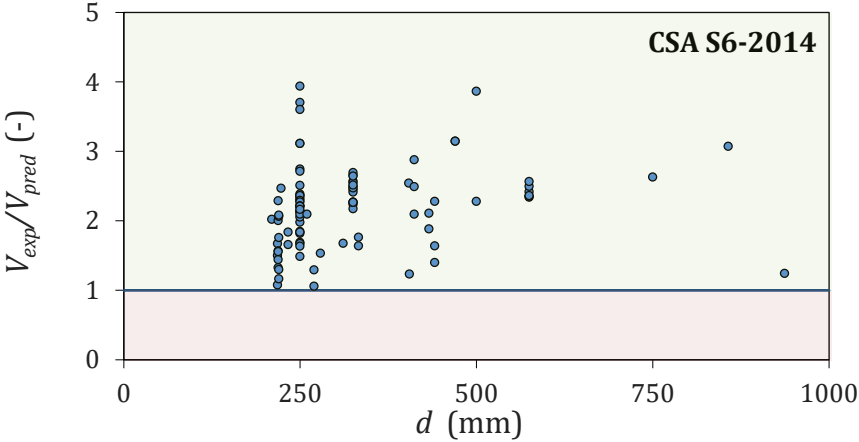
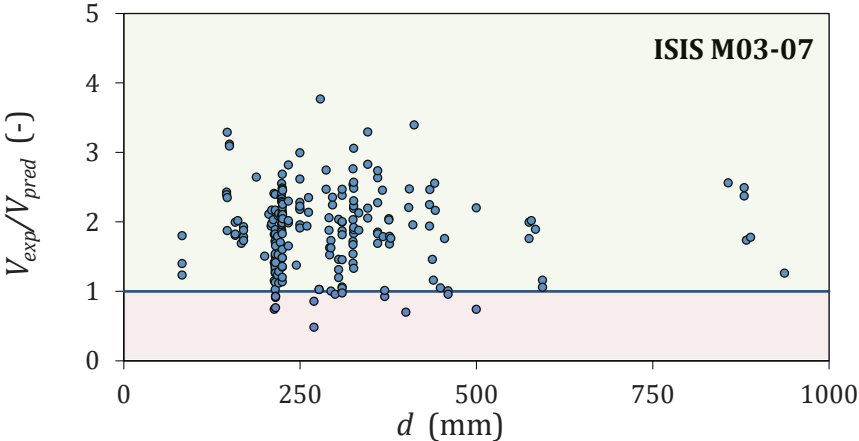**Figure 2-26** Predictions of the experimental values according to CSA (2014)
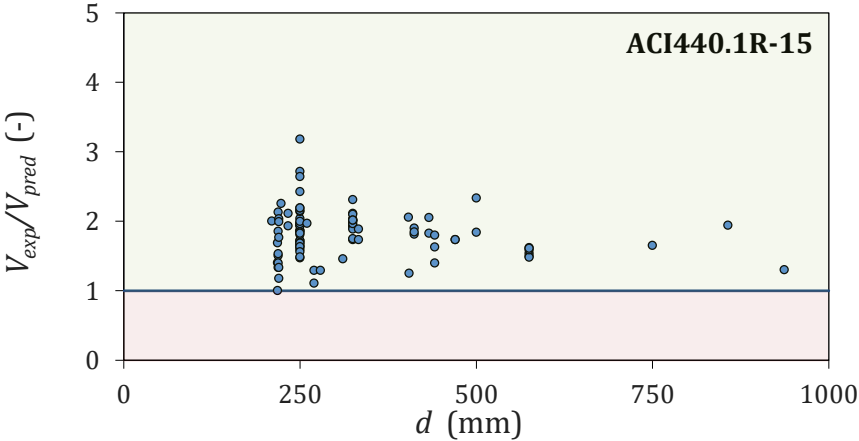
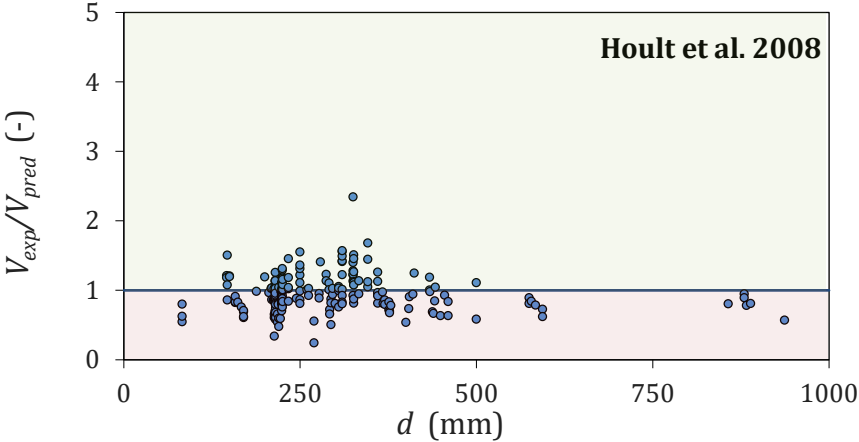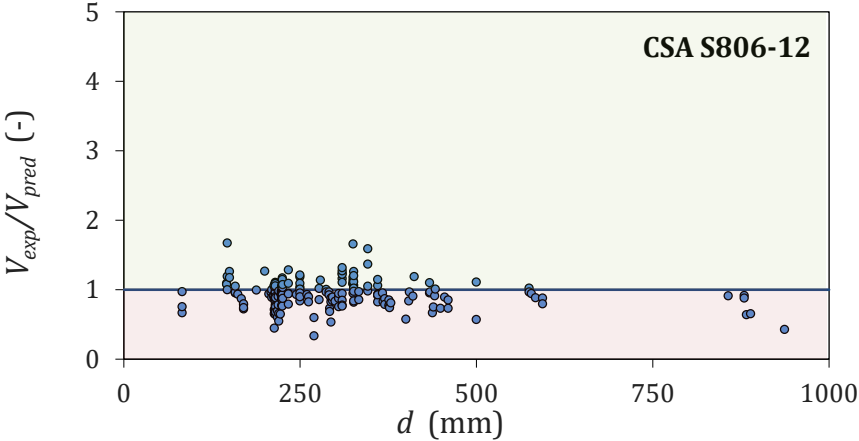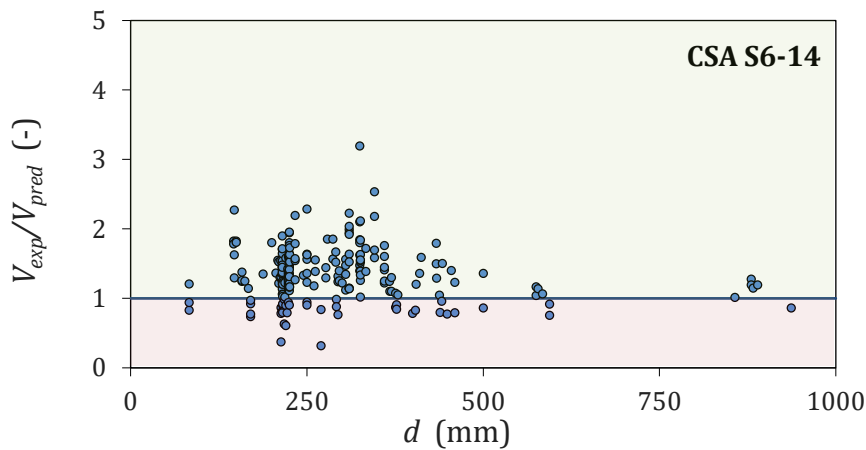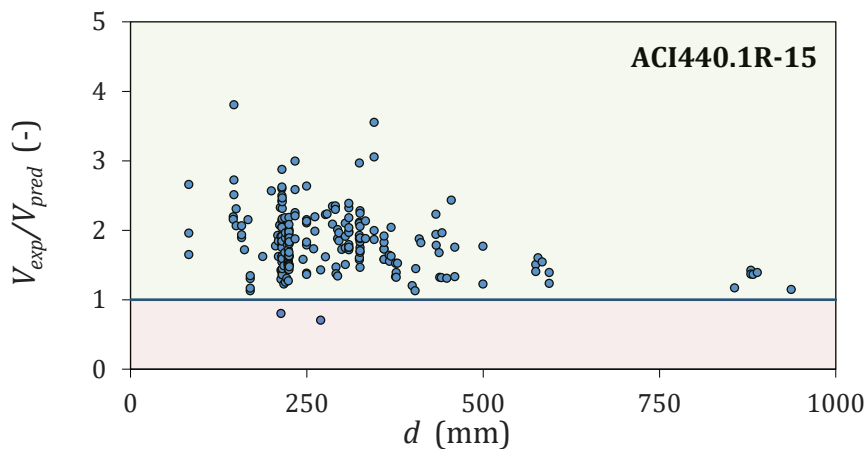**Figure 2-27** Predictions of the experimental values according to ACI (2015)
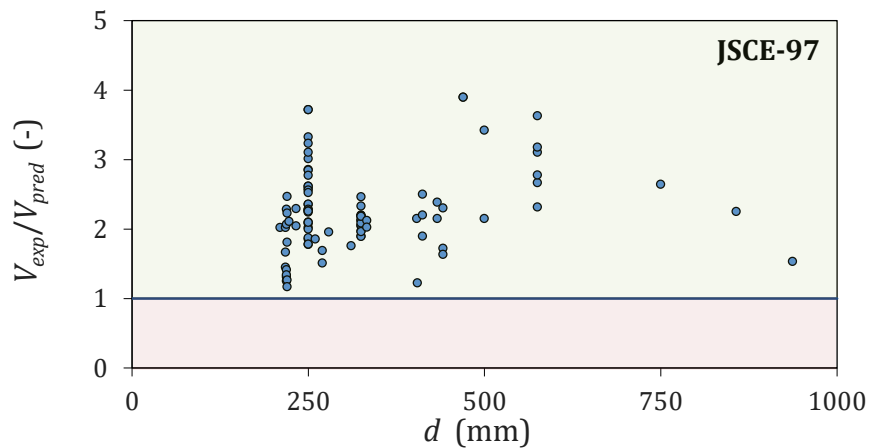
2.6   Conclusions

A comprehensive database including FRP RC beams with and without shear reinforcement is presented and the performance of existing design-oriented models for FRP RC beams is evaluated. The review of available literature lead to the following conclusions:

- The same resisting mechanisms develop in elements with steel and FRP reinforcement. Owing to the different mechanical properties of FRPs, however, the relative magnitudes of these mechanisms differs from that observed in steel RC.

- Similarly to steel RC beams, experimental studies confirm that size effect in FRP RC elements is significant primarily in beams without web reinforcement and is mitigated by the presence of shear reinforcement.

- A detailed analysis of the large database of FRP RC beams collected as part of this research and a database of steel RC beams available in the literature confirms the hypothesis that size effect is more prominent in FRP RC beams than in steel RC beams. Current design provisions, however, cannot accurately capture this behaviour.

- The experimental results available in the literature show that strain in FRP shear reinforcement largely exceeds the strain limits imposed by the current design models; however, these strain values decrease with increasing axial stiffness of the reinforcement. The strain in the shear reinforcement seems to be a function of member's depth and increases with increasing effective depth.

- The most conservative estimate of shear contribution of concrete is given by ISIS M03-07 and ACI 440.1R-15 models, with average experimental-to-theoretical ratios equal to 1.88 and 1.83, respectively (COV=30.2% and 23.9%, respectively). Slightly unconservative results are obtained using the shear provisions proposed by *fib* bulletin 40, CNR-DT203/2006, CSA S806-12 and Hoult et al. 2008; however, these models show the lowest standard deviations between experimental results and predicted values. The best approximation is obtained by implementing the equation proposed in CSA

S806-12, with a mean value of V_{exp}/V_{pred} equal to 0.93 and a COV equal to 20.3%.

- The most conservative predictions for beams with shear reinforcement are achieved using JSCE-97 with a mean value of V_{exp}/V_{pred} equal to 2.63, COV= 46.2%. This suggests that this design approach, although it allows calculating the strain in FRP shear reinforcement, provides non-uniform predictions and greatly underestimates contribution of V_f. The best performance, though slightly conservative, is achieved using the provisions given in *fib* bulletin 40, with a mean value of V_{exp}/V_{pred} = 1.21 and a COV=19.7%.

Based on the discussion presented above, an experimental programme was designed to assess the effect of member's depth on the shear behaviour of FRP RC beams, including strain development in flexural and shear reinforcement, contribution of concrete and shear reinforcement to overall shear resistance, crack initiation and development. This will be introduced in Chapter 3 and Chapter 4.

2.7   References

- Alam, M. S., and Hussein, A. (2012). "Size effect on shear strength of FRP reinforced concrete beams without stirrups." J. Compos. Constr., 10.1061/(ASCE)CC.1943-5614.0000346, 507-516.

- American Concrete Institute (ACI). Guide for the design and construction of concrete reinforced with FRP bars. Technical Committee Document No. 440.1R-15, Farmington Hills, Mich; 2015.

- Angelakos, D., Bentz, E. C., and Collins, M. P. (2001). "Effect of concrete strength and minimum stirrups on shear strength of large members." J. Struct. Eng., 98(3), 290–300.

- Ashour, A. F., and Kara, I. F. (2014). "Size effect on shear strength of FRP reinforced concrete beams." Compos. Part B., 60, 612-620.

- Bazant, Z. P., and Kazemi, M. T. (1991). "Size effect on diagonal shear failure of beams without stirrups." ACI Struct. J., 88(3), 268-276.

- Bazant, Z. P., and Kim, J. K. (1984). "Size effect in shear failure of longitudinally reinforced beams." ACI Journal., 8, 456-468.

- Bazant, Zdenek P., and Hsu-Huei Sun. "Size effect in diagonal shear failure: influence of aggregate size and stirrups." ACI Materials Journal 84, no. 4 (1987): 259-272.

- Bentz, E. C., Massam, L., and Collins, M. P. (2010). "Shear strength of large concrete members with FRP reinforcement." J. Compos. Constr., 10.1061/(ASCE)CC.1943-5614.0000108, 637-646.

- British Institution of Structural Engineers (BISE). Interim guidance on the design of reinforced concrete structures using fiber composite reinforcement. IStructE, SETO Ltd., London; 1999.

- Canadian Standards Associations (CSA). Canadian Highway Bridge Design Code. CSA S6-14, Mississauga, ON, Canada; 2014.

- Canadian Standards Associations (CSA). Design and construction of building components with fibre-reinforced polymers. Canadian Standards S806-12, Rexdale, Ontario, Canada; 2012.

- Cao, Shen. "Size effect and the influence of longitudinal reinforcement on the shear response of large reinforced concrete members." MSc thesis., Department of Civil Engineering, University of Toronto, Toronto, Ontario, Canada (2001).

- CNR-DT 203/2006. Guide for the design and construction of concrete structures reinforced with fiber-reinforced polymer bars. National Research Council, Rome, Italy; 2006.

- Collins, M. P., and Kuchma, D. (1999). "How safe are our large, lightly reinforced concrete beams, slabs, and footings? " ACI Struct. J., 96(4), 482-490.

- Duranovic N, Pilakoutas K, Waldron P. Tests on concrete beams reinforced with glass fibre reinforced plastic bars. In: Proceedings of FRPRCS-3 Conference. 1997; pp. 479-486.

- Fenwick, R. C., and Paulay, T. (1968). "Mechanisms of Shear Resistance of Concrete

- *fib* (Fédération internationale du béton). (2007). "FRP reinforcement in RC structures, technical". fib bulletin 40, Technical report. Lausanne, Switzerland Joint ACI-ASCE

- Frosch R. J. (2000). Behavior of large-scale reinforced concrete beams with minimum shear reinforcement ACI Struct. J., 97(6), 814-820.

- Guadagnini M, Pilakoutas K, Waldron P. Shear resistance of FRP RC beams: Experimental study. J. Compos. Constr. 2006; 10.1061/(ASCE)1090-0268(2006)10:6(464), 464-473.

- Hordijk DA. Tensile and tensile fatigue behaviour of concrete, experiments, modelling and analyses. Heron 1992;37(1):3–79.

- Hoult NA, Sherwood EG, Bentz EC, Collins MP. Does the use of FRP reinforcement change the one-way shear behavior of reinforced concrete slabs? J. Compos. Constr. 2008; 10.1061/(ASCE)1090-0268(2008)12:2(125), 125-133.

- ISIS Canada. Reinforcing concrete structures with fiber reinforced polymers. ISIS-M03-07, Canadian network of centers of excellence on intelligent sensing for innovative structures, Univ. of Winnipeg, Winnipeg, Man; 2007.

- Issa MA, Ovitigala T, Ibrahim M. Shear Behavior of Basalt Fiber Reinforced Concrete Beams with and without Basalt FRP Stirrups. J. Compos. Constr. 2015, 20(4), 04015083.

- Jang, H., M. Kim, J. Cho, and C. Kim. "Concrete shear strength of beams reinforced with FRP bars according to flexural reinforcement ratio and shear span to depth ratio." In Proceedings of 9th International Symposium on Fiber Reinforced Polymer Reinforcement for Concrete Structures, FRPRCS, vol. 9. 2009.

- Japan Society of Civil Engineers (JSCE). In: Machida A, editor, Recommendations for design and construction of concrete structures using continuous fibre reinforced materials. Concrete Engineering Series 23, Tokyo, Japan; 1997.

- Johnson, David T., and Shamim A. Sheikh. "Experimental Investigation of Glass Fiber-Reinforced Polymer-Reinforced Normal-Strength Concrete Beams." ACI Structural Journal 113, no. 6 (2016): 1165.

- Joint ACI-ASCE Committee 445, "Recent Approaches to Shear Design of Structural Concrete." J. Struct. Eng.-ASCE, V. 124, No. 12, Dec. 1998, 1375-1417.

- Kanakubo, T., and Shindo, M. (1997). "Shear Behaviour of Fiber-Mesh Reinforced Beams." Journal of the Structural Division, Proceedings of the American Society of Civil Engineering, 94(No. ST10), 2325-2350.

- Kani, G. N. J. (1966). "Basic facts concerning shear failure" *ACI Journal,* 63(6)*,* 675-692.

- Kani, G. N. J. (1967). "How Safe Are Our Large Reinforced Concrete Beams?" Journal of the American Concrete Institute, 64(3), 128-141.

- Kaszubska, Monika, Renata Kotynia, Joaquim AO Barros, and Hadi Baghi. "Shear behavior of concrete beams reinforced exclusively with longitudinal glass fiber reinforced polymer bars: Experimental research." Structural Concrete 19, no. 1 (2018): 152-161.

- Lee, C., S. Lee, and S. Shin. "Shear capacity of RC beams with carbon fiber-reinforced polymer stirrups with rectangular section." Journal of Composites for Construction 20, no. 4 (2015): 04015085.

- Lubell, A., Sherwood, T., Bentz, E., and Collins, M. (2004). "Safe shear design of large wide beams." Concrete International., 26(1), 66-78.

- Mahmoud, K., and El-Salakawy, E. (2016). "Size Effect on Shear Strength of Glass Fiber-Reinforced Polymer-Reinforced Concrete Continuous Beams." ACI Struct. J., 113(1), 125.

- Maruyama, K., and Zhao, W. J. (1994). "Flexural and Shear Behaviour of Concrete Beams Reinforced with FRP Rods." Corrosion and Corrosion Protection of Steel in Concrete, University of Sheffield, UK, 1330-1339.

- Massam, L., "The Behaviour of GFRP Reinforced Concrete Beams in Shear," MSc thesis, Department of Civil Engineering, University of Toronto, Toronto, Ontario, Canada (2001).

- Matta, F., El-Sayed, A. K., Nanni, A., and Benmokrane, B. (2013). "Size effect on concrete shear strength in beams reinforced with fiber-reinforced polymer bars." ACI Struct. J., 110(4), 617.

- Matta, F., Nanni, A., Galati, N., and Mosele, F. (2007). "Size effect on shear strength of concrete beams reinforced with FRP bars." Proc., 6th International Conf. on Fracture Mech. of Concr. and Concr. Struct. (FraMCoS-6)., Balkema/Taylor & Francis, ed., Vol. 2, pp. 17-22.

- Nakamura, H., and Higai, I. (1995). "Evaluation of Shear Strength on Concrete Beams Reinforced with FRP" Concrete Library, JSCE, 26, 111-123 pp.

- Plates." Third International Symposium on Non-Metallic (FRP) Reinforcement for Concrete Structures, Sapporo, Japan, 317-324.

- Podgorniak-Stanik, Bogdan A. "The influence of concrete strength, distribution of longitudinal reinforcement, amount of transverse reinforcement and member size on shear strength of reinforced concrete members." MSc thesis, Department of Civil Engineering, University of Toronto, Toronto, Ontario, Canada (1998).

- Razaqpur, A. G., and Isgor, O. B. (2006). "Proposed shear deign method for FRP-reinforced concrete members without stirrups." ACI Struct. J., 103(1), 93–102.

- Razaqpur, A. G., Isgor, B. O., Greenaway, S., and Selley, A. (2004). "Concrete contribution to the shear resistance of fiber reinforced polymer reinforced concrete members." J. Compos. Constr., 10.1061/(ASCE)1090-0268(2004)8:5(452), 452-460.

- Reineck, Karl-Heinz, Evan C. Bentz, Birol Fitik, Daniel A. Kuchma, and Oguzhan Bayrak. "ACI-DAfStb Database of Shear Tests on Slender Reinforced Concrete Beams without Stirrups." ACI Structural Journal 110, no. 5 (2013).

- Sherwood, E. G.; Bentz, E. c.; and Collins, M. P. (2008), "Prediction of the Shear Strength of FRP-Reinforced Slabs using the 2004 CSA A23 Design Code," CSCE Annual Conference, Quebec. Canada, June 10-13

- Sherwood, E.G. " One-Way Shear Behaviour of Large, Lightly-Reinforced Concrete Beams and Slabs." PhD thesis, Department of Civil Engineering, University of Toronto, Toronto, Ontario, Canada (2008).

- Shioya, T., Iguro, M., Nojiri, Y., Akiyama, H., and Okada, T. (1989). "Shear strength of large reinforced concrete beams." Special Publication, 118, 259-280.

- Steiner. S.; El-Sayed, A. K. and Benrnokranc, B. (2008), "Shear Behaviour of LargeSize Concrete Beams Reinforced with Glass I'RP Bars," CSCE Annual Conference, Quebcc,Canada, June 10-13.

- Stratford T, Burgoyne CJ. (). Shear Analysis of Concrete with Brittle Reinforcement. J. Compos. Constr. 2003; 7(4), pp. 323-330.

- Taylor, H. P. J. (1970). "Investigation of the Forces Carried Across Cracks in Reinforced Concrete Beams in Shear by Interlock of Aggregate." 42.447, Cemen and Concrete Association, London.

- Tottori, S., and Wakui, H. (1993). "Shear Capacity of RC and PC Beams Using FRP Reinforcement." International Symposium on Fiber Reinforced Plastic Reinforcement for Concrete Structures, 615-632.

- Vecchio FJ, Collins MP. The modified compression field theory for reinforced concrete elements subjected to shear. ACI J. 1986; 83(2), 219–231.

- Walraven, J. C. (1981). "Fundamental Analysis of Aggregate Interlock." Journal of the Structural Division, Proceedings of the American Society of Civil Engineering, 107(No.ST11), 2245-2269.

- Yoshida, Yoichi. "Shear reinforcement for large lightly reinforced concrete members." MASc thesis, Department of Civil Engineering, University of Toronto, Toronto, Ontario, Canada (2000).

Chapter 3

Effect of Beam Depth on Shear Behaviour of FRP RC Beams

Cholostiakow, S., *Di Benedetti, M., Pilakoutas, Guadagnini, M., 2019. Effect of Beam Depth on Shear Behaviour of FRP RC Beams. Journal of Composites for Construction, 10.1061/(ASCE)CC.1943-5614.0000914*

Abstract*: The behaviour of shear critical fibre-reinforced-polymer (FRP) reinforced concrete (RC) elements is characterised by the development of comparatively large strains and crack widths, which can be strongly influenced by their relative geometrical size. This paper investigates experimentally the size effect on the shear behaviour of FRP RC beams with and without shear reinforcement and overall depth varying from 260 mm to 460 mm. The results confirm a considerable size effect for members without shear reinforcement, showing an average reduction in normalized shear strength of about 19 %, with maximum value up to 40 %. It is also shown that current design provisions are overall conservative, but with non-uniform margins of safety that decrease with increasing member depth. It is anticipated that the results of this study will help improve the efficiency of future design equations for the shear strength of FRP RC.*

This chapter consists of a "stand alone" journal paper and includes a relevant bibliography at the end of the chapter. Additional information and further test results are presented in Appendix C, D and E.

3.1   Introduction

Owing to its non-corrosive characteristics, fibre-reinforced polymer (FRP) reinforcement is primarily used in structures exposed to severe environments, such as bridges. Although FRP reinforcement is widely used in concrete bridge decks (e.g. Morristown Bridge in Vermont, US; Irvine Creek Bridge in Ontario, Canada; Saint Catharine twin overpass bridges in Sherbrook, Canada), FRPs are not used extensively in other bridge elements. This may be attributed to the lack of understanding of shear performance of large FRP reinforced concrete (RC) elements, combined with the overly conservative nature of existing design recommendations, which makes such designs uneconomic (Zoghi 2013).

Even for conventional steel reinforcement, the lack of a universally accepted rational shear theory has led to the development of many simplified empirical design rules, which, although generally conservative, have also been shown to lead to unsafe design, especially for large structural elements, potentially with catastrophic consequences (Burgoyne and Scantlebury 2006; Collins et al. 2008).

The shear performance of large steel reinforced concrete elements has been examined by various researchers (Kani 1967; Shioya et al. 1990; Bazant and Kazemi 1991; Walraven and Lehwalter 1994; Collins and Kuchma 1999; Frosch 2000; Angelakos et al. 2001; Bentz 2005; Hassan et al. 2008, Yu et al. 2013), and it was found that for geometrically similar members shear strength at failure reduces with increasing beam depth; i.e. there is a "size effect". The Joint ASCE and ACI Committee 445 on Shear and Torsion (ASCE-ACI 1998) attributed size effect mainly to a reduction in the resistance offered by aggregate interlock as a result of larger crack openings. The size effect may also be affected by shear span-to-depth-ratio, aggregate size, presence of shear reinforcement, and longitudinal reinforcement ratio. Various models based on empirical observations and plasticity theory have been developed over the years to account for size effect (e.g. Reineck 1991; Collins et al. 1996; Lubell et al. 2004) and implemented in design codes (EN 1992; JSCE 1997; AASHTO 2007; CSA 2004; ISIS 2007; CSA 2012; CSA 2014; Model Code 2010). Other researcher tried to model size effect as a function of energy release at failure

caused by macro crack growth (Bazant 1984; Bazant and Kim 1984; Bazant and Kazemi 1991).

Experimental evidence (Nanni 1993; Benmokrane et al. 1995; Alsayed et al. 2000; Yost et al. 2001; Pilakoutas et al. 2002; Razaqpur et al. 2004; Guadagnini et al. 2006; El Sayed et al. 2006) suggests that, although the same resisting mechanisms are mobilised, the shear capacity of FRP RC elements is lower than that of their equivalent steel reinforced concrete counterparts. Under similar loading conditions, FRP RC elements develop much higher deformations, thus exhibiting wider and deeper cracks (Tureyen and Frosh 2002). In turn, larger strain in the FRP flexural reinforcement results in a reduced portion of concrete resisting shear in compression and weakened aggregate interlock along cracks.

Current shear design recommendations for FRP RC (JSCE 1997; BISE 1999; CSA 2012; CNR 2006; ISIS 2007; CSA S6-2014; ACI 2015) are based on modifications of models originally developed for conventional steel RC, but account somehow for the lower stiffness of the FRP bars. Size effect, when included, is modelled through the use of empirically derived (based on the experimental observations rather than theoretical approach) parameters calibrated against experimental data collected from steel RC specimens. These assumptions may potentially result in unsafe design or produce low margins of safety for large FRP RC beams having overall depth greater than 300 mm (Razaqpur and Isgor 2006; Razaqpur et al. 2011).

The aim of the current study is to investigate experimentally the shear behaviour of FRP RC beams with and without shear reinforcement, examining in detail the effect of beam size on crack initiation and development, strain distribution and failure mode. The performance of current design oriented shear models including ACI440.1R-15, CSA S6-2014, CSA 806-12, Hoult et al. (2008) and *fib* 2007 is also assessed. The results are expected to assist in the development of more reliable shear design equations for large FRP RC members.

3.2   Experimental programme

The experimental programme was designed to investigate size effect on shear behaviour of FRP RC beams with and without shear reinforcement. A total of fifteen tests on FRP RC beams were carried out (full details are shown in Figure 3-1 Details of geometry and reinforcement layout for all beams). The specimens were divided into two groups, comprising beams without shear reinforcement (GB54-GB58, GB58R, GB59R, GB58-0 and GB59-0) and beams with closed external FRP links (GB60-GB65), respectively. The parameters investigated in this study were: effective depth, d; presence of shear links; and concrete strength, f'_c. All other parameters, including beam width, b_w, longitudinal tensile reinforcement ratio, ρ_f, shear-span-to-depth ratio, a/d, were kept constant.

3.2.1   Test specimens

As summarised in Figure 3-1, testing of each beam was carried out in two consecutive phases (that was not a case for one of the beams with overall depth of 260 mm, which faced some experimental complications and only one test was performed - GB58) so as to allow an in-depth examination of the behaviour of the two shear spans and to minimize the variability in the test results. For instance, tests GB64 and GB65 were performed on the same specimen. During the first phase of testing, the damage was induced primarily on the left shear span, keeping clear span ($a+a'$) equal to 2300 mm (see Figure 3-1). During the second phase, the shear span tested in the first phase was cut off and the second test was performed on shorter clear span, a'=1400 mm, yet keeping the same shear span length, a=900 mm. For beams with the overall depth 460 mm, the second phase of testing was performed without cutting off the tested shear span "a" so as to keep the same clear span (2300 mm) during both test phases. In addition, post-tensioned metal straps (PTMS) (Helal et al. 2016) were used to strengthen the tested shear span and, in case of GB61, a cement grout was used to repair the beam before testing. PTMS were also provided along span a' of some of the specimens to ensure that failure occurred in the instrumented shear span. More information can be found in Appendix C.
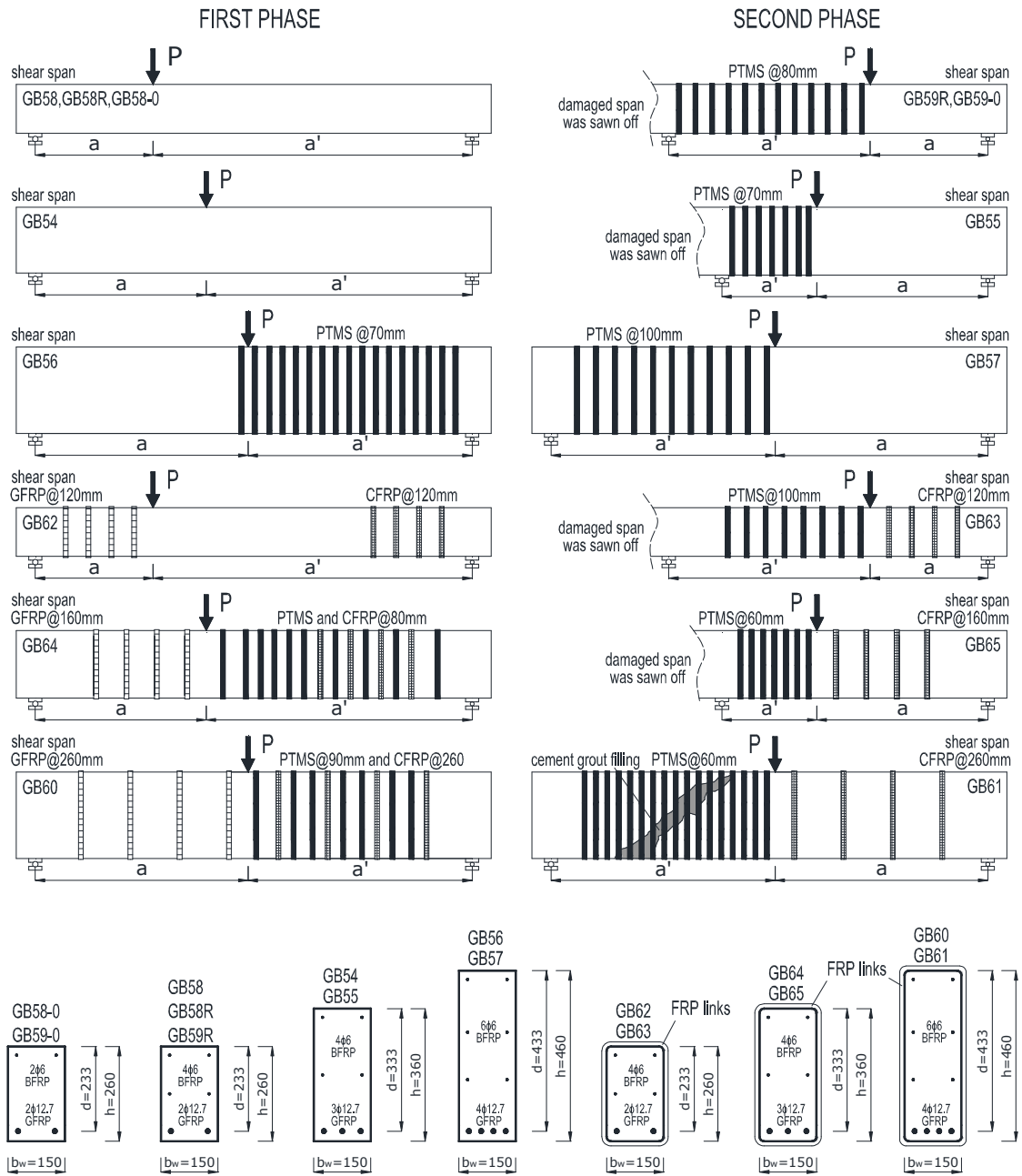
Figure 3-1 Details of geometry and reinforcement layout for all beams

3.2.2 Concrete

The beams were cast in three batches using normal weight ready-mix concrete with a maximum aggregate size of 20 mm, a water-to-cement ratio of 0.55, and cement type 52,5N CEM I. Beams GB58R, GB59R, GB58-0 and GB59-0 were cast using concrete with angular aggregates (limestone), while round river aggregates were

used for the remaining beams. The compressive concrete strength was determined on the day of testing from three 100 mm cubes cured under the same conditions as the beams. The concrete cylinder compressive strength, $f'c$, was taken as 80 % of the cube compressive strength (Table 3-1).

Table 3-1 Specimen geometry and concrete properties

| Beam	a (mm)	a' (mm)	h (mm)	d (mm)	a/d (mm)	a'/d (mm)	f'_c (MPa)	E_c [a] (GPa)	ρ_f (%)	Type of links	s (mm)
GB58-0		1680				7.2	41.6	30.3		-	-
GB59-0		1060				4.6	48.4	32.7		-	-
GB58		1680				7.2	36.6	28.4		-	-
GB58R	620	1680	260	233	2.65	7.2	47.0	32.2	0.82	-	-
GB59R		1060				4.6	48.6	32.7		-	-
GB62		1680				7.2	52.7	34.4		GFRP	120
GB63		1060				4.5	50.9	32.4		CFRP	
GB54		1400				4.2	30.2	28.5		-	-
GB55	900	500	360	333	2.70	1.5	30.2	28.5	0.86	-	-
GB64		1400				4.2	47.5	32.4		GFRP	160
GB65		500				1.5	47.5	32.4		CFRP	
GB56							38.0	29.0		-	-
GB57	1120	1180	460	433	2.58	2.7	36.6	28.4	0.88	-	-
GB60							38.4	29.1		GFRP	260
GB61							38.4	29.1		CFRP	

Note: [a] values calculated according to ACI 440.1R-15

3.2.3 FRP Reinforcement

The details and layout of the FRP internal and external reinforcement are shown in Figure 3-1, Table 3-2, and Table 3-3. The main flexural reinforcement comprised commercially available sand coated GFRP bars (Figure 3-2a) with nominal diameter of 12.7 mm (average measured 13.5 mm). The number of bars was selected to prevent flexural failure prior to shear failure, resulting in a longitudinal reinforcement ratio of about 0.85 %. As such, failure due to diagonal shear was designed to occur at about 60% of bending capacity. In addition, longitudinal sand coated basalt FRP (BFRP) bars with nominal diameter of 6 mm were used at specific heights within the web of the specimens. It should be noted that, although the use of

skin reinforcement has been shown to mitigate size effect (Collins and Kuchma 1999; Bentz 2010), the BFRP bars used in this study were selected to be sufficiently small to offer negligible contribution to shear resistance, yet enable the installation of strain gauges at various locations of interest within the test spans. Beams GB58-0 and GB59-0 served as control specimens and were constructed without the skin reinforcement to assess the contribution of the BFRP bars to the overall shear capacity of the beams.

External FRP links (Figure 3-2b) were employed as shear reinforcement to facilitate the monitoring of deformations and to gain an additional insight into strain distribution along the link length using Digital Image Correlation. The FRP links were wrapped continuously around the beam, with an overlap in the top part of the beam perimeter eliminating the possibility of premature delamination.
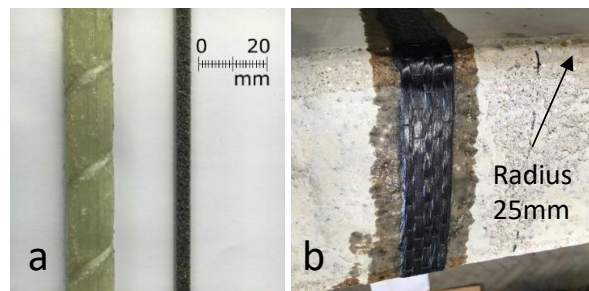
Figure 3-2 FRP reinforcement: (a) Longitudinal reinforcement; (b) CFRP link bonded to the beam

Table 3-2 Mechanical properties of the FRP longitudinal reinforcement

Flexural bars	Bar diameter (mm)	Cross-sectional area (mm^2)	Modulus of elasticity (GPa)	Tensile strength (MPa)
GFRP bars	13.5	143.0	46.0	758
BFRP bars[a]	6.0	28.3	42.0	1,297

Note:[a] Data from Serbescu et al. 2014

The external FRP links were manufactured in the laboratory using continuous strips of glass and carbon fibre sheets impregnated with an epoxy resin. The two types of fibres were used to investigate the influence of link stiffness on the cracking and overall shear behaviour of the beams. GFRP links were used in specimens GB60,

GB62 and GB64, while CFRP links were used in GB61, GB63 and GB65. The shear reinforcement was designed to provide the minimum shear reinforcement ratio of $\rho_{fv,min}=0.35/f_{fv}$ recommended in ACI 440.1R-15 (Table 3-3).

Strain developed on the external links can be slightly different from that in equivalent internal links mainly to the expected different bond behaviour. However, given that the links are fully anchored (fully wrapped around the section, see also Figure 4-1), once mobilised, their behaviour is expected to be similar to internally placed stirrups. As it will be shown later in Figure 3 - 13, no strain is observed away from the crack confirming good bond between shear links and concrete. As long as they are effectively anchored, the contribution of shear links can be calculated based on the truss analogy and the effective strength of the links (also a function of the geometry of the bent portions). The shear depth considered in design (i.e. the distance between the centroid of the area of concrete in compression and the tension reinforcement) is only determined by the position of the flexural reinforcement. This is also reflected in current design approaches for internal and external links. It should be also mentioned that, externally placed links confine the whole beam section, not only the reinforcement cage as in case of stirrups, which in theory would result in a slightly steeper inclination of the critical shear crack, and thus, slightly smaller shear resistance. However, as the distance between the centroid of the stirrup and centroid of the shear link would be only about 20 mm, this difference in shear strength is expected to have a negligible importance.

Table 3-3 Mechanical properties of the FRP shear reinforcement

| Beam	Type	f_{fv} [a] (MPa)	Cross-sectional area[a] (mm^2)	Modulus of elasticity[a] (GPa)	Tensile strength[a] (MPa)
GB60	GFRP	260	40.5	65	1,700
GB61	CFRP	964	10.5	241	4,140
GB64	GFRP	260	28.4	65	1,700
GB65	CFRP	964	8.4	241	4,140
GB62	GFRP	260	21.6	65	1,700
GB63	CFRP	964	6.3	241	4,140

Note:[a] Determined for dry fibres

3.2.4 Test Setup and Instrumentation

All beams were simply supported and tested in an asymmetric 3-point bending configuration. The load was applied in displacement control at a rate of 0.25 mm/min. The dimensions of loading and bearing steel plates were identical and equal to 75x150x20 mm. The loading procedure consisted of two load cycles followed by a final load ramp up to failure. The cycles were performed at load levels inducing strain in the main longitudinal reinforcement of about 3,000 με and 4,500 με, which were taken as the strain levels expected under typical service conditions and corresponding to the maximum allowable strain limit in the reinforcement, respectively. Specimens with overall depth of 460 mm failed during the second cycle before the target strain of 4,500 με could be attained.

The typical test setup is shown in Figure 3-3 (GB65). The instrumentation was designed to measure load, vertical displacement of the beam and strains in the FRP reinforcement.
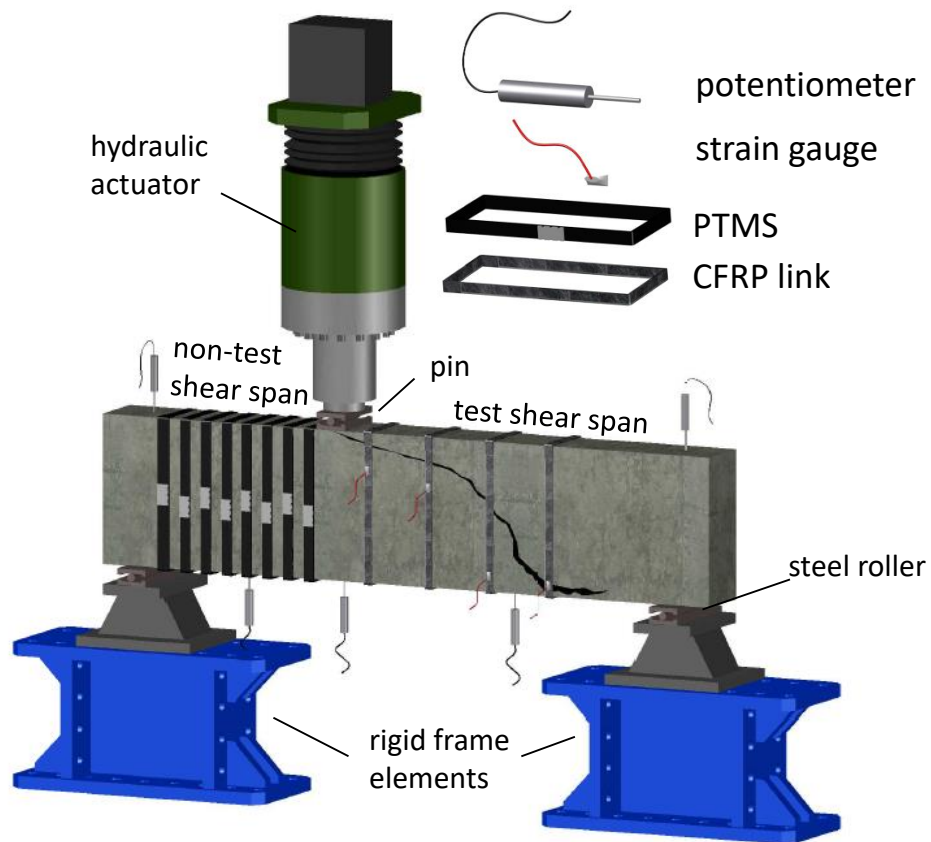
Figure 3-3 Typical test setup (GB65)

The deflection profile of the beam was measured by 3 potentiometers placed under the loading point and at the middle of each shear span. To account for any support movement, two additional potentiometers were used to measure the displacement at each support. Strain in the reinforcement was monitored by electrical resistance strain gauges (5 and 10 mm length for the BFRP and GFRP bars, respectively) bonded to the longitudinal reinforcement on a grid of 150 mm and distributed spatially so as to capture the initiation and development of the expected shear crack (Figure 3-4). Additional gauges were installed on the FRP shear links to enable a more accurate estimate of their contribution to shear resistance.

3.3   Test Results and Discussion

The main results obtained in the experimental program are summarised in Table 3-4. All beams exhibited a brittle diagonal tension shear failure caused by the development of diagonal cracks (Figure 3-5).The shear cracks initiated from flexural cracks within the shear span (see white circles in Figure 3-5) and propagated towards the compression zone under the loading point. The location of the initiation point depended on the member size and, the taller the beam, the lower the initiation point. For instance, the onset of the shear crack in GB58 and GB62 was almost at mid-height of the beam ($0.61d$ and $0.55d$, respectively), whereas in GB56 and GB60 it was near the level of the tensile reinforcement ($0.87d$ and $0.78d$, respectively). As the load increased, the flexural cracks propagated higher and additional smaller cracks developed from and along the shear crack. Just before failure, the shear crack "pushed" the bottom concrete cover off and propagated along the longitudinal reinforcement towards the support.

Table 3-4 Main test results

Beam	$\varepsilon_{l,max}$ ($\mu\varepsilon$)	$\varepsilon_{t,max}$ ($\mu\varepsilon$)	P_{ult} (kN)	k_1	V_{exp} (kN)	v_{norm} (MPa)	θ_{exp} (deg)	Eq.3-5 (deg)	Eq.3-10 (deg)
GB58-0	7,100	-	38.9	0.73	28.4	0.13	60	52	48
GB59-0	6,600	-	39.8	0.63	25.1	0.10	56	50	47
GB58	7,100[a]	-	51.0	0.73	37.3	0.18	40	59	48
GB58R	7,900[a]	-	47.2	0.73	34.4	0.14	45	57	48
GB59R	6,700[a]	-	47.8	0.63	30.2	0.12	50	54	48
GB62	11,000[a]	12,900	66.1	0.73	48.2	0.19	60	60	48

GB63	12,000[a]	6,800	86.0	0.63	54.2	0.22	45	60	48
GB54	4,400[a]	-	51.5	0.61	31.3	0.11	52	47	46
GB55	5,500[a]	-	132.5	0.36	47.3	0.17	50	55	50
GB64	10,000	9,000	101.4	0.61	61.7	0.18	59	60	50
GB65	8,900[b]	10,500	177.5	0.36	63.4	0.18	50	60	50
GB56	4,100[a]	-	85.6		43.9	0.11	44	47	47
GB57	4,500[a]	-	97.4	0.51	50.0	0.13	40	49	50
GB60	8,300[a]	16,800	150.5		77.2	0.19	53	60	52
GB61	x	13,500	166.4		85.4	0.21	45	60	52

Note: x = gauge did not work
[a]Average value from two strain gauges placed on opposite side of the beam
[b]Value presents the last reading from the gauge at shear load of about 60 kN
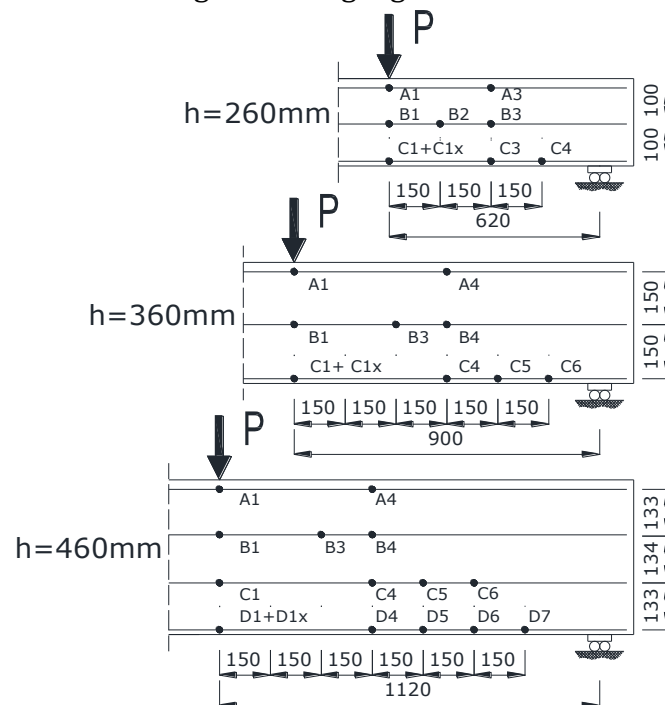
*Strain gauges marked with an "x" represent transducers placed at the same distance from the support but on the opposite side of the beam.

Figure 3-4 Typical strain gauge arrangement on the longitudinal reinforcement (dimensions in mm).

The diagonal shear failure of the members reinforced with shear links was abrupt and caused the rupture of the links. The fracture usually started from the link closest to the initiation point. No premature failure of the links due to debonding or anchorage failure was observed in any of the beams.

3.3.1 Load-Deflection Behaviour and Stiffness

The plots of shear load (in the critical span) versus net deflection under the loading point for all beams are shown in Figure 3-6. Each plot compares the response of beams tested under the same setup. The black and red curves represent the beams without external shear links, while the grey curves correspond to the beams with external shear links. The beams without skin reinforcement GB58-0 and GB59-0 (red curves) developed shear in the tested span about 5 kN lower than the corresponding beams with the mid-height bars.
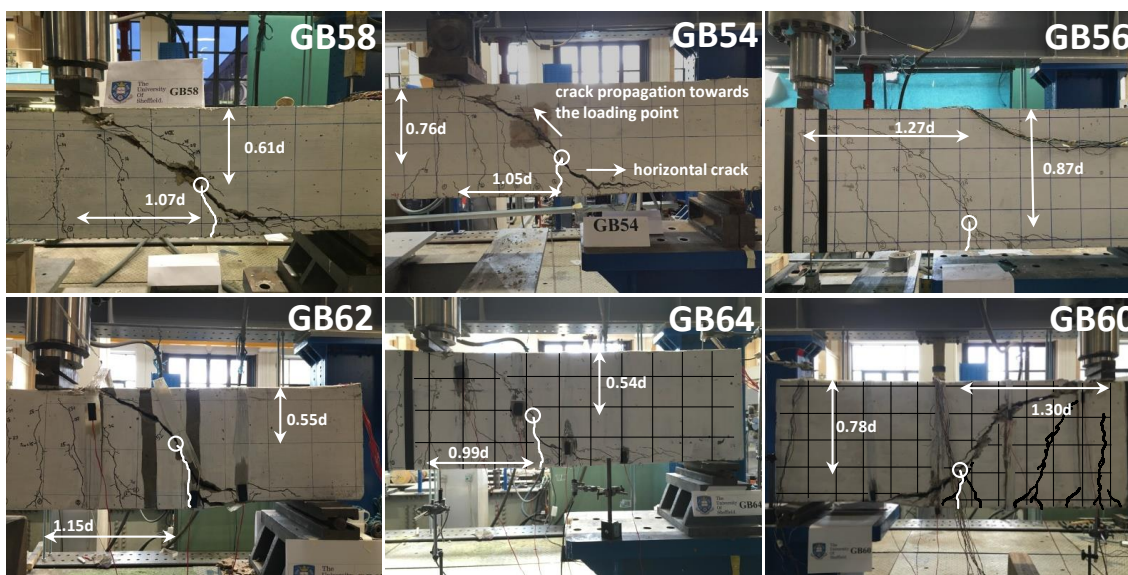
Figure 3-5 Failure modes of beams tested in the first phase

This indicates that basalt bars at the mid-height of the beam slightly contributed to shear and helped maintain beam stiffness after development of the critical shear crack. However, this additional strength is expected to decrease in larger members due to larger and deeper shear cracks and is not expected to affect significantly the overall shear capacity. In general, the shear capacity of the beams without external shear links increased with increasing member depth. Only GB54 developed slightly lower (about 15 %) shear capacity than its scaled counterparts GB58 and GB58R. Although within the expected variability of results, this can be mainly attributed to the lower strength measured for the concrete of GB54 (30.1 MPa).
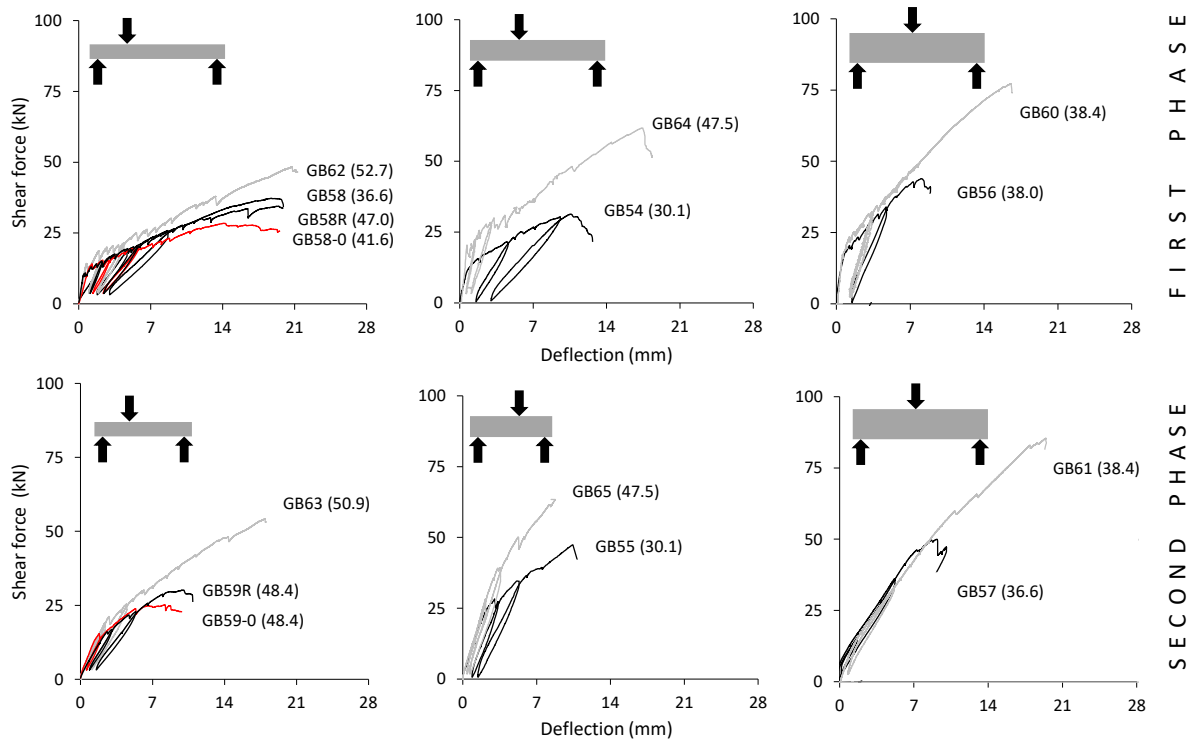
Figure 3-6 Shear load-deflection plots for all beams. Values in parentheses correspond to compression strength of concrete $f'c$ (in MPa)

The higher concrete strength of beams GB62-GB65 affected both stiffness and cracking behaviour. In general, an increase in the stiffness and cracking load was observed when compared to beams without shear links. The higher stiffness and shear capacity exhibited by GB65 in comparison to GB55 can be attributed to the ability of the shear links to control diagonal crack opening along the test span, thus enabling the further development of a stiffer truss-like transfer mechanism. On the other hand, GB60 and GB61 showed very similar initial shear load-deflection behaviour to the beams without shear links (GB56 and GB57), but developed a higher shear capacity through the contribution of the shear reinforcement.

The critical shear span length was kept identical in both testing phases and, as expected, a similar shear resistance was recorded, with differences usually not exceeding 10 %. However, in case of GB55, the tested shear span from the previous test (GB54) was sawn off, and the test was performed on a shorter beam, yet keeping the same test shear span of 900 mm. This resulted in much smaller shear span deflection, which could possibly affect the rotation of the shear crack and provide

slightly higher shear capacity. As a result, GB55 developed a shear strength almost 35 % higher than GB54. This suggests that the relative length of the shear spans, even though *a/d* ratio was kept the same, might have an influence on the overall behaviour and relative contribution of the resisting mechanisms. Such behaviour could be a result of material's natural variability but warrants further investigations.

3.3.2 Crack Development

Figure 3-7 shows the crack patterns for all beams along with the values of the angles of the main shear cracks estimated at mid-height. In general, analogous crack patterns were observed for geometrically equivalent elements. However, the beams with external GFRP links (first phase tests) showed steeper shear crack inclinations in comparison to the unreinforced beams. This confirms that the external shear links were effectively engaged and able to control the opening of the shear cracks. Crack spacing increased with member depth, which is in agreement with the observations from other studies (e.g. Alam and Hussein 2012).
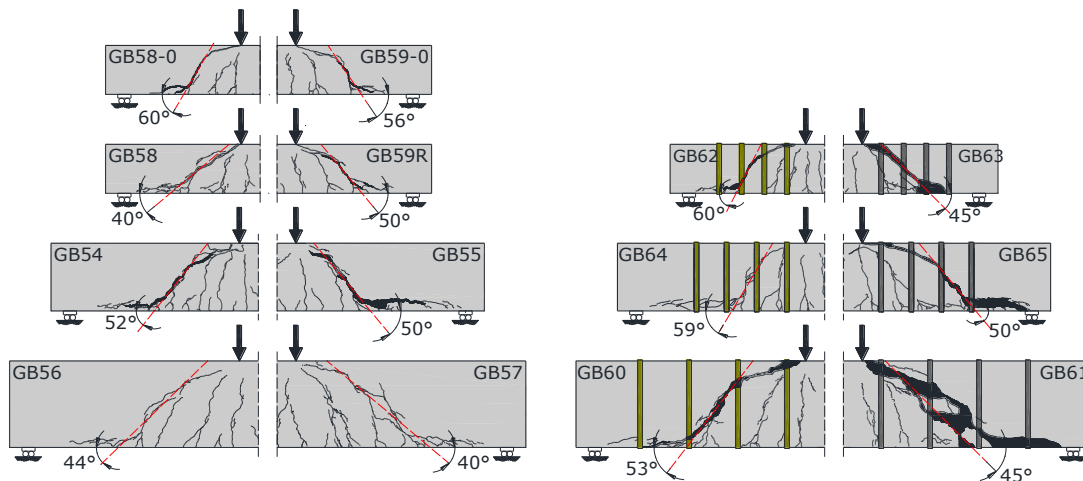
Figure 3-7 Crack patterns for all beams

3.3.3 Strains in Reinforcement

The strain recorded in the main reinforcement under the loading point for the first and second phase of testing is shown in Figure 3-8a and Figure 3-8b, respectively. The maximum allowable strain of 4500 με proposed in Guadagnini et al. (2003) is

indicated in the Figure with dashed lines. All beams with overall depth 360 mm (green curves) and 260 mm (red curves) exceeded this strain, which confirms that this strain limit provides a reasonable margin of safety for beams of this size and smaller. However, strain levels of 4,100 με and 4,500 με were recorded for GB56 and GB57, thus indicating that the strain limit of 4,500 με may not be suitable for larger FRP RC beams without shear reinforcement and, hence, needs to be reassessed.
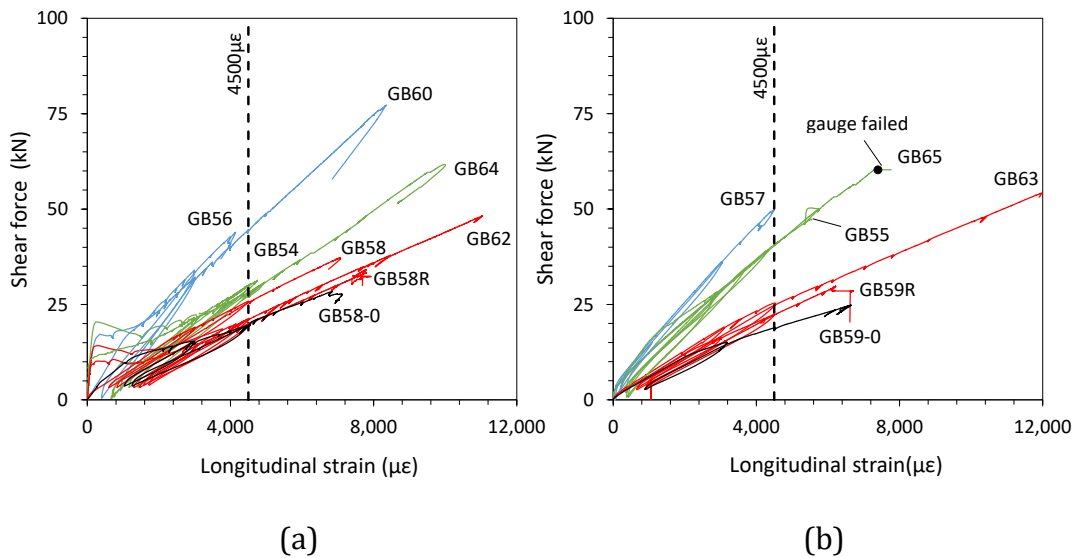
Figure 3-8 Shear load-strain behaviour for all beams: (a) first phase of testing; (b) second phase of testing

Figure 3-9, Figure 3-10 and Figure 3-11 show the strain distributions at different shear load levels (indicated with different markers) for beams GB58, GB54 and GB56. The top graphs plot strain in the longitudinal bars (B, C in Figures 3-9 and 3-10 and D in Figure 3-11) along the beam length, while the bottom ones show the strain profiles over beam depth at various sections. The section 1-1 is the section under the loading point, while sections 3-3 and 4-4 (only in case of 460 mm beams) were the sections across the shear crack. The red dashed lines correspond to strain at failure load estimated using cross-section analysis. The highest strain values were recorded in the lateral BFRP bars near the location of the main shear crack, usually at about mid-height of the beam (bar B in GB58 and GB54 and bar C in GB56). As can be observed, strains measured in different reinforcement layers did not change linearly within the beam height as it is expected from the plane section principle,

both at sections crossing a shear crack (sections 3-3 or 4-4) and at those where maximum bending moment was attained (section 1-1).
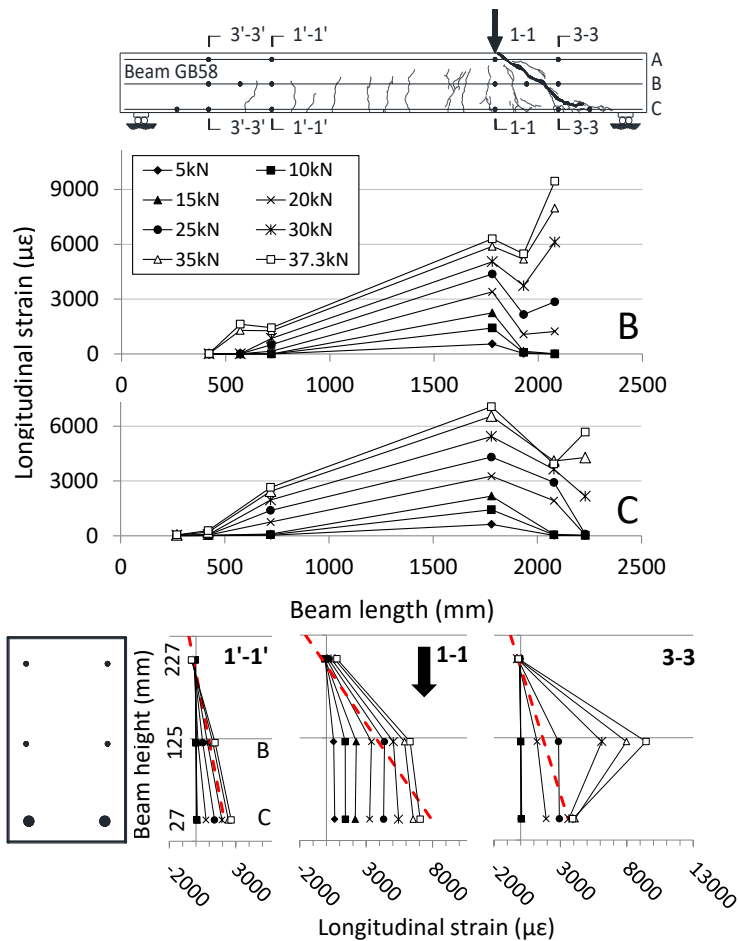
Figure 3-9 Strain distribution in longitudinal reinforcement in beam GB58 (at a given shear load in test shear span)

The strain in the main GFRP reinforcement immediately below the load (section 1-1) was close to that estimated by cross-section analysis (red dashed lines), while strain values in the lateral BFRP bars at mid-height were largely underestimated (see strain profiles in Figure 3-9, Figure 3-10 and Figure 3-11). The high strain values recorded at mid-depth of the tested beams were significantly higher than those predicted by beam theory only within the disturbed regions of the beams, which were subjected to a high interaction of shear and bending.
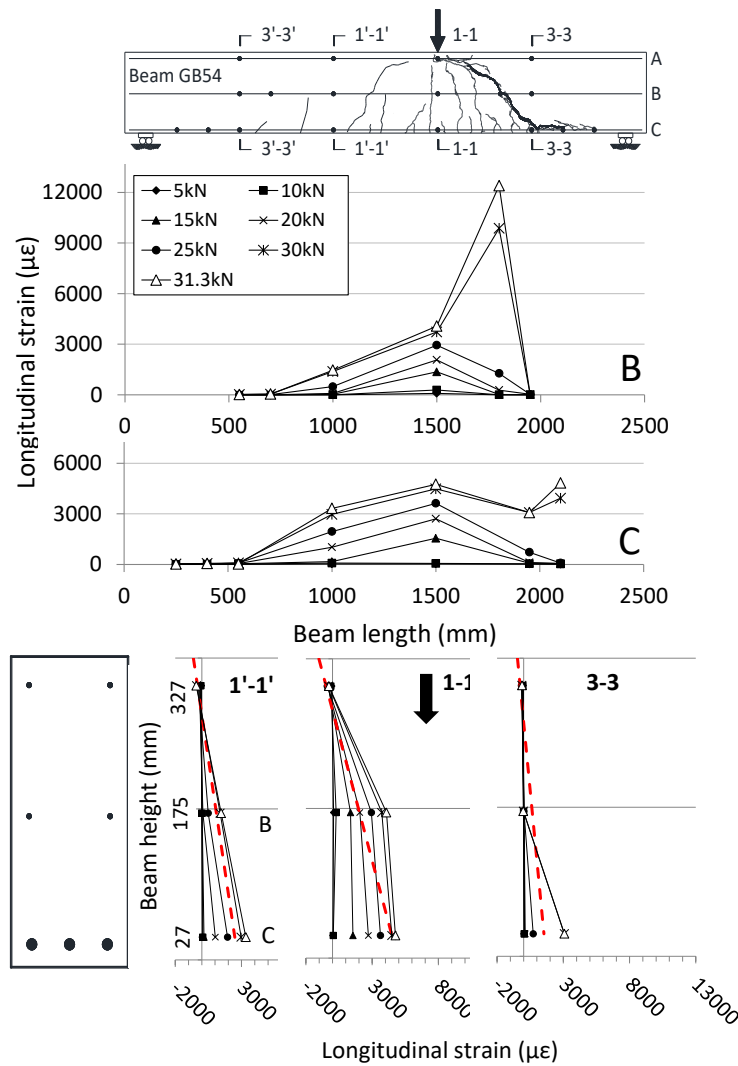
Figure 3-10 Strain distribution in longitudinal reinforcement in beam GB54 (at a given shear load in test shear span)

However, these measurements are local and do not necessarily conflict with the assumption that plane sections can be considered to remain plane in undisturbed regions. Disturbance of plane section strains due to shear cracks is well known and additional deformations due to shear cracks have been documented (e.g. Imjai et al. 2016). The local strain measurements are also affected by the bond between the longitudinal bars used in the test and the surrounding concrete. In contrast, strain profiles of relatively undamaged sections not subjected to large shear deformations (e.g. section 1'-1' in Figures 3-9 and 3-10), were similar to the analytical predictions, showing a linear trend along the beam depth.
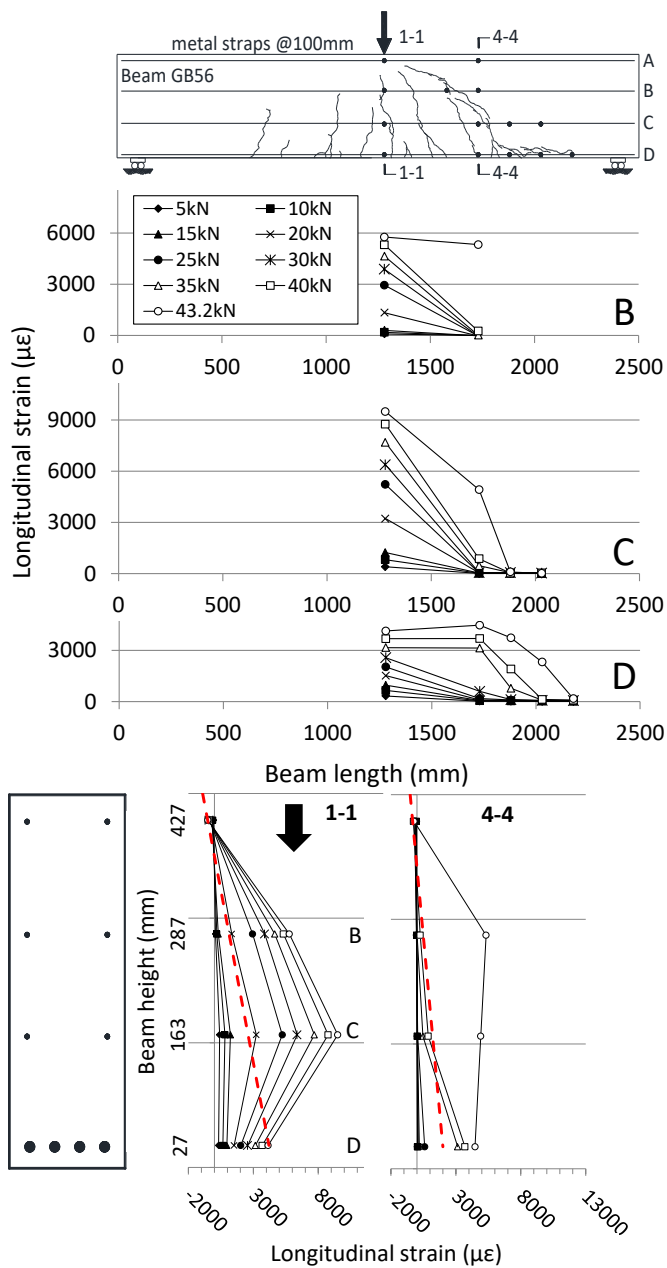
Figure 3-11 Strain distribution in longitudinal reinforcement in beam GB56 (at a given shear load in test shear span)

Figure 3-12 shows the strain distribution of GB62 as representative of the typical behaviour observed for all of the tested beams with external GFRP shear links. The strain distribution is similar to that of its unreinforced counterpart (GB58), albeit higher strains were obtained after shear cracks developed. For shear loads above 30 kN, when the shear crack started to form, GB62 developed slightly higher strain values than GB58 at mid-height of section 1-1 (of about 1,000 µε), while much larger

strains were recorded at ultimate (up to 13,000 με). A similar shift in strain values after shear cracking (about 1,500 με) was observed in GB64 and GB60, thus providing evidence that external shear links effectively controlled the opening of the diagonal cracks and changed the strain distribution along the beam span and across the beam height. In fact, shear links successfully reduced strains in the section across the shear crack. For instance, GB62 recorded no strains at mid-height of the critical section 3-3 up to a load of 35 kN. In contrast, the strain values measured in GB58 at the same load level were above 9,000 με and the beam was approaching failure.
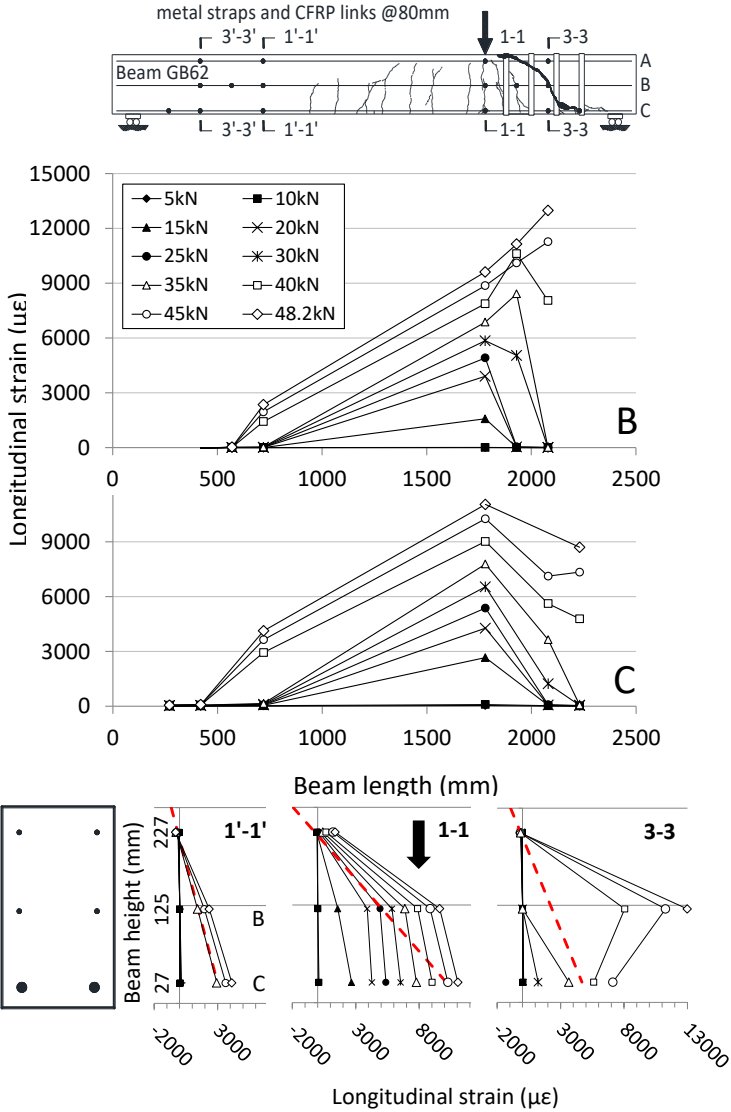
Figure 3-12 Strain distribution in longitudinal reinforcement in beam GB62 (at a given shear load in test shear span)

Figure 3-13 shows the strain distribution in the GFRP links of beam GB60, which is representative of what was experimentally observed in all other specimens. The beam failed by rupture of link 3 in the region where the shear crack was the widest and strain values reached about 16,800 με. The full-field map of vertical strain obtained from DIC (bottom image in Figure 3-13) clearly shows that no significant strains were recorded in the links along the un-cracked areas, thus indicating good bond between the concrete and the FRP links and effective anchorage of the shear reinforcement. This also evidence that strain distribution recorded in the external links may be used to estimate the contribution of the shear reinforcement in similar manner as internally placed stirrups.
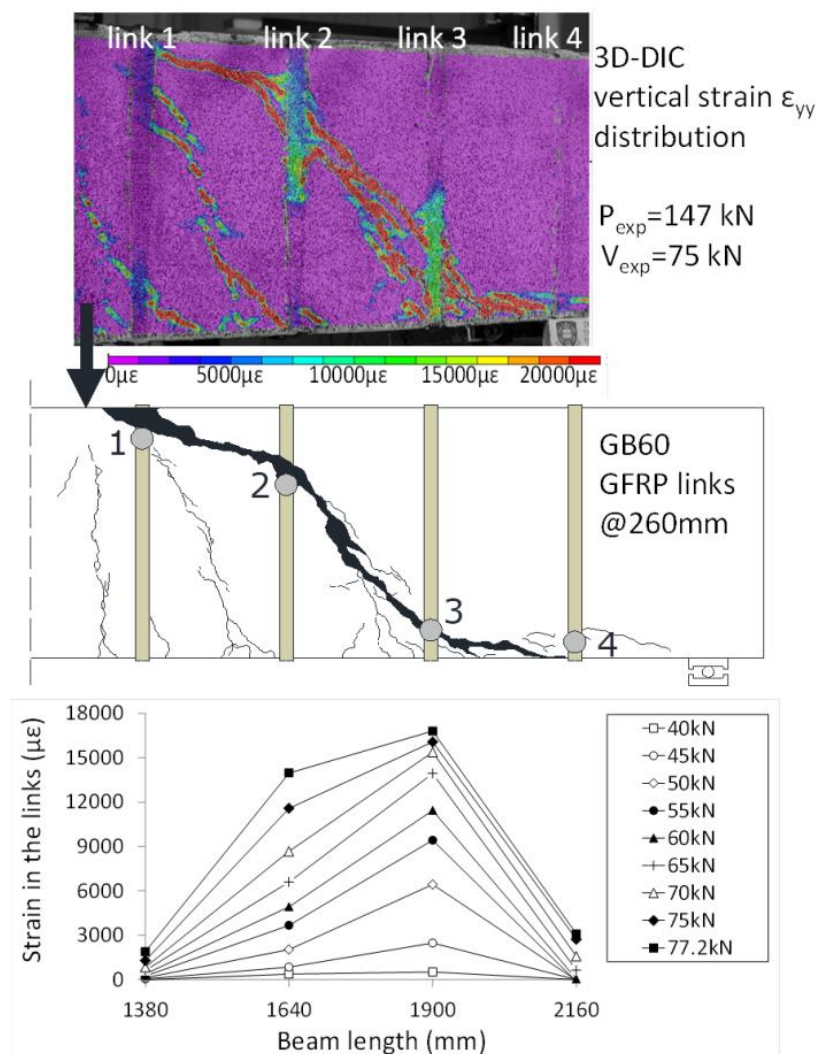
Figure 3-13 Strain distribution along the GFRP shear links of beam GB60 just before failure (applied load Pexp=147 kN)

3.3.4 Effect of Member Depth

Figure 3-14 and Figure 3-15 show the normalized shear strength as a function of beam effective depth. As can be seen, size effect is observed in the beams without external shear links, and a reduction up to 40 % can be observed between minimum and maximum experimental values (Figure 3-14). However, the average reduction in normalized shear strength between 260 mm and 460 mm beams (grey markers) is about 19 %. This seems to be in agreement with results published by Alam and Hussein (2012) who reported a strength decrease of 20 % for similarly reinforced specimens with effective depths ranging from 305 mm to 440 mm.
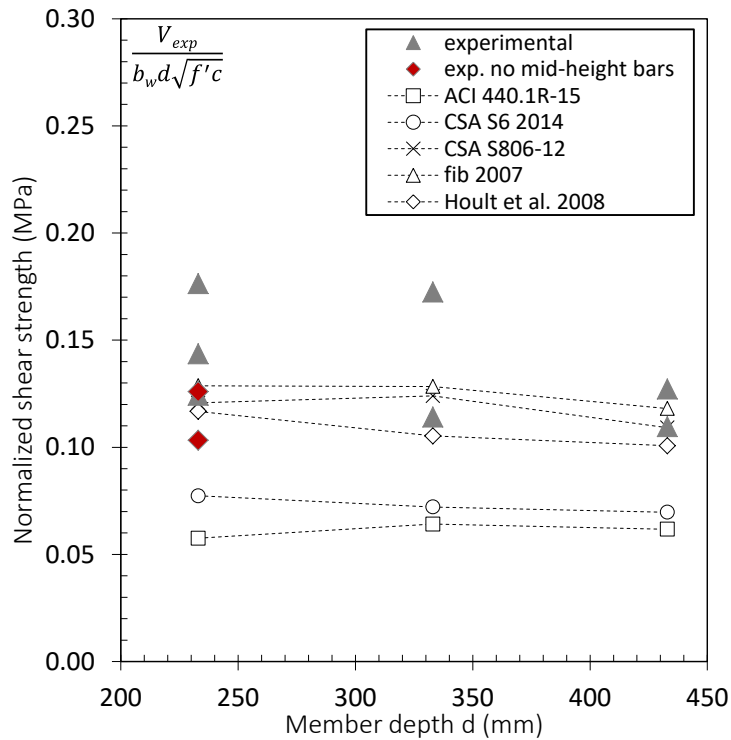
Figure 3-14 Size effect on normalized shear strength of beams without shear reinforcement

The scattered values of shear strength in Figure 3-14 (in particular for the shallowest members) may be mainly attributed to material variability and the geometry of the critical shear crack. It is worth noting that the tests performed on the two beams without mid-height BFRP reinforcement (red markers) showed an average reduction in shear strength of about 10 % and an increase in the angle of the shear crack (see Figure 3-7) with respect to the same beams with mid-height bars. This shows that such bars can help resisting shear; however, not necessarily

eliminating size effect. On the other hand, the presence of shear links mitigates effectively size effect (Figure 3-15) and reduces the variability in the results.
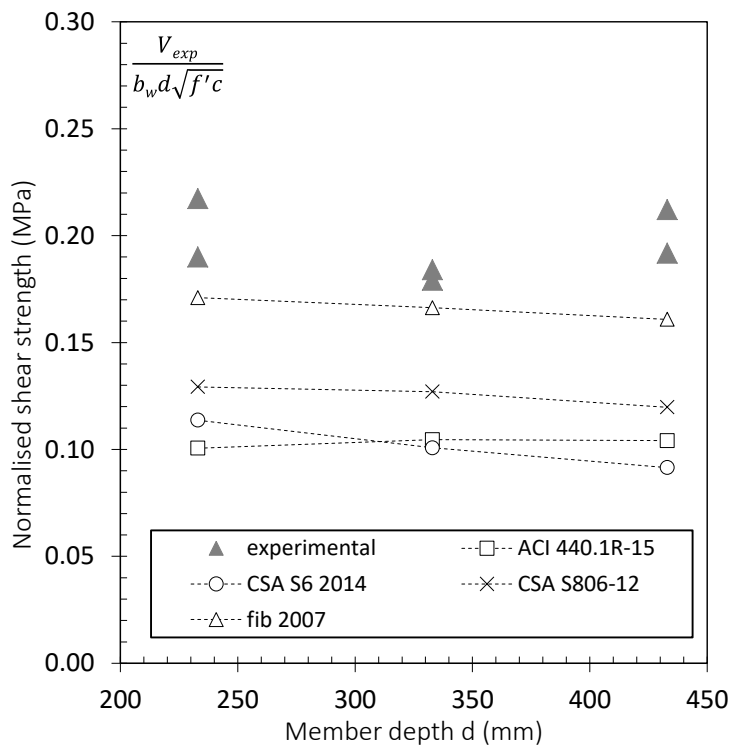
Figure 3-15 Size effect on normalised shear strength of beams with shear reinforcement

Although the beams investigated in this study do not cover large-scale elements, the observed decrease in normalized shear strength is aligned with that observed in studies examining a wider range of beam depths. For instance, Bentz et al. (2010) reported size effect up to 32 % in beams with an average reinforcement ratio of 0.44 % as the effective depth is increased from 188 mm to 860 mm. Matta et al. (2013) observed a strength decrease up to 36 % between beams having effective depths varying from 146 mm to 880 mm and flexural reinforcement ratio of 0.24 %.

3.4   Discussion and Comparison of Results

Existing shear design approaches for FRP RC estimate the total shear capacity of an element by considering the contribution of both concrete (V_c) and shear links (V_f). However, this is true only when shear crack openings (notably larger in FRP RC than in steel RC) are controlled, and all shear resisting mechanisms are effectively

mobilised. This is included implicitly in current guidelines by imposing strain limits on shear reinforcement. However, as discussed in the following, current design guidelines (e.g. ACI Committee 440 2015, CSA S6 2014, CSA S806 2012, *fib* bulletin 40 2007) recommend different limiting strain values and adopt different models to estimate the contribution of concrete (V_c).

In ACI, the total shear contribution is given by the sum of the following equations:

$$V_c = \frac{2}{5}\sqrt{f'_c}\,b_w d k \tag{3-1}$$

$$V_f = \frac{A_{fv} f_{fv} d}{s}; \qquad f_{fv} = 0.004 E_f \leq f_{fb} \tag{3-2}$$

In this approach, the allowable stress in the shear reinforcement is the minimum between the stress corresponding to a strain level of 0.4 % and the maximum stress level that can be developed at the bent portion of the link (f_{fb}). In addition, the inclination of the concrete strut is assumed to be 45 degrees and no provision for size effect is included.

The CSA design equation recognizes size effect only in concrete members without transverse reinforcement having effective depth greater than 300 mm (k_s). In addition, the code equations account for the flexure-shear interaction (k_m) and limit the maximum strain in the shear links to 0.5 %. The angle of the concrete strut is calculated using Eq. 3-5. The contribution of both concrete and shear reinforcement is calculated as a sum of the following:

$$V_c = 0.05 \lambda \phi_c k_m k_r k_s f'^{1/3}_c b_w d_v \tag{3-3}$$

$$V_f = \frac{0.4 \phi_F A_{fv} f_{fu} d_v}{s} \cot \theta \tag{3-4}$$

where the inclination of the concrete strut θ is calculated as following:

$$30° \leq \theta = 30 + 7000\varepsilon_x \leq 60° \tag{3-5}$$

The Canadian Highway Bridge Design Code (CHBDC) CSA S6 2014 recommends calculating the total shear resistance of FRP RC beams reinforced with external fully wrapped links as a sum of the following:

$$V_c = \beta \phi_C \sqrt{f'_c}\, b d_v \tag{3-6}$$

$$V_f = \frac{\phi_{FRP} E_{FRP} 0.004 A_{FRP} d_{FRP} \cot \theta}{s_{FRP}} \tag{3-7}$$

This model relies on the modified compression field theory (MCFT) and it is based on a variable angle truss model and a variable concrete contribution. The parameter β models the ability of concrete to transmit tensile stresses, and for FRP reinforced concrete sections should be computed using the general method (Eq. 3-8).

$$\beta = \left(\frac{0.4}{1+1500\varepsilon_x}\right)\left(\frac{1300}{1000+s_{ze}}\right) \tag{3-8}$$

The longitudinal strain at mid-depth, ε_x, for the specimens presented in this study was calculated as follows:

$$\varepsilon_x = \frac{\dfrac{M_a}{d_v}+V_a}{2(A_{fl}E_{fl})} \leq 3,000\mu\varepsilon \tag{3-9}$$

where M_a and V_a correspond to the applied moment and the shear force at failure at a distance d_v from the loading. The contribution of shear links is calculated assuming that FRP shear links are fully anchored in the compression zone and maximum strain in the links is limited to 0.4 %. The inclination of the shear crack was calculated as follows:

$$\theta = (29+7000\varepsilon_x)(0.88+s_{ze}/2500) \tag{3-10}$$

The accuracy of Eq. 3-6 can be further improved using a refined "second order" MCFT algorithm (Hoult et al. 2008)(Eq. 3-11), which was derived to account for the larger strains typically attained in FRP RC beams at ultimate.

$$V_c = \left(\frac{0.3}{0.5+(1000\varepsilon_x+0.15)^{0.7}}\right)\left(\frac{1300}{1000+s_{ze}}\right)\sqrt{f'_c}bd_v \tag{3-11}$$

The theoretical shear resistance of the tested beams is also calculated using the "Sheffield Approach" (Guadagnini et al. 2003) as included in *fib* bulletin 40 (*fib* 2007), and accounting for the different stiffness of the FRP tensile reinforcement through the modular ratio E_f/E_s. A ratio of 1.8 is also introduced to account for the higher strain that can be developed in the FRP longitudinal reinforcement upon shear failure (4,500 µε) when compared to the level of strain that can be mobilized at yielding in the more conventional steel reinforcement (about 2,500 µε).

66

The same strain limit of 4,500 με (0.45%) was also adopted to calculate the contribution of the links and a fixed crack inclination of 45° was assumed (Eq. 3-13). The design equations are shown below:

$$V_c = \left[\frac{0.18}{\gamma_c} \cdot \left(1 + \sqrt{\frac{200}{d}}\right) \cdot (100 \frac{A_{fl}}{b_w d} \cdot \frac{E_{fl}}{E_s} \cdot 1.8 \cdot f_{ck})^{\frac{1}{3}} \right] b_w d \qquad (3\text{-}12)$$

$$V_f = \frac{A_{fv}}{s} 0.0045 E_{fv} z \qquad (3\text{-}13)$$

The theoretical predictions for all tested beams are shown in Table 3-5. For the sake of comparison, all safety and material factors were omitted in the calculations. As can be seen, the models examined significantly underestimate the shear capacity of the tested elements. The ACI equation yields the most conservative predictions with an average experimental-to-theoretical shear capacity ratio for beams without reinforcement above 2.0, while the best correlation was obtained when *fib* 2007 and CSA 2012 model was used.

Table 3-5 Comparison of the experimental and theoretical shear capacity

Beam	ACI 440.1R-15		*fib* 2007		CSA S 806-12		CSA S6 2014		Hoult et al. 2008
	V_c	V_f	V_c	V_f	V_c	V_f	V_c	V_f	V_c
	kN		kN		kN		kN		kN
GB580	13.1	-	29.3	-	27.5	-	15.9	-	23.9
GB590	13.7		30.8	-	28.9	-	17.1	-	26.7
GB58	12.7	-	28.1	-	26.3	-	16.4	-	24.7
GB58R	13.6	-	30.5	-	28.6	-	18.5	-	28.0
GB59R	13.7	-	30.8	-	28.9	-	18.8	-	28.4
GB62	14.0	10.9	31.7	11.0	29.7	2.8	19.6	8.8	26.9
GB63	13.9	11.8	31.3	11.9	27.1	3.1	19.3	9.5	26.5
GB54	17.6	-	35.2	-	34.0	-	21.6	-	30.7
GB55	17.6	-	35.2	-	34.0	-	18.0	-	27.1
GB64	19.9	15.3	41.0	15.5	39.4	4.0	22.5	11.6	34.0
GB65	19.9	16.9	41.0	17.1	37.6	4.4	22.5	12.7	34.0
GB56	24.6	-	47.2	-	43.6	-	29.4	-	41.7
GB57	24.4	-	46.6	-	43.1	-	26.0	-	38.2
GB60	24.7	17.5	47.3	17.8	42.3	4.6	24.6	12.4	37.2
GB61	24.7	16.9	47.3	17.1	40.5	4.4	24.6	11.9	37.2

Table 3 - 1: Comparison of the experimental and theoretical shear capacity
continued.

Beam	ACI 440.1R-15		*fib* 2007		CSA S 806-12		CSA S6 2014		Hoult et al. 2008
	$V_{exp}/$ V_c	$V_{exp}/$ V_c+V_f	$V_{exp}/$ V_c	$V_{exp}/$ V_c+V_f	$V_{exp}/$ V_c	$V_{exp}/$ V_c+V_f	$V_{exp}/$ V_c	$V_{exp}/$ V_c+V_f	$V_{exp}/$ V_c
GB580	2.16	-	0.97	-	1.03	-	1.79	-	1.19
GB590	1.83	-	0.81	-	0.87	-	1.47	-	0.94
GB58	2.94	-	1.33	-	1.42	-	2.28	-	1.51
GB58R	2.53	-	1.13	-	1.20	-	1.86	-	1.23
GB59R	2.21	-	0.98	-	1.05	-	1.61	-	1.06
GB62	-	1.93	-	1.13	-	1.48	-	1.70	-
GB63	-	2.11	-	1.25	-	1.79	-	1.88	-
GB54	1.78	-	0.89	-	0.92	-	1.45	-	1.02
GB55	2.69	-	1.34	-	1.39	-	2.63	-	1.74
GB64	-	1.75	-	1.09	-	1.42	-	1.81	-
GB65	-	1.72	-	1.09	-	1.51	-	1.80	-
GB56	1.78	-	0.93	-	1.01	-	1.50	-	1.05
GB57	2.05	-	1.07	-	1.16	-	1.92	-	1.31
GB60	-	1.83	-	1.19	-	1.65	-	2.08	-
GB61	-	2.06	-	1.33	-	1.90	-	2.33	-
Average	**2.22**	**1.90**	**1.05**	**1.18**	**1.12**	**1.63**	**1.83**	**1.93**	**1.21**
St Dev	**0.40**	**0.15**	**0.18**	**0.09**	**0.18**	**0.17**	**0.38**	**0.21**	**0.24**
COV	**0.18**	**0.08**	**0.17**	**0.07**	**0.16**	**0.11**	**0.21**	**0.11**	**0.20**

The mean value of V_{exp}/V_{calc} obtained using the CHBDC method was equal to 1.83 for the beams without shear links, which is in agreement with the findings of other researchers (El-Sayed and Benmokrane 2008; Mahmoud and El-Salakawy 2015). The implementation of Hoult et al. (2008) model yielded a better estimate of the shear capacity of beams without shear links with an average V_{exp}/V_{calc} ratio of 1.21.

The normalized shear strength predicted by ACI for the beams without shear reinforcement (square markers in Figure 3-14) is almost constant as no size effect parameter is included in the original formulation, and the only deviations are caused by the slightly different reinforcement ratios.

Although size effect is accounted for in the CHBDC equation (Eq. 3-8), the observed values of normalized shear strength are similar to those derived using the ACI

equation. The conservative predictions can be mainly attributed to the fact that the higher values of strain calculated in the FRP flexural reinforcement result in low values of β. The model proposed by Hoult et al. (2008) attempts to address this issue and yields less conservative results (diamond markers in Figure 3-14).

The use of CSA and *fib* (cross and triangular markers, respectively, in Figure 3-14) yielded similar predictions for the beams without shear reinforcement and produced estimates close to the average of the experimental values. However, both are still conservative in their predictions of the beams with shear reinforcement, with the *fib* producing the best results (Figure 3-15). The high degree of safety can be partly attributed to the conservative values adopted as limiting strain for shear reinforcement as well as conservative assumptions for calculating V_f using CSA 2012.

The experimental strain values recorded at failure in the links ranged from about 9,000 με to 16,800 με for GFRP links and from about 6,800 με to 13,500 με for CFRP links (see Table 3-4), and are much higher than the limitations specified in current design recommendations (ranging from 4,000 με to 5,000 με). This provides further evidence that the contribution of shear links to overall shear resistance can be substantially underestimated by the current FRP design codes. It should be noted that the local strain measured on the externally bonded links adopted in this research programme is expected to be lower than the maximum strain that would be developed in internal links (due to local debonding) and, hence, can still be used to inform the selection of design limiting values. When considering the adoption of less conservative limiting values, however, it should be kept in mind that high strain values in FRP links result in larger crack widths and degradation of the shear resisting mechanisms, thus leading to an overall reduction in shear capacity.

The relative shear strength of shear-reinforced beams did not change when increasing beam depth (though it shows variability). This may be attributed to the ability of the shear links to effectively control cracking and maintain an adequate level of shear transfer across the cracks. For instance, at an applied shear force of approximately 30 kN, a maximum crack width of 1.8 mm was observed in the shear span of GB58, whilst the maximum crack width for GB62 and GB63 at the same load

level was only 0.3 mm and 0.2 mm, respectively. In beams with larger depth, the difference in shear crack width at comparable levels of applied shear force between beams without and with shear reinforcement was less pronounced, e.g. 0.6 mm for GB56 and 0.4 mm for GB60. This suggests that the relative contribution of concrete and shear reinforcement to the overall shear capacity is also a function of beam depth.

3.5   Conclusions

Fifteen shear tests were performed on FRP RC beams with and without shear reinforcement to investigate their shear behaviour with a specific focus on the effect of beam depth. The experimentally determined distribution of both horizontal and vertical strain within the shear span of the tested beams was presented and discussed. The results were compared with the predictions obtained from current design equations to verify their accuracy in terms of overall capacity and contributions of different resisting mechanisms. From the discussion and results presented in this study, the following conclusions can be drawn:

- All tested beams failed in diagonal tension. The depth at which flexural cracks transition to diagonal shear cracks is a function of the overall depth of the beams. In particular, the taller the beam, the lower the depth of initiation of the diagonal crack. As already observed in steel RC beams, crack spacing was confirmed to be a function of beam size, with larger spacing being developed in deeper specimens.
- The maximum strain in the FRP reinforcement (both flexural and shear) generally exceeded allowable design limits. A decrease in the maximum strain developed in the flexural reinforcement was observed with increasing member depth. The maximum values measured in the flexural reinforcement ranged from 4,100 με to 7,900 με in beams without shear links and from 8,300 με to 12,000 με in beams with shear links. The maximum strain in the shear reinforcement ranged from 9,000 με to 16,800 με for GFRP links and from 6,800 με to 13,500 με for CFRP links.

- Although the same *a/d* ratio was maintained for the test shear-span of all specimens, the relative stiffness of the shear spans appears to affect overall performance and relative shear strength. Such behaviour has not been reported in previous literature and could be a result of material's natural variability but requires further investigation.

- Current FRP design equations do not predict the shear strength of FRP RC beams of different sizes with a uniform margin of safety.

- The results confirm that shear strength of FRP members without shear links is somehow affected by their size. The CSA (2012) and *fib* (2007) models account for this sufficiently, while ACI and CHBDC (CSA 2014) predictions are overly conservative. The model proposed by Hoult et al. (2008) yields a better estimate of V_c than the equation originally implemented in CHBDC. No significant size effect is found in beams with shear reinforcement, which appears to control crack width sufficiently, even at larger strains than allowed by current design models. Overall, the model included in *fib* 2007 predicts reasonably well the performance of shear-reinforced beams, even though the relative contribution of individual shear resisting mechanisms needs to be re-examined.

Based on the experimental results and the discussion presented above, a decomposition of the shear resisting components is performed in Chapter 4 to assess the individual contributions of concrete and FRP shear links to the overall shear resistance.

3.6   References

- AASHTO. (2007). *LRFD Bridge design specifications*, 4th Ed., Washington, DC.

- ACI (American Concrete Institute). (2015). "Guide for the design and construction of structural concrete reinforced with FRP bars." ACI 440.1R-15, Farmington Hills, MI.

- Alam, M. S., and Hussein, A. (2012). "Size effect on shear strength of FRP reinforced concrete beams without stirrups." *J. Compos. Constr.*, 10.1061/(ASCE)CC.1943-5614.0000346, 507-516.

- Alsayed, S. H., Al-Salloum, Y. A., and Almusallam, T. H. (2000). "Performance of glass fiber reinforced plastic bars as a reinforcing material for concrete structures." *Compos. Part B.*, 31(6), 555-567.

- Angelakos, D., Bentz, E. C., and Collins, M. P. (2001). "Effect of concrete strength and minimum stirrups on shear strength of large members." *J. Struct. Eng.*, 98(3), 290–300.

- Ashour, A. F., and Kara, I. F. (2014). "Size effect on shear strength of FRP reinforced concrete beams." *Compos. Part B.,* 60, 612-620.

- Bazant, Z. P. (1984). "Size effect in blunt fracture: concrete, rock, metal." *J. Eng. Mech.,* 110(4), 518-535.

- Bazant, Z. P., and Kazemi, M. T. (1991). "Size effect on diagonal shear failure of beams without stirrups." *ACI Struct. J.*, 88(3), 268-276.

- Bazant, Z. P., and Kim, J. K. (1984). "Size effect in shear failure of longitudinally reinforced beams." *ACI Journal,* 8, 456-468.

- Benmokrane, B., Chaallal, O., and Masmoudi, R. (1995). "Glass fibre reinforced plastic (GFRP) rebars for concrete structures." *Constr Build. Mater.,* 9(6), 353-364.

- Bentz, E. C. (2005). "Empirical modeling of reinforced concrete shear strength size effect for members without stirrups." *ACI Struct. J.*, 102(2), 232.

- Bentz, E. C., Massam, L., and Collins, M. P. (2010). "Shear strength of large concrete members with FRP reinforcement." *J. Compos. Constr.*, 10.1061/(ASCE)CC.1943-5614.0000108, 637-646.

- BISE (British Institution of Structural Engineers). (1999) "Interim guidance on the design of reinforced concrete structures using fiber composite reinforcement". IStructE, SETO Ltd., London, UK.

- Burgoyne, C. J., and Scantlebury, R. (2006). "Why did Palau Bridge collapse?" *The Structural Engineer*, 84. pp. 30-37. ISSN 0039-2553

- Collins, M. P., and Kuchma, D. (1999). "How safe are our large, lightly reinforced concrete beams, slabs, and footings? " *ACI Struct. J.*, 96(4), 482-490.

- Collins, M. P., D. Mitchell, and E. C. Bentz. (2008). "Shear design of concrete structures." *The Structural Engineer.,* 86.10, 32-39.

- Collins, M. P., Mitchell, D., Adebar, P., and Vecchio, F. J. (1996). "A general shear design method." *ACI Struct. J.*, 93(1), 36-45.

- Comité Européen de Normalisation (CEN). (2004). "Eurocode 2: Design of Concrete Structures: Part 1-1: General Rules and Rules for Buildings" EN 1992-1-1, Brussels, Belgium.

- CSA (Canadian Standards Association). (2012). "Design and construction of building structures with fibre-reinforced polymers." S806-12, Mississauga, ON, Canada.

- CSA (Canadian Standards Association). (2014). "Canadian Highway Bridge Design Code." CSA S6-14, Mississauga, ON, Canada.

- El-Sayed, A. K., and Benmokrane, B. (2008) "Evaluation of the new Canadian highway bridge design code shear provisions for concrete beams with fiber-reinforced polymer reinforcement." *Can. J. Civ. Eng.* 35, 6, 609-623.

- El-Sayed, A. K., El-Salakawy, E. F., and Benmokrane, B. (2006). "Shear strength of FRP-reinforced concrete beams without transverse reinforcement." *ACI Struct. J.*, 103(2), 235.

- *fib* (Fédération internationale du béton). (2007). "FRP reinforcement in RC structures, technical". *fib* bulletin 40, Technical report. Lausanne, Switzerland.

- *fib* (Fédération internationale du béton). (2013). "Model Code for Concrete Structures 2010". Ernest&Sohn, ed., Weinheim.

- Frosch R. J. (2000). Behavior of large-scale reinforced concrete beams with minimum shear reinforcement *ACI Struct. J.*, 97(6), 814-820.

- Guadagnini, M., Pilakoutas, K., and Waldron, P. (2003). "Shear performance of FRP reinforced concrete beams." *J. Reinf. Plast. Compos.,* 22(15), 1389-1407.

- Guadagnini, M., Pilakoutas, K., and Waldron, P. (2006). "Shear resistance of FRP RC beams: Experimental study." *J. Compos. Constr.*, 10.1061/(ASCE)1090-0268(2006)10:6(464), 464-473.

- Hassan, T. K., Seliem, H. M., Dwairi, H., Rizkalla, S. H., and Zia, P. (2008). "Shear behavior of large concrete beams reinforced with high-strength steel." *ACI Struct. J.*, 105(2), 173.

- Helal, Y., Garcia, R., Pilakoutas, K., Guadagnini, M., and Hajirasouliha, I. (2016). "Strengthening of short splices in RC beams using Post-Tensioned Metal Straps." *Mater. Struct.,* 49(1-2), 133-147.

- Hoult, N. A., Sherwood, E. G., Bentz, E. C., and Collins, M. P. (2008). "Does the use of FRP reinforcement change the one-way shear behavior of reinforced concrete slabs?" *J. Compos. Constr.*, 10.1061/(ASCE)1090-0268(2008)12:2(125), 125-133.

- Imjai, T., Guadagnini, M., Garcia R. and Pilakoutas, K. (2016) "A practical method for determining shear crack induced deformation in FRP RC beams." *Eng. Struct.* 126, 353-364.

- ISIS Canada. (2007). "Reinforcing concrete structures with fiber reinforced polymers." ISIS-M03-07, Canadian Network of Centers of Excellence on Intelligent Sensing for Innovative Structures, Univ. of Winnipeg, Winnipeg, Canada.

- Joint ACI-ASCE Committee 445, "Recent Approaches to Shear Design of Structural Concrete." *J. Struct. Eng.-ASCE*, V. 124, No. 12, Dec. 1998, 1375-1417.

- JSCE (Japan Society of Civil Engineers). (1997). "Recommendation for design and construction of concrete structures using continuous fiber reinforcing materials." *Concrete Engineering Series 23*, A. Machida, ed., Tokyo, Japan.

- Kani, G. (1967). "How safe are our large reinforced concrete beams? " *In Journal Proceedings.,* 64, 3, 128-141).

- Lubell, A., Sherwood, T., Bentz, E., and Collins, M. (2004). "Safe shear design of large wide beams." *Concrete International.*, 26(1), 66-78.

- Mahmoud, K., and El-Salakawy, E. (2015) "Shear strength of glass fiber reinforced polymer–reinforced concrete continuous beams without transverse reinforcement." *Can. J. Civ. Eng.* 42, 12, 1073-1082.

- Mahmoud, K., and El-Salakawy, E. (2016). "Size Effect on Shear Strength of Glass Fiber-Reinforced Polymer-Reinforced Concrete Continuous Beams." *ACI Struct. J.*, 113(1), 125.

- Matta, F., El-Sayed, A. K., Nanni, A., and Benmokrane, B. (2013). "Size effect on concrete shear strength in beams reinforced with fiber-reinforced polymer bars." *ACI Struct. J.*, 110(4), 617.

- Matta, F., Nanni, A., Galati, N., and Mosele, F. (2007). "Size effect on shear strength of concrete beams reinforced with FRP bars." *Proc., 6th International Conf. on Fracture Mech. of Concr. and Concr. Struct. (FraMCoS-6).,* Balkema/Taylor & Francis, ed., Vol. 2, pp. 17-22.

- Massam, L., "The Behaviour of GFRP Reinforced Concrete Beams in Shear." MSc thesis, University of Toronto, Toronto, ON, Canada, 2001, 304 pp.

- Nanni, A. (1993). "Flexural behavior and design of RC members using FRP reinforcement." *J. Struct. Eng.,* 119(11), 3344-3359.

- National Research Council. (2006). "Guide for the design and construction of concrete structures reinforced with fiber-reinforced polymer bars." CNR-DT 203, Rome, Italy.

- Pilakoutas, K., Neocleous, K., and Guadagnini, M. (2002). "Design philosophy issues of fiber reinfored polymer reinforced concrete structures." *J. Compos. Constr.*, 10.1061/(ASCE)1090-0268(2002)6:3(154), 154-161.

- Razaqpur, A. G., Isgor, B. O., Greenaway, S., and Selley, A. (2004). "Concrete contribution to the shear resistance of fiber reinforced polymer reinforced concrete members." *J. Compos. Constr.*, 10.1061/(ASCE)1090-0268(2004)8:5(452), 452-460.

- Razaqpur, A. G., and Isgor, O. B. (2006). "Proposed shear deign method for FRP-reinforced concrete members without stirrups." *ACI Struct. J.*, 103(1), 93–102.

- Razaqpur, A. G., Shedid, M., and Isgor, B. (2010). "Shear strength of fiber-reinforced polymer reinforced concrete beams subject to unsymmetric loading." *J. Compos. Constr.*, 10.1061/(ASCE)CC.1943-5614.0000184, 500-512.

- Reineck, K.-H. (1991). "Ultimate shear force of structural concrete members without transverse reinforcement derived from a mechanical model." *ACI Struct. J.* 88, (5), 592-602.

- Serbescu, A., Guadagnini, M., and Pilakoutas, K. (2014). "Mechanical characterization of basalt FRP rebars and long-term strength predictive model." *J. Compos. Constr.*, 10.1061/(ASCE)CC.1943-5614.0000497, 04014037.

- Shioya, T., Iguro, M., Nojiri, Y., Akiyama, H., and Okada, T. (1990). "Shear strength of large reinforced concrete beams." *Special Publication*, 118, 259-280.

- Tureyen, A. K., and Frosch, R. J. (2002). "Shear tests of FRP-reinforced concrete beams without stirrups."*Struct. J.*, 99(4), 427-434.

- Walraven, J., and Lehwalter, N. (1994). "Size effect in short beams loaded in shear." *ACI Struct. J.*, 91(5), 585–593.

- Yost, J. R., Gross, S. P., and Dinehart, D. W. (2001). "Shear strength of normal strength concrete beams reinforced with deformed GFRP bars." *J. Compos. Constr.*, 5(4), 268-275.
- Yu, L., Che, Y., and Song, Y. (2013). "Shear Behavior of Large Reinforced Concrete Beams without Web Reinforcement." *Adv Struct Eng.*, 16(4), 653-665.
- Zoghi, M. (2013). The international handbook of FRP composites in civil engineering, CRC Press, Boca Raton, Florida.

Chapter 4

Shear Resisting Mechanisms in FRP RC Beams

Abstract*: Current approaches treat the shear design of fibre-reinforced-polymer (FRP) reinforced concrete beams in a similar manner as that of steel reinforced concrete beams. However, the different mechanical characteristics and lack of plasticity of FRPs may lead to different relative contributions of concrete and shear reinforcement, especially since larger strains are expected to develop in FRP reinforcement than in conventional steel reinforcement. This paper presents pioneering experimental evidence on the development of shear resisting components in FRP reinforced concrete beams with different overall depths, utilizing detailed strain measurements obtained from digital image correlation and strain gauges. It was found that the contribution of concrete decreases gradually after diagonal cracking with increasing strain and crack width. A comprehensive analysis of key design oriented shear models for FRP reinforced concrete is also presented and the results indicate that the adoption of a variable angle truss model, though possible, would require an appropriate reduction in the contribution of concrete.*

This chapter consists of a "stand alone" journal paper and includes a relevant bibliography at the end of the chapter. Additional information and further test results are presented in Appendix C, E.

4.1   Introduction

Shear transfer in steel reinforced concrete (RC) has been extensively examined and numerous explanatory theories exist (Mitchell and Collins 1974; Vechhio and Collins 1986; Nielsen 1984; Kotsovos 1988; Reineck 1991). Although the overall understanding of shear behaviour of RC has been significantly improved, the precise estimate of total shear resistance is still difficult as it depends on many parameters including the development and geometry of shear cracks.

Current shear design approaches rely on the basic assumption that overall shear resistance of RC beams is determined by the contribution provided by shear reinforcement (V_s) and the contribution of concrete (V_c). V_s depends on the number of stirrups bridging shear cracks and can be estimated using the well-established truss analogy (Morsh 1909). V_c is a function of concrete tensile strength and consists of several internal shear transfer mechanisms including shear resistance offered by non-cracked concrete in the compression zone, aggregate interlock across shear cracks and dowel action of the flexural reinforcement. In addition, experimental studies (Kani 1967; Shoya et al. 1990; Bazant and Kazemi 1991) have shown that larger beam elements without shear reinforcement and with similar geometry show a decrease in shear strength (size effect), caused by the reduction of internal shear transfer mechanisms due to aggregate interlock (ACI-ASCE 1998).

Various studies (Duranovic et al. 1997; Yost et al. 2006; Guadagnini et al. 2006; El-Sayed et al. 2006; Hoult et al. 2008) showed that the same shear resisting mechanisms can be assumed for beams with fibre-reinforced-polymer (FRP) reinforcement, as long as the lower stiffness of the FRP bars is accounted for. However, these resisting mechanisms degrade at higher rates than in steel RC. This is because, at similar loading conditions, FRP reinforced beams develop larger and deeper cracks (Mikani et al. 1989; Tureyen and Frosh 2002) than in equivalent steel reinforced beams, and hence, it is expected that less shear can be transferred by aggregate interlock than in steel RC beams (*fib* 2007). In addition, in FRP RC beams the neutral axis decreases faster, reducing the amount of concrete resisting shear in

compression and dowel action is much lower than that in steel RC and has a negligible contribution to the overall shear resistance (Razaqpur et al. 2004).

Although the better understanding of shear developed over the years allowed codes of practice to utilise more advanced design models for steel RC, such as allowing the use of a variable compressive strut angle e.g. (CEN 2004; *fib* 2010; CSA 2012; CSA 2014), only the Canadian Standard Association (CSA) decided to extend their shear models to FRP RC members. The remaining codes and design guidelines e.g. (ACI 2015; fib 2007; ISIS 2007; BISE 1999; JSCE 1997; CNR 2006) still follow the V_c+V_s approach to determine the total shear resistance and adopt the fixed compressive strut angle approach ($\theta = 45°$), and impose different strain limits on the FRP shear stirrups/links.

According to Eurocode 2, the steel RC beams with shear reinforcement can be designed using the modified truss model, which does not include the contribution of concrete. Some researches already reported that this may lead to excessively conservative predictions for low shear reinforcement ratios and to unsafe predictions for high reinforcement ratios (Caldera and Mari 2007). FRP RC beams currently are designed using the assumption that, when shear reinforcement is provided, the concrete contribution remains constant (even after shear cracking) and is not affected by crack width or longitudinal strain. This approach, well-established for steel RC, relies on the plastic theory and the assumption that redistribution of stresses can occur following yielding of the steel shear reinforcement. However, it can be argued that this concept is not valid for FRP RC members as no yielding occurs in the FRP reinforcement (Stratford and Burgoyne 2003). Research evidence (Nagasaka et al. 1993; Tomlison and Fam 2014; Issa et al. 2015) shows that current FRP shear provisions can be used to estimate the capacity of the FRP RC beams with some degree of conservatism, however, no comprehensive discussion exists on the relative contributions of V_c and V_s as well as on the choice of θ for FRP RC beams.

Experimental assessment of the contribution of shear reinforcement requires the accurate monitoring of the strain in the reinforcements near the main shear crack. However, the failure path of the shear cracks is not known a priori as it is affected

by material natural variability and develops along the weakest path. Digital Image Correlation (DIC, Sutton et al. 2009), an optical measuring technique offering distributed measuring capabilities, can be employed to enhance our understanding of the surface strain field beyond the conventionally used localised strain measurements on re-bars (Sabau et al. 2018).

This paper aims to investigate, for the first time, the contributions of concrete (V_c) and FRP shear links (V_f) to the overall shear resistance of FRP RC beams varying in depth, based on detailed DIC and strain gauge measurements. The results are used to evaluate the performance of current shear design models accounting for FRP reinforcement (ACI 440.1R-15, fib bulletin 40 and CSA S806-12). The outcomes of this work will provide a better understanding of the relative shear contributions of V_c and V_f and are expected to assist in future improvements of FRP design guidelines.

4.2 Testing programme

The experimental tests described herein are part of a larger programme that aims to investigate the shear behaviour of FRP RC beams with overall depth varying from 260 to 460 mm (Cholostiakow et al. 2018). The results of the tests carried out on three of these beams are further discussed and analysed in depth to assess the relative contribution of FRP shear reinforcement on overall shear capacity (full details for all beams are shown in Figure 4-1 and Table 4-1). Fully wrapped external FRP shear links were used as shear reinforcement so as to allow the better monitoring of strains through Digital Image Correlation (DIC).

4.2.1 Test specimens and instrumentation

The two ends of each beam were tested in two consecutive loading phases. In each phase the length of the critical shear span, *a*, was kept constant. In GB63 and GB65, the left shear span damaged during phase I was sawn off before phase II was carried out, thus reducing their overall clear span (Table 4-1). In GB61 the damaged span was repaired using a cement grout and the test was performed on the same clear span as GB60. In addition, post-tensioned metal straps (PTMS) (Helal et al. 2016) were provided along the shear spans of some of the beams to ensure that failure occurred in the investigated, undamaged opposite shear span (Figure 4-1).
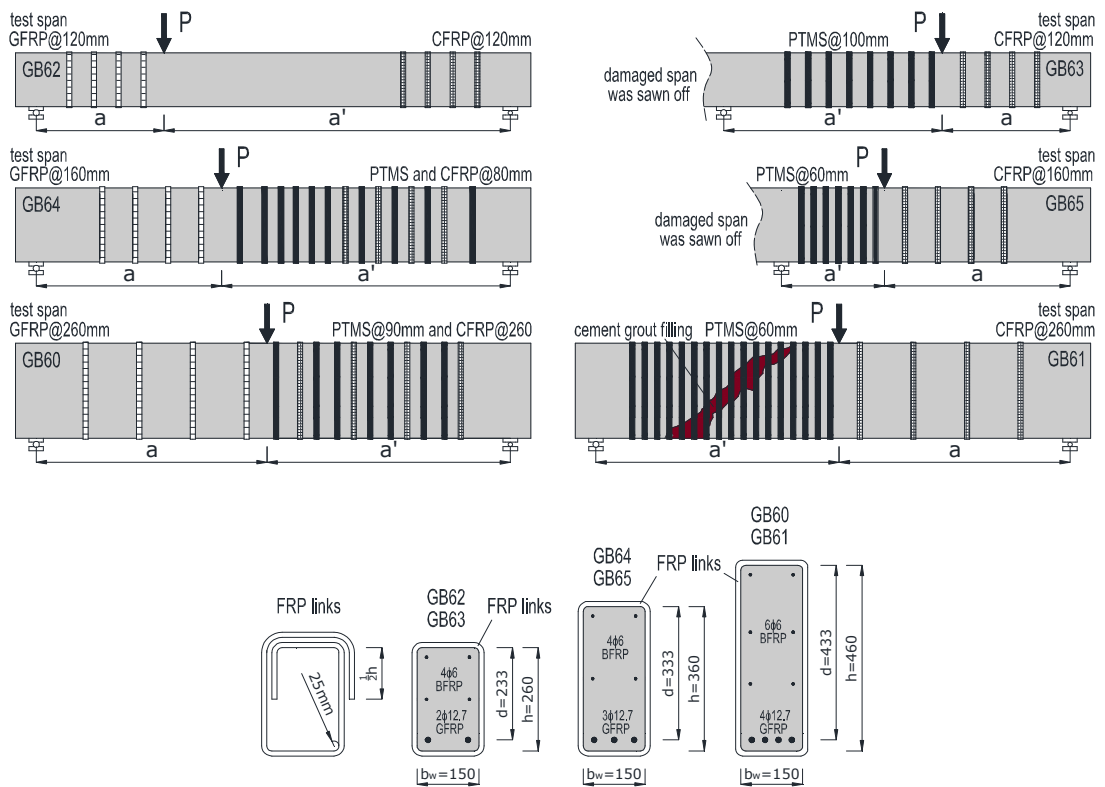
Figure 4-1 Reinforcement layout and geometry for all beams

All of the beams were simply supported and tested in displacement control under a three-point bending configuration. The applied load was measured using a load cell, while displacement and strains were recorded using potentiometers and electrical strain gauges, respectively. Displacements were measured under the load point and at the supports to determine net deflection. Strain gauges were placed along the longitudinal reinforcement on the test side of the beam, as well as on the shear links in the vicinity of the potential diagonal crack (see blue markers in Figure 4-3).

Table 4-1 Beams geometry and material properties

Beam	a (mm)	a' (mm)	L (mm)	h (mm)	d (mm)	a/d (mm)	ρ_{fl} (%)	f'_c (MPa)	Link type	s (mm)	A_{fv} (mm^2)	E_{fv} (GPa)	DIC
GB62	620	1680	2300	260	233	2.65	0.82	52.7	GFRP	120	21.6	65	YES
GB63	620	1060	1680	260	233	2.65	0.82	50.9	CFRP	120	6.3	241	NO
GB64	900	1400	2300	360	333	2.70	0.86	47.5	GFRP	160	28.3	65	YES
GB65	900	500	1400	360	333	2.70	0.86	47.5	CFRP	160	8.4	241	NO
GB60	1120	1180	2300	460	433	2.58	0.88	38.4	GFRP	260	40.5	65	YES
GB61	1120	1180	2300	460	433	2.58	0.88	38.4	CFRP	260	10.5	241	YES

Along with electrical strain gauges, DIC was also used to monitor the strain distribution in the shear links of beams GB62, GB64, GB60 and GB61, albeit on the opposite face. The collected images were processed using VIC-3D (Correlated Solutions, Inc.) to obtain the horizontal and vertical displacement fields from which the strain in the links was calculated. The software calculates the strain between any two points within the area covered by the speckle pattern using "virtual extensometers" placed along the shear links (Figure 4-2). The base length of the extensometers was selected as the minimum length bridging the width of the shear crack at a load level close to failure to ensure that the strain in the links is calculated only on the debonded part of the links and, hence, provides an accurate estimate of the maximum mobilised average strain.

4.2.2 DIC setup and reliability of the measurements

Digital Image Correlation (DIC) is a contactless measuring technique for full-field displacements and strains. The full-field measurements are obtained by comparing local correlation between two images, before and after deformation, based on gray-scale variations of a continuous pattern, divided on unique subsets. The subsets of an image are identified and matched based on the stochastically distributed image information (i.e. light intensity), and the multi-dimensional displacement of each subset is determined relative to its initial position. The individual displacement of all subsets in an image constitutes the displacement field. DIC has become an accepted method for measuring the surface displacement, strains, and displacement gradients in solid mechanics.

The quality of the correlation between the images was assessed based on the statistical confidence margin (given in pixels), which in VIC-3D software is defined as sigma parameter. Sigma value of "0" indicates perfect match; higher numbers indicate a noise, which can be associated with blurriness, poor speckle pattern, discontinuities in the measuring field or reflections. In order to ensure the validity of the DIC measurements, a subset size giving an optimal match confidence (sigma) of 0.01 pixel was assumed in all analysed images.

DIC was employed to obtain distributed strain measurements within the shear span of the beams, and in particular, a three dimensional (3D) configuration was used to compensate the effects of possible out of plane displacement of the specimens during testing (i.e., generation of apparent strains) (Di Benedetti et al. 2015). Images were acquired with two CMOS digital cameras having a 4272×2848 pixel resolution (Canon EOS 1100D) and equipped with zoom lenses with F-number and focal length of 3.5-5.6 and 18-55 mm, respectively (Canon EF S 18 55mm f/3.5 5.6 IS II). The two cameras were rigidly connected and positioned 2 m apart from the specimen and a light-emitting diode (LED) lamp was used to uniformly illuminate the measurement surface. The stereo vision system was calibrated by taking images of a known pattern with different positions and orientations (Sutton et al. 2009). During the load test, the shutter was remotely triggered every 10 seconds by the data acquisition system recording the point wise sensors in order to synchronize all data. After whitewashing the beams, speckles with an approximate diameter of 1 mm were spray painted in the region of interest (shear span under investigation) with a stencil technique. The speckle size was chosen to fit the recommendations in desirable range of 2-5 pixels (Zhou 2001).
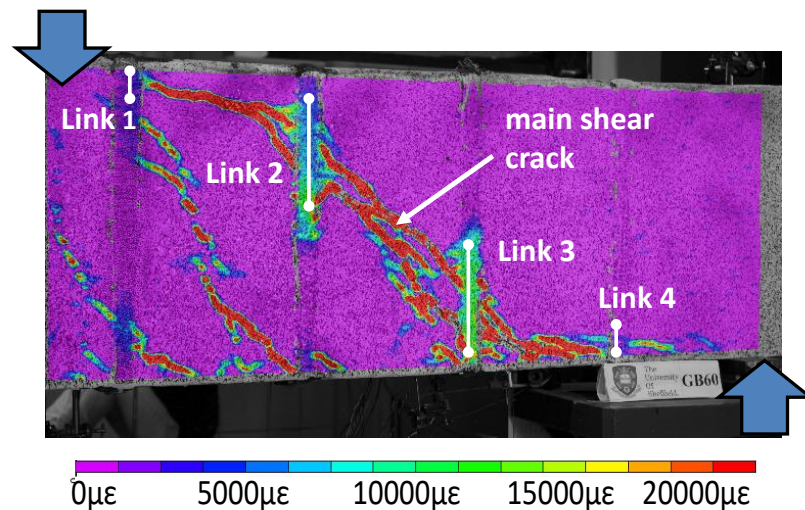
Figure 4-2 Location of the "virtual extensometers" along the shear links in beams GB60 (contour map shows the distribution of vertical strain)

4.2.3   Material properties

All the beams were cast using ready-mixed concrete with round river aggregates of maximum size of 20 mm and cement type 52.5N CEM I (mix proportions: cement - 150 kg; GGBS – 150 kg; 4/20 mm graded gravel – 1097 kg; 0/4 mm sand gravel - 804 kg; water 82 kg; Plasticiser – 1.95 l). Table 4-1 gives the compressive cylinder concrete strength for each beam taken as 80 % of the mean strength value obtained from three 100 mm concrete cubes.

The longitudinal reinforcement comprised sand-coated glass FRP bars of a nominal diameter of 12.7 mm as main flexural reinforcement and basalt FRP bars with nominal diameter of 6 mm as side distributed reinforcement so as to determine longitudinal strain at this level. The nominal modulus of elasticity was equal to 46 GPa for GFRP bars and 42 GPa for BFRP bars (determined by Serbescu et al. 2014). Details of shear reinforcement and its configuration for each beam are shown in Table 4-1 and Figure 4-1. The shear links were prepared in the laboratory using continuous strips of glass and carbon fibre sheets impregnated with epoxy resin. The FRP links were wrapped continuously around the beam, with an overlap in the top part of the beam perimeter (in compression). In addition, to reduce stresses at the bent portions of the links, the corners of the beams were rounded to a radius of 25 mm. GFRP links were used in specimens GB60, GB62 and GB64, while CFRP links were used in GB61, GB63 and GB65. The amount of shear reinforcement was designed to provide the minimum reinforcement ratio according to ACI.440.1R-15, thus the GFRP and the CFRP links offered the same theoretical additional shear capacity. The two types of fibres were used to investigate the influence of material stiffness on the cracking and overall shear behaviour of the beams.

4.3   Test results

The main test results are summarised in Table 4-2. The failure load, $P_{ult,}$ is the maximum applied external load, while V_{scr} and V_{exp} correspond to the shear force at diagonal cracking and at failure, respectively. V_{con} is the estimated contribution of concrete. The parameter k_1 is the ratio between the shear load V_{exp} and the applied load P_{ult}. The values $\varepsilon_{l,max}$ and $\varepsilon_{t,max}$ represent the peak strain in longitudinal and

transverse reinforcement as measured by the strain gauges, respectively. The values $\varepsilon_{t,max,DIC}$ and $w_{,max,DIC}$ correspond to the maximum strain in the shear links measured through DIC and maximum measured crack width, respectively.

Table 4-2 Main test results

Beam	P_{ult} (kN)	k_1 (-)	V_{scr} (kN)	V_{exp} (kN)	Service load (kN)	V_{con}/V_{scr} (at 4,500με) (%)	V_{con}/V_{exp} (at ultimate) (%)	$\varepsilon_{l,max}$ (με)	$\varepsilon_{t,max}$ (gauges) (με)	$\varepsilon_{t,maxDIC}$ (DIC) (με)	$w_{,max,DIC}$ (DIC) (mm)
GB62	66.1	0.73	37.8	48.2	32.1	78	30	11,000[a]	12,900	12,600	1.7
GB63	86.0	0.63	29.6	54.2	36.1	98	43	12,000[a]	6,800	-	1.7*
GB64	101.4	0.61	33.4	61.7	41.1	82	38	10,000	9,000	9,600	2.5
GB65	177.5	0.36	41.5	63.4	42.3	85	34	8,900[b]	10,500	-	2.1*
GB60	150.5	0.51	36.8	77.2	51.5	93	19	8,300[a]	16,800	12,400	3.3
GB61	166.4	0.51	40.8	85.4	56.9	93	22	-	13,500	8,800	3.6

Note: [a] average value from two strain gauges placed on opposite side of the beam; [b] last reading from the gauge at shear load of about 60 kN;* the cracks widths in elements GB63 and GB65 were measured with a manual microscope.

4.3.1 Failure mode and cracking patterns

The crack patterns at failure for all beams are shown in Figure 4-3. The numbers 1-4 indicate the position of the links along the shear span, with link 1 being located nearest to the loading point.
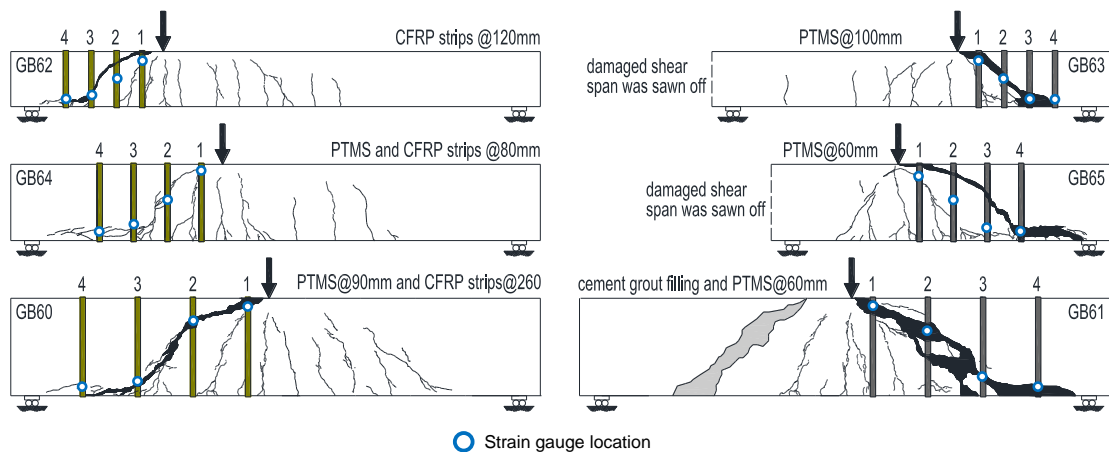
Figure 4-3 Cracking diagrams for all beams (blue markers show the location of strain gauges)

All tested beams exhibited diagonal tension failure caused by the development of a diagonal shear crack within links 2 and 3, with link 3 generally failing first followed by links 2 and 1, while link 4 usually remained undamaged. All four links in GB65 and GB61 fractured as a result of large horizontal splitting cracks that developed along the flexural reinforcement. No premature delamination of the shear links was observed.

4.3.2 Deflection and strain in the flexural reinforcement

Figure 4-4 shows the shear force along the tested shear span against the net deflection under the loading point for all beams. An increase in shear capacity was observed with increasing member depth. Similar shear resistance was achieved in beams of the same overall depth; however, shear spans reinforced with CFRP links developed slightly higher capacity than their counterparts with GFRP links.
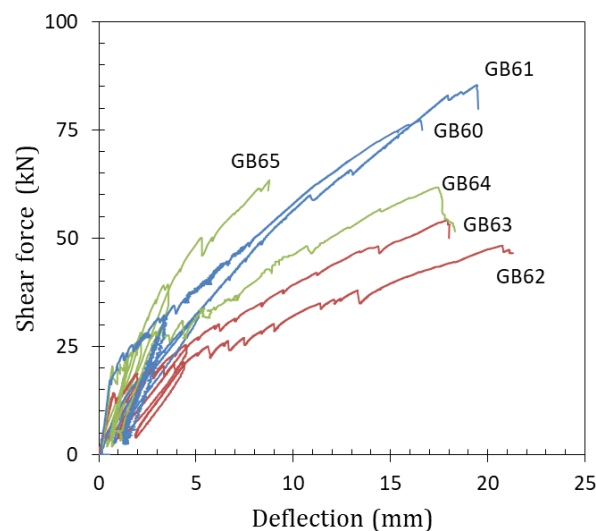
Figure 4-4 Load-deflection behaviour for all beams

Figure 4-5 shows the average longitudinal strain in the flexural reinforcement measured by two strain gauges located at the section under the loading point but on the two external bars of each beam. The largest longitudinal strain at ultimate was recorded in the shallowest beams (red curves) reaching values of about 12,000 με (GB63) and decreasing values were observed with increasing member depth.
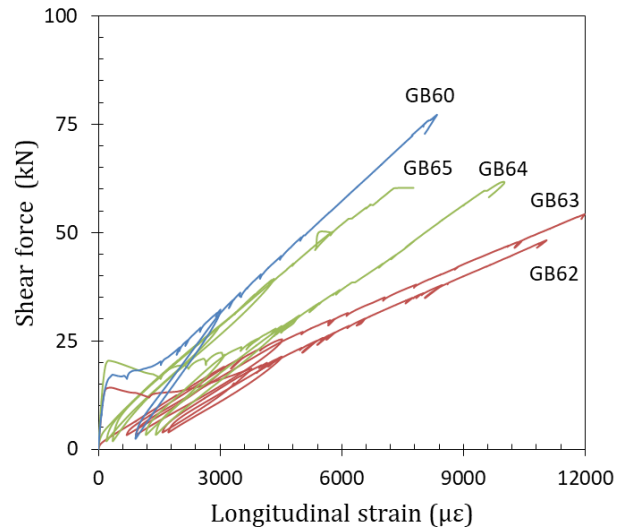
Figure 4-5 Load-strain curves for all beams

The beams were subjected to one or two load cycles (two for the elements with overall depth of 260 mm and 360 mm, and one cycle for 460 mm beams) at two strain levels in the flexural reinforcement of: 3,000 με, corresponding to typical SLS strain values and 4,500 με corresponding to a level of strain expected to induce significant level of shear damage. Note that GB61 is not shown as the strain gauge failed during the first phase of testing (GB60).

4.3.3   Strain in the shear links

The development of strain in the FRP shear links of all beams, measured using both conventional strain gauges and DIC, is shown in Figure 4-6. It can be seen that the strain evolution obtained from DIC (Figure 4-6: d-g) is in agreement with that recorded by the electrical strain gauges (Figure 4-6: a-c, and j). Any discrepancies in terms of maximum recorded values (see Table 4-2) between the two measuring methods may be attributed to the fact that electrical strain gauges provide local measurements, while average measurements along a longer gauge length at the exact crack location were obtained from DIC. In addition, it should be noted that these measurements were taken on opposite sides of the shear span and differences in cracking patterns resulting from material variability and, possibly torsion, may have affected the overall strain distribution and make a direct comparison more difficult. The DIC results will be used in all further analyses of GB60, GB61, GB62 and

GB64 as they can provide a more representative estimate of the force developed in each of the links.
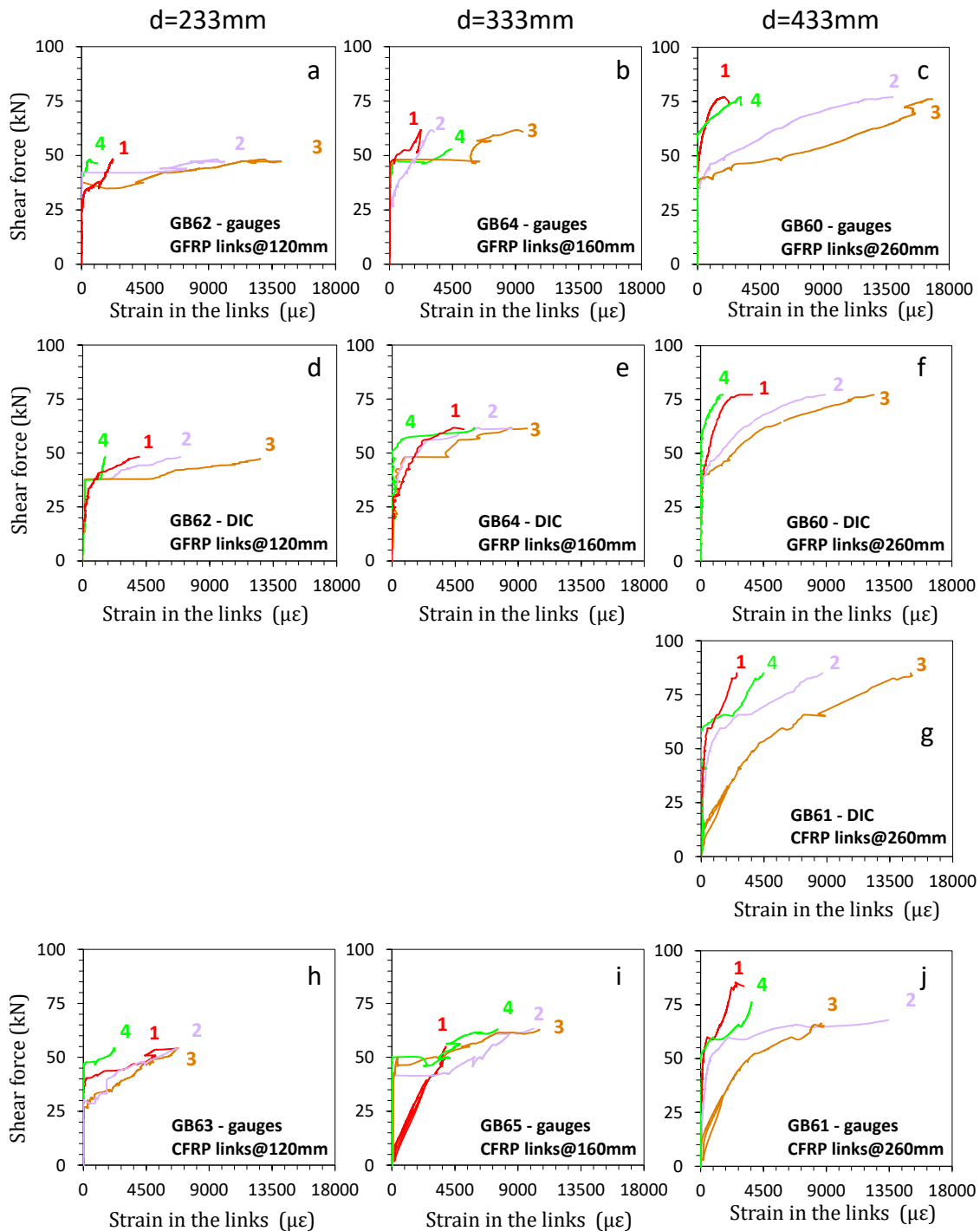
Figure 4-6 Strain evolution in the shear links (see also Figure 4-3)

4.4 Estimation of shear components

Figure 4-7, Figure 4-8 and Figure 4-9 show typical decompositions of shear resisting components in three beams of different sizes. The individual contribution of each link ($F_{sl,i} = E_{fv}A_{fv}\varepsilon_{ti}$) was estimated on the basis of the strain mobilised in the links across the crack that led to failure and measured through DIC. The relative contribution of the concrete (shaded area under the dashed curve) was determined by subtracting the cumulative force developed in the links contributing to the overall shear capacity (links 1-3) from the total shear resisted along the test shear span (black curves). As such, the estimated concrete contribution includes: shear resistance of the uncracked concrete, aggregate interlock, and dowel action. Links 4 were not taken into account in this analysis as they did not directly contribute to shear resistance and were only activated just before failure at the onset of the horizontal splitting crack along the flexural reinforcement.
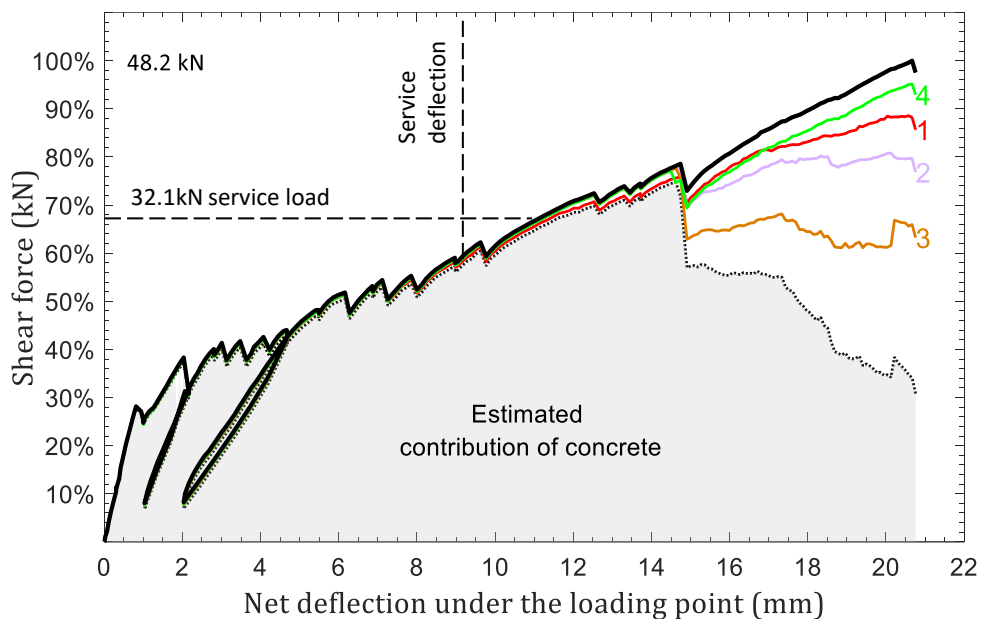
Figure 4-7 Shear resisting components in GB62

The shear links were only activated after the critical shear crack initiated and following the stress transfer between cracked concrete and the transverse reinforcement, which was characterised by a sudden drop in load. For example, in GB62 (Figure 4-7), the main shear crack developed at a shear force of about 37.8 kN

(about 78 % of the total shear capacity), with links 3 and 2 developing increasingly higher levels of strain at increasing load levels. The load at which the main shear crack developed within the tested shear span, V_{scr}, ranged from 29.6 kN (GB63) to 41.5 kN (GB65) as shown in Table 4-2. The experimental values of V_{scr} and the deflection attained at those load levels are compared to service conditions (Table 4-2).
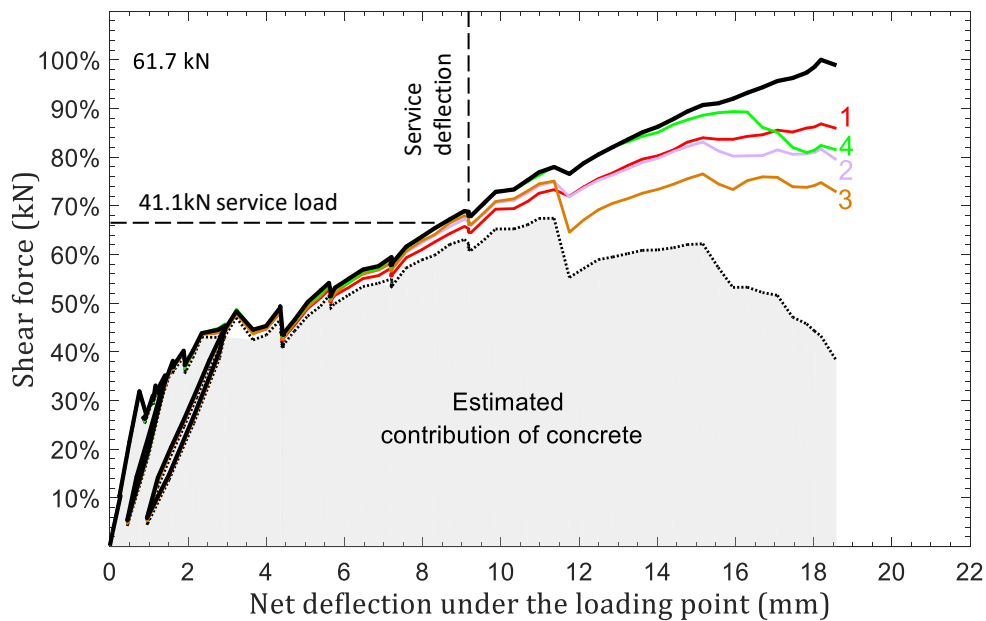
Figure 4-8 Shear resisting components in GB64

The service load is considered to be the experimental capacity divided by a factor equal to 1.5, representing an average value of load factors used in design codes (e.g. Eurocode 2, ACI). The service deflection (vertical dashed line) was calculated as $L/250$, where L is the clear span of the beam. As can be seen from Figure 4-7, Figure 4-8 and Figure 4-9 and the values reported in Table 4-2, the shear crack developed at a load lower than the estimated service load for the beams with an overall depth of 260 mm (GB62) and 360 mm (GB64), while diagonal cracking occurred at about 70% of service load for the beams with an overall depth of 460 mm (GB60).
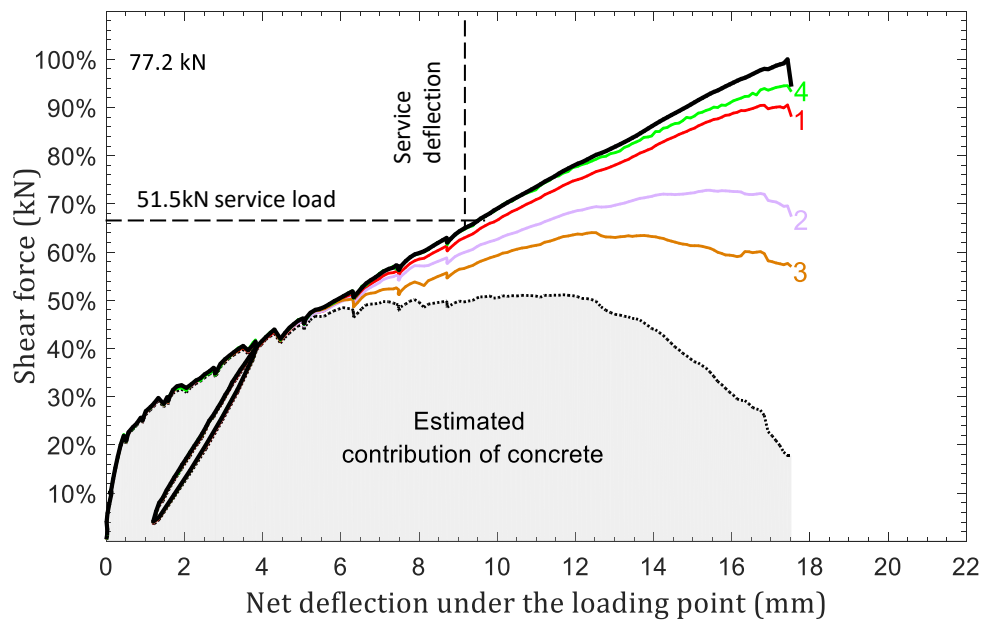
Figure 4-9 Shear resisting components in GB60

After the initiation of the shear crack, V_c decreases with increasing load. In general, the initial reduction of concrete resistance is fairly linear (GB64, GB65) or remains almost constant (GB60, GB61, GB63), suggesting that shear links effectively controlled the opening of the shear crack and shear resisting mechanisms were sufficiently mobilised. A more brittle behaviour was observed in GB62 where shear cracking was followed by a significant decrease in concrete contribution and by a rapid increase in the strain developed in the shear reinforcement (Figure 4-7). The estimated value of concrete contribution at failure (V_{con}) in GB62 (Figure 4-7) and GB64 (Figure 4-8) was about 30-38 % of their respective total shear capacities (see Table 4-2). In GB60, the residual contribution of concrete at failure was only about 20 % (Figure 4-9), suggesting that in larger elements a larger proportion of vertical shear is resisted by V_f rather than V_c. Similar values of V_{con}/V_{exp} was achieved for beams with CFRP links (see Table 4-2), indicating that the stiffness of the fibres did not have significant influence on the cracking behaviour of the beams.

4.5 Comparison with code predictions and design recommendations

The experimental results presented above are used to evaluate the performance of existing design models in predicting the contribution of concrete and FRP shear reinforcement to the total shear resistance of FRP RC beams. Key international design approaches (ACI 440.1R-15, *fib* bulletin 40 and CSA S806) are selected so as to compare different models estimating V_c as well as different strain limits recommended for the design of FRP shear reinforcement (see equations in Table 4-3).

Table 4-3 Shear design provisions

Reference	Shear provisions	
ACI440.1R-15 (ACI 2015)	$V_c = \dfrac{2}{5}\sqrt{f'_c}\,b_w d k$	Eq. 4-1
	$V_f = \dfrac{A_{fv} f_{fv} d}{s};\qquad f_{fv} = 0.004 E_f \le f_{fb}$	Eq. 4-2
	$f_{fb} = \left(0.3 + 0.05\dfrac{r}{d_b}\right) f_{FRP} \le f_{FRPu}$	Eq. 4-3
fib bulletin 40 (*fib* 2007)	$V_c = \left[\dfrac{0.18}{\gamma_c}\cdot\left(1+\sqrt{\dfrac{200}{d}}\right)\cdot\left(100\dfrac{A_{fl}}{b_w d}\cdot\dfrac{E_{fl}}{E_s}\cdot 1.8\cdot f_{ck}\right)^{\frac{1}{3}}\right] b_w d$	Eq. 4-4
	$V_f = \dfrac{A_{fv}}{s}\,0.0045 E_{fv} z$	Eq. 4-5
	$V_c = 0.05\lambda\phi_c k_m k_r k_s {f'_c}^{1/3} b_w d_v$	Eq. 4-6
	$V_f = \dfrac{0.4\phi_F A_{fv} f_{fu} d_v}{s}\cot\theta$	Eq. 4-7
CSA S806-12 (CSA 2012)	$f_{fu} \le 0.005 E_{fv}$	Eq. 4-8
	$30° \le \theta = 30° + 7000\varepsilon_x \le 60°$	Eq. 4-9
	$\varepsilon_x = \dfrac{\dfrac{M_a}{d_v}+V_a}{2(A_{fl}E_{fl})}$	Eq. 4-10

In ACI the design stress in the shear reinforcement is taken as the minimum between the strength of the bent portion of the FRP stirrup (f_{fb} in Eq. 4-3) and the stress corresponding to a strain level of 4,000 µε (Eq. 4-2). As a bending radius of 25 mm

was ensured for all of the FRP shear links used in this experimental programme, the predicted f_{fb} is close to the ultimate strength of the link (f_{FRPu}), and the design strength is governed by the limiting strain value. The design approach implemented in *fib* bulletin 40, originally proposed by (Guadagnini et al. 2003), considers a level of stress in the FRP flexural reinforcement and FRP shear links corresponding to a maximum allowable strain of 4,500 με (Eq.4-4, Eq. 4-5). Both ACI and *fib* models implicitly adopt a fixed angle for the concrete strut equal to 45°. In the Canadian design code CSA S806-12, the recommended maximum strain level in FRP links is equal to 5,000 με (Eq. 4-8) and an additional reduction factor equal to 0.4 (Eq. 4-7) is introduced to account for the reduced strength of the bent portions of the links (El-Sayed et al. 2011). However, some researchers (e.g. Razaqpur and Spadea 2014) suggest that the reduction factor is not an integral part of the design equation and that the maximum stress level in the FRP reinforcement is to be taken as the smallest of $0.005E_{fv}$, $0.4f_{fv}$ or 1200 MPa. The inclination of the shear crack can be calculated using Eq. 4-8 and Eq. 4-9 and varies between 30° and 60°.

Although the equations used to calculate V_f are for RC members with internal FRP stirrups, given that the links used in the testing programme presented here were fully anchored (fully wrapped around the section and with appropriate overlap), these provisions can be also adopted to estimate the shear resistance offered by the external shear links. As long as the shear links are anchored well, their contribution can be estimated based on the truss analogy and the effective strength of the links.

Figure 4-10, Figure 4-11, and Figure 4-12 show the development of total shear resistance (black curves) and experimentally determined contribution of concrete (grey curves) with the variation of strain in the shear links (taken as the average strain recorded in links 2 and 3 as these two links started resisting shear from the opening of the critical shear crack and developed the largest strains). The red curves show the theoretical predictions according to ACI 440.1R-15, *fib* bulletin 40 and CSA S806-12. The experimental and theoretical results are normalized by the corresponding design V_c values (Table 4-3). This procedure can help evaluate the accuracy of the design models and assist in estimating how much concrete shear

93

resistance is effectively mobilised after the occurrence of diagonal cracking with respect to the theoretical assumptions.
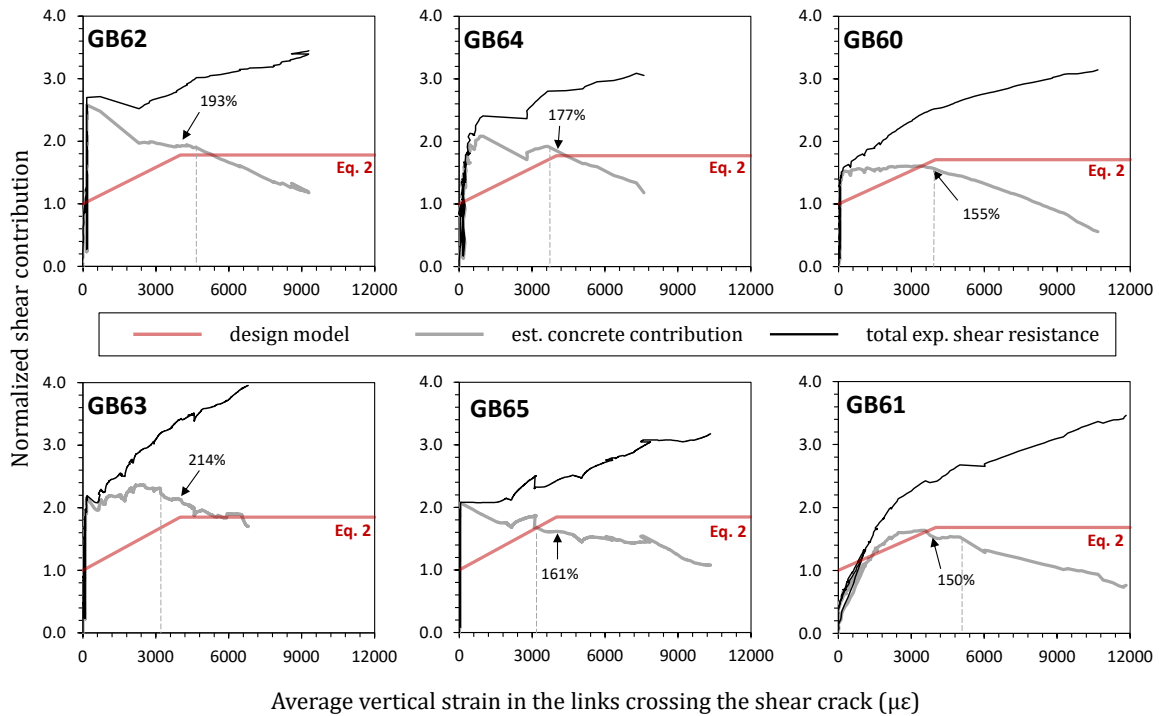
Figure 4-10 Experimental results and theoretical predictions according to ACI 440 design guideline
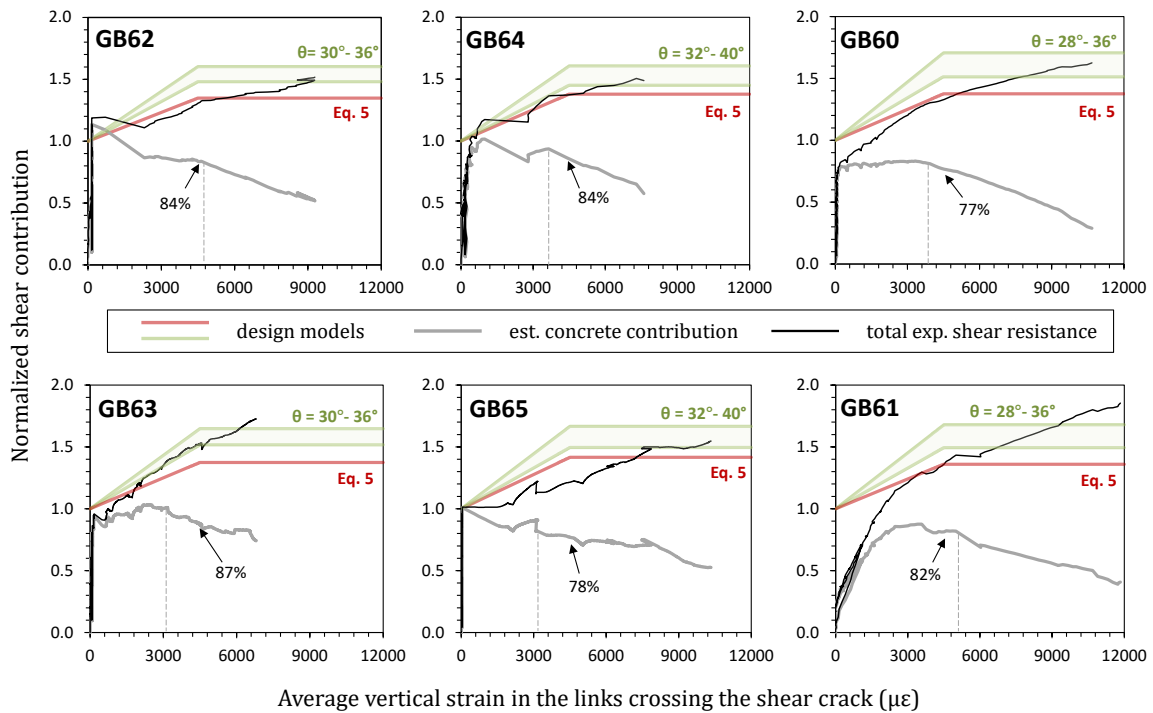
Figure 4-11 Experimental results and theoretical predictions according to *fib* model

All examined design approaches provide conservative estimates of the total shear resistance, with the ACI provisions being the most conservative with a mean value of experimental-to-theoretical shear resistance close to 2.0 (Table 4-4). From Figure 4-10, it can be seen that, for the majority of the specimens, the theoretical total shear resistance (red horizontal line starting at the strain level of 4,000 με) is lower than the load causing diagonal cracking and that the model fails to accurately estimate the relative contribution of the two main resisting components. A better agreement between the experimental and theoretical values is attained using the *fib* and CSA approaches (Figure 4-11, Figure 4-12).
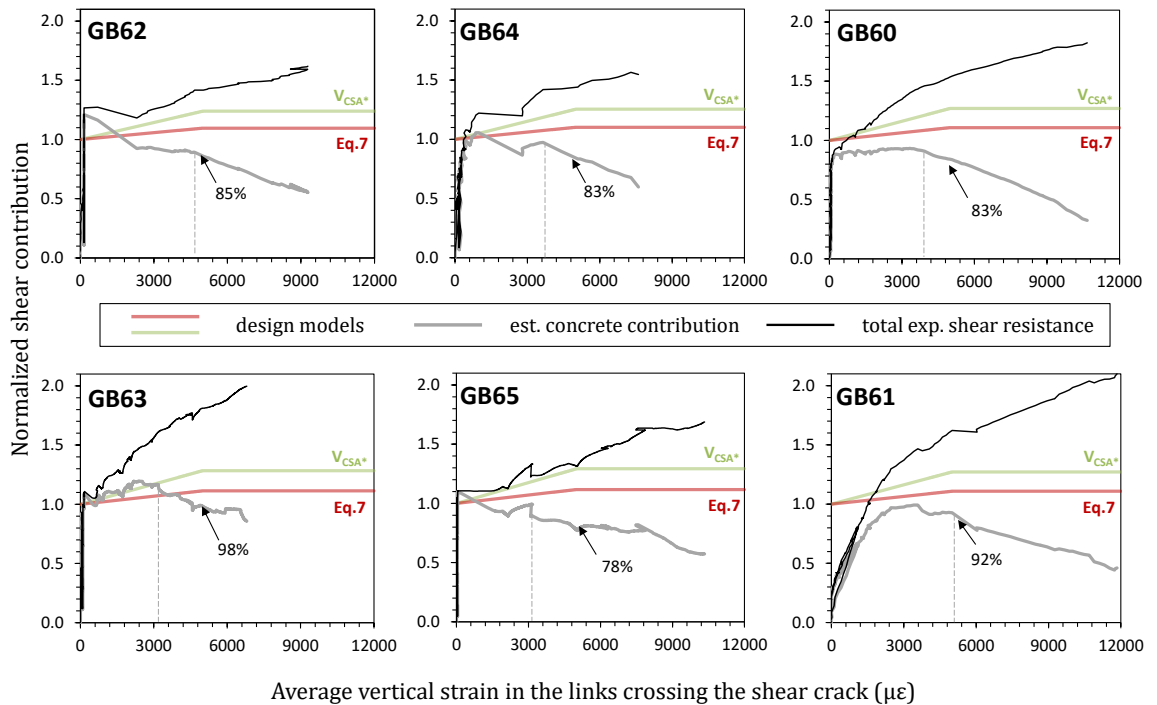
Figure 4-12 Experimental results and theoretical predictions according to CSA S806 design code

The ratios of $V_{scr}/V_{c,fib}$ and $V_{scr}/V_{c,CSA}$ are equal to 0.93 and 0.99, while V_{exp}/V_{fib} and V_{exp}/V_{CSA} produce values of 1.18 and 1.63, respectively. When the factor that accounts for the reduction in strength of bent stirrups is not taken into account (no failure has been observed to be triggered by the rupture of the links at their corner), the experimental-to-theoretical shear resistance V_{exp}/V_{CSA*} reduces to 1.37.

Table 4-4 Comparison of the experimental shear resistance with values predicted by design guidelines

Beam	ACI 440.1R-15		*fib* bulletin 40		CSA S806-12		
	$V_{scr}/V_{c,ACI}$	V_{exp}/V_{ACI}	$V_{scr}/V_{c,fib}$	V_{exp}/V_{fib}	$V_{scr}/V_{c,CSA}$	V_{exp}/V_{CSA}	V_{exp}/V_{CSA*}
GB62	2.70	1.93	1.19	1.13	1.27	1.48	1.31
GB63	2.13	2.11	0.96	1.25	1.01	1.79	1.46
GB64	1.68	1.75	0.81	1.09	0.84	1.42	1.24
GB65	2.08	1.72	1.01	1.09	1.05	1.51	1.25
GB60	1.49	1.83	0.78	1.19	0.84	1.65	1.40
GB61	1.65	2.06	0.86	1.33	0.93	1.90	1.56
Average	**1.96**	**1.90**	**0.93**	**1.18**	**0.99**	**1.63**	**1.37**
StDev	0.41	0.15	0.14	0.09	0.15	0.17	0.11
COV	0.21	0.08	0.15	0.07	0.15	0.11	0.08

Note: design safety factors set equal to 1; V_{CSA*} - total shear resistance determined without including the factor accounting for the reduction in strength of bent stirrups

Although the initial shear force causing diagonal cracking (V_{scr}) is on average predicted very well by *fib* and CSA, the values predicted for individual specimens exhibit variable margins of safety, which decrease with increasing member depth (see Figure 4-13a and Table 4-4). The highest reduction is seen in the ACI approach and can be attributed to the lack of a size effect factor in Eq. 4-1. However, the predictions of the total shear capacity (including the contribution of the shear links) are less affected by the size of the specimens (Figure 4-13b).
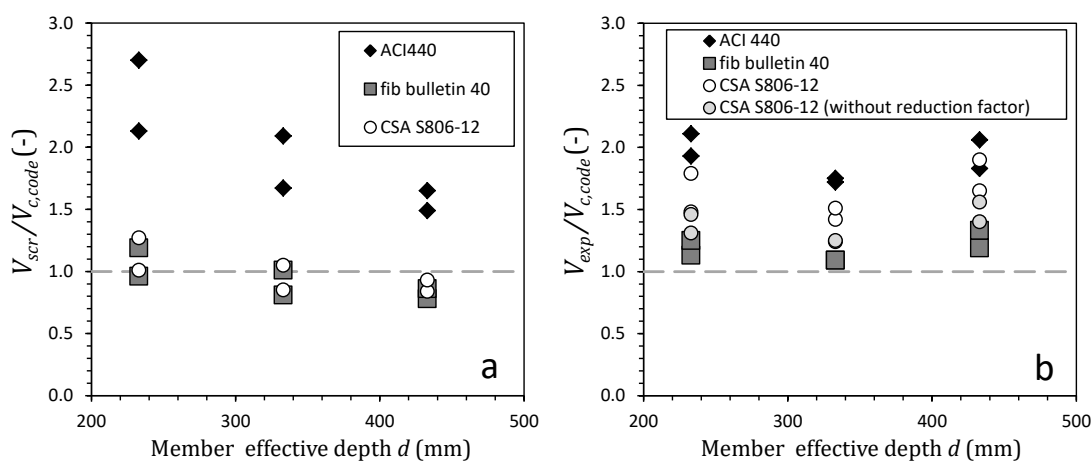
Figure 4-13 Comparison of experimental results to theoretical predictions with respect to member effective depth; a- predictions of the diagonal cracking load; b – predictions of the total shear capacity

4.6   Contribution of concrete

The shear resistance offered by concrete is considered constant up to failure by the current existing design guidelines, which imply that it is not affected by the development of the critical shear crack. However, the experimental evidence shows that the contribution of concrete (grey curves in Figure 4-10, Figure 4-11 and Figure 4-12) decreases with increasing strain in the shear links. For instance, at the average strain in the FRP links corresponding to 4,500 με, the contribution of concrete varies between 77 % (GB60) and 87 % (GB63) of the theoretical value calculated by *fib* (Figure 4-11). Similarly, at the allowable strain recommended by CSA (5,000 με), the residual concrete contribution ranges between 78 % (GB65) and 98 % (GB63) of $V_{c,CSA}$ (Figure 4-12). On the other hand, ACI greatly underestimates the contribution offered by the concrete even when the links develop the maximum allowable strain of 4,000 με (Figure 4-10), with experimentally estimated values ranging from 150 % (GB61) to 214 % (GB63) of that predicted using Eq. 4-1.

The grey dashed lines (Figure 4-10, Figure 4-11 and Figure 4-12) represent the strain level in the shear links at which the degradation of concrete resistance is more pronounced and decreases almost linearly until failure. These strain values range from 3,200 με (GB63) to 5,100 με (GB61). However, from close examination of Figure 4-14, which shows the variation in normalised experimental contribution of concrete (V_{con}/V_{scr}) with shear crack growth, it can be seen that the concrete contribution exceeds 75 % of the total shear resistance even at crack widths exceeding 0.5 mm and strain levels of 4,500 με (circle markers). The maximum crack width observed at failure increases with increasing member depth and ranged from 1.7 mm (GB62, GB63) to 3.7 mm (GB61), with the maximum crack width not exceeding 2 mm at the recommended design strain levels (see coloured markers in Figure 4-14).
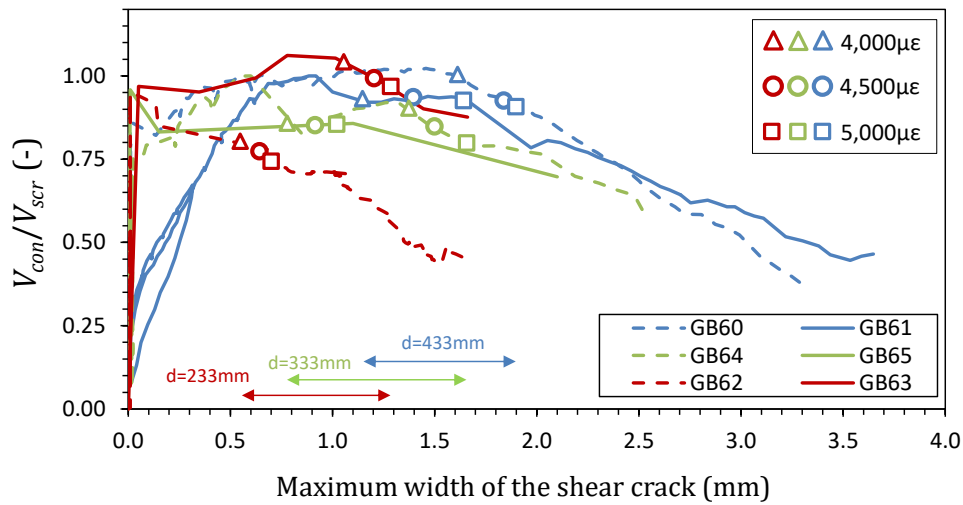
Figure 4-14 Reduction of concrete contribution with respect to the width of the shear crack

The contribution of concrete to the total shear capacity (V_{con}/V_{exp}) as a function of the longitudinal strain measured in the flexural reinforcement at maximum moment is shown in Figure 4-15.
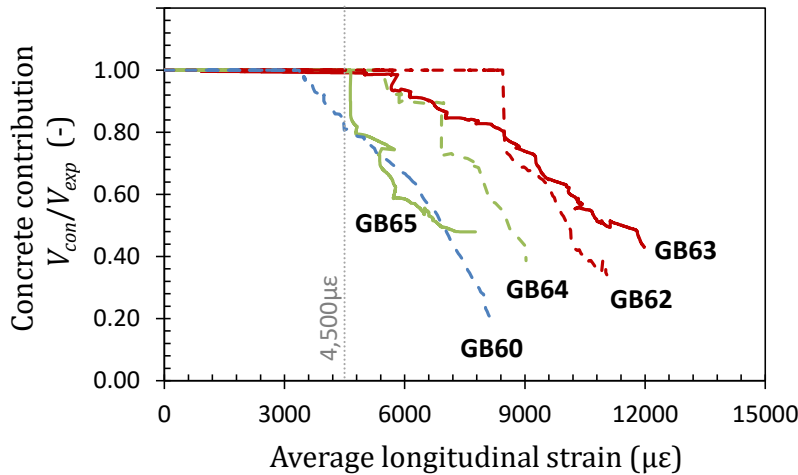
Figure 4-15 Degradation of concrete contribution

Even though only a limited number of specimens was tested and there are natural variabilities between them, it can still be seen that the shallowest beams (red curves) developed shear cracks at higher longitudinal strains indicating that size effect affects their behaviour. For those beams, it can be seen that no shear crack developed at the longitudinal strain of 4,500 με, which is the strain value that is allowed to be developed in the flexural reinforcement when estimating V_c according to *fib* bulletin 40. However, the beam with the largest depth (GB60, blue curve)

developed diagonal cracking at lower level of flexural strain indicating that to control shear failure effectively, there is scope for an approach (like that of *fib*) that limits strains in the longitudinal reinforcement, which may be a function of beam depth.

4.7   Contribution of shear links

FRP shear design provisions allow different strain limits in FRP shear reinforcement, varying from 2,500 to 5,000 µε. The maximum recorded strain at failure in the shear reinforcement ranged from 9,000 µε to 16,800 µε for the specimens reinforced with GFRP links and from 6,800 µε to 13,500 µε for members with CFRP links (based on the readings from strain gauges, Table 4-2). Figure 4-10, Figure 4-11, Figure 4-12 and Figure 4-14 indicate that the shear resisting mechanisms can be sufficiently mobilized even above the current design limits.

Although the *fib* model somewhat overestimates the contribution of concrete (Figure 4-11), the total shear capacity is still reasonably estimated provided the correct number of mobilized shear links is used. Experimental results show that a total of three links participated in resisting shear, with link 1 contributing less than the other two links. As a fixed inclination of the compressive strut ($\cot\theta = 1$) is implicitly assumed (Eq. 4-5), for a spacing of 0.5d, the model considers that only two of the shear links contribute in resisting shear after diagonal cracking. Even when only the contribution of two links is assumed, the value of total shear force resisted at the strain level corresponding to the recommended design limit (4,500 µε) is predicted fairly well, without the need to reduce the contribution of concrete (see black and red plots in Figure 4-11). The green curves show the results assuming that all three shear links contribute to the overall shear resistance. As such, for the adopted link spacing, the inclination of the shear crack can vary from about 28° to 40°. Figure 4-11 clearly shows that when a shallower θ is used the model overestimates the experimental shear capacity and eventually leads to unsafe design at ultimate limit state (e.g. GB61, GB62, GB64, and GB65) suggesting that the contribution of concrete should be reduced. On the other hand, reduction of the concrete contribution to zero, as is recommended in the latest version of Eurocode

2 for all members with shear reinforcement, would result in overly conservative predictions for lightly shear-reinforced FRP RC beams.

The shear provisions given by CSA S806-12 (Figure 4-12) implement the use of a variable angle truss model and the inclination of the strut (Eq. 4-8) is determined based on mid-depth longitudinal strains (Eq. 4-9). The red and green curves model the behaviour of the tested beams with and without the inclusion of the reduction factor for bent FRP stirrups (taken as 0.4), respectively. As can be seen, both approaches (with and without reduction parameter) underestimate the contribution of the shear links. This can be mainly attributed to the very steep values of θ resulting from Eq. 4-8, although limited to 60° (cotθ = 0.58) according to the code provisions.

On the basis of the above discussion, it can be concluded that, even though the adoption of a fixed truss angle (i.e. 45 °) and the currently recommended strain limits generally underestimate the contribution of shear links, provided that a reliable estimate of V_c is made, reasonable predictions of total shear capacity can be obtained (e.g. *fib* model). On the other hand, the truss angle estimated by CSA does not correspond to experimental observations and the predicted steeper angles underestimate the contribution made by the links. A variable angle truss in line with EC2 provisions, which result in shallower angles, may reflect better the observed critical crack angles. However, the adoption of shallower angles would also require adjustments in V_c to reflect the gradual loss in concrete contribution seen with increasing longitudinal and vertical strain and crack widths.

Though this paper does not deal with steel RC elements, lessons may also be learned for that case. It is clear that concrete contribution to shear decreases gradually with increasing strains in the flexural and shear reinforcement. As after yielding of the steel reinforcement, either in shear or flexure, the strains increase at a much faster rate than for FRP reinforcement, then the concrete contribution is also likely to decrease more rapidly. Hence, the implicit use of plastic theory is not valid and there is scope for introducing strain limits on the reinforcements or reducing the value of V_c even in steel RC design.

4.8   Conclusions

The results of six tests carried out on FRP RC beams with shear FRP reinforcement are presented and discussed in detail so as to gain important insights on the development and magnitude of shear resisting mechanisms. Based on experimental evidence and critical DIC measurements, the relative contributions of shear reinforcement and concrete were estimated and compared with shear design provisions given by ACI440 (2015), *fib* bulletin 40 (2007) and CSA S806 (2012). The main conclusions drawn from this study can be summarized as follows:

- All tested elements failed in diagonal tension followed by fracture of shear links. For the given minimum shear reinforcement, the critical shear crack was resisted mainly by three shear links, with the links placed in the middle of the shear span usually developing much higher strains than the link closest to the loading point. The links crossing the horizontal splitting crack (closest to the support) had a negligible contribution to overall shear resistance.

- Strains recorded in the shear links and longitudinal reinforcement always exceeded the limits recommended by the design guidelines. The maximum strain developed in the shear reinforcement ranged from 9,000 με to 16,800 με for the elements reinforced with GFRP links and from 6,800 με to 13,500 με for members with CFRP links. The maximum longitudinal strain in flexural GFRP reinforcement varied from 8,300 με to 12,000 με, with maximum strain values decreasing with increasing member depth.

- The *fib* and CSA models appear to be fairly accurate in predicting the shear load at which diagonal crack develops (V_{scr}), with experimental-to-theoretical ratios equal to 0.94 and 0.99, respectively. The ACI equation, however, greatly underestimates the experimental values ($V_{scr}/V_{c,ACI}$ = 1.96) and predicts the diagonal cracking loads with non-uniform safety margins, which decrease with increasing member depth.

- The width of the main diagonal crack increased with increasing beam depth. However, at the strain levels currently allowed by design models, crack widths did not exceed 2 mm and at least 75 % of the initial concrete contribution was still effectively mobilized.

- After the development of the critical shear crack, the contribution of concrete decreases gradually as the load increases. The residual contribution of concrete just before failure is a function of beam depth and ranges from about 20 % to 40 % of the beam total shear capacity. Although existing design models do not take this into account and only consider a constant concrete contribution, a reasonable estimate of total shear capacity, with a reasonable margin of error, is obtained when a simplified fixed angle of the concrete strut (45°) is assumed. The design philosophy included in the latest version of Eurocode 2 allows for the use of a more refined variable angle truss (from 21.8° to 45°) but neglects the contribution of concrete whenever shear reinforcement is provided. However, this results in overly conservative predictions and the experimental evidence indicates that an additive nature of shear resisting components can be still maintained, as long as the concrete contribution is adequately accounted for.

- Although the presence of even a minimum amount of shear reinforcement can effectively mitigate size effect in terms of overall shear capacity, local phenomena (crack width and strain distribution) seem to be a function of beam depth and can affect the development of shear resisting mechanisms and their relative contribution.

- DIC shows a great potential in capturing strains and crack widths. In addition, DIC allows to measure strain along the shear links using larger base lengths than conventional electrical gauges, thus making the results more reliable.

- Lessons learned here may also improve the design of steel RC. As concrete shear contribution is shown to decrease with increasing stain, the implicit use of plastic theory principles is not valid, and either the value of V_c needs to be reduced or strain limits introduced in shear design.

4.9 References

- American Concrete Institute (ACI). Guide for the design and construction of concrete reinforced with FRP bars. Technical Committee Document No. 440.1R-15, Farmington Hills, Mich; 2015.

- Bazant ZP, Kazemi, M. T. Size effect on diagonal shear failure of beams without stirrups. ACI Struct. J 1991;88(3):268-276.

- British Institution of Structural Engineers (BISE). Interim guidance on the design of reinforced concrete structures using fiber composite reinforcement. IStructE, SETO Ltd., London; 1999.

- Canadian Standards Associations (CSA). Canadian Highway Bridge Design Code. CSA S6-14, Mississauga, ON, Canada; 2014.

- Canadian Standards Associations (CSA). Design and construction of building components with fibre-reinforced polymers. Canadian Standards S806-12, Rexdale, Ontario, Canada; 2012.

- CEN European Committee for Standardization. Eurocode 2. Design of concrete structures – general rules and rules for buildings. EN 1992-1-1, Brussels, Belgium; 2004. p. 225.

- Cholostiakow S, Di Benedeti M, Pilakoutas K, Guadagnini M. Effect of beam depth on shear behaviour of FRP RC beams. J Compos Constr 2018; 10.1061/(ASCE)CC.1943-5614.0000914 (*in press*).

- Cladera A, Mari AR. Shear strength in the new Eurocode 2. A step forward? Structural Concrete-London-Thomas Telford Limited, 2007; *8*(2), 57.

- CNR-DT 203/2006. Guide for the design and construction of concrete structures reinforced with fiber-reinforced polymer bars. National Research Council, Rome, Italy; 2006.

- Di Benedetti M, Cholostiakow S, Fergani H, Zappa E, Cigada A, Guadagnini M. 3D-DIC for strain measurement in small scale GFRP RC specimens. In: Proceedings of SMAR 2015 Conference. Antalya. September, 2015. pp. 1-8.

- Duranovic N, Pilakoutas K, Waldron P. Tests on concrete beams reinforced with glass fibre reinforced plastic bars. In: Proceedings of FRPRCS-3 Conference. 1997; pp. 479-486.

- El-Sayed AK, El-Salakawy EF, Benmokrane B. Shear strength of FRP-reinforced concrete beams without transverse reinforcement. ACI Struct. J. 2006;103(2), 235.

- El-Sayed AK, Soudki K. Evaluation of Shear Design Equations of Concrete Beams with FRP Reinforcement. J. Compos. Constr. 2011; 15(1), pp.9–20.

- *fib* (Fédération internationale du béton). FRP reinforcement in RC structures. *fib* bulletin 40, Technical report. Lausanne, Switzerland, 2007.

- *fib* (Fédération internationale du béton). Model Code for Concrete Structures 2010. Ernest&Sohn, ed., Weinheim. 2013.

- Guadagnini M, Pilakoutas K, Waldron P. Shear performance of FRP reinforced concrete beams. J. Reinf Plast Compos. 2003;22(15), 1389-1407.

- Guadagnini M, Pilakoutas K, Waldron P. Shear resistance of FRP RC beams: Experimental study. J. Compos. Constr. 2006; 10.1061/(ASCE)1090-0268(2006)10:6(464), 464-473.

- Helal Y, Garcia R, Pilakoutas K, Guadagnini M, Hajirasouliha I. Strengthening of short splices in RC beams using Post-Tensioned Metal Straps. Mater. Struct., 2016. 49(1-2), 133-147.

- Hoult NA, Sherwood EG, Bentz EC, Collins MP. Does the use of FRP reinforcement change the one-way shear behavior of reinforced concrete slabs? J. Compos. Constr. 2008; 10.1061/(ASCE)1090-0268(2008)12:2(125), 125-133.

- ISIS Canada. Reinforcing concrete structures with fiber reinforced polymers. ISIS-M03-07, Canadian network of centers of excellence on intelligent sensing for innovative structures, Univ. of Winnipeg, Winnipeg, Man; 2007.

- Issa MA, Ovitigala T, Ibrahim M. Shear Behavior of Basalt Fiber Reinforced Concrete Beams with and without Basalt FRP Stirrups. J. Compos. Constr. 2015, 20(4), 04015083.

- Japan Society of Civil Engineers (JSCE). In: Machida A, editor, Recommendations for design and construction of concrete structures using continuous fibre reinforced materials. Concrete Engineering Series 23, Tokyo, Japan; 1997.

- Joint ACI-ASCE Committee 445, Recent Approaches to Shear Design of Structural Concrete. J. Struct. Eng. V. 124, No. 12, Dec. 1998, 1375-1417.

- Kani G. How safe are our large reinforced concrete beams? In: Journal Proceedings*.*, 1967;64, 3, 128-141.

- Kotsovos MD. Compressive force path: Basis for ultimate limit state reinforced concrete design. ACI Struct*. J.* 1988*;* 85(1), pp. 68–75.

- Mikani H, Katoh M, Takeuchi H, Tamura T. Flexural and shear behaviour of RC beams reinforced with braided FRP rods in spiral shape. Transactions of the Japan Concrete Institute, 1989;11(1), 119-206.

- Mitchell D, Collins MP. Diagonal compression field theory - A rational model for structural concrete in pure torsion. ACI J. 1974;71(8), 396–408.

- Morsh E. Concrete-steel construction. E. P. Goodrich, translator, McGraw-Hill, New York, 1909

- Nagasaka T, Fukuyama H, Tanigaki M. Shear performance of concrete beams reinforced with FRP stirrups. In: Proc., Int. Symp. on Fiber Reinforced-Plastic Reinforcement for Concrete Structures, Nanni, A., Dolan, C. W. eds., American Concrete Institute, Detroit, 789–811,1993.

- Nielsen MP. Limit analysis and concrete plasticity. Prentice-Hall Inc., Englewood Cliffs, N.J, 1984.

- Razaqpur AG Spadea S. Shear strength of FRP reinforced concrete members with stirrups. J. Compos. Constr. 2014; 19(1), 04014025.

- Razaqpur AG, Isgor BO, Greenaway S, Selley A. Concrete contribution to the shear resistance of fiber reinforced polymer reinforced concrete members. J. Compos. Constr. 2004; 10.1061/(ASCE)1090-0268(2004)8:5(452), 452-460.

- Reineck KH. Ultimate shear force of structural concrete members without transverse reinforcement derived from a mechanical model. ACI Struct. *J.* 1991; 88, (5), 592-602.

- Sabau C, Popescu C, Sas G, Blanksvärd, T, Täljsten B. Axially Loaded RC Walls with Cutout Openings Strengthened with FRCM Composites. J. Compos. Constr. 2018; *22*(6), 04018046.

- Serbescu A, Guadagnini M, Pilakoutas K. Mechanical characterization of basalt FRP rebars and long-term strength predictive model. J. Compos. Constr. 2014; 10.1061/(ASCE)CC.1943-5614.0000497, 04014037.

- Shioya T, Iguro M, Nojiri Y, Akiyama H, Okada T. Shear strength of large reinforced concrete beams. Special Publication. 1990; 118, 259-280.

- Stratford T, Burgoyne CJ. (). Shear Analysis of Concrete with Brittle Reinforcement. J. Compos. Constr. 2003; 7(4), pp. 323-330.

- Sutton MA, Orteu JJ, Schreier HW. Image Correlation for Shape, Motion and Deformation Measurements - Basic Concepts, Theory and Applications." New York: Springer Science+Business Media. 2009.

- Tomlinson D, Fam A. Performance of concrete beams reinforced with basalt FRP for flexure and shear. J. Compos. Constr. 2014; 19(2), 04014036.

- Tureyen AK, Frosch RJ. Shear tests of FRP-reinforced concrete beams without stirrups. Struct. J. 2002; 99(4), 427-434.

- Vecchio FJ, Collins MP. The modified compression field theory for reinforced concrete elements subjected to shear. ACI J. 1986; 83(2), 219–231.

- Yost JR, Gross SP, Dinehart DW. Shear strength of normal strength concrete beams reinforced with deformed GFRP bars. J. Compos. Constr. 2001; 5(4), 268-275

- Zhou P, Goodson KE. Subpixel displacement and deformation gradient measurement using digital image/speckle correlation. Optical Engineering. 2001; 40(8), pp.1613-1621.

Chapter 5

Shear Design Recommendations for FRP RC Beams

On the basics of the remarks and conclusions drawn from the previous Chapters, a new model based on a modified EC2 approach is proposed for the unified design of FRP and steel RC beams. The accuracy of the model is then validated against the FRP RC databases presented in Chapter 2 and the steel RC database recently published in ACI Structural Journal.

The content of this chapter is part of a paper under preparation to be submitted to a peer reviewed research journal.

5.1 Introduction

The analysis of the shear behaviour of FRP RC beams without shear reinforcement presented in Chapter 2 provided evidence that a significant size effect is observed in FRP RC elements. Although different size effect models have been proposed for steel RC beams and have been incorporated directly in current shear design-oriented equations for FRP reinforced elements, these approaches do not capture adequately the experimentally observed behaviour of large beams.

Based on the experimental observations of the strain development in the longitudinal and shear FRP reinforcement, as well as analysis of the cracking behaviour, a new design approach is proposed to determine V_c and V_f. The model controls strain in the FRP flexural and shear reinforcement and is more reliable in determining the individual shear contributions of concrete and FRP shear reinforcement.

5.2 Contribution of concrete

Based on experimental studies on FRP RC beams (Duranovic et al. 1995a; Duranovic 1995b; Duranovic 1997) and FRP RC flat slabs (El-Ghandour et al. 1999a; El-Ghandour et al. 1999b) carried out at the University of Sheffield, it was concluded that current shear design approaches impose unnecessarily conservative strain limits on the FRP reinforcement. It was observed that much higher strain can be developed in FRP bars (reaching values up to 10,000 με), and as a result, some modifications to the strain approach (see §2.5.1) were proposed (e.g. Sheffield Approach). The proposed approach assumed that the equivalent area of longitudinal reinforcement is equal to:

$$A_{eq} = A_{FRP} \cdot \frac{E_{FRP}}{E_s} \cdot \phi_\varepsilon \qquad \text{(Eq. 5-1)}$$

Where the term ϕ_ε is equal to 1.8, which corresponds to the ratio between the maximum allowed strain in the FRP longitudinal reinforcement (conservatively assumed as 4,500 με) and the strain attained at yielding of steel (typically 2,500 με). Further studies (Guadagnini et al. 2003; Guadagnini et al. 2006) confirmed that for

strain levels up to 4,500 με (for both flexural and shear FRP reinforcement) shear cracks are effectively controlled, the additive nature of V_c and V_f is maintained and in general no failure should occur. This design approach was later included in *fib* bulletin 40 (2007) as a modification of the EC2 equation for V_c and proved to approximate the shear behaviour of FRP RC beams without shear reinforcement with a reasonable degree of accuracy (see §2.5.4). However, it can be argued that this strain limit was validated only against small scale specimens with an effective depth of about 250 mm and does not necessarily apply for all beam sizes. In addition, the same size effect parameter as for steel RC was adopted without further examination of its suitability for FRP RC beams.

5.2.1   Effect of member depth on longitudinal strain

Based on the results from the experimental programme reported in Chapter 3, it was observed that the maximum strain values attained in the flexural reinforcement at ultimate decrease with increasing beam depth, and the limit of 4,500 με may not be suitable for larger FRP RC beams without shear reinforcement (see §3.3.3). This indicates that a more reliable model that can account for beam's depth would be more suitable to control strain in the flexural reinforcement, especially when dealing with large specimens.

Chapter 4 concludes that both the longitudinal strains in flexural reinforcement and V_c are a function of beam's size. In addition, although the contribution of concrete after diagonal cracking decreases, this occurs gradually, even at strain levels higher than 4,500 με (Figure 4-15).

Figure 5-1 shows the effect of member depth on the maximum strain that developed in the flexural FRP reinforcement of the beams without shear reinforcement tested as part of this study, as well as beams reported by various researchers. It can be clearly seen that the strain in the flexural reinforcement is size dependent and decreases with increasing effective depth. This can be attributed to the moment-shear interaction and to the fact that, although failure is dominated by the development of critical shear stresses, in taller beams these generally develop at lower values of curvature. Although the proposed limiting strain of 4,500 με seems

to be reasonable for elements with an effective depth smaller than 350 mm and provide conservative predictions, it can lead to an overestimate of the shear capacity of larger elements.
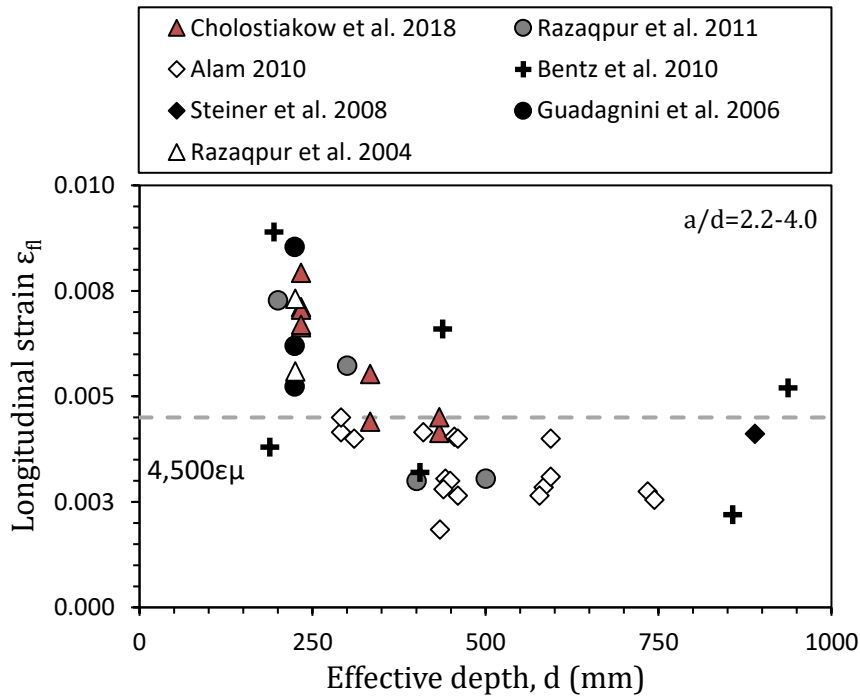
Figure 5-1 Effect of member depth on longitudinal strain in flexural reinforcement

As some of the variability in the strain values reported in Figure 5-1 can be attributed to the different values of a/d, a smaller subset, including only specimens with similar *a/d* ratios (Figure 5-2), was considered when assessing the effect of member's depth on the maximum strain that can be developed in the longitudinal reinforcement at shear failure (Eq. 5-2).

$$\varepsilon_{fl} = \frac{0.504}{d^{0.807}}$$
(Eq. 5-2)

If the strain provided by Eq. 5-2 is normalised by the yielding strain of conventional steel reinforcement (about 2,500 με), Eq. 5-3 is derived.

$$\varepsilon_{fl,norm} = \frac{202.8}{d^{0.807}} \approx \frac{200}{d^{0.8}}$$
(Eq. 5-3)

110
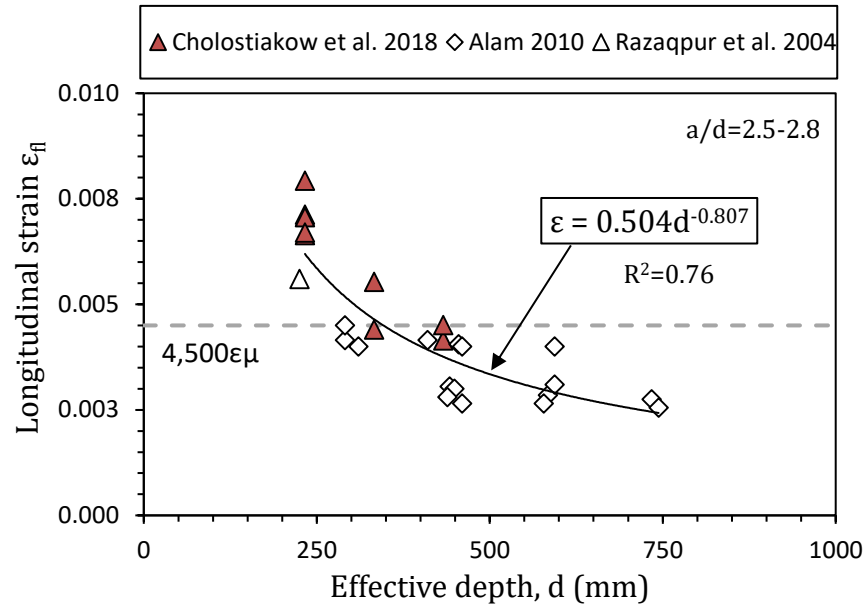
Figure 5-2 Effect of member depth on longitudinal strain in flexural reinforcement of beams with *a/d* ratio ranging from 2.5 to 2.8.

The Eq. 5-6 is derived based on the results form 26 beams: 9 from the present study and 17 from other studies (Razaqpur et al. 2004 and Alam 2010). The correlation between the model and the input variables is measured by R-squared value. The R-squared value of the model showed in Figure 5-2 is equal to 0.76, which means that more than 75 % of the observed variation can be captured by the model.

5.2.2 Design recommendations

Based on the discussion presented in Section 5.2.1, Eq. 5-3 can be adopted to provide a more accurate estimate of the strain values expected to develop in the flexural reinforcement at shear failure. Hence, a modification to the Sheffield Approach (Eq. 5-4) is proposed as shown in Eq. 5-5 to estimate the concrete contribution.

Sheffield Approach:

$$V_c = \left[C_{Rd,c} \cdot k \cdot \left(\frac{0.0045}{0.0025} \right)^{1/3} \left(100 \cdot \frac{A_{fl}}{b_w \cdot d} \cdot \frac{E_f}{E_s} \cdot f_{ck} \right)^{1/3} \right] \cdot b_w \cdot d \qquad \text{(Eq. 5-4)}$$

where $k = \left(1 + \sqrt{\frac{200}{d}} \right) \leq 2.0$

Proposed equation:

$$V_c = \left[C_{Rd,c} \cdot k \cdot k_\varepsilon \left(100 \cdot \frac{A_{fl}}{b_w \cdot d} \cdot \frac{E_f}{E_s} \cdot f_{ck} \right)^{1/3} \right] \cdot b_w \cdot d \qquad \text{(Eq. 5-5)}$$

where $k_\varepsilon = \left(\dfrac{200}{d^{0.8}} \right)^{1/3}$ and $\varepsilon_{fl,norm} = \dfrac{200}{d^{0.8}} \leq \dfrac{0.0045}{0.0025}$

The parameter k_ε uses the experimentally calibrated strain to account for the effect of size on various parameters, such as moment-shear interaction and cracking, and the development of shear resisting mechanisms. In keeping with the recommendation of the Sheffield Approach, the maximum strain that can be developed in FRP flexural reinforcement, ε_{fl}, is conservatively limited to a value of 4,500 με, which results in $k_\varepsilon \leq 1.2$. This represents an upper bound for elements having an effective depth smaller than about 350 mm. In other words, this limit assumes that for beams with $d<350$ mm a strain level in the flexural reinforcement corresponding to at least 4,500 με can be attained before failure. For design purposes, the parameter k_ε can be replaced by the following simplified formula:

$$k_\varepsilon = \left(\frac{800}{d} \right)^{1/4} \leq 1.2 \, ; \, (d \text{ in mm}) \qquad \text{(Eq. 5-6)}$$

Figure 5-3 shows a comparison between the way in which size effect is accounted for in the Sheffield Approach (adopted from the current EC2 equation) and in the newly proposed model.
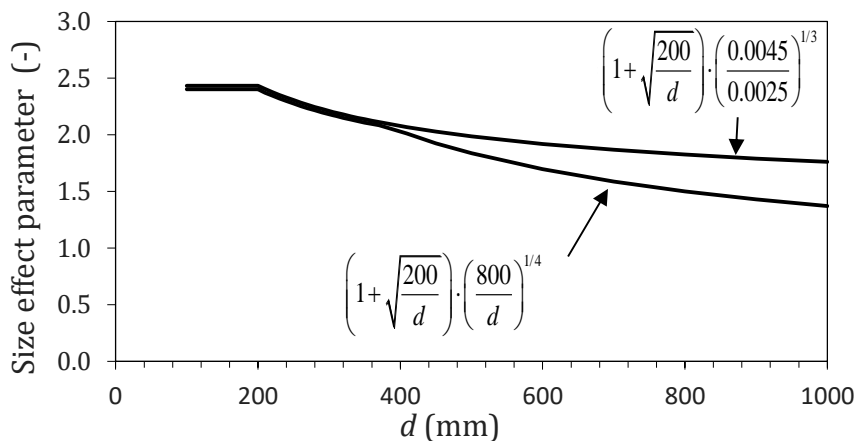
Figure 5-3 Comparison between the proposed size effect parameter and that adopted for the shear design of steel RC according to EC2

The strain factor recommended in the Sheffield approach is included to ease the comparison between the two models. It can be seen that, in line with the discussion presented in Section 2.4 and 5.2.1, the value of the proposed parameter decreases at a faster rate than that adopted in the current adaptation of the EC2 model. It is clear that the use of the proposed parameter would yield consistently lower predictions for beams with a depth larger than about 350mm and, as discussed in the next section, better approximate the experimental results.

5.2.3 Validation of the proposed approach with database

The performance of Eq. 5-5 in predicting V_c was verified against a subset of 216 FRP RC beams without shear reinforcement having a/d ratios ranging from 2.5 to 4.5 (see § 2.3). Table 5-1 compares the performance of the proposed model with that of the approaches evaluated in Chapter 2 in terms of mean value, standard deviation, variation, and COV.

Table 5-1 Statistical performance of the proposed model and various shear design-oriented models – beams without shear reinforcement

Design provision	AVERAGE		SD		VAR		COV (%)	
	All	d > 400mm	All	d > 400mm	All	d > 400mm	All	d > 400mm
JSCE-97	1.33	1.33	0.29	0.21	0.08	0.05	21.5	16.0
BISE-99	1.39	1.26	0.30	0.20	0.09	0.04	21.4	16.1
CNR-DT 203/06	0.90	0.91	0.23	0.22	0.05	0.05	25.6	24.3
fib bulletin 40	0.89	0.86	0.19	0.14	0.04	0.02	21.4	16.2
ISIS M03-07	1.88	1.85	0.57	0.61	0.32	0.38	30.2	33.0
Hoult et al. 2008	0.95	0.84	0.26	0.17	0.07	0.03	27.2	20.2
CSA S806-12	0.93	0.87	0.19	0.16	0.04	0.03	20.3	19.0
CSA S6-2014	1.35	1.14	0.39	0.26	0.15	0.07	28.9	23.2
ACI 440 1R-15	1.83	1.55	0.44	0.32	0.19	0.10	23.9	20.7
Eq.5-5	**0.91**	**0.95**	**0.19**	**0.14**	**0.04**	**0.02**	**21.1**	**14.7**
Eq.5-5 ($C_{Rd}=0.16$)	**1.02**	**1.06**	**0.22**	**0.16**	**0.05**	**0.02**	**21.1**	**14.7**

Figure 5-4 and Figure 5-5 illustrate the performance of the Sheffield Approach and the proposed model (Eq. 5-5), respectively. Eq. 5-5 predicts the shear resistance of larger elements (with d greater than 400) with a higher degree of accuracy and

reduced COV (from 16.2% to 14.7%). It is worth noting that, although the average experimental-to-theoretical ratio did not improve significantly, this value can be easily calibrated (e.g. by adjusting C_{Rd}, see Table 5-1 and Figure 5-6).
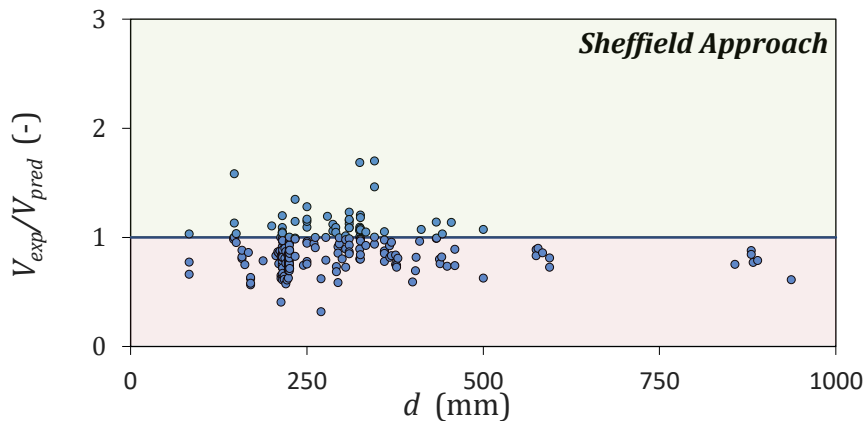
Figure 5-4 Predictions of the experimental values according to Sheffield Approach (*fib* 2007)
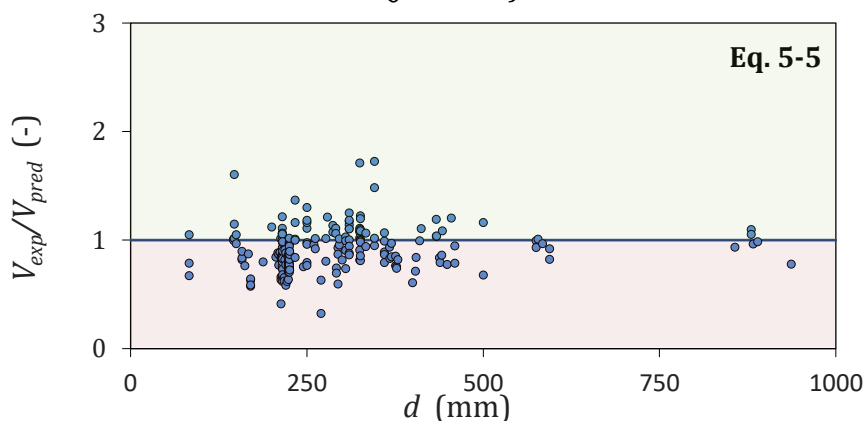
Figure 5-5 Predictions of the experimental values according to the proposed model (Eq. 5-5)
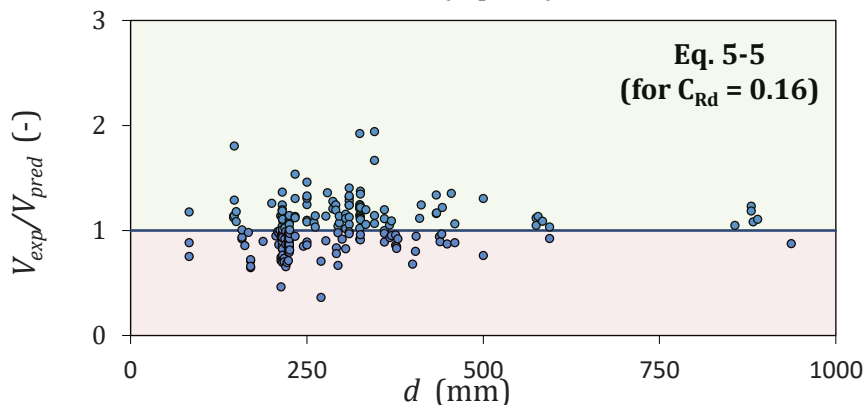
Figure 5-6 Predictions of the experimental values according to the proposed model (for $C_{Rd} = 0.16$)

5.2.4 Validation of the proposed model against steel RC beams

Eq. 5-5 may be also used to improve shear predictions for steel RC beams. Figure 5-7 and Figure 5-8 show the performance of the shear model for steel RC beams according to the current version of EC2 and the approach proposed in Eq. 5-5, respectively, based on a subset of data (a/d ranging from 2.5 to 4.5) collected by Reineck et al. (2013).
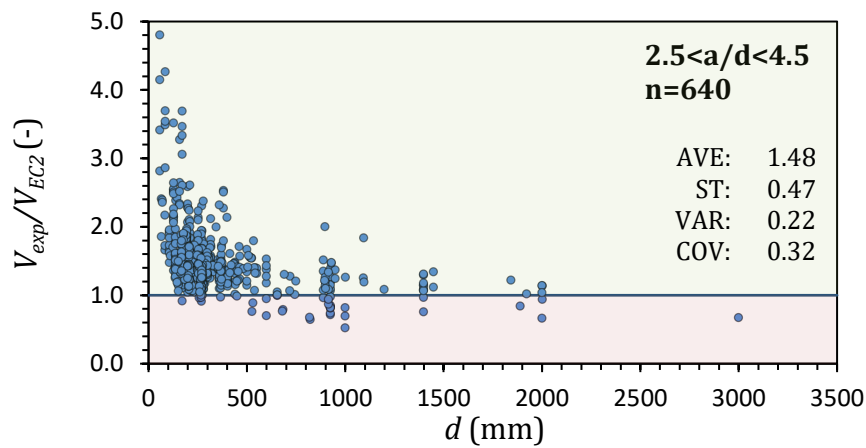
Figure 5-7 Predictions of the experimental values using EC2 provisions
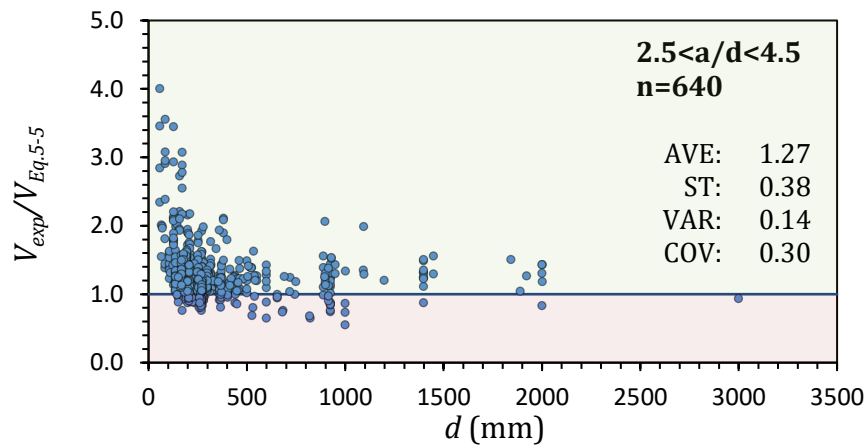
Figure 5-8 Predictions of the experimental values using Eq. 5-5

As can be seen, the implementation of the factor k_ε, which provides an additional way to account for the effect of size on the development of shear resisting mechanisms based on the strain demand on the flexural reinforcement, reduces the COV by 2% and produces safer estimates for very large elements ($d>1000$mm). In addition, it can be clearly seen that such approach improves also the variability in the predictions for beams with $d<500$ mm.

In the case of conventional steel reinforcement, the high strain that develops beyond yielding at the section subjected to maximum moment does not propagate as rapidly into the shear span as for FRP RC beams. As a result, the shear transfer mechanisms mobilised along the shear span are expected to be less affected by the more localised strain demand on the flexural reinforcement and higher maximum strain can be developed at shear failure. This can often be the case for small, shear-deficient beams subjected to high moments. If the upper cap previously set to 4,500 $\mu\varepsilon$ for FRP RC beams with *d* smaller than about 350mm reinforcement is removed, Eq. 5-5 seems to yield less conservative and more consistent predictions for steel RC beams within this lower depth range (Figure 5-9). When the entire set of data is considered, Eq. 5-5 is affected by a COV=24% (32% for EC2).
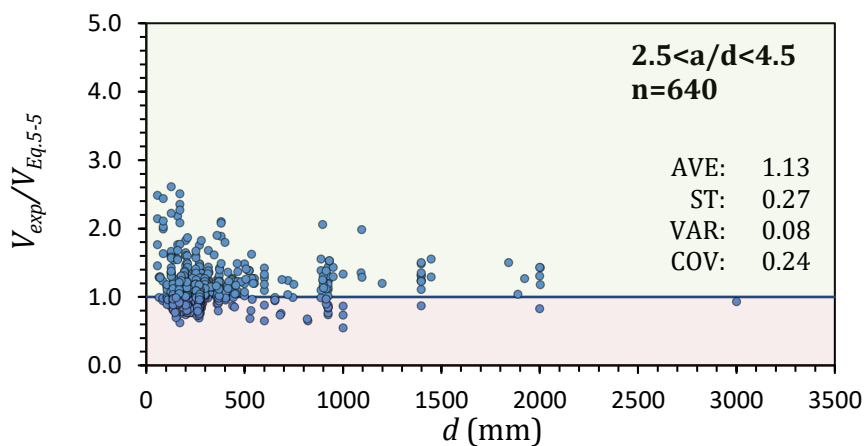
Figure 5-9 Predictions of the experimental values using Eq. 5-5
(k_ε without the upper cap)

These results clearly show that there is a scope for introducing the use of the proposed strain factor also in the design of steel RC beams, and that the proposed approach can improve predictions not only in the case of larger elements but also for smaller elements. However, more work is required to confirm these observations.

5.3   Contribution of shear reinforcement

The experimental studies carried out on FRP RC beams with shear reinforcement (Maruyama and Zhao 1994; Duranovic et al. 1997; Guadagnini et al .2006; Issa et al 2016; Lee et al. 2016; Johnson and Sheikh, as well as the work presented herein) showed that the strain levels that are typically attained in shear reinforcement at failure can be substantially larger (up to 4 times) than that considered by current FRP design guidelines (Figure 2-9 in §2.4). These conservative strain limits are imposed to ensure the integrity of all shear resisting mechanisms and to guarantee the validity of the assumption that V_c and V_f can be added. As a result, however, most of the shear models, even if accurate in predicting V_c, tend to underestimate V_f and yield overall conservative predictions (see § 2.5.5).

The analysis presented in Figure 4-14 clearly shows that, even when using the minimum amount of reinforcement, a larger average strain is mobilised in the shear links, and considerable amount of concrete contribution is still effectively mobilised (more than 75 %), and the additive nature of V_c and V_f can be still maintained.

Figure 4-14 also shows that wider shear cracks can be observed in larger beams and this affects both V_c and V_f. As such, the larger the crack width, the smaller the contribution of V_c and the greater the contribution of V_f at ultimate (i.e. the larger crack widths developed in larger elements would result into larger strain being mobilised in the shear reinforcement –see Figure 4-7, Figure 4-8 and Figure 4-9).

Hence, a model that could account for a more accurate distribution of strain along the links bridging the failure shear crack would lead to a more realistic assessment of the magnitude of the shear resisting components. Such a model could be based on the implementation of an average design strain value and a parameter accounting for the effect of beam depth on crack width.

5.3.1   Effect of member's depth on strain in shear reinforcement

Figure 5-10 shows the effect of the beam's effective depth on the average strain measured in the shear reinforcement. The average strain was determined from the experimental strain values measured in the links that effectively bridged the critical

shear crack at failure. In order to focus solely on the effect of member's depth and to exclude the influence of different shear reinforcement configurations, only the specimens having a similar range of a/d and $E_{fw}\rho_{fw}$ were considered. As can be seen, the average strain in the shear links increases with increasing effective depth as described by Eq. 5-7.

$$\varepsilon_{fw,ave} = 0.0013d^{0.33} \approx 0.001d^{0.33}$$ (Eq. 5-7)
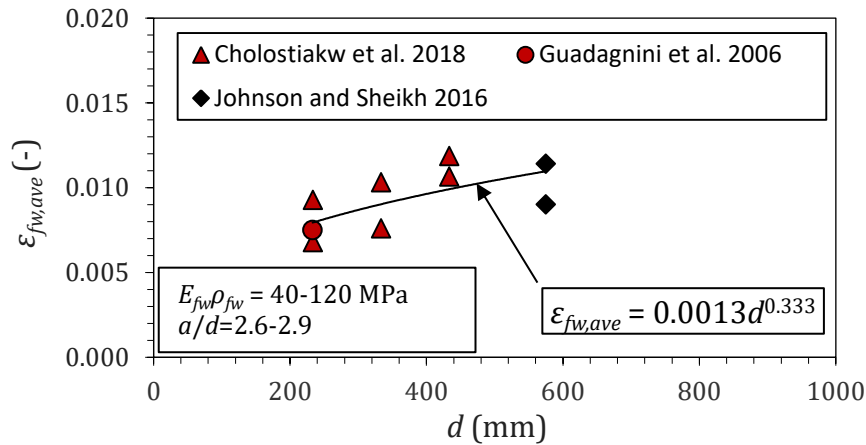
Figure 5-10 Effect of member's depth on the average strain in shear reinforcement

5.3.2 Design recommendations

Based on the discussion presented in the preceding sections, a new design approach for the shear resistance of FRP RC beams with shear reinforcement is proposed. Following the concept of levels of approximation introduced in Model Code 2010, two approximation levels are defined, yet still implementing the proven truss analogy approach (Eq. 5-8).

$$V_f = \frac{A_{fv}f_{fv}z}{s}\cot\theta$$ (Eq. 5-8)

where f_{fv} is the maximum allowable design stress level in FRP shear links, which shall not be taken more than the strength of the bent portions of the links (Eq. 5-9).

$$f_{fb} = \left(0.05\frac{r_b}{d_s} + 0.3\right)f_{fu} \le f_{fu}$$ (Eq. 5-9)

Level I

The total shear resistance is determined as V_c+V_f, where V_c is given by the newly proposed Eq. 5-5, which includes a more accurate estimate of size effect in FRP RC beams, and V_f by Eq. 5-8. The maximum allowable design strain that can be developed in the shear links is conservatively taken as that previously proposed in the *fib*/Sheffield Approach (i.e. 4,500 με) and the angle of inclination of the strut is considered to be fixed at 45° (i.e. $\cot\theta=1$).

Level II

The total shear resistance is still determined as V_c+V_f and the angle of inclination of the strut is still considered to be fixed at 45° (i.e. $\cot\theta=1$). V_c is again determined according to Eq. 5-5, whilst the maximum allowable design strain that can be developed in the shear links (Eq. 5-10) relies on a less conservative estimate of average strain and accounts for the effect of size on crack width and overall distribution of strain in the shear reinforcement.

$$f_{fv} = \frac{\sqrt[3]{d}}{1000} \cdot E_{fw} \leq \varepsilon_{fw,\max} \cdot E_{fw} \ (d \text{ in mm})$$
(Eq. 5-10)

Although higher strain values were observed in the tests conducted as part of this research and by other researchers (Figure 5-10), a maximum design strain level of $\varepsilon_{fw,max}$=6,500 με is recommended so as to limit overall damage (e.g. development of cracks that are too large to enable the local transfer of shear stresses or create high transverse forces on the shear reinforcement) and ensure that the contribution of concrete and shear reinforcement are still effectively mobilised and can be relied upon. This strain limit also corresponds to a minimum average strain level experimentally observed in the elements tested within this study.

5.3.3 Validation of the proposed model

The performance of the proposed approach in predicting the total shear resistance was verified against a subset of 93 FRP RC beams with FRP shear reinforcement and *a/d* ratios ranging from 2.5 to 4.5 (see § 2.3). The theoretical total shear resistance was calculated as V_c+V_f, using the two levels of approximations described in the

previous section. Table 5-2 compares the performance of the proposed model with that of the approaches evaluated in Chapter 2 in terms of mean value, standard deviation, variance and COV.

Table 5-2 Statistical coefficients of shear predictions according to the proposed model and various shear design-oriented models

Design provision	AVERAGE		SD		VAR		COV (%)	
	All	d > 400mm	All	d > 400mm	All	d > 400mm	All	d > 400mm
JSCE-97	2.63	2.61	1.22	0.87	1.48	0.76	46.2	33.4
CNR-DT 203/06	0.89	1.06	0.23	0.26	0.05	0.07	25.3	25.0
fib bulletin 40	1.21	1.25	0.24	0.20	0.06	0.04	19.7	15.8
ISIS M03-07	2.50	2.80	0.67	0.62	0.45	0.38	27.0	22.1
CSA S806-12	1.63	1.85	0.42	0.55	0.18	0.30	26.0	29.7
CSA S6-2014	2.21	2.37	0.61	0.38	0.37	0.38	27.5	26.2
ACI 440 1R-15	1.83	1.72	0.35	0.25	0.12	0.06	19.1	14.6
Level I	**1.23**	**1.32**	**0.24**	**0.21**	**0.06**	**0.04**	**19.7**	**15.7**
Level II	**1.09**	**1.14**	**0.21**	**0.17**	**0.04**	**0.03**	**19.5**	**15.3**

The proposed approach (Figure 5-11 and Figure 5-12) produces a mean value of experimental-to-theoretical ratio of 1.23 and 1.09 for approximation Levels I and II, respectively. Although only relatively small improvement in terms of COV is achieved when Level I and II are used, the new approach is more accurate in approximating the relative contributions of V_c and V_f (see also Table 5-1). The performance of the proposed model improves predictions for large elements when Level II is adopted, reducing COV to 15.3%. This also supports the observation that shear resisting mechanisms can be sufficiently mobilised even at higher strain levels than those proposed by current design guidelines, and that an approach that relies on the additive nature of V_c and V_f can still be used in design.

Although the proposed value of $\varepsilon_{fw,d}$ provides reasonable estimates of the strength developed in beams with different depths, this is based on a database including a limited number of large beams and should be re-assessed when more data becomes available.
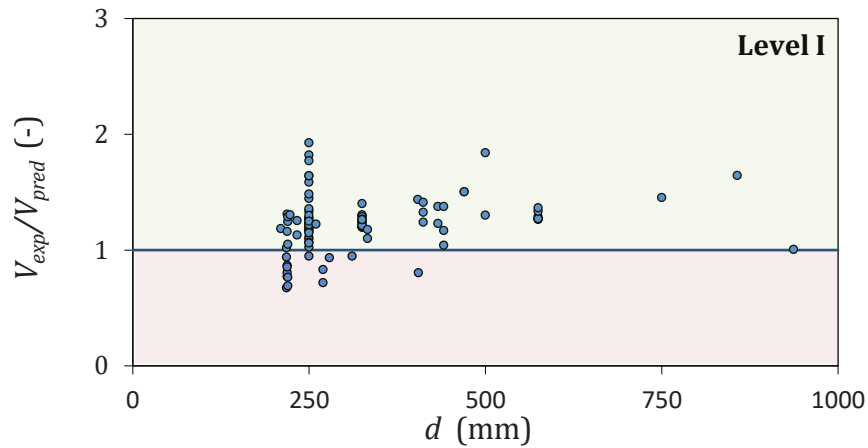
Figure 5-11 Predictions of the experimental values using Level I approximation
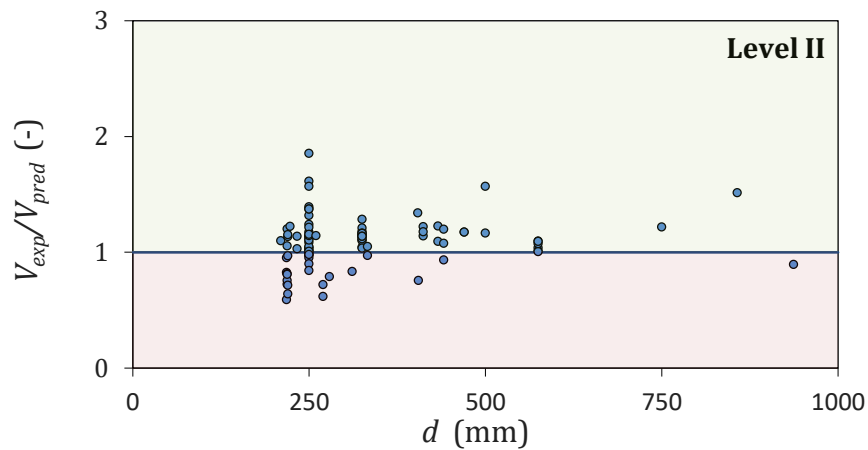
Figure 5-12 Predictions of the experimental values using Level II approximation

5.4 Discussion

In accordance to most current design guidelines, both Levels I and II assume the simple concept of a fixed strut angle (θ=45°) and consider a constant contribution of V_c. However, as discussed in Chapter 4, the contribution of V_c was found to decrease with increasing strain level in the shear reinforcement as the increased level of damage can affect some of the concrete shear transfer mechanisms (notably the aggregate interlock). Although this simplistic approach can still yield conservative results, the models do not allow a reliable estimate of the relative contribution of the two main shear resisting components and tend to underestimate the contribution of the shear reinforcement (more links are effectively mobilised than estimated through the implementation of a 45° truss) and overestimate the

contribution of concrete. In addition, owing to concrete's natural variability, the geometry of shear cracks is difficult to determine analytically and the typical assumption that one single angle can be used to describe the crack geometry and determine the number of links effectively bridging the main shear crack may not correctly reflect the true utilisation of the shear reinforcement. Figure 5-13 shows the experimental and theoretical contributions of V_c and V_f at an average strain in the links corresponding to 4,500 με. Although the experimental evidence showed that 3 links were always engaged in resisting shear (albeit providing different contributions), For a fixed inclination of the concrete strut of 45 ° and a link spacing of 0.5d (as used in the experimental programme) the single shear crack would cross, and effectively engage, only two links and the resulting total shear resistance ($V_{c,100\%}$ + $V_{f,cot(\theta=45°)}$ at 4,500 με) would correctly predict the applied shear load at that strain level but underestimate the maximum shear capacity.

When Level II approximation is implemented and larger stain values are allowed to develop in the shear links (e.g. 6,500 με in the case of beam GB64), a better approximation of the contribution of the shear links at ultimate is achieved but the total shear resistance is still slightly underestimated, with an experimental-to-theoretical ratio equal to 1.05. Although the total shear capacity is adequately predicted, the ability of the model to capture the relative contribution of the shear resisting mechanisms is limited by the use of a fixed strut angle and a maximum allowable strain that can be developed in the shear reinforcement. A better approximation of the contribution of the shear reinforcement would be achieved by considering a more accurate estimate of both strain developed at failure (e.g. 7,600με in the case of beam GB64) and number of contributing links (i.e. correct strut angle inclination). Experimental evidence shows that, in the case of GB64, three shear links contributed to V_f, the number of which would be more accurately estimated by using theoretical angles ranging from 32° to 40° (see Figure 5-13). This however, would lead to an increase in V_f (in comparison to the value estimated in Level II) and an un-conservative estimate of total shear capacity, if V_c was taken as a constant value as determined in Level I and II. Hence, a more refined level of approximation (Level III) should also include provisions to estimate the degradation

of concrete shear resistance, ΔV_c, so as to lead to better overall predictions and more reliable estimate of the main carrying mechanisms.
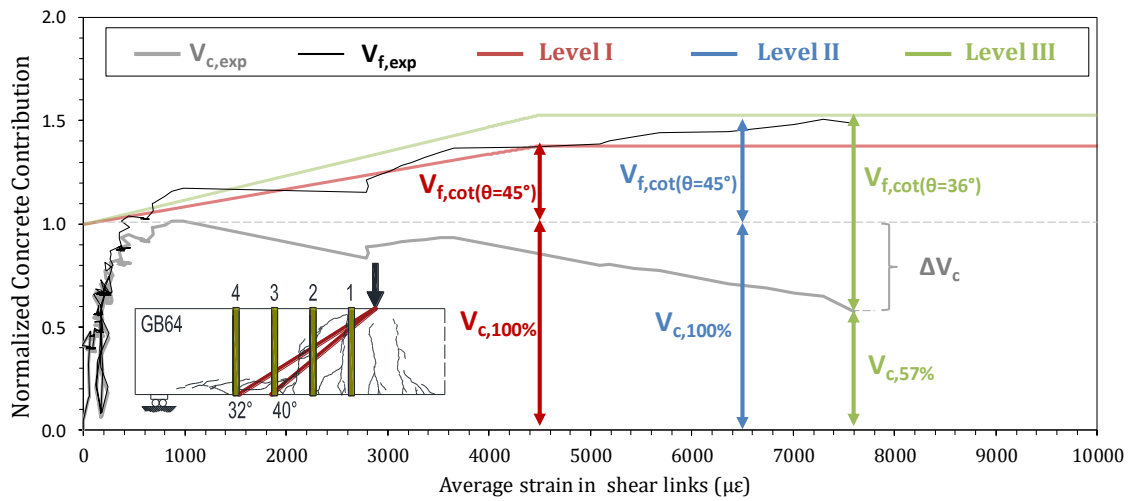
Figure 5-13 Experimental and theoretical contributions of V_c and V_f at different average strain values (Beam GB64)

Additional work needs to be carried out, however, before a model to estimate the degradation of concrete contribution can be proposed. Such model should consider the interaction between concrete and shear reinforcement and estimate the degradation of the concrete shear contribution as a function of shear reinforcement mechanical ratio ($E_{fw}\rho_{fw}$) and ultimate strain level (see also Figure 5-14).
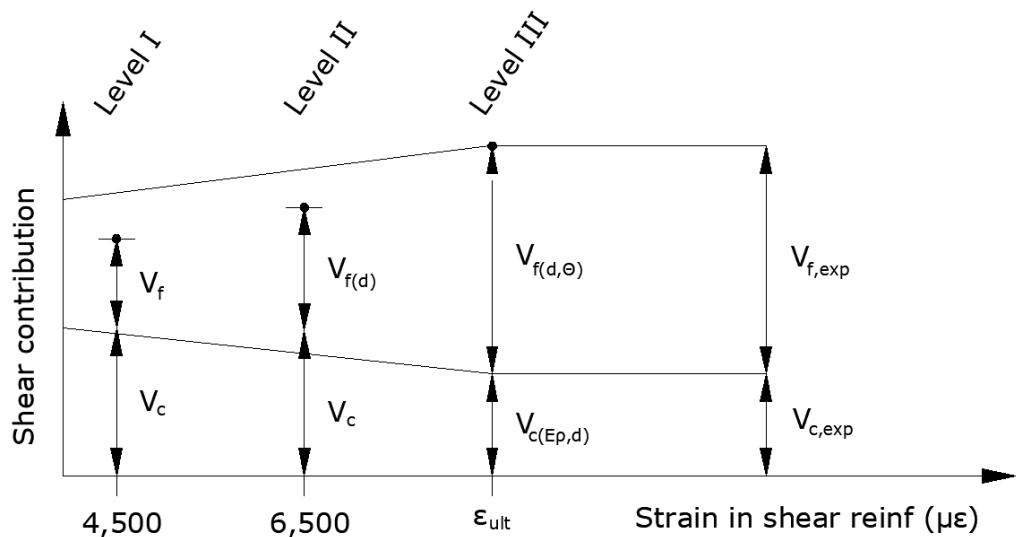
Figure 5-14 Model's accuracy in predicting V_c and V_f

5.5   Concluding remarks

A unified equation for calculating V_c is proposed. The new approach introduces a new factor to account for the effect of member's depth on the development of shear resisting mechanisms based on the strain demand on the flexural reinforcement and can predict shear resistance of FRP/steel RC beams with a higher degree of accuracy than current shear design provisions.

In addition, a new approach to determine the allowable stress level in FRP stirrups/links is recommended. This approach can account for the fact that larger cracks can develop in larger elements, thus affecting the contribution of shear reinforcement (i.e. larger strain).

The proposed model better approximates the experimental contributions offered by concrete and shear reinforcement to total shear resistance.

5.6   References

- Alam, M. "Influence of different parameters on shear strength of FRP reinforced concrete beams without web reinforcement." PhD Thesis., Memorial University of Newfoundland, 2010.

- Bentz, E. C., Massam, L., and Collins, M. P. (2010). "Shear strength of large concrete members with FRP reinforcement." J. Compos. Constr., 10.1061/(ASCE)CC.1943-5614.0000108, 637-646.

- Comité Européen de Normalisation (CEN). (2004). "Eurocode 2: Design of Concrete Structures: Part 1-1: General Rules and Rules for Buildings" EN 1992-1-1, Brussels, Belgium.

- Duranovic N, Pilakoutas K, Waldron P. Tests on concrete beams reinforced with glass fibre reinforced plastic bars. In: Proceedings of FRPRCS-3 Conference. 1997; pp. 479-486.

- Duranovic, N. (1995a). "Beam tests - GB1 - SB4, EUROCRETE Project, Internal progress report." CCC/95/19A, University of Sheffield, Sheffield.

- Duranovic, N. (1995b). "Beam tests - GB5 - SB8, EUROCRETE Project, Internal progress report." CCC/95/20A, University of Sheffield, Sheffield.

- El-Ghandour, A. W., Pilakoutas, K., and Waldron, P. (1999a). "Development of Design Guidelines for FRP Reinforced Concrete." Proceedings of the Second Middle East Symposium on Structural Composites for Infrastructure Applications, Hurgada, Egypt, 200-213.

- El-Ghandour, A. W., Pilakoutas, K., and Waldron, P. (1999b). "New Approach for the Punching Shear Capacity Prediction of FRP RC Flat Slab." Fourth International Symposium Fiber Reinforced Polymers for Reinforced Concrete Structures (FRPRCS-4), Baltimore (USA), 135-144.

- Guadagnini M, Pilakoutas K, Waldron P. Shear resistance of FRP RC beams: Experimental study. J. Compos. Constr. 2006; 10.1061/(ASCE)1090-0268(2006)10:6(464), 464-473.

- Issa MA, Ovitigala T, Ibrahim M. Shear Behavior of Basalt Fiber Reinforced Concrete Beams with and without Basalt FRP Stirrups. J. Compos. Constr. 2015, 20(4), 04015083.

- Johnson, David T., and Shamim A. Sheikh. "Experimental Investigation of Glass Fiber-Reinforced Polymer-Reinforced Normal-Strength Concrete Beams." ACI Structural Journal 113, no. 6 (2016): 1165.

- Maruyama, K., and Zhao, W. J. (1994). "Flexural and Shear Behaviour of Concrete Beams Reinforced with FRP Rods." Corrosion and Corrosion Protection of Steel in Concrete, University of Sheffield, UK, 1330-1339.

- Razaqpur, A. G., Isgor, B. O., Greenaway, S., and Selley, A. (2004). "Concrete contribution to the shear resistance of fiber reinforced polymer reinforced concrete members." J. Compos. Constr., 10.1061/(ASCE)1090-0268(2004)8:5(452), 452-460.

- Razaqpur, A. G., Shedid, M., and Isgor, B. (2010). "Shear strength of fiber-reinforced polymer reinforced concrete beams subject to unsymmetric loading." *J. Compos. Constr.*, 10.1061/(ASCE)CC.1943-5614.0000184, 500-512.

- Reineck, Karl-Heinz, Evan C. Bentz, Birol Fitik, Daniel A. Kuchma, and Oguzhan Bayrak. "ACI-DAfStb Database of Shear Tests on Slender Reinforced Concrete Beams without Stirrups." ACI Structural Journal 110, no. 5 (2013).

- S Cholostiakow, M Di Benedetti, K Pilakoutas, M Guadagnini (2018). Effect of Beam Depth on Shear Behavior of FRP RC Beams. J. Compos. Constr., 10.1061/(ASCE)CC.1943-5614.0000914.

- Steiner. S.; El-Sayed, A. K. and Benmokrane, B. (2008), "Shear Behaviour of Large Size Concrete Beams Reinforced with Glass I'RP Bars," CSCE Annual Conference, Qucbcc, Canada, June 10-13.

Chapter 6

Conclusions and Recommendations for Future Research

This section summarises the main conclusions drawn from each chapter. In addition, some recommendations for future work are proposed.

6.1   Conclusions

The aim of this project was to contribute to the understanding of how beam's depth affects overall shear capacity and the relative contributions of the shear resisting components in FRP RC beams and to develop more reliable shear design provisions for RC beams. Several objectives were set to achieve the aim and all of them have been accomplished during the project. The study evaluated the performance of current FRP shear design-oriented approaches in terms of size effect provisions being used, as well as the accuracy in predicting V_c and V_f for different elements' sizes, based on comprehensive shear database of FRP RC beams (Obj. 1-3). Subsequently, a comprehensive experimental programme designed to focus on the critical range of depths was carried out (Obj. 4). Based on the experimental observations as well as the detailed analysis of strains developed in flexural and shear reinforcement, a new design approach was proposed (Obj. 5-7). The model predicts the shear behaviour of larger FRP RC beams with a higher accuracy than the available design guidelines and codes of practice and reflects the individual magnitudes of shear resisting components in a more realistic manner. On the basics of the discussion and findings presented in Chapters 2-5, the major conclusions are presented hereafter.

6.1.1   Review of shear design models for FRP RC beams (Obj. 1-3)

A comprehensive database including FRP RC beams with and without shear reinforcement was presented and the performance of existing design-oriented models for FRP RC beams was evaluated. The following conclusions were drawn:

- The analysis of a large database including both FRP RC beams (collected as part of this research) and steel RC beams (available in the literature) confirms the hypothesis that size effect is more pronounced in FRP RC beams than in steel RC beams. Current design provisions, however, cannot accurately capture this behaviour and still rely on size effect provisions that were originally developed for steel RC.

- Current shear design-oriented models predict the shear resistance of FRP RC beams without shear reinforcement with non-uniform margins of safety, which

in case of ISIS M03-07 and ACI 440.1R-15 models decrease with increasing member's depth. Also these models yield the most conservative estimate of V_c, with average experimental-to-theoretical ratios equal to 1.88 and 1.83, respectively.

- Slightly unconservative predictions of shear capacity are obtained using the shear provisions proposed by *fib* bulletin 40, CNR-DT203/2006, CSA S806-12 and Hoult et al. 2008; however, these models show the lowest variability between the experimental results and predicted values.

- The model incorporated in CSA S806-12 is the most accurate in predicting V_c, with a mean value of V_{exp}/V_{pred} equal to 0.93 and a COV equal to 20.3%. However, it can be argued that this model does not predict the behaviour of the large elements with a sufficient margin of safety (mean=0.87, COV=19% for d>400mm).

- The most conservative predictions for beams with shear reinforcement are achieved using JSCE-97, with a mean value of V_{exp}/V_{pred} equal to 2.49. This suggests that this design approach, although it allows to calculate the strain in the shear reinforcement, greatly underestimates its contribution.

- The best estimate of the shear resistance of FRP RC beams with shear reinforcement, though slightly conservative, is achieved using the provisions given in *fib* bulletin 40, with a mean value of V_{exp}/V_{pred} equal to 1.21 and a standard deviation equal to 0.24.

6.1.2   Experimental programme (Obj. 4-5)

Fifteen tests were performed on FRP RC beams with and without shear reinforcement to investigate their shear behaviour with a specific focus on the effect of beam's depth. The results were compared with current shear predictions to verify their accuracy in terms of predicting overall shear capacity, diagonal cracking load, and size effect. Based on the code comparison as well as the experimental observations of the overall shear behaviour and the initiation and development of shear cracks, the following conclusions can be summarized:

- All tested beams failed in diagonal tension. The depth at which flexural cracks transition to diagonal shear cracks was found to be a function of the overall

depth of the beams. In particular, the taller the beam, the lower the depth of initiation of the diagonal crack.

- As already observed in steel RC beams, crack spacing was confirmed to be a function of beam size, with larger spacing being developed in deeper specimens.

- Beams with FRP external shear links failed in diagonal tension followed by fracture of shear links. For the given minimum shear reinforcement, the critical shear crack was resisted mainly by three shear links, with the links placed in the middle of the shear span usually contributing more than the link closest to the loading point. The links crossing the horizontal splitting crack (closest to the support) had a negligible contribution to overall shear resistance.

- The results confirm that the shear strength of FRP members without shear links is size dependent. On the other hand, no significant size effect was found in beams with shear reinforcement, which appeared to control crack width sufficiently, even when minimum amount of shear reinforcement was provided. Local phenomena (crack width and strain distribution), however, were found to be a function of beam depth and affected the development of shear resisting mechanisms and their relative contribution.

- Current FRP design equations for V_c do not predict the shear strength of FRP RC beams of different sizes with a uniform margin of safety. This safety margins decrease with increasing member's depth.

- The fib and CSA models appear to predict the shear load at which diagonal crack develops (V_{scr}) in beams with shear reinforcement with an acceptable degree of accuracy, with experimental-to-theoretical ratios equal to 0.94 and 0.99, respectively. The ACI equation, however, greatly underestimates the experimental values ($V_{scr}/V_{c,ACI}$ = 1.96).

- The relative contribution of the individual shear resisting mechanisms needs to be re-examined.

6.1.3 Distribution of strain in the flexural and shear reinforcement

The experimentally determined distribution of both horizontal and vertical strain within the shear span of the tested beams was presented and discussed. Based on

detailed DIC and strain gauge measurements, as well as the data reported in other research studies, the following conclusions can be formed:

- The experimental results available in the literature and test results obtained from this study confirm that strain in FRP shear reinforcement largely exceeds the strain limits imposed by the current design models; however, these strain values decrease with increasing axial stiffness of the reinforcement. The strain in the shear reinforcement is a function of member's depth and, for similar axial stiffness, increases with increasing effective depth.

- A decrease in the maximum strain developed in the flexural reinforcement was observed with increasing member depth. The maximum values measured in the flexural reinforcement ranged from 4,100 με to 7,900 με in beams without shear links and from 8,300 με to 12,000 με in beams with shear links.

- The maximum strain in the shear reinforcement ranged from 9,000 με to 16,800 με for GFRP links and from 6,800 με to 13,500 με for CFRP links.

- As the maximum strain values attained in the flexural reinforcement decrease with increasing beam depth, the limit of 4,500 με appears to be not suitable for larger FRP RC beams without shear reinforcement and leads to an overestimation of V_c.

- Strains measured in different reinforcement layers along the shear span did not change linearly within the beam height as expected from the plane section principle. The strain values recorded at mid-depth of the tested beams were significantly higher than those predicted by beam theory only within the disturbed regions of the beams, which were subjected to a high interaction of shear and bending.

- DIC shows a great potential in capturing strains and crack widths. In addition, DIC allows to measure strain along the shear links using larger base lengths than conventional electrical gauges, thus making the results more reliable.

6.1.4 Analysis of shear resisting mechanisms (Obj. 6)

Based on experimental evidence and critical DIC measurements, the relative contributions of shear reinforcement and concrete were estimated. The main conclusions drawn from this study can be summarized as follows:

- After the development of the critical shear crack, the contribution of concrete decreases gradually as the load increases. The residual contribution of concrete just before failure is a function of beam depth and ranges from about 20 % to 40 % of the beam total shear capacity.

- The analysis of the shear cracks confirms that wider shear cracks can be observed in larger beams and this affects both V_c and V_f. As such, the larger the crack width, the smaller the contribution of V_c and the greater the contribution of V_f at ultimate.

- Even when a large average strain is mobilised in the shear links, a considerable amount of concrete contribution is still effectively mobilised and the additive nature of V_c and V_f can still be assumed in design. The design philosophy included in the latest version of Eurocode 2, which neglects the contribution of concrete whenever shear reinforcement is provided, results in overly conservative predictions.

- For the given minimum shear reinforcement ratio the contribution of V_c was about 75 % (at a strain level in the links corresponding to 4,500 $\mu\varepsilon$). More tests should be carried out to determine the minimum V_c contribution that can be used in design for different shear reinforcement ratios.

- At the strain levels currently allowed by design models, crack widths did not exceed 2 mm and at least 75 % of the initial concrete contribution was still effectively mobilised.

- Although existing design models only consider a constant concrete contribution, a reasonable estimate of total shear capacity, with a reasonable margin of error, can be still obtained when a simplified fixed angle of the concrete strut (45°) is assumed. In case of a model considering a variable strut angle, the contribution of V_c must be adequately modified to reflect the relative contribution of all resisting mechanisms.

6.1.5 Shear design recommendations for FRP RC beams (Obj. 7)

Based on the experimental results and detailed analysis of strain and shear resisting components, the following design recommendations for FRP RC beams and steel RC are proposed:

- The use of an additional size effect parameter, based on the strain demand on longitudinal reinforcement, k_ε, is proposed to more accurately estimate the concrete contribution of FRP RC beams. This parameter takes into account the effect of several aspects, such as moment-shear interaction, cracking behaviour, and NA depth, and better predicts the overall shear capacity of larger FRP RC beams. k_ε can be also directly applied to the current EC2 equation for steel RC beams and reduce the variability of the model by 25%.

- The contribution of the links can be estimated using different levels of approximation suitable for design and analysis. For Level I (design), a strain limit of 0.0045 is maintained; for Level II (analysis), a strain limit of $0.001\sqrt[3]{d} \le$ 6,500 με is proposed.

- Due to the limited experimental data, a fixed, conservative value of the inclination of the concrete strut (45°) and a constant contribution of concrete are recommended for Levels I and II. For Level III a more refined concept, including the use of a variable strut angle as well as variable contributions of V_c and V_f, is suggested.

- The design stress of the shear reinforcement can be limited by the maximum stress that can be developed in the bent corners of the links and this can be estimated using available models.

The findings presented herein help to better understand how the main shear resisting components, as well as strains in flexural and shear reinforcement, are affected by the element's geometry. The results clearly show that strain distribution in both flexural and shear reinforcement is greatly affected by beam's depth, which in turn, can lead to inaccurate predictions of Vc and Vf. Therefore, new strain design limits based on the effective depth should be considered. It is believed that this study will lay a foundation for a new research on size effect, which will closely focus on the strain distribution in FRP RC beams and will lead to a more in-depth understanding on size effect.

6.1.6 Recommendations for future research

On the basis of the findings of this study, the following issues should be further investigated:

- Future experimental work should focus on examining the relative contributions of V_c and V_f in beams with a wider range of flexural and shear reinforcement ratios and a/d ratios.

- The behaviour of beams with a wider range of large effective depths (>500mm) should be examined to assess the influence of cracking on the development and deterioration of shear resisting mechanisms.

- Further experimental work is required to investigate the relationship between the initiation point of the shear crack and beam's effective depth. This parameter is possibly a measure of the effect of both size and moment/shear interaction and could be used to develop more reliable analysis methods.

- The use of a variable strut angle would enable a more accurate estimate of the contribution of the shear reinforcement. The use of an average inclination of the failure crack seems to enable a more reliable estimate of the number of links that are effectively engaged in resisting shear. However, the strut angle to be used in design is not easily determined and it also proves difficult to be measured experimentally. Different shear reinforcement layouts (diameter and spacing of shear links) should be examined to assess the effect of the internal reinforcement on the initiation and development of diagonal cracking. Detailed DIC measurements could be used to examine the kinematics of the shear crack to determine its local evolution (e.g. relative contributions of mode I and mode II crack opening) and enable a more reliable assessment of existing theoretical approaches and numerical models (e.g. rotating crack theory). This could also yield invaluable data that can be used to assess shear transfer across cracks (i.e. aggregate interlock and friction).

- The strain distribution in the disturbed regions (i.e. across the shear cracks) warrants further studies. In this research, the distribution of strain along the height of the beams was measured using small diameter, low stiffness reinforcing bars fitted with strain gauges. Although interesting data was

134

obtained, the measurements are local and very much affected by the relative location of the cracks. While DIC cannot assist in this task, the use of a fibre optic system could help in capturing the real distribution of internal strain and assist in improving current understanding of the behaviour of elements subjected to a combination of high moment and shear forces and characterised by the formation of large disturbed regions (e.g. deep elements, transfer beams). A more in-depth understanding of strain distribution in disturbed regions could also help to validate the performance of existing shear models based on the strain effect (e.g. Hoult et al. 2008, CSA S6-14) or develop new, refined models.

- Although the same a/d ratio was maintained for the test shear-span of all specimens, the relative stiffness of the shear spans appears to affect overall performance and relative shear strength. Such behaviour has not been reported in previous literature and could be a result of material's natural variability but requires further investigation.

- Eq. 5-5 approximates the shear resistance of steel RC beams significantly better if no upper limits to k_ε are applied. However, this implies that considerably large strain may be potentially attained in the flexural reinforcement, which may result in flexural failure prior to shear failure. Hence, further experimental investigation should focus on examining shear-bending interaction and its effect on strain in flexural reinforcement.

Page intentionally left blank.

Appendix A

Database of FRP RC Beams without Shear Reinforcement

This database collects the main experimental results from the tests performed on the FRP reinforced concrete beams without shear reinforcement. This appendix includes the results of the code comparison discussed in Chapter 2 for the elements with shear span-to-depth-ratio ranging from 2.5 to 4.5. The full database can be downloaded under the following URL: **https://doi.org/10.15131/shef.data.5057527.v1**

Appendix A: *Database of FRP RC beams without shear reinforcement*

Beam	d (mm)	V_{exp} (kN)	$V_{exp}/$ V_{JSCE}	$V_{exp}/$ V_{BISE}	$V_{exp}/$ V_{CNR}	$V_{exp}/$ V_{fib}	$V_{exp}/$ V_{ISIS}	$V_{exp}/$ V_{Hoult}	$V_{exp}/$ V_{CSA} $S806$	$V_{exp}/$ $V_{CSA\ S6}$	$V_{exp}/$ V_{ACI}	$V_{exp}/$ $Eq5\text{-}5$
A1	83	20.0	1.05	1.23	0.57	0.66	1.23	0.81	0.67	0.83	1.65	0.67
A5	83	25.0	1.32	1.54	0.67	0.77	1.40	0.86	0.76	0.94	1.96	0.78
A9	83	36.0	1.90	2.22	0.89	1.03	1.80	0.79	0.97	1.20	2.66	1.05
S6-0.24-1B	146	33.0	1.46	1.62	1.03	1.00	2.43	0.83	1.09	1.82	2.19	1.01
S6-0.24-2B	146	32.5	1.43	1.60	1.01	0.98	2.39	0.72	1.08	1.78	2.16	1.00
S6-1	147	28.6	1.58	1.85	0.91	1.00	1.87	0.70	1.00	1.29	2.51	1.01
S6-2	147	36.8	2.31	2.56	1.68	1.58	3.29	0.67	1.67	2.27	3.81	1.60
S6-3	147	26.3	1.65	1.83	1.20	1.13	2.35	0.78	1.19	1.62	2.72	1.15
G01	150	33.1	1.51	1.68	1.42	1.03	3.12	0.54	1.26	1.82	2.31	1.05
G02	150	36.3	1.39	1.54	1.21	0.95	3.09	0.73	1.18	1.80	2.06	0.96
GFRP1	158	27.0	1.18	1.31	0.92	0.81	1.80	0.90	0.95	1.24	1.89	0.82
GFRP2	158	28.0	1.20	1.33	0.92	0.82	1.82	0.94	0.96	1.26	1.93	0.83
GFRP3	158	29.0	1.29	1.43	1.03	0.88	1.99	1.25	1.05	1.37	2.06	0.89
Beam 7	162	17.5	1.10	1.29	0.80	0.75	2.02	1.00	0.94	1.25	1.72	0.76
Beam 1	167	12.5	1.26	1.39	0.94	0.86	1.69	1.18	0.87	1.14	2.15	0.87
I	170	12.7	0.91	1.01	0.83	0.62	1.79	0.98	0.78	0.92	1.30	0.63
II	170	13.7	0.83	0.92	0.78	0.57	1.93	0.69	0.73	0.73	1.13	0.57
III	170	14.2	0.92	1.02	0.77	0.63	1.73	0.66	0.80	0.97	1.34	0.64
IV	170	15.4	0.84	0.94	0.72	0.58	1.88	0.85	0.74	0.77	1.17	0.59
S20-0	188	74.0	1.15	1.27	0.99	0.79	2.64	1.04	1.00	1.35	1.62	0.80
B1	200	64.0	1.68	1.96	0.80	1.10	1.50	0.63	1.27	1.80	2.56	1.12
B-3.3-R5	206	30.0	1.24	1.43	0.83	0.83	2.11	0.93	0.94	1.36	1.77	0.84
B-3.3-R4	209	28.0	1.29	1.49	0.86	0.87	1.94	0.63	0.97	1.54	1.93	0.88
GB2	210	26.0	1.25	1.37	0.94	0.85	2.17	0.84	1.00	1.52	1.84	0.87
GB6	210	22.0	1.11	1.22	0.88	0.76	1.97	1.11	0.89	1.21	1.62	0.77
Beam 3	212	17.5	1.28	1.40	1.08	0.88	2.03	0.58	0.91	1.30	2.07	0.89
Beam 9	213	27.5	1.47	1.68	1.07	1.00	2.41	0.89	1.06	1.54	2.32	1.01

C-L-18-R3-1,2	214	15.3	0.59	0.65	0.37	0.41	0.74	0.81	0.45	0.37	0.80	0.41
C-L-27-R3-1,2	214	26.2	0.95	1.04	0.56	0.65	1.15	0.84	0.72	0.78	1.30	0.66
G-L-18-R3-1,2	214	15.3	0.91	0.99	0.71	0.62	1.41	0.79	0.66	0.87	1.42	0.63
G-L-27-R3-1,2	214	21.5	1.21	1.32	0.88	0.83	1.82	0.73	0.87	1.30	1.91	0.84
C-2.5-R1	215	35.4	1.45	1.58	0.79	0.99	1.35	0.62	0.95	1.53	2.14	1.00
C-2.5-R2	215	25.2	1.25	1.36	0.73	0.85	1.28	0.80	0.83	1.13	1.78	0.87
C-2.5-R3	215	26.1	1.06	1.15	0.68	0.72	1.32	0.94	0.71	0.81	1.42	0.73
G-2.5-R1	215	25.7	1.52	1.66	1.00	1.04	1.71	0.89	0.95	1.34	2.60	1.06
G-2.5-R2	215	24.4	1.75	1.91	1.23	1.20	2.17	0.78	1.11	1.70	2.87	1.21
G-2.5-R3	215	27.2	1.60	1.74	1.23	1.09	2.39	0.81	1.04	1.90	2.42	1.11
C-3.5-R1	215	29.5	1.21	1.31	0.66	0.82	1.13	0.57	0.93	1.45	1.78	0.84
C-3.5-R2	215	27.0	1.34	1.46	0.78	0.91	1.38	0.81	1.05	1.64	1.91	0.93
C-3.5-R3	215	29.7	1.21	1.31	0.77	0.82	1.50	0.86	0.96	1.24	1.62	0.84
G-3.5-R1	215	25.9	1.54	1.67	1.01	1.05	1.73	0.79	1.00	1.35	2.62	1.06
G-3.5-R2	215	21.2	1.52	1.66	1.07	1.04	1.88	0.83	1.09	1.48	2.50	1.05
G-3.5-R3	215	20.6	1.21	1.32	0.93	0.83	1.81	0.72	0.93	1.44	1.83	0.84
C-4.5-R1	215	26.8	1.10	1.19	0.60	0.75	1.02	0.70	0.96	1.40	1.62	0.76
C-4.5-R2	215	24.7	1.23	1.33	0.71	0.84	1.26	0.67	1.09	1.71	1.75	0.85
C-4.5-R3	215	28.3	1.15	1.25	0.74	0.79	1.43	0.78	1.04	1.37	1.54	0.80
G-4.5-R1	215	20.2	1.20	1.30	0.79	0.82	1.35	0.54	0.78	1.06	2.04	0.83
G-4.5-R2	215	17.3	1.24	1.35	0.87	0.85	1.54	0.73	0.89	1.21	2.04	0.86
G-4.5-R3	215	20.7	1.22	1.32	0.94	0.83	1.82	0.90	1.06	1.44	1.84	0.84
C-L-18-R1-1,2	216	25.8	1.05	1.15	0.54	0.72	0.93	0.94	0.76	1.05	1.59	0.73
C-L-18-R2-1,2	216	18.9	0.94	1.02	0.51	0.64	0.91	1.25	0.68	0.81	1.36	0.65
C-L-27-R1-1,2	216	23.2	0.89	0.97	0.43	0.61	0.76	1.00	0.64	0.79	1.36	0.62
C-L-27-R2-1,2	216	21.1	0.98	1.07	0.51	0.67	0.93	1.18	0.72	0.90	1.44	0.68
G-L-18-R1-1,2	216	20.7	1.30	1.41	0.82	0.88	1.41	0.98	0.75	1.02	2.31	0.90

G-L-18-R2-1,2	216	18.6	1.41	1.53	0.95	0.96	1.69	0.69	0.90	1.22	2.41	0.97
G-L-27-R1-1,2	216	20.4	1.20	1.30	0.71	0.82	1.26	0.66	0.68	0.92	2.16	0.83
G-L-27-R2-1,2	216	20.0	1.42	1.55	0.90	0.97	1.65	0.85	0.88	1.20	2.46	0.98
B-3.3-R3	218	18.6	0.96	1.09	0.60	0.64	1.23	1.04	0.70	0.98	1.49	0.65
B-2.5-R3	218	27.0	0.91	1.04	0.65	0.61	1.79	0.63	0.60	0.63	1.23	0.62
B-3.3-R2	219	23.1	1.34	1.52	0.79	0.90	1.53	0.93	0.90	1.22	2.18	0.91
B-2.5-R2	219	31.6	1.20	1.37	0.80	0.81	2.09	0.63	0.78	1.02	1.67	0.82
TB6B	220	29.2	1.29	1.46	0.89	0.87	2.12	0.84	0.98	1.58	1.89	0.88
B-3.3-R1	220	17.0	1.13	1.29	0.61	0.76	1.12	1.11	0.66	0.90	1.96	0.77
B-2.5-R1	220	19.5	0.86	0.97	0.57	0.57	1.28	0.58	0.55	0.60	1.25	0.58
F-3GF	222	19.5	0.89	0.96	0.70	0.61	1.70	0.89	0.65	0.79	1.31	0.62
GB43	223	27.2	1.23	1.33	0.90	0.84	2.07	0.81	0.93	1.42	1.79	0.85
5a,b,c-37-NS	224	47.4	1.16	1.25	0.90	0.79	2.37	0.84	0.98	1.38	1.61	0.80
6a,b,c-37-NS	224	42.2	1.11	1.20	0.89	0.76	2.35	0.79	0.94	1.26	1.53	0.77
5FRPa	224	37.7	0.92	0.99	0.72	0.63	1.88	0.73	0.77	0.94	1.27	0.63
5FRPb	224	51.0	1.24	1.33	0.97	0.85	2.55	0.62	1.05	1.60	1.72	0.86
5FRPc	224	46.6	1.13	1.22	0.89	0.77	2.33	0.80	0.96	1.36	1.57	0.78
6FRPa	224	43.5	1.14	1.22	0.92	0.78	2.41	0.94	0.96	1.34	1.56	0.79
6FRPb	224	42.0	1.10	1.18	0.89	0.75	2.33	0.89	0.93	1.26	1.51	0.76
6FRPc	224	41.3	1.08	1.16	0.87	0.74	2.29	0.78	0.91	1.22	1.48	0.75
3a,b,c-27-HS	224	35.8	1.23	1.39	0.71	0.70	1.86	0.81	0.87	1.20	1.49	0.71
4a,b,c-37-HS	224	46.4	1.22	1.38	0.75	0.69	1.96	0.57	0.86	1.13	1.44	0.70
1FRPa	225	39.0	1.30	1.40	1.00	0.89	2.15	0.81	1.07	1.56	1.94	0.90
1FRPb	225	38.5	1.28	1.38	0.99	0.88	2.13	0.86	1.05	1.54	1.91	0.89
1FRPc	225	36.8	1.23	1.32	0.94	0.84	2.03	0.79	1.01	1.47	1.83	0.85
2FRPa	225	28.1	1.11	1.20	0.86	0.76	2.00	0.83	0.92	1.36	1.61	0.77
2FRPb	225	35.0	1.39	1.49	1.08	0.95	2.49	0.72	1.15	1.80	2.01	0.96

2FRPc	225	32.0	1.27	1.36	0.98	0.86	2.27	0.70	1.05	1.64	1.83	0.88
3FRPa	225	40.0	1.15	1.24	0.89	0.79	2.21	0.67	0.96	1.44	1.63	0.80
3FRPb	225	48.6	1.40	1.51	1.09	0.96	2.68	0.78	1.17	1.94	1.99	0.97
3FRPc	225	44.7	1.29	1.39	1.00	0.88	2.47	0.54	1.08	1.76	1.83	0.89
4FRPa	225	43.8	1.02	1.09	0.79	0.69	1.98	0.73	0.85	1.11	1.43	0.70
4FRPb	225	45.9	1.07	1.15	0.82	0.73	2.08	0.90	0.89	1.20	1.50	0.74
4FRPc	225	46.1	1.07	1.15	0.83	0.73	2.09	0.94	0.89	1.21	1.51	0.74
1a,b,c-26-HS	225	38.0	1.26	1.43	0.72	0.72	1.60	1.25	0.85	1.16	1.63	0.73
2a,b,c-26-HS	225	32.5	1.31	1.48	0.75	0.75	1.83	1.00	0.91	1.32	1.63	0.76
BR1	225	36.0	1.42	1.53	0.65	0.97	1.14	1.18	0.94	1.56	2.18	0.98
BR2/BA2	225	47.0	1.40	1.59	0.70	0.94	1.35	0.98	0.93	1.41	1.97	0.95
BR3	225	47.0	1.36	1.47	0.76	0.93	1.48	0.69	0.93	1.31	1.88	0.94
BR4	225	43.0	1.11	1.20	0.65	0.76	1.36	0.66	0.77	0.90	1.49	0.77
BA3	225	47.0	1.47	1.59	0.79	1.00	1.48	0.85	1.15	1.95	2.08	1.02
BA4	225	38.0	1.19	1.28	0.64	0.81	1.20	1.04	1.04	1.60	1.68	0.82
1a,b,c-26-NS	226	38.1	1.27	1.36	0.97	0.87	2.10	0.63	1.04	1.52	1.89	0.88
2a,b,c-26-NS	226	31.7	1.25	1.34	0.97	0.85	2.25	0.93	1.03	1.63	1.81	0.86
3a,b,c-36-NS	226	44.5	1.29	1.39	1.00	0.88	2.45	0.63	1.08	1.72	1.83	0.89
4a,b,c-46-NS	226	45.3	1.05	1.12	0.81	0.71	2.04	0.84	0.87	1.16	1.47	0.72
GB58	234	37.3	1.97	2.10	1.43	1.35	2.82	1.11	1.29	2.19	2.99	1.37
GB58R	234	34.4	1.68	1.88	1.12	1.14	2.30	0.58	1.09	1.79	2.59	1.16
GB59R	234	30.2	1.48	1.65	0.96	0.99	1.98	0.89	0.95	1.54	2.25	1.01
GB58-0	234	28.4	1.44	1.56	1.00	0.98	2.02	0.81	0.94	1.57	2.21	1.00
GB59-0	234	25.1	1.23	1.38	0.80	0.83	1.65	0.84	0.79	1.27	1.87	0.84
NC	245	29.2	1.16	1.29	0.66	0.74	1.37	0.79	0.93	1.33	1.58	0.75
FN1	250	38.3	1.88	1.97	1.25	1.28	2.19	0.73	1.19	2.28	2.63	1.30
FN2	250	43.8	1.60	1.68	1.09	1.09	2.28	0.62	1.04	1.56	2.11	1.11
FN3	250	48.3	1.68	1.76	1.19	1.15	2.62	0.80	1.09	1.63	2.15	1.16

FN4	250	59.1	1.71	1.79	1.17	1.17	2.99	0.94	1.21	1.62	2.13	1.18
No1	250	45.0	1.41	1.48	0.94	0.96	2.18	0.89	1.01	1.35	1.79	0.97
No6	250	46.0	1.14	1.20	0.87	0.78	2.22	0.78	0.95	0.94	1.38	0.79
No15	250	40.5	1.11	1.16	0.77	0.76	1.96	0.81	0.84	0.90	1.36	0.77
No24	250	38.4	1.39	1.45	0.93	0.95	1.91	0.57	0.90	1.23	1.83	0.96
No 1	260	62.2	1.38	1.44	0.89	0.94	1.94	0.81	0.93	1.18	1.73	0.96
Beam 5	262	25.0	1.47	1.52	1.25	1.00	2.35	0.86	0.90	1.55	2.19	1.01
Beam 11	262	30.0	1.33	1.45	0.96	0.91	2.14	0.79	0.82	1.38	1.98	0.92
NT	270	20.6	0.99	1.07	0.48	0.62	0.85	0.83	0.60	0.84	1.43	0.63
NB	270	11.5	0.50	0.55	0.26	0.32	0.48	0.72	0.34	0.32	0.70	0.32
B-300-2	277	32.9	1.47	1.50	0.67	1.00	1.03	0.70	1.02	1.44	2.22	1.01
B-300-4	277	32.9	1.16	1.19	0.64	0.79	1.03	0.67	0.86	1.29	1.62	0.80
BM7	279	53.4	1.75	1.78	1.60	1.19	3.77	0.78	1.14	1.85	2.23	1.21
BM8	287	36.0	1.64	1.66	1.39	1.12	2.47	0.54	1.01	1.85	2.34	1.13
BM9	287	40.0	1.55	1.57	1.36	1.06	2.74	0.73	0.97	1.56	2.09	1.07
G-50	291	75.6	1.79	1.90	1.04	1.09	2.06	0.90	0.97	1.66	2.35	1.11
G-70	291	80.2	1.90	2.02	0.99	1.05	1.88	0.94	0.93	1.52	2.30	1.06
S3-0.24-1B	292	22.0	1.07	1.09	0.76	0.73	1.63	1.25	0.73	0.98	1.47	0.74
S3-0.24-2B	292	20.6	1.01	1.02	0.71	0.68	1.52	1.00	0.69	0.88	1.37	0.69
S3-1	294	15.2	0.93	0.99	0.54	0.58	1.00	1.18	0.53	0.76	1.34	0.59
S3-2	294	19.3	1.34	1.35	0.98	0.91	1.73	0.98	0.88	1.32	2.01	0.93
S3-3	294	18.1	1.26	1.27	0.92	0.86	1.62	0.69	0.83	1.23	1.88	0.87
G-2.5-350(1)	296	65.5	1.38	1.39	1.00	0.94	2.24	0.66	0.84	1.25	1.84	0.95
G-2.5-350(2)	296	70.9	1.46	1.50	1.04	1.00	2.35	0.85	0.89	1.39	1.96	1.01
B2	300	61.0	1.23	1.29	0.55	0.80	0.95	1.04	0.83	1.22	1.72	0.81
G-2.5	305	61.0	1.49	1.48	1.04	1.01	2.03	0.63	0.89	1.56	2.10	1.03
G-3.5	305	43.7	1.07	1.06	0.75	0.73	1.46	0.93	0.76	1.12	1.50	0.74
C-2.5	305	64.6	1.44	1.44	0.78	0.98	1.31	0.63	0.88	1.34	1.91	0.99
C-3.5	305	58.9	1.31	1.31	0.71	0.89	1.20	0.84	0.95	1.47	1.74	0.90

C07N1	310	49.0	1.81	1.80	1.08	1.23	1.99	1.11	1.24	2.22	2.32	1.25
C07N2	310	46.0	1.70	1.69	1.01	1.16	1.87	0.58	1.16	1.99	2.18	1.17
C10N1	310	48.0	1.45	1.48	0.86	0.99	1.81	0.89	1.11	1.63	1.79	1.00
C10N2	310	53.0	1.61	1.63	0.96	1.09	2.00	0.81	1.22	1.94	1.98	1.11
C15N1	310	56.0	1.66	1.64	1.08	1.12	2.38	0.84	1.27	1.92	1.97	1.14
C15N2	310	58.0	1.72	1.70	1.11	1.16	2.47	0.79	1.32	2.04	2.04	1.18
C-0.5-350	310	58.7	1.60	1.62	0.66	1.09	1.06	0.73	0.94	1.52	2.38	1.10
C-2.5-350	310	72.5	1.37	1.36	0.80	0.93	1.45	0.62	0.85	1.14	1.72	0.94
C-50	310	71.6	1.43	1.49	0.60	0.87	1.04	0.80	0.78	1.14	1.75	0.88
C-70	310	77.8	1.55	1.62	0.59	0.85	0.98	0.94	0.76	1.13	1.75	0.86
Beam 4	325	147.0	2.49	2.57	1.31	1.69	1.72	0.89	1.66	3.19	2.97	1.71
Beam 5	325	93.0	1.58	1.63	0.83	1.07	1.67	0.78	1.13	1.62	1.88	1.08
Beam 6	325	78.0	1.32	1.36	0.69	0.89	1.40	0.81	1.10	1.47	1.57	0.91
Beam 8	325	62.0	1.57	1.62	1.00	1.06	2.03	0.57	1.09	1.84	2.12	1.07
Beam 9	325	47.0	1.19	1.22	0.76	0.80	1.54	0.81	0.95	1.39	1.60	0.81
G15N1	325	49.0	1.61	1.58	1.25	1.09	2.76	0.86	1.18	2.10	2.10	1.11
G15N2	325	45.0	1.48	1.45	1.15	1.00	2.54	0.79	1.08	1.80	1.92	1.02
CN-1	326	78.0	1.21	1.24	0.65	0.80	1.33	0.83	0.82	1.02	1.47	0.81
GN-1	326	71.0	1.63	1.68	1.07	1.08	2.19	0.72	1.06	1.63	2.28	1.10
CN-2	326	104.0	1.46	1.49	0.85	0.99	1.83	0.70	1.03	1.39	1.75	1.00
GN-2	326	60.0	1.24	1.26	0.87	0.84	1.89	0.67	0.84	1.25	1.68	0.85
CN-3/CN-1.7	326	125.0	1.58	1.59	0.93	1.07	2.23	0.78	1.12	1.52	1.83	1.08
GN-3/GN-1.7	326	78.0	1.45	1.46	1.03	0.98	2.48	0.54	0.99	1.54	1.88	1.00
CH-1.7	326	130.0	1.60	1.65	0.80	0.98	1.92	0.73	1.02	1.34	1.70	0.99
GH-1.7	326	87.0	1.58	1.63	0.96	0.97	2.30	0.90	0.98	1.55	1.89	0.98
CH-2.2	326	174.0	1.96	2.03	1.01	1.20	2.57	0.94	1.26	1.83	2.05	1.22
GH-2.2	326	115.5	1.92	1.98	1.20	1.18	3.06	1.25	1.20	2.11	2.24	1.20
GB54	334	31.3	1.37	1.33	1.04	0.93	1.88	1.00	0.86	1.38	1.88	0.94
GB55	334	35.5	1.55	1.51	1.17	1.05	2.12	1.18	0.97	1.71	2.13	1.06

G07N1	346	55.0	2.16	2.09	1.53	1.46	2.83	0.98	1.37	2.18	3.05	1.48
G07N2	346	64.0	2.51	2.43	1.78	1.70	3.29	0.69	1.59	2.53	3.55	1.72
G10N1	346	43.0	1.38	1.37	0.98	0.94	2.05	0.66	0.98	1.58	1.86	0.95
G10N2	346	46.0	1.48	1.47	1.05	1.00	2.20	0.85	1.05	1.69	1.99	1.02
V-G1-1	360	108.0	1.28	1.22	0.93	0.87	1.85	1.04	0.92	1.41	1.73	0.88
V-G2-1	360	95.0	1.15	1.10	0.85	0.78	1.69	0.63	0.82	1.22	1.58	0.79
V-A-1	360	115.0	1.30	1.24	0.92	0.88	1.83	0.93	0.93	1.44	1.73	0.89
V-G1-2	360	137.0	1.26	1.23	0.91	0.85	2.28	0.63	0.93	1.25	1.58	0.87
V-G2-2	360	153.0	1.44	1.41	1.05	0.98	2.63	0.84	1.06	1.60	1.82	0.99
V-A-2	360	177.0	1.56	1.52	1.09	1.05	2.74	1.11	1.15	1.76	1.92	1.07
G-318/118-30-15	367	47.7	1.36	1.30	1.04	0.92	2.45	0.58	0.95	1.24	1.64	0.93
G-312/212-30-15	368	34.8	1.21	1.15	0.92	0.82	1.79	0.89	0.83	1.10	1.55	0.83
B-400-2	370	32.9	1.42	1.34	0.65	0.96	0.92	0.81	0.87	1.30	2.04	0.97
B-400-4	370	36.1	1.23	1.17	0.69	0.83	1.01	0.84	0.79	1.10	1.63	0.84
G-318-30-15	376	38.6	1.24	1.17	0.99	0.84	2.04	0.79	0.85	1.07	1.53	0.85
G-418-30-15	376	38.2	1.12	1.06	0.88	0.75	2.02	0.73	0.77	0.87	1.33	0.76
G-316-30-15	377	31.7	1.10	1.04	0.87	0.74	1.68	0.62	0.75	0.90	1.39	0.75
G-416-30-15	377	34.8	1.08	1.02	0.84	0.73	1.79	0.80	0.74	0.84	1.32	0.74
G-512-30-15	379	34.3	1.20	1.13	0.92	0.81	1.76	0.94	0.81	1.05	1.52	0.82
B3	400	55.0	0.91	0.89	0.41	0.59	0.70	0.89	0.58	0.78	1.20	0.60
Q-A-5L	404	118.4	1.03	0.98	0.87	0.69	2.21	0.78	0.84	0.83	1.13	0.71
M20-0	405	138.0	1.22	1.13	1.01	0.82	2.47	0.81	0.97	1.20	1.45	0.84
G-500	410	77.2	1.43	1.38	0.98	0.96	1.95	0.57	0.91	1.36	1.88	0.99
Q-A-3L	412	154.3	1.60	1.52	1.34	1.07	3.39	0.81	1.19	1.59	1.82	1.11
GB56	434	43.9	1.48	1.37	1.05	0.99	1.94	0.86	0.96	1.49	1.94	1.03
GB57	434	50.0	1.70	1.58	1.22	1.14	2.24	0.79	1.10	1.79	2.23	1.19
G-2.5-500	434	92.2	1.48	1.38	1.12	0.99	2.46	0.83	0.97	1.29	1.78	1.04

M05-0	438	86.0	1.19	1.11	0.85	0.80	1.46	0.72	0.67	1.04	1.68	0.84
C-2.5-500	439	82.5	1.13	1.07	0.63	0.76	1.16	0.70	0.75	0.79	1.32	0.79
Q-C-2L	441	145.8	1.22	1.17	1.01	0.82	2.55	0.67	0.91	0.95	1.32	0.86
G-500-70	442	116.1	1.80	1.76	1.04	1.03	2.16	0.78	1.01	1.50	1.96	1.08
C-500-70	449	100.4	1.28	1.26	0.58	0.74	1.05	0.54	0.73	0.77	1.31	0.78
G-0.5-500	455	68.0	1.70	1.58	1.07	1.14	1.76	0.73	0.89	1.40	2.43	1.20
C-500	460	74.1	1.11	1.05	0.58	0.74	1.01	0.90	0.73	0.79	1.33	0.78
C-0.5-500	460	70.3	1.33	1.27	0.59	0.89	0.96	0.94	0.85	1.23	1.75	0.94
No30	500	142.8	1.61	1.50	1.16	1.07	2.20	1.25	1.11	1.35	1.77	1.16
B4	500	68.0	0.98	0.96	0.44	0.63	0.74	1.00	0.57	0.86	1.22	0.68
JSC32-NT	575	154.0	1.34	1.25	1.06	0.89	1.99	1.18	1.03	1.16	1.51	0.99
JSV40-NT	575	163.5	1.26	1.17	0.90	0.83	1.76	0.98	0.97	1.04	1.41	0.93
G-650-70	578	155.2	1.59	1.56	0.97	0.90	2.02	0.69	0.94	1.14	1.60	1.01
G-650	584	103.7	1.30	1.21	1.02	0.86	1.89	0.66	0.88	1.06	1.54	0.97
C-650	594	112.9	1.23	1.15	0.71	0.81	1.16	0.85	0.88	0.91	1.39	0.92
C-650-70	594	146.1	1.29	1.26	0.61	0.73	1.06	1.04	0.80	0.75	1.23	0.82
L20-0	857	232.0	1.18	1.10	0.94	0.75	2.56	0.63	0.91	1.01	1.17	0.93
S1B-1	880	220.7	1.38	1.28	1.11	0.88	2.49	0.93	0.92	1.27	1.42	1.09
S1B-2	880	216.2	1.32	1.23	1.05	0.84	2.37	0.63	0.88	1.19	1.37	1.05
S1-1	883	154.1	1.21	1.12	0.90	0.77	1.74	0.84	0.64	1.14	1.36	0.96
A1	889	159.0	1.24	1.15	0.92	0.79	1.78	1.11	0.65	1.19	1.39	0.98
L05-0	937	135.0	0.97	0.94	0.61	0.61	1.26	0.58	0.43	0.86	1.15	0.78

Appendix B

Database of FRP RC Beams with FRP Shear Reinforcement

This database collects the main experimental results from the tests performed on the FRP reinforced concrete beams with shear reinforcement. This appendix includes the results of the code comparison discussed in Chapter 2 for the elements with shear span-to-depth-ratio ranging from 2.5 to 4.5. The full database can be downloaded under the following URL: **https://doi.org/10.15131/shef.data.5267722.v1**

Appendix B: *Database of FRP RC beams with FRP shear reinforcement*

Beam	d (mm)	V_{exp} (kN)	V_{exp}/V_{JSCE}	V_{exp}/V_{CNR}	V_{exp}/V_{fib}	V_{exp}/V_{ISIS}	$V_{exp}/V_{CSA\,S806}$	$V_{exp}/V_{CSA\,S6}$	V_{exp}/V_{ACI}	$V_{exp}/Level\,I$	$V_{exp}/Level\,II$
GB11	210	49.0	2.02	0.87	1.18	2.75	1.67	2.02	2.00	1.18	1.10
GB50-P150	218	30.0	1.45	0.36	0.67	1.34	1.07	1.07	1.00	0.67	0.59
CB51-P150	218	41.9	2.02	0.51	0.94	1.88	1.49	1.50	1.40	0.94	0.82
GB52-P80	218	47.2	1.67	0.66	1.02	1.87	1.18	1.67	1.69	1.02	0.95
TB1A	219	35.1	1.25	0.53	0.77	1.65	0.99	1.33	1.33	0.77	0.72
TB1B	219	39.6	1.41	0.59	0.87	1.86	1.13	1.56	1.50	0.87	0.81
TB2A	219	36.8	1.31	0.55	0.81	1.73	1.04	1.44	1.40	0.81	0.75
TB2B	219	65.8	2.29	0.81	1.31	2.77	1.86	2.29	2.13	1.31	1.20
TB3A	219	60.0	2.07	0.70	1.16	2.43	1.67	2.00	1.85	1.16	1.05
TB3B	219	36.9	1.34	0.62	0.85	1.85	1.07	1.56	1.53	0.85	0.81
TB4A	220	32.9	1.27	0.53	0.76	1.72	0.99	1.30	1.33	0.76	0.71
TB4B	220	59.3	2.23	0.77	1.25	2.74	1.77	2.06	2.03	1.25	1.14
TB5A	220	47.6	1.81	0.68	1.05	2.34	1.44	1.76	1.77	1.05	0.97
TB5B	220	67.1	2.47	0.74	1.29	2.78	1.93	2.08	1.99	1.29	1.15
TB6A	220	30.6	1.17	0.72	0.69	1.54	0.91	1.16	1.18	0.69	0.64
GB43R	223	57.1	2.11	1.08	1.30	3.22	1.62	2.47	2.25	1.30	1.22
GB62	233	48.2	2.04	0.70	1.13	2.20	1.34	1.65	1.93	1.13	1.03
GB63	233	54.2	2.29	0.94	1.25	2.44	1.52	1.84	2.11	1.25	1.14
No.27	250	66.3	2.58	1.02	1.33	2.25	1.68	2.32	2.04	1.33	1.17
No.28	250	79.1	2.86	0.83	1.17	2.00	1.77	1.98	1.59	1.17	0.97
No.29	250	72.8	2.28	1.05	1.28	2.50	1.49	2.39	1.94	1.28	1.14
No.30	250	82.9	2.02	1.05	1.23	2.85	1.45	1.85	1.86	1.23	1.12
No.34	250	131.5	2.24	0.60	1.11	1.84	1.50	2.12	1.65	1.11	0.98
No.35	250	138.6	2.35	0.95	1.16	1.91	1.58	2.21	1.72	1.16	1.02
No.36	250	117.3	2.08	0.64	1.09	1.79	1.38	2.14	1.72	1.09	0.99
No.37	250	134.7	2.36	0.99	1.21	2.00	1.59	2.36	1.87	1.21	1.08
FF1-20	250	59.0	2.28	0.89	1.18	1.99	1.48	2.05	1.81	1.18	1.04

FF1-10	250	84.0	3.01	0.87	1.24	2.11	1.87	2.09	1.69	1.24	1.03
FF2-20	250	72.8	2.26	1.03	1.27	2.49	1.48	2.36	1.93	1.27	1.13
FF2-10	250	89.0	2.62	0.90	1.20	2.33	1.65	2.29	1.63	1.20	1.01
FF3-10	250	95.0	2.62	0.95	1.24	2.52	1.64	2.27	1.68	1.24	1.05
FF4-10	250	119.5	2.85	1.14	1.44	3.19	1.98	2.51	1.97	1.44	1.24
FF4-13	250	86.0	2.10	0.94	1.15	2.60	1.46	1.69	1.63	1.15	1.01
FF4-16	250	75.0	1.85	0.89	1.07	2.45	1.30	1.49	1.56	1.07	0.95
FF4-20	250	82.5	2.00	1.03	1.22	2.82	1.43	1.82	1.85	1.22	1.10
No.10	250	113.7	2.26	0.82	1.36	3.30	1.87	2.21	1.97	1.36	1.21
No.14	250	125.9	2.77	0.81	1.93	5.20	2.45	3.93	3.18	1.93	1.85
No.16	250	116.2	2.56	0.83	1.48	3.37	1.96	2.74	2.14	1.48	1.32
No.19	250	73.3	1.87	0.55	1.02	2.13	1.31	1.67	1.47	1.02	0.90
GG05-10	250	83.0	2.52	0.77	1.30	3.08	1.76	2.21	2.00	1.30	1.14
GG10-10	250	100.0	3.10	0.94	1.58	3.77	2.16	2.71	2.43	1.58	1.39
GG05-10	250	56.0	1.78	0.79	1.06	2.69	1.26	1.84	1.83	1.06	0.98
GG10-20	250	66.0	2.09	0.93	1.25	3.17	1.49	2.16	2.15	1.25	1.15
No.25	250	110.0	3.32	1.22	1.82	3.56	2.26	3.70	2.72	1.82	1.61
No.26	250	107.0	3.23	1.19	1.77	3.46	2.19	3.60	2.64	1.77	1.57
No.27	250	131.0	3.72	0.95	1.64	3.14	2.47	3.11	2.19	1.64	1.37
No.28	250	131.0	3.72	0.95	1.64	3.14	2.47	3.11	2.19	1.64	1.37
FC	250	53.5	1.78	0.69	0.95	1.74	1.49	1.63	1.49	0.95	0.84
No.32	260	80.8	1.85	0.87	1.22	3.29	1.41	2.09	1.97	1.22	1.14
FT	270	36.4	1.51	0.47	0.72	1.11	0.99	1.06	1.11	0.72	0.62
FB	270	44.9	1.69	0.57	0.83	1.35	1.21	1.29	1.29	0.83	0.72
BM2	279	71.2	1.96	0.69	0.93	2.24	1.18	1.53	1.29	0.93	0.79
B1	311	69.0	1.76	0.85	0.95	2.11	1.23	1.68	1.46	0.95	0.83
No.10	325	103.0	1.90	0.85	1.20	1.89	1.41	2.45	1.93	1.20	1.11
No.11	325	107.3	1.97	0.88	1.24	1.96	1.47	2.57	2.00	1.24	1.15
No.12	325	102.0	1.89	0.84	1.22	1.92	1.41	2.50	2.02	1.22	1.15

No.15	325	117.8	2.13	0.99	1.30	2.06	1.59	2.66	2.03	1.30	1.18
No.16	325	112.9	2.04	0.95	1.24	1.98	1.52	2.55	1.95	1.24	1.13
No.17	325	111.9	2.06	1.06	1.30	2.05	1.54	2.69	2.11	1.30	1.21
No.18	325	119.2	2.13	0.93	1.29	2.04	1.59	2.64	2.00	1.29	1.17
No.19	325	128.3	2.20	0.89	1.20	1.93	1.62	2.41	1.73	1.20	1.04
No.20	325	103.9	1.96	0.84	1.20	1.93	1.45	2.47	1.89	1.20	1.10
No.21	325	87.7	2.09	0.96	1.26	2.46	1.52	2.27	2.10	1.26	1.16
No.22	325	94.0	2.19	0.87	1.25	2.41	1.58	2.23	1.97	1.25	1.11
No.23	325	110.0	2.47	0.74	1.21	2.31	1.74	2.17	1.75	1.21	1.03
No.24	325	93.3	2.18	0.95	1.26	2.44	1.58	2.26	2.01	1.26	1.14
No.25	325	93.3	2.18	0.95	1.26	2.44	1.58	2.26	2.01	1.26	1.14
No.26	325	98.1	2.33	1.26	1.40	2.72	1.69	2.51	2.31	1.40	1.28
GB64	333	66.1	2.12	0.72	1.18	2.24	1.39	1.76	1.89	1.18	1.05
GB65	333	63.4	2.02	0.81	1.10	2.08	1.32	1.64	1.73	1.10	0.97
Q-C-5R	404	250.0	2.15	1.78	1.40	4.17	1.81	2.54	2.06	1.44	1.34
M20-1	405	154.0	1.22	0.76	0.78	2.16	0.99	1.23	1.25	0.80	0.75
Q-A-3R	412	301.0	2.50	1.41	1.38	3.46	1.91	2.88	1.90	1.41	1.22
Q-A-4L	412	220.0	1.90	1.31	1.20	3.30	1.48	2.09	1.82	1.24	1.14
Q-A-4R	412	266.0	2.20	1.34	1.29	3.34	1.70	2.49	1.85	1.33	1.18
GB60	433	77.2	2.15	0.76	1.19	2.37	1.45	1.88	1.83	1.23	1.09
GB61	433	85.4	2.39	1.07	1.33	2.65	1.61	2.11	2.06	1.37	1.22
Q-C-1L	441	252.0	1.72	1.21	1.12	3.03	1.34	1.64	1.63	1.17	1.08
Q-C-1R	441	362.0	2.30	1.34	1.33	3.31	1.76	2.28	1.80	1.38	1.20
Q-C-2R	441	240.0	1.63	1.07	1.00	2.63	1.24	1.40	1.40	1.04	0.93
CC-3	470	305.0	3.90	1.04	1.46	2.68	2.99	3.15	1.74	1.50	1.17
CG-3	470	305.0	3.90	1.04	1.46	2.68	2.99	3.15	1.74	1.50	1.17
No.31	500	172.0	2.15	1.03	1.22	2.04	1.46	2.28	1.84	1.30	1.17
No.30	500	370.0	3.42	1.17	1.74	3.42	2.37	3.87	2.33	1.84	1.57
JSC32-22B	575	387.5	2.66	0.87	1.19	2.37	2.03	2.34	1.54	1.27	1.04

JSC32-40B	575	450.5	3.11	0.83	1.19	2.35	2.21	2.35	1.49	1.26	1.01
JSC32-50B	575	547.5	3.63	0.81	1.23	2.38	2.48	2.41	1.48	1.29	1.00
JSV40-22B	575	374.5	2.32	0.89	1.18	2.32	1.83	2.36	1.59	1.27	1.07
JSV40-40B	575	447.5	2.77	0.90	1.25	2.43	2.13	2.49	1.62	1.33	1.10
JSV40-50B	575	533.5	3.18	0.88	1.29	2.48	2.38	2.56	1.61	1.36	1.09
No.32	750	590.0	2.64	0.86	1.29	2.65	1.93	2.63	1.65	1.45	1.22
L20-1	857	500.0	2.25	1.30	1.36	4.04	1.82	3.07	1.94	1.64	1.51
L05-1	937	237.0	1.53	0.64	0.83	1.65	0.72	1.24	1.30	1.00	0.89

Appendix C

Data Acquisition

GB58-0 (first phase of testing)

Main flexural reinforcement: 2Ø12.7 mm GFRP bars
Compression reinforcement: 2Ø6 mm BFRP bars
Vertical reinforcement (to ease cage construction): 6 mm steel stirrups

GB59-0 (second phase of testing)

Main flexural reinforcement: 2Ø12.7 mm GFRP bars
Compression reinforcement: 2Ø6 mm BFRP bars
Vertical reinforcement (to ease cage construction): 6 mm steel stirrups

GB58 (first phase of testing)

Main flexural reinforcement: 2∅12.7 mm GFRP bars
Compression reinforcement: 2∅6 mm BFRP bars
Mid-depth reinforcement: 2∅6 mm BFRP bars
Vertical reinforcement (to ease cage construction): 6 mm steel stirrups
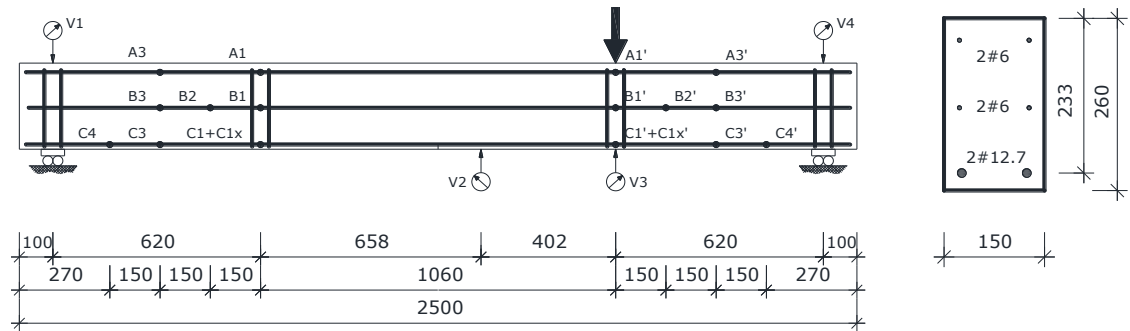
GB59 (second phase of testing)

Main flexural reinforcement: 2∅12.7 mm GFRP bars
Compression reinforcement: 2∅6 mm BFRP bars
Mid-depth reinforcement: 2∅6 mm BFRP bars
Vertical reinforcement (to ease cage construction): 6 mm steel stirrups
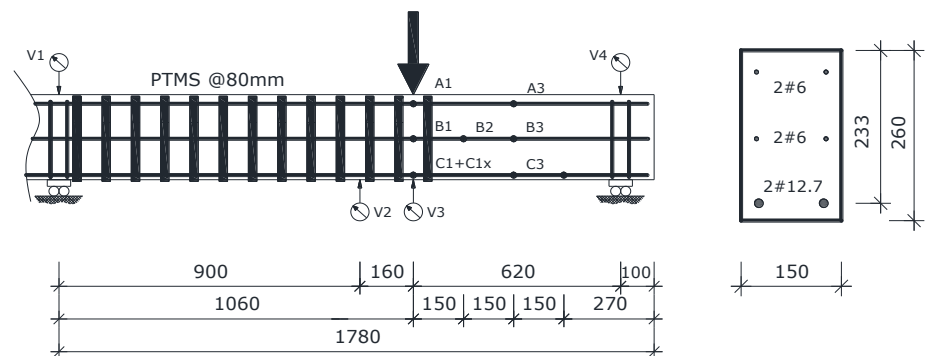
GB58-R (first phase of testing)

Main flexural reinforcement: 2∅12.7 mm GFRP bars
Compression reinforcement: 2∅6 mm BFRP bars
Mid-depth reinforcement: 2∅6 mm BFRP bars
Vertical reinforcement (to ease cage construction): 6 mm steel stirrups

GB59-R (second phase of testing)

Main flexural reinforcement: 2∅12.7 mm GFRP bars
Compression reinforcement: 2∅6 mm BFRP bars
Mid-depth reinforcement: 2∅6 mm BFRP bars
Vertical reinforcement (to ease cage construction): 6 mm steel stirrups

GB54 (first phase of testing)

Main flexural reinforcement: 3∅12.7 mm GFRP bars
Compression reinforcement: 2∅6 mm BFRP bars
Mid-depth reinforcement: 2∅6 mm BFRP bars
Vertical reinforcement (to ease cage construction): 6 mm steel stirrups

GB55 (second phase of testing)

Main flexural reinforcement: 3∅12.7 mm GFRP bars
Compression reinforcement: 2∅6 mm BFRP bars
Mid-depth reinforcement: 2∅6 mm BFRP bars
Vertical reinforcement (to ease cage construction): 6 mm steel stirrups

155
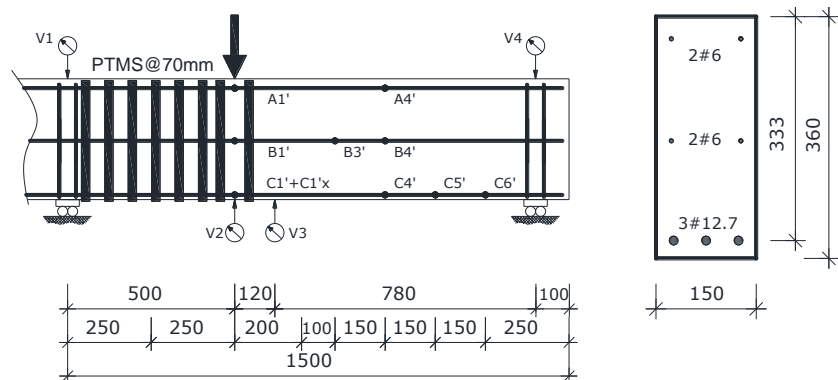
GB56 (first phase of testing)

Main flexural reinforcement: 4Ø12.7 mm GFRP bars
Compression reinforcement: 2Ø6 mm BFRP bars
Mid-depth reinforcement: 4Ø6 mm BFRP bars
Vertical reinforcement (to ease cage construction): 6 mm steel stirrups
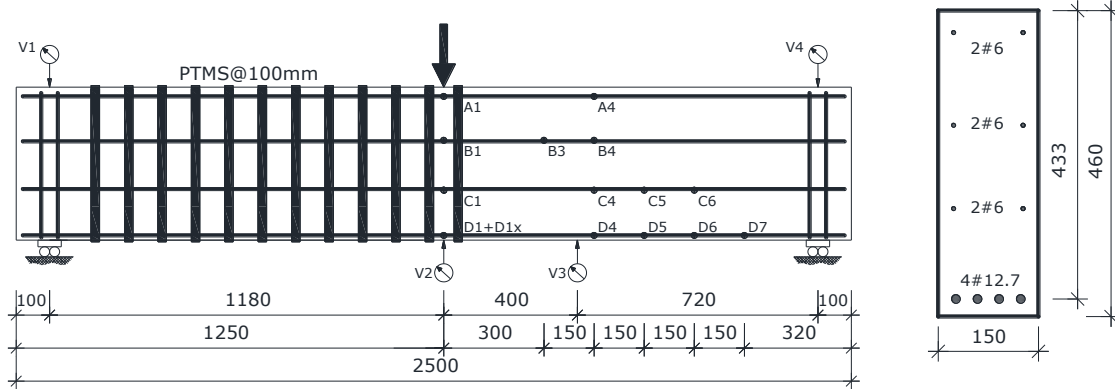
GB57 (second phase of testing)

Main flexural reinforcement: 4Ø12.7 mm GFRP bars
Compression reinforcement: 2Ø6 mm BFRP bars
Mid-depth reinforcement: 4Ø6 mm BFRP bars
Vertical reinforcement (to ease cage construction): 6 mm steel stirrups
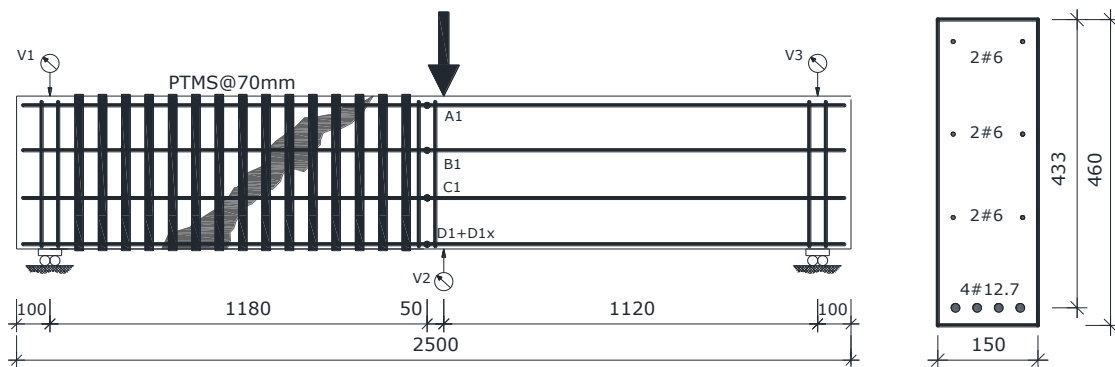
GB62 (first phase of testing)

Main flexural reinforcement: 2∅12.7 mm GFRP bars
Compression reinforcement: 2∅6 mm BFRP bars
Shear reinforcement: GFRP links@120 mm
Mid-depth reinforcement: 2∅6 mm BFRP bars
Vertical reinforcement (to ease cage construction): 6 mm steel stirrups
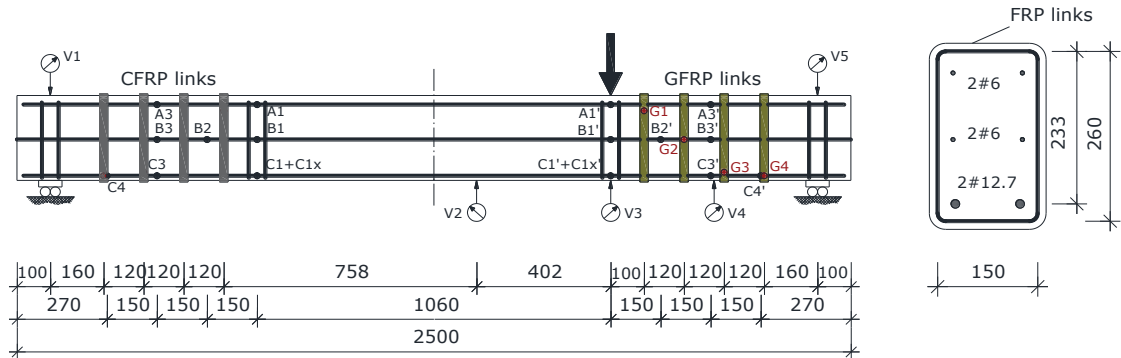
GB63 (second phase of testing)

Main flexural reinforcement: 2∅12.7 mm GFRP bars
Compression reinforcement: 2∅6 mm BFRP bars
Shear reinforcement: CFRP links@120 mm
Mid-depth reinforcement: 2∅6 mm BFRP bars
Vertical reinforcement (to ease cage construction): 6 mm steel stirrups

157
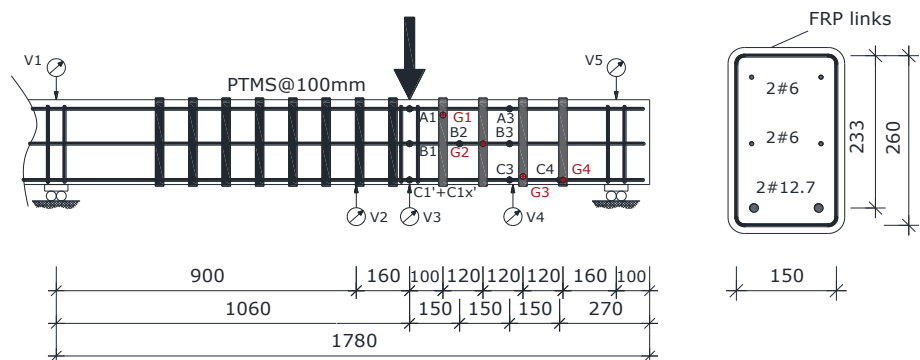
GB64 (first phase of testing)

Main flexural reinforcement: 3Ø12.7 mm GFRP bars
Compression reinforcement: 2Ø6 mm BFRP bars
Shear reinforcement: GFRP links@160 mm
Mid-depth reinforcement: 2Ø6 mm BFRP bars
Vertical reinforcement (to ease cage construction): 6 mm steel stirrups
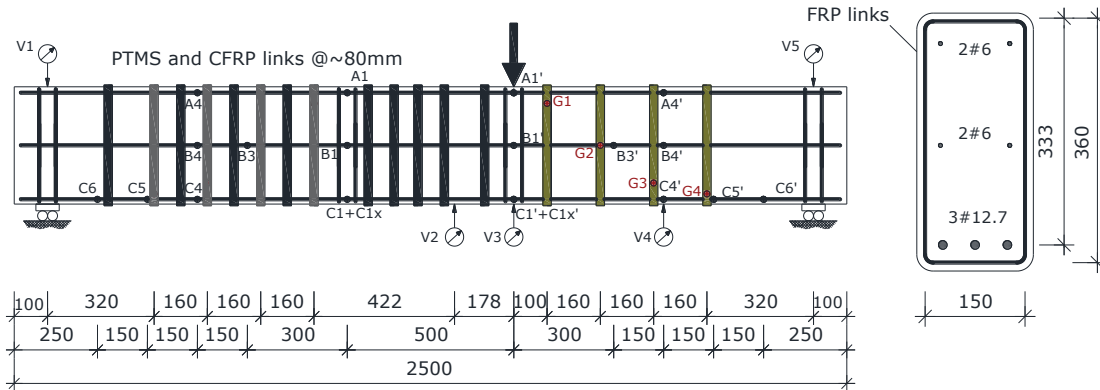
GB65 (second phase of testing)

Main flexural reinforcement: 3Ø12.7 mm GFRP bars
Compression reinforcement: 2Ø6 mm BFRP bars
Shear reinforcement: CFRP links@160 mm
Mid-depth reinforcement: 2Ø6 mm BFRP bars
Vertical reinforcement (to ease cage construction): 6 mm steel stirrups
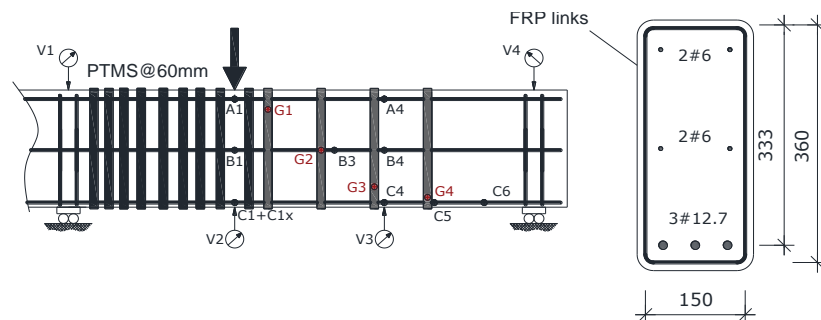
GB60 (first phase of testing)

Main flexural reinforcement: 4∅12.7 mm GFRP bars
Compression reinforcement: 2∅6 mm BFRP bars
Shear reinforcement: GFRP links@260 mm
Mid-depth reinforcement: 4∅6 mm BFRP bars
Vertical reinforcement (to ease cage construction): 6 mm steel stirrups
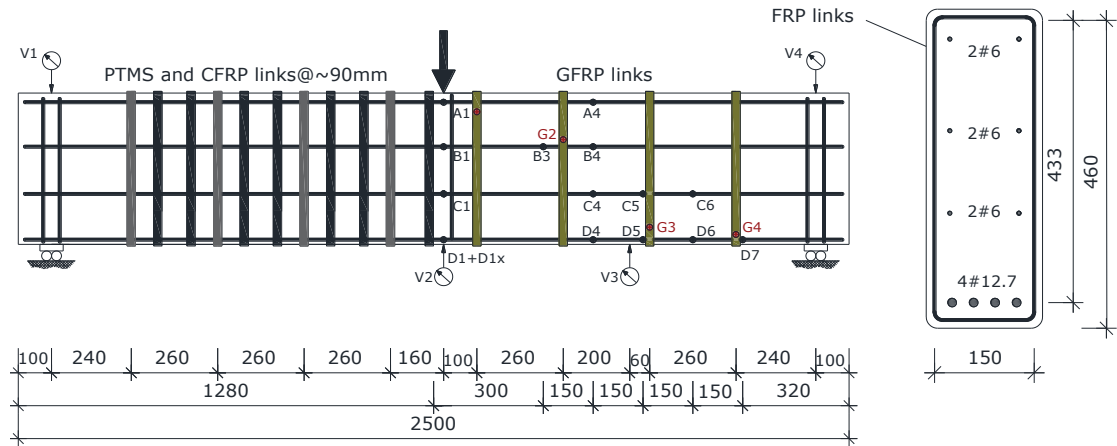
GB61 (first phase of testing)

Main flexural reinforcement: 4∅12.7 mm GFRP bars
Compression reinforcement: 2∅6 mm BFRP bars
Shear reinforcement: CFRP links@260 mm
Mid-depth reinforcement: 4∅6 mm BFRP bars
Vertical reinforcement (to ease cage construction): 6 mm steel stirrups
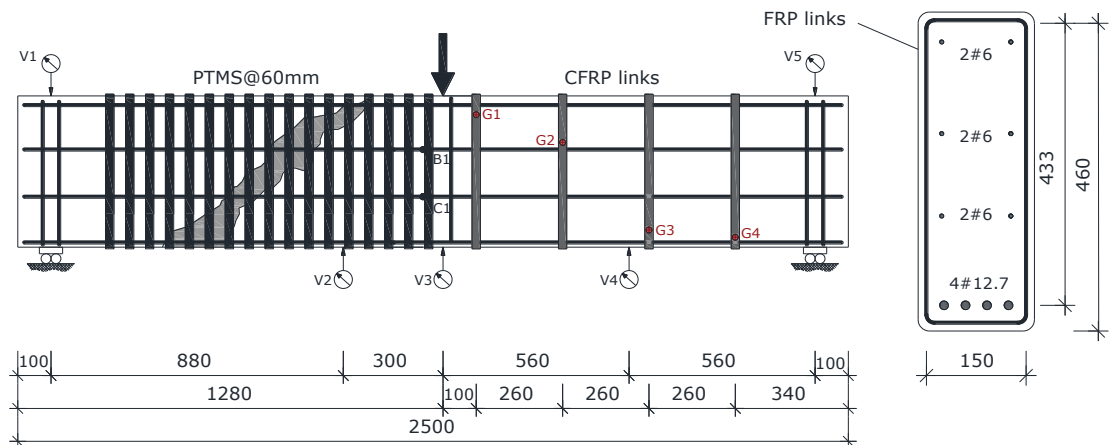
Appendix D

Experimental Results: Beams without Shear Reinforcement

GB58-0

Deflections measured on top of the supports
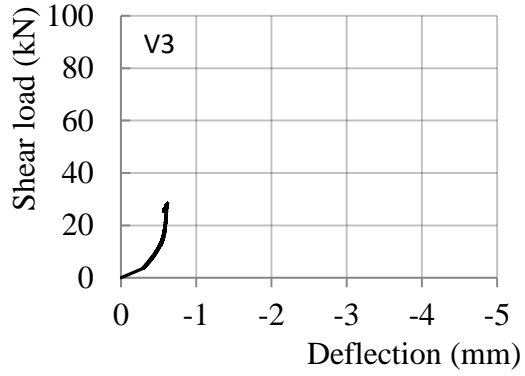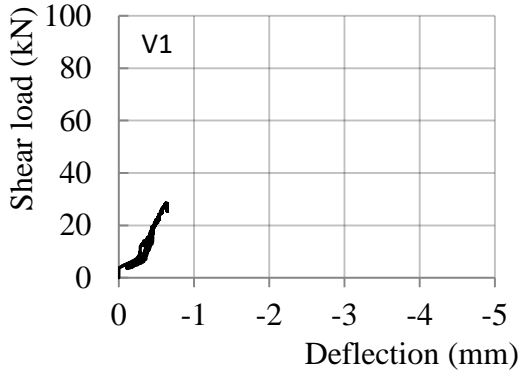
Deflections measured on the bottom of the beam
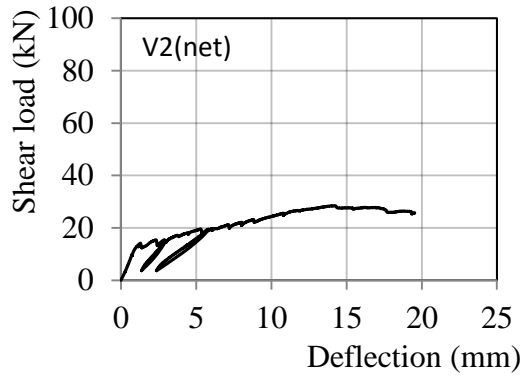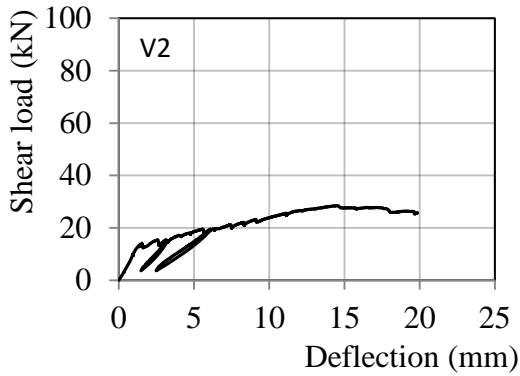
Strain measured in longitudinal reinforcement
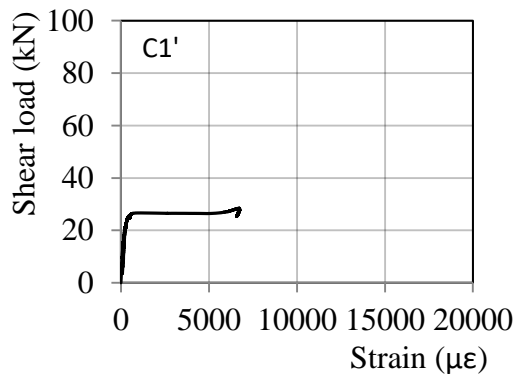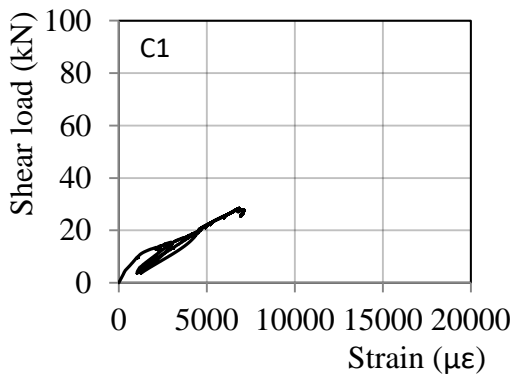
GB59-0

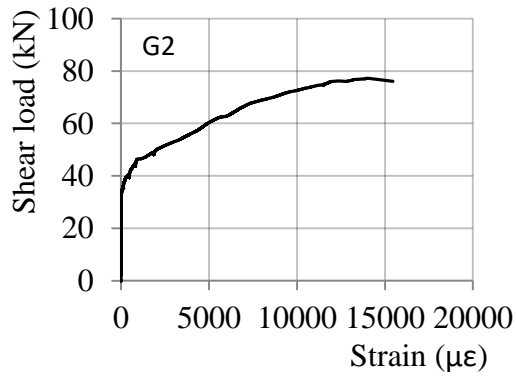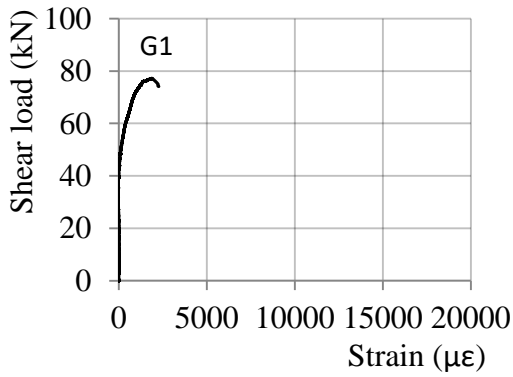*Deflections measured on top of the supports*
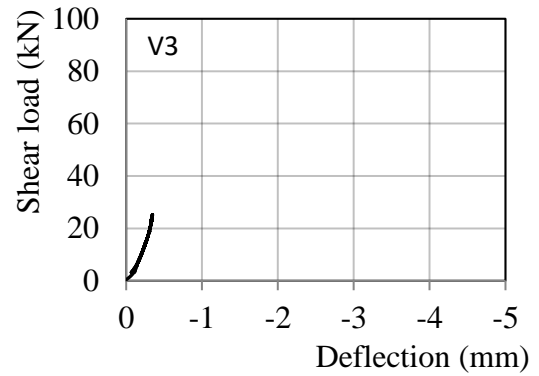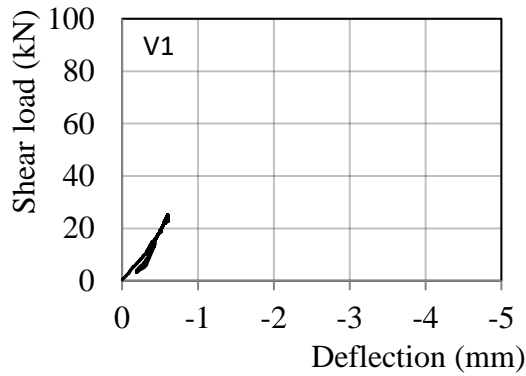
Deflections measured on the bottom of the beam
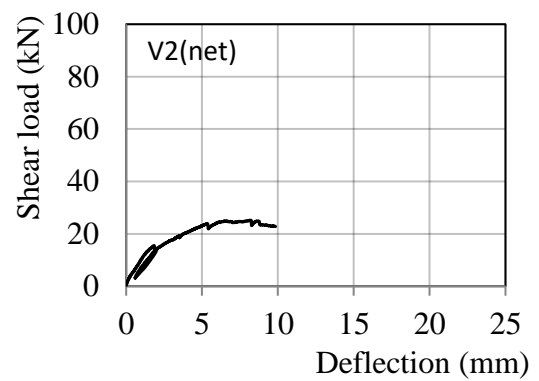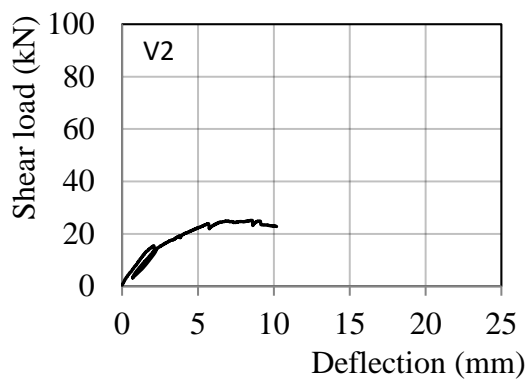
Strain in flexural reinforcement
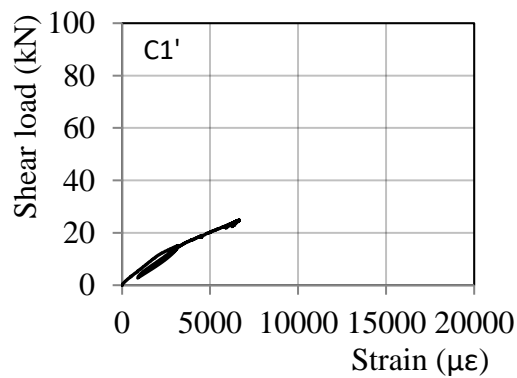
GB58

Deflections measured on top of the supports
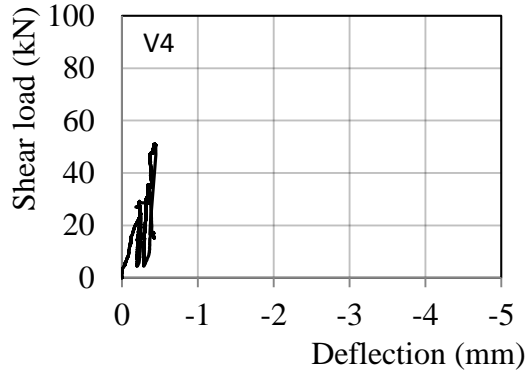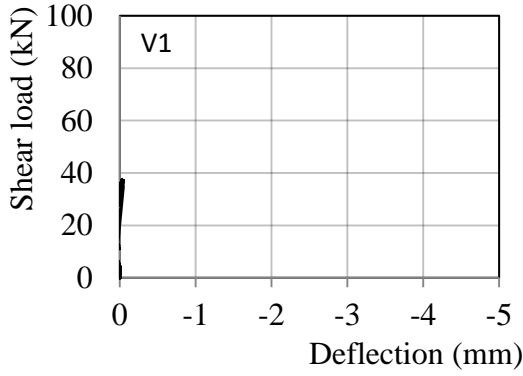
Deflections measured on the bottom of the beam
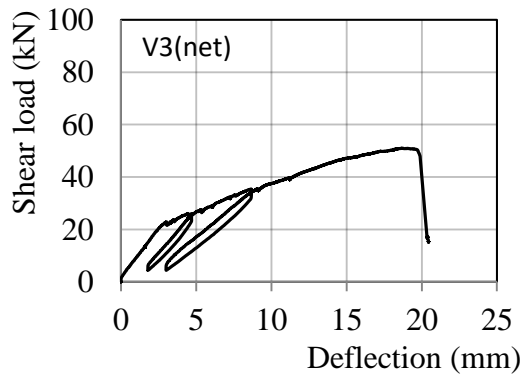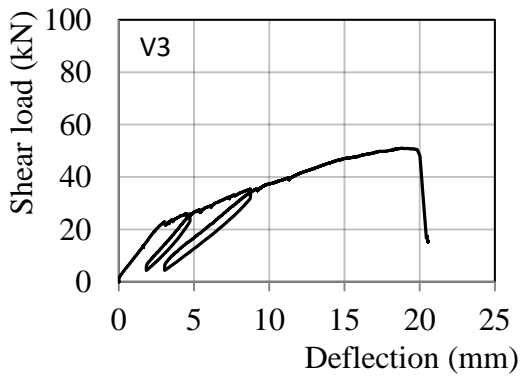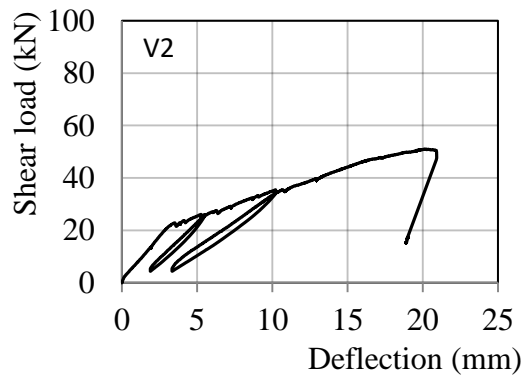
Strain in longitudinal reinforcement – non-test shear span
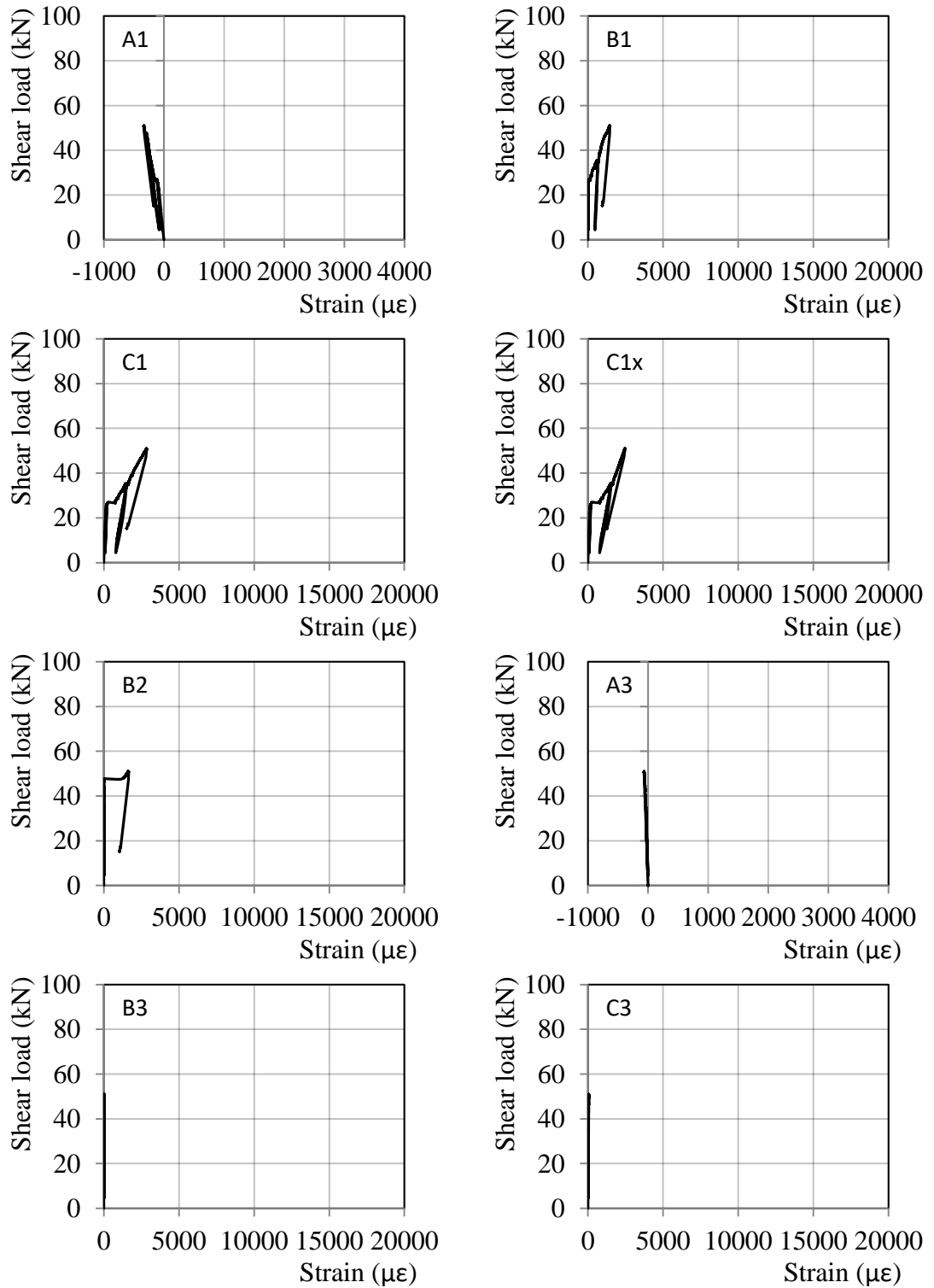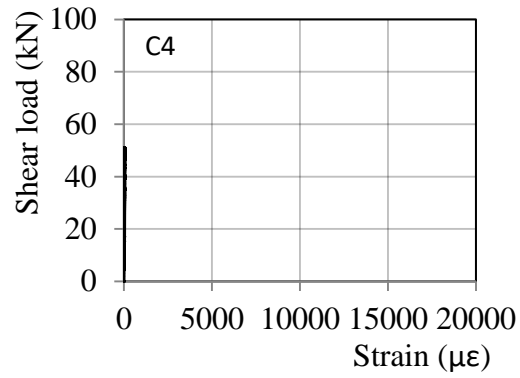
Strain in longitudinal reinforcement –test shear span
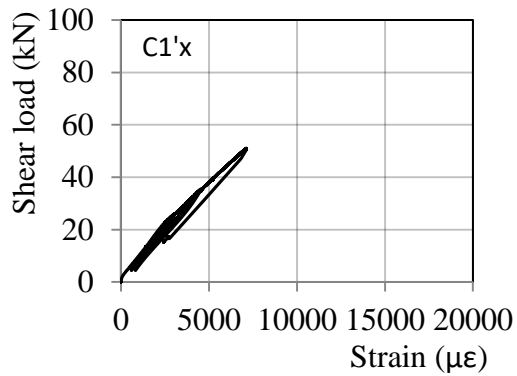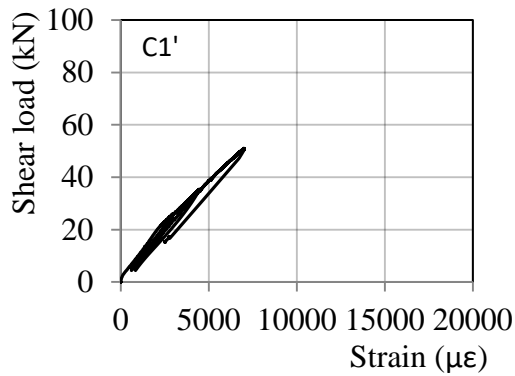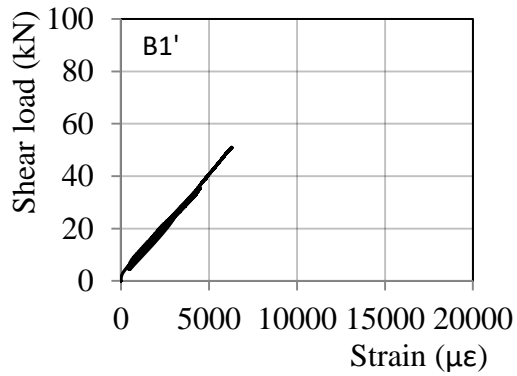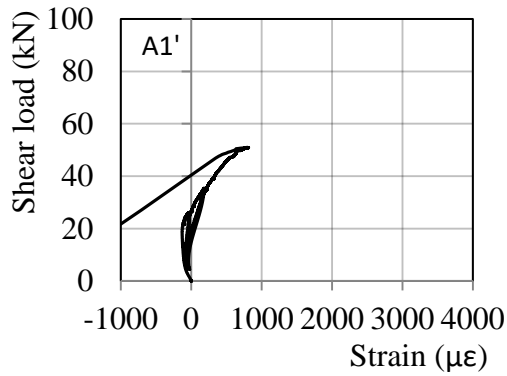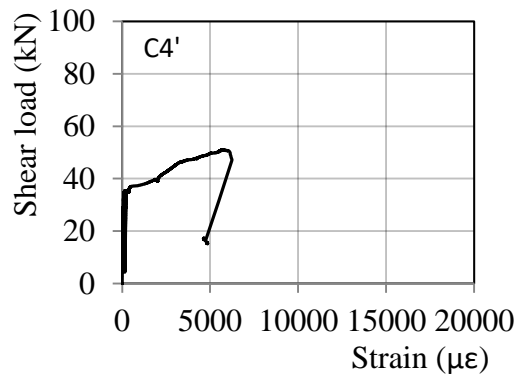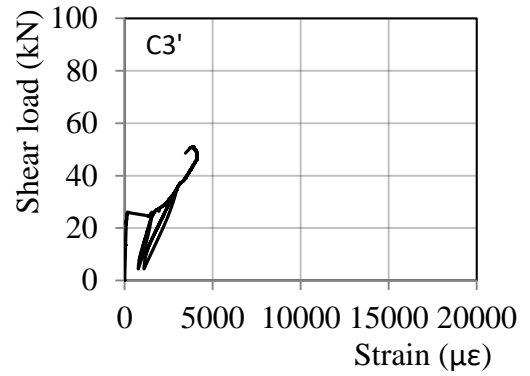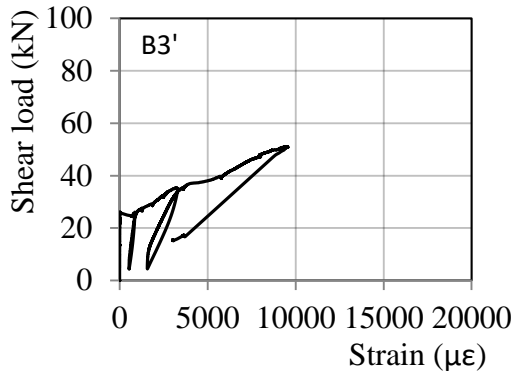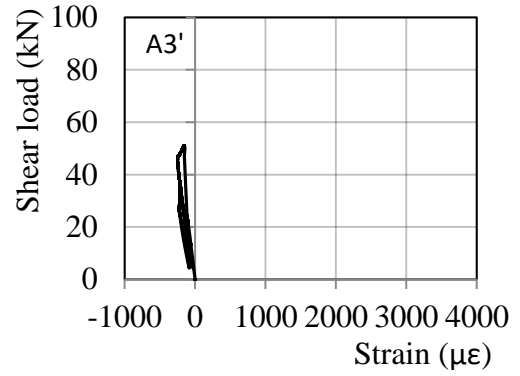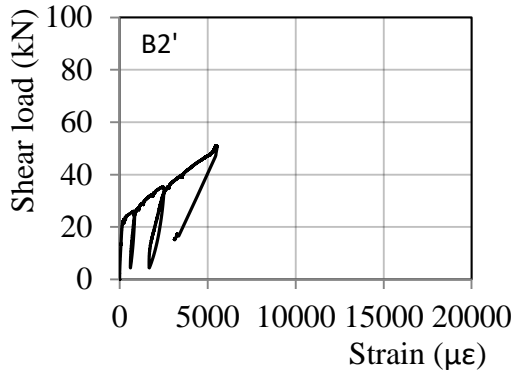
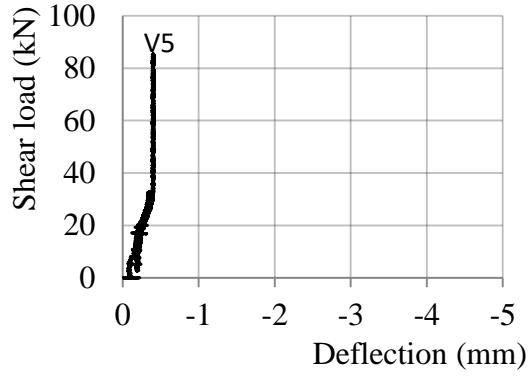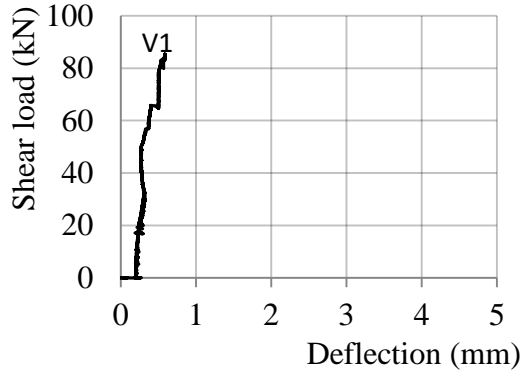# GB59

Deflections measured on top of the supports
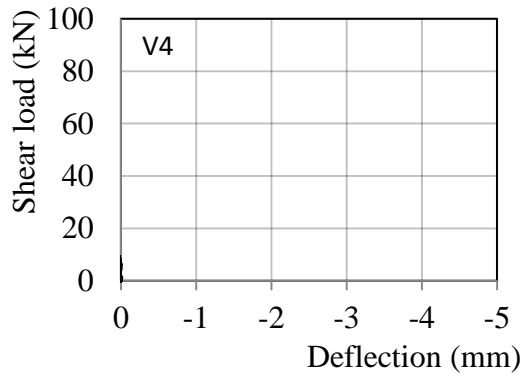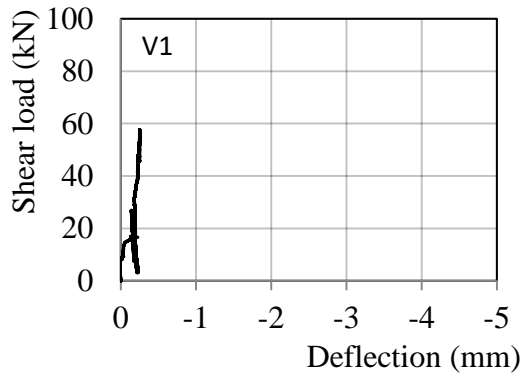
Deflections measured on the bottom of the beam
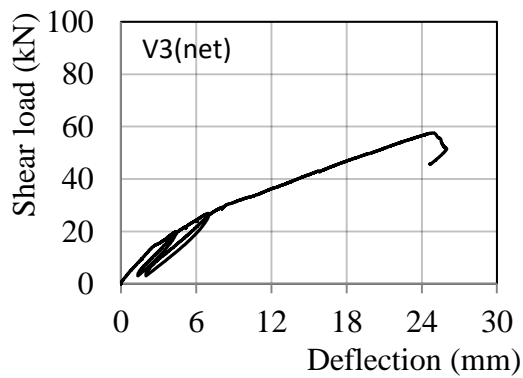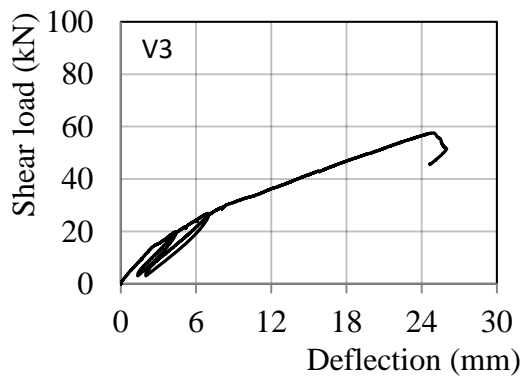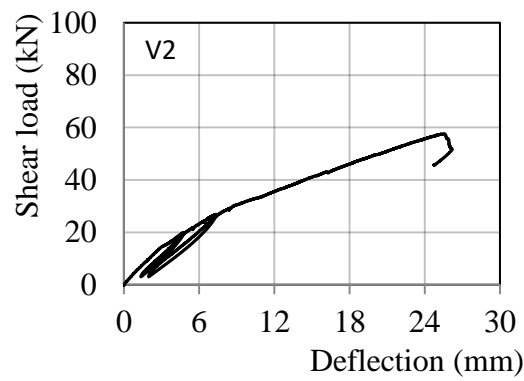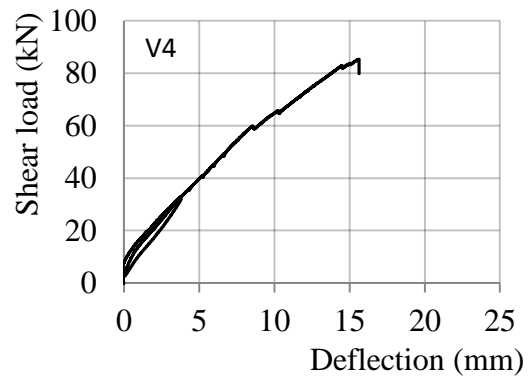
Strain in longitudinal reinforcement –-test shear span
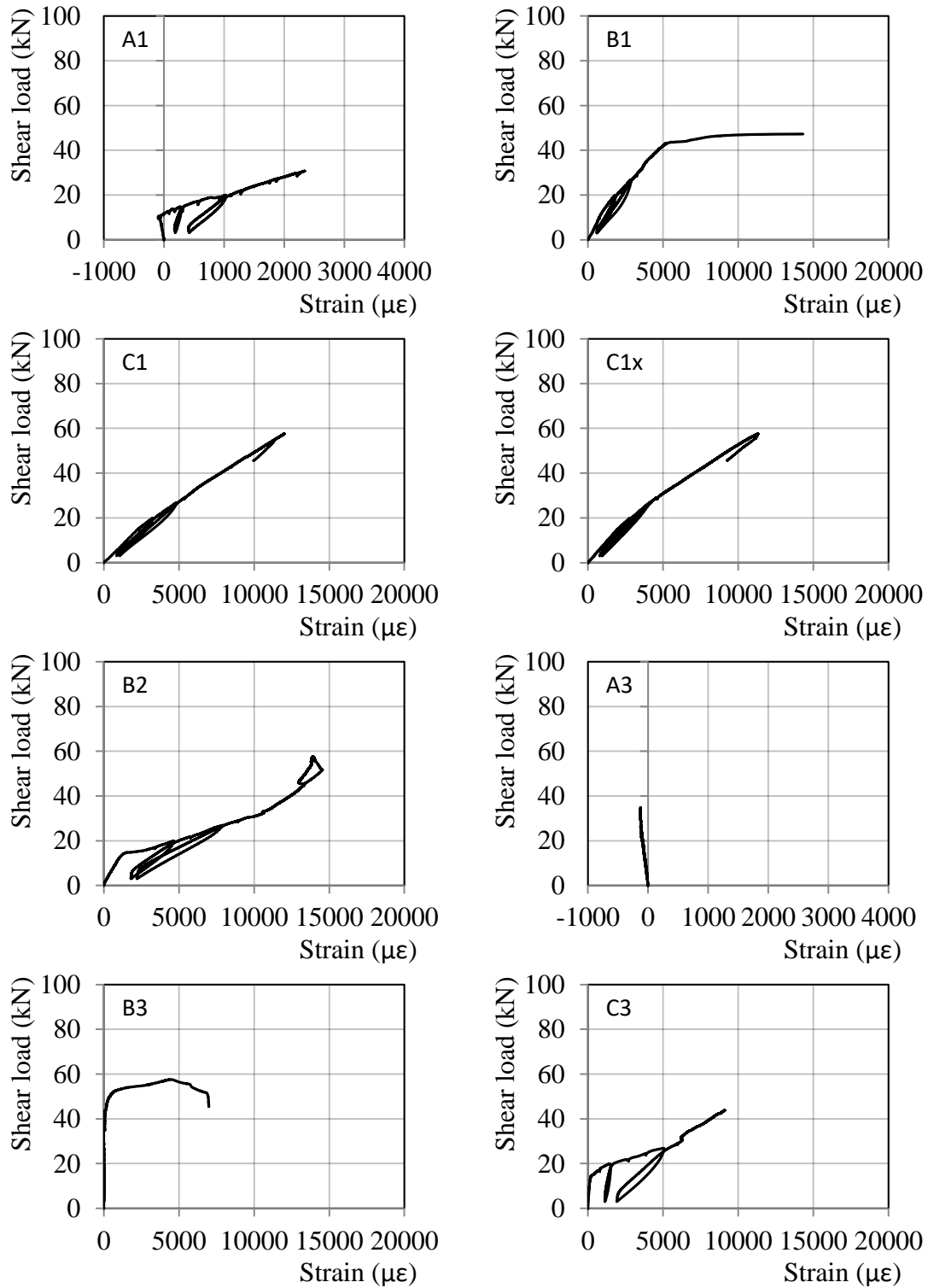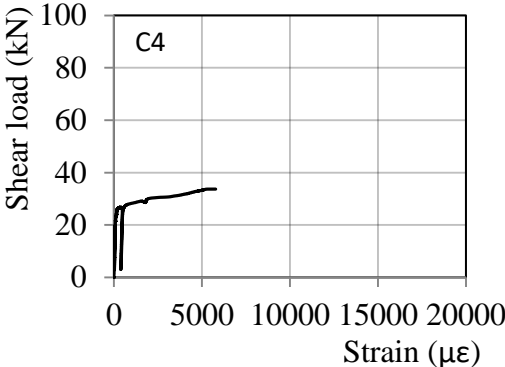
GB58-R

Deflections measured on top of the supports
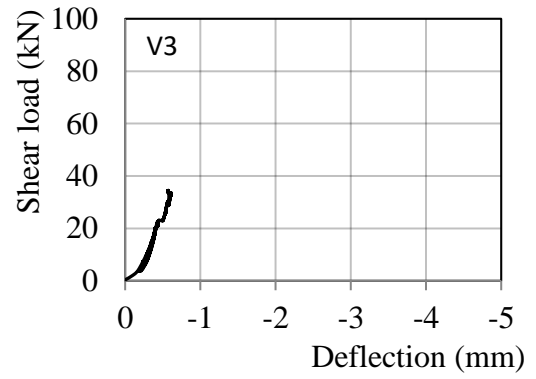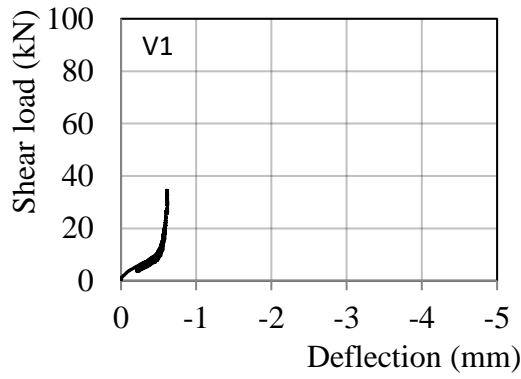
Deflections measured on the bottom of the beam
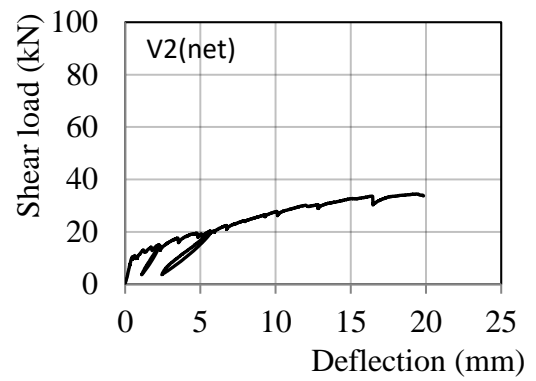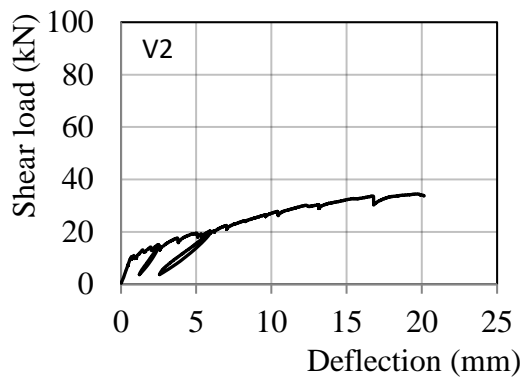
Strain in longitudinal reinforcement – non-test shear span
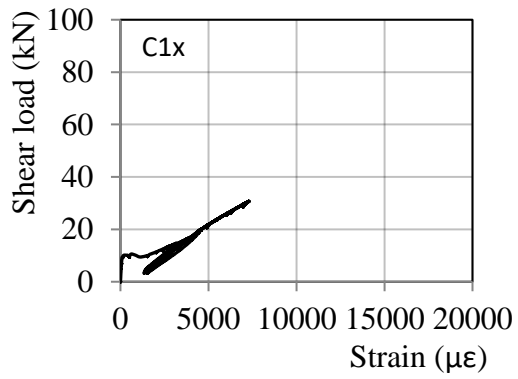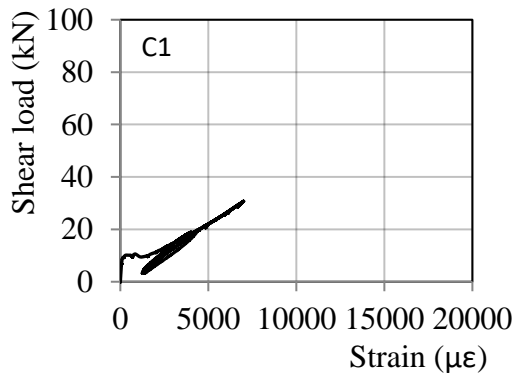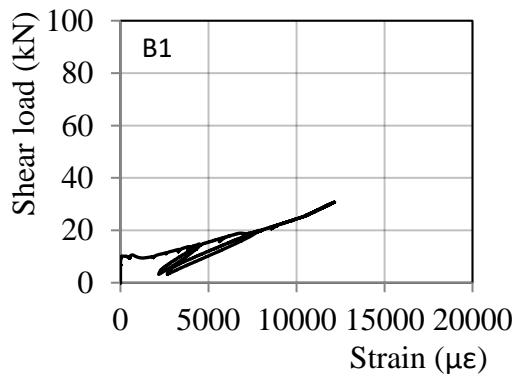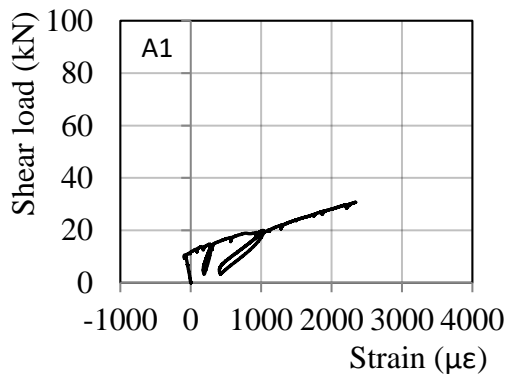
*Strain in longitudinal reinforcement –-test shear span*
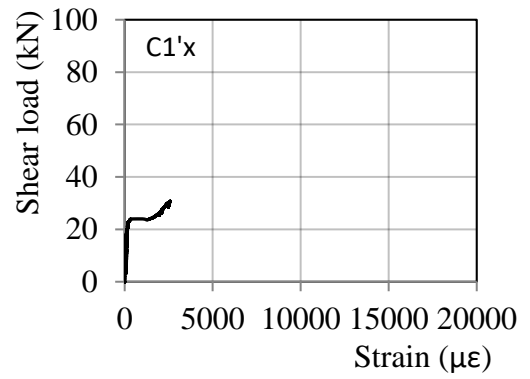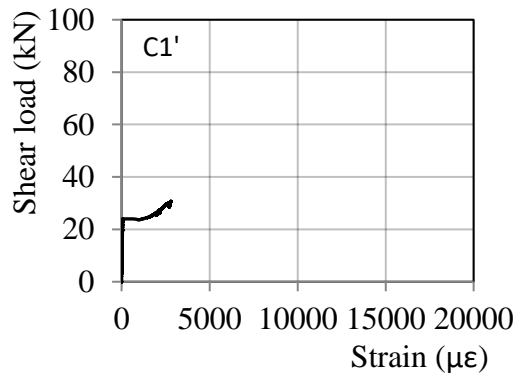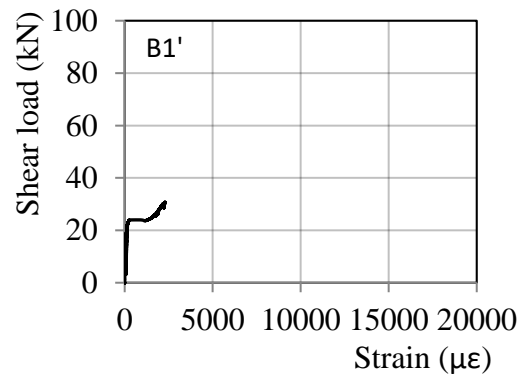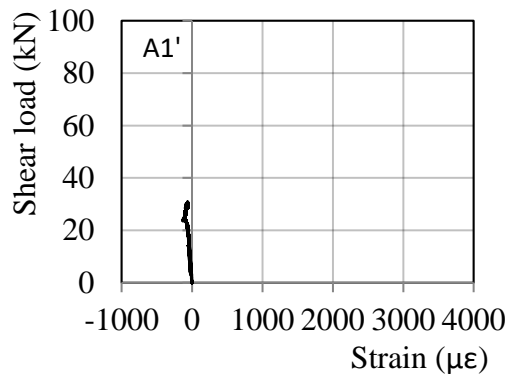
GB59-R

Deflections measured on top of the supports
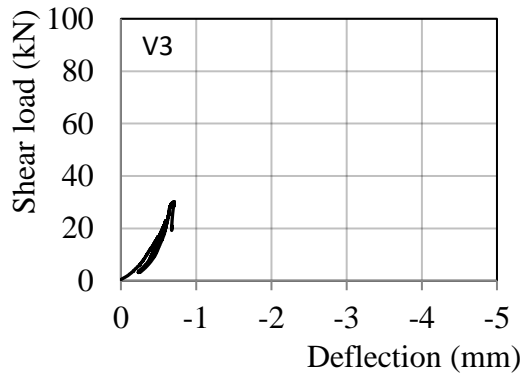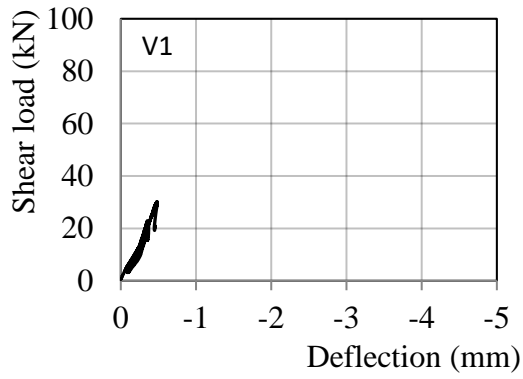
Deflections measured on the bottom of the beam
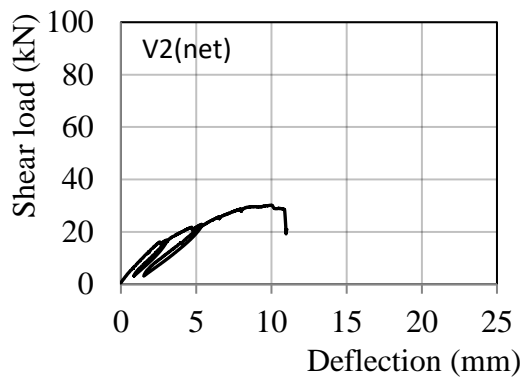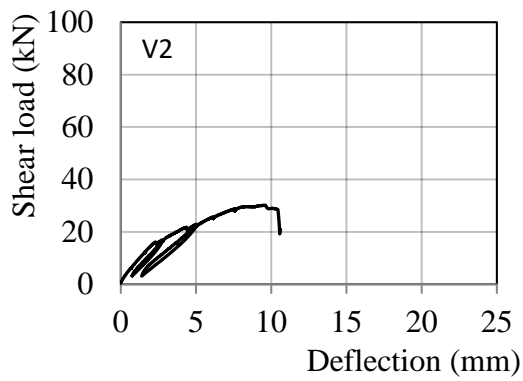
Strain in longitudinal reinforcement –-test shear span
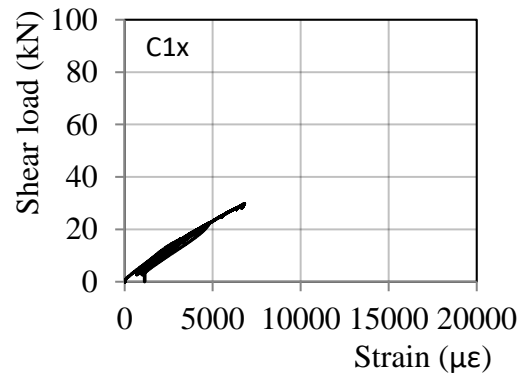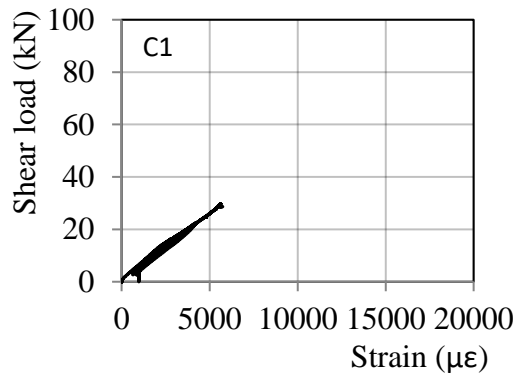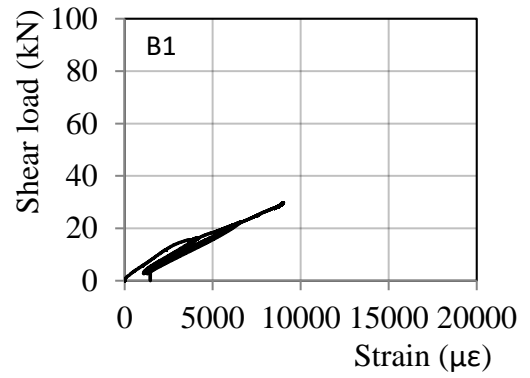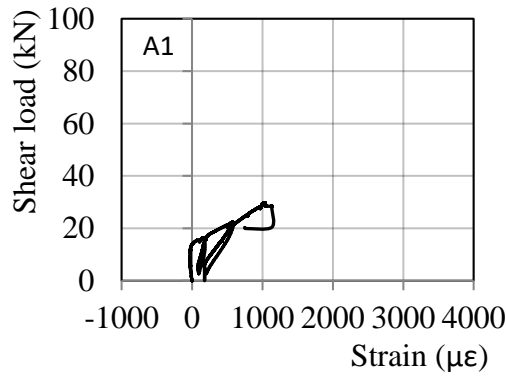
GB54

Deflections measured on top of the supports
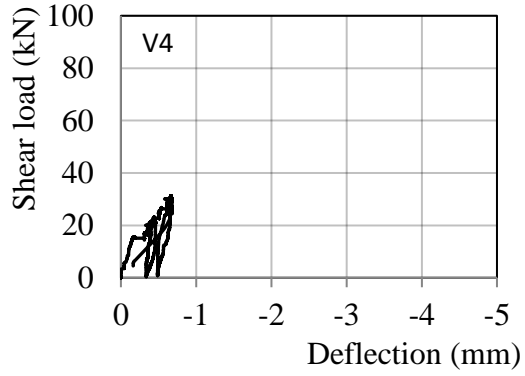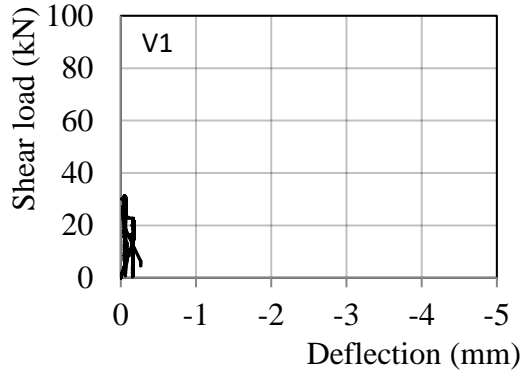

Deflections measured on the bottom of the beam
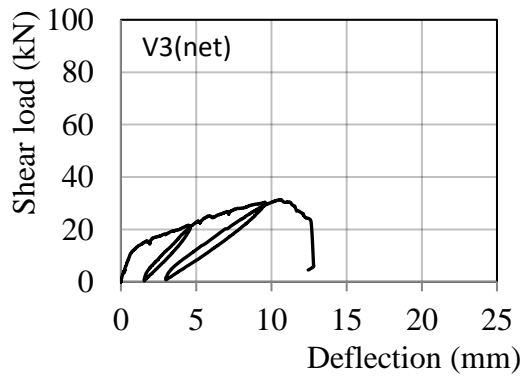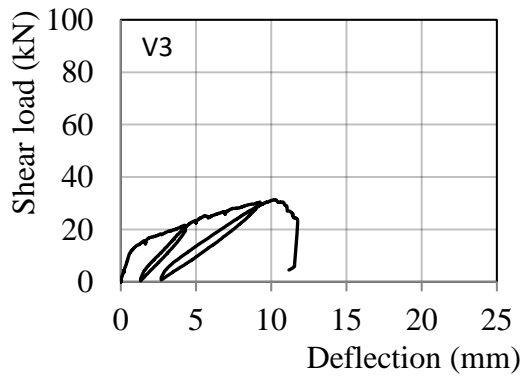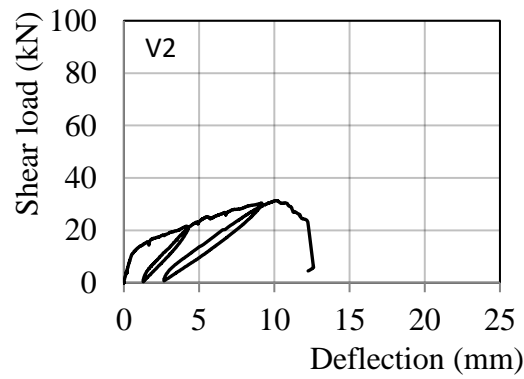
Strain in longitudinal reinforcement – non-test shear span
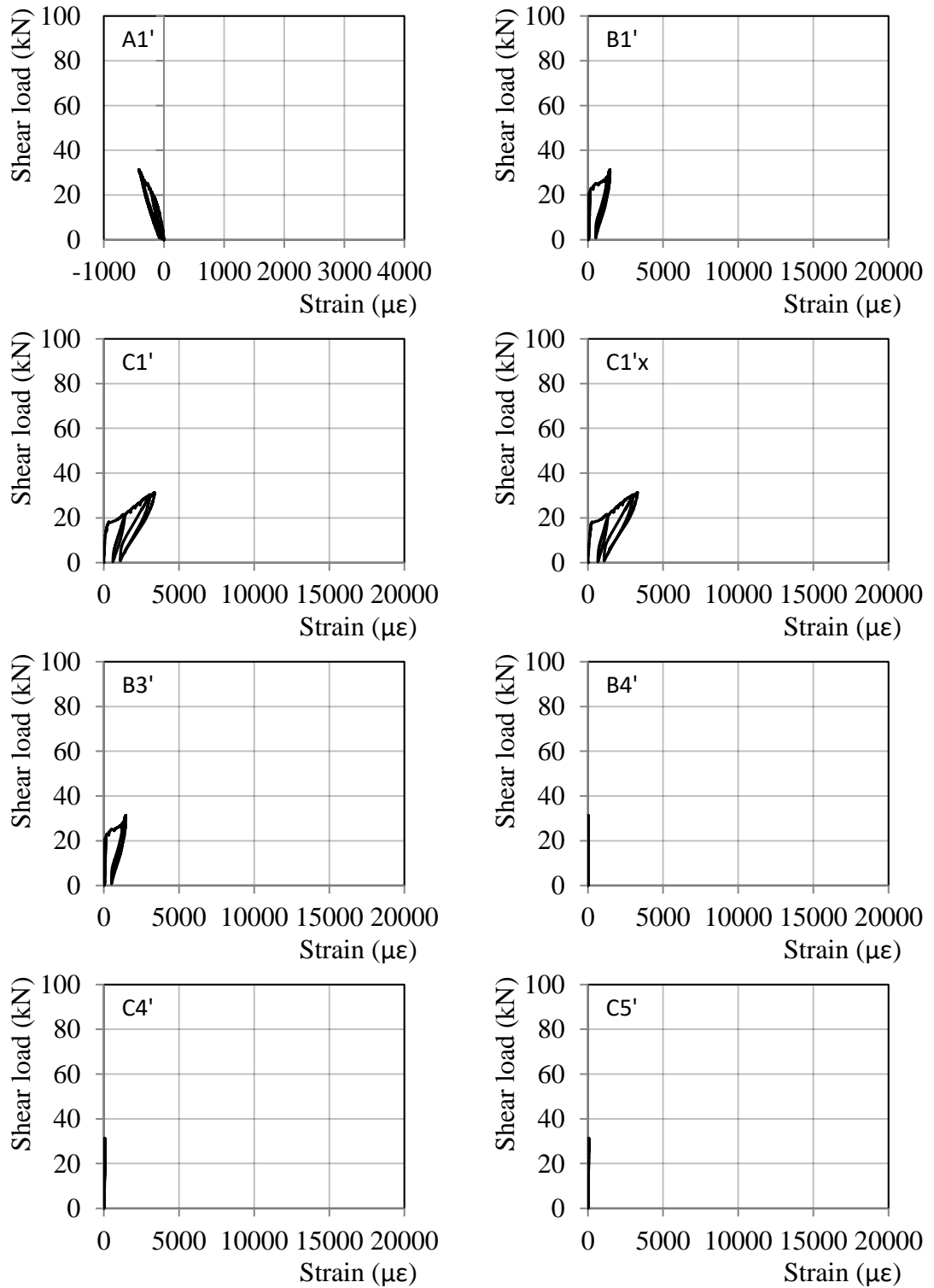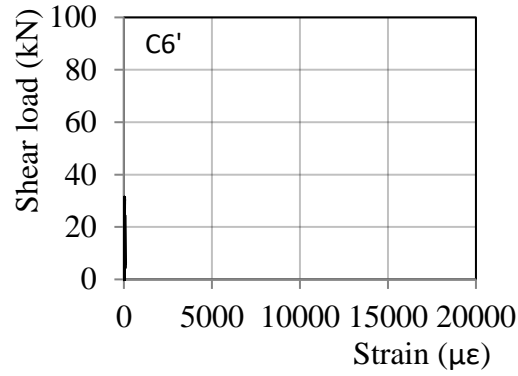
Strain in longitudinal reinforcement –test shear span
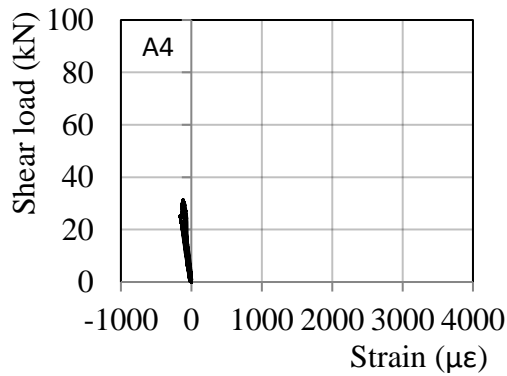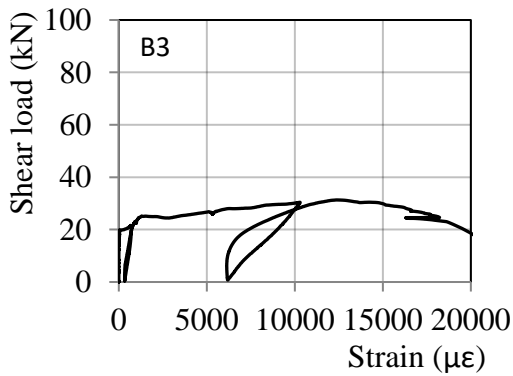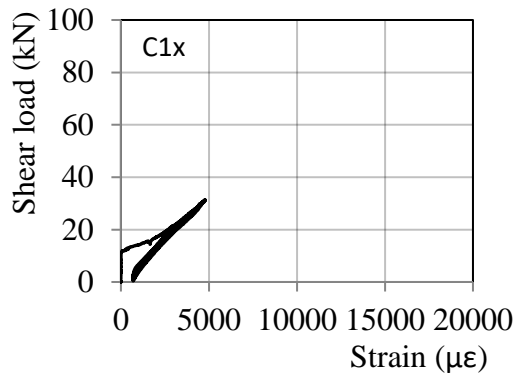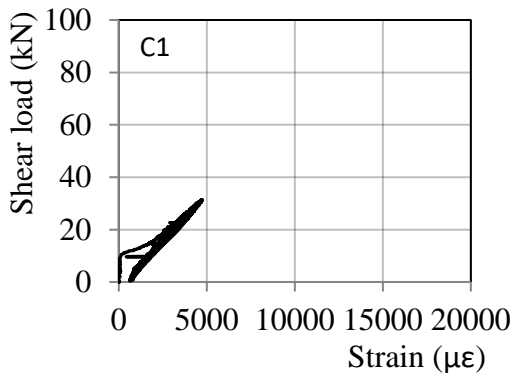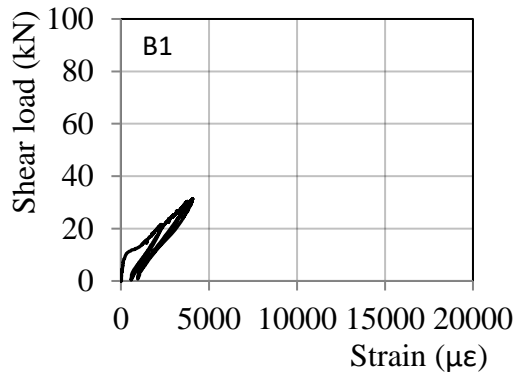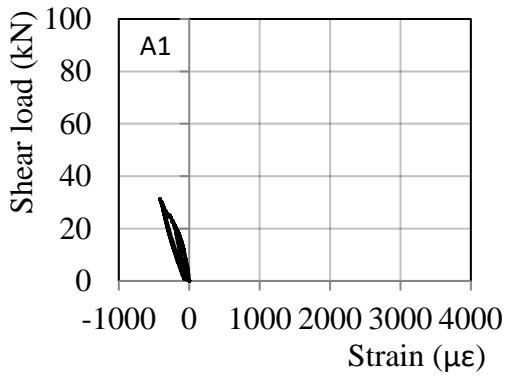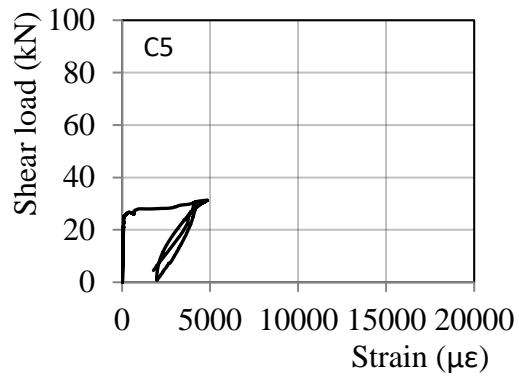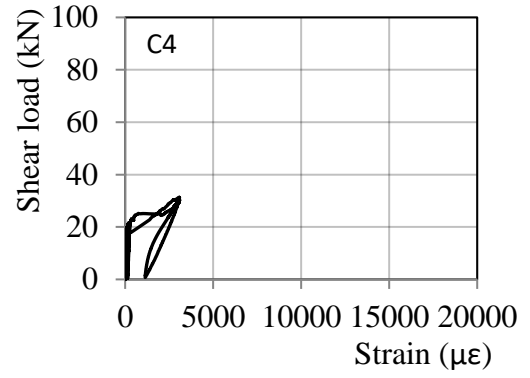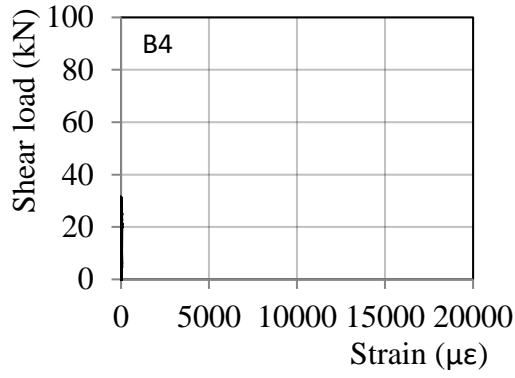
GB55

Deflections measured on top of the supports
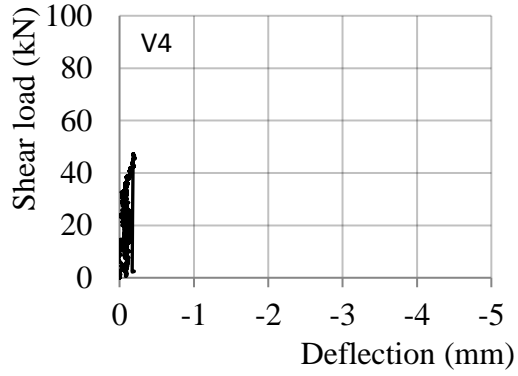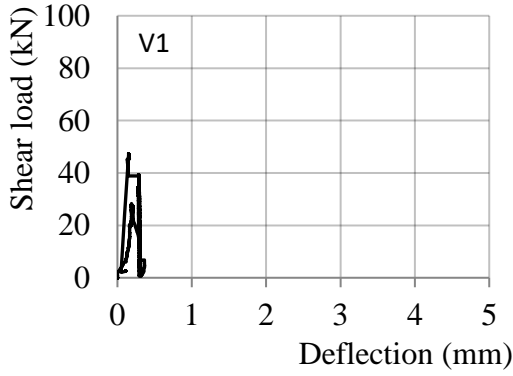
Deflections measured on the bottom of the beam
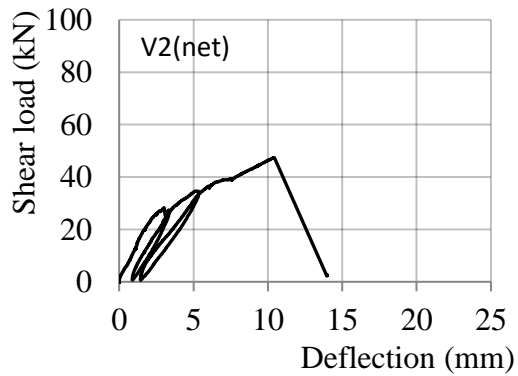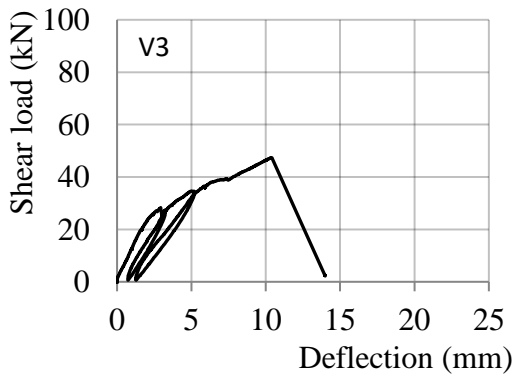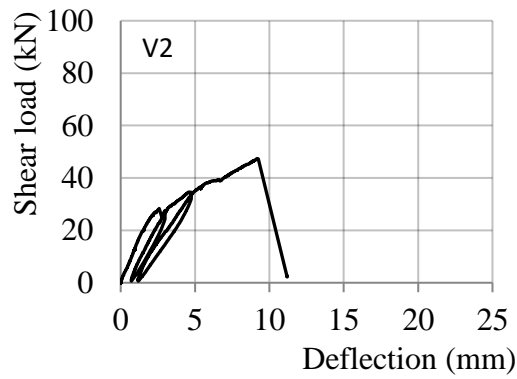
Strain in longitudinal reinforcement –test shear span
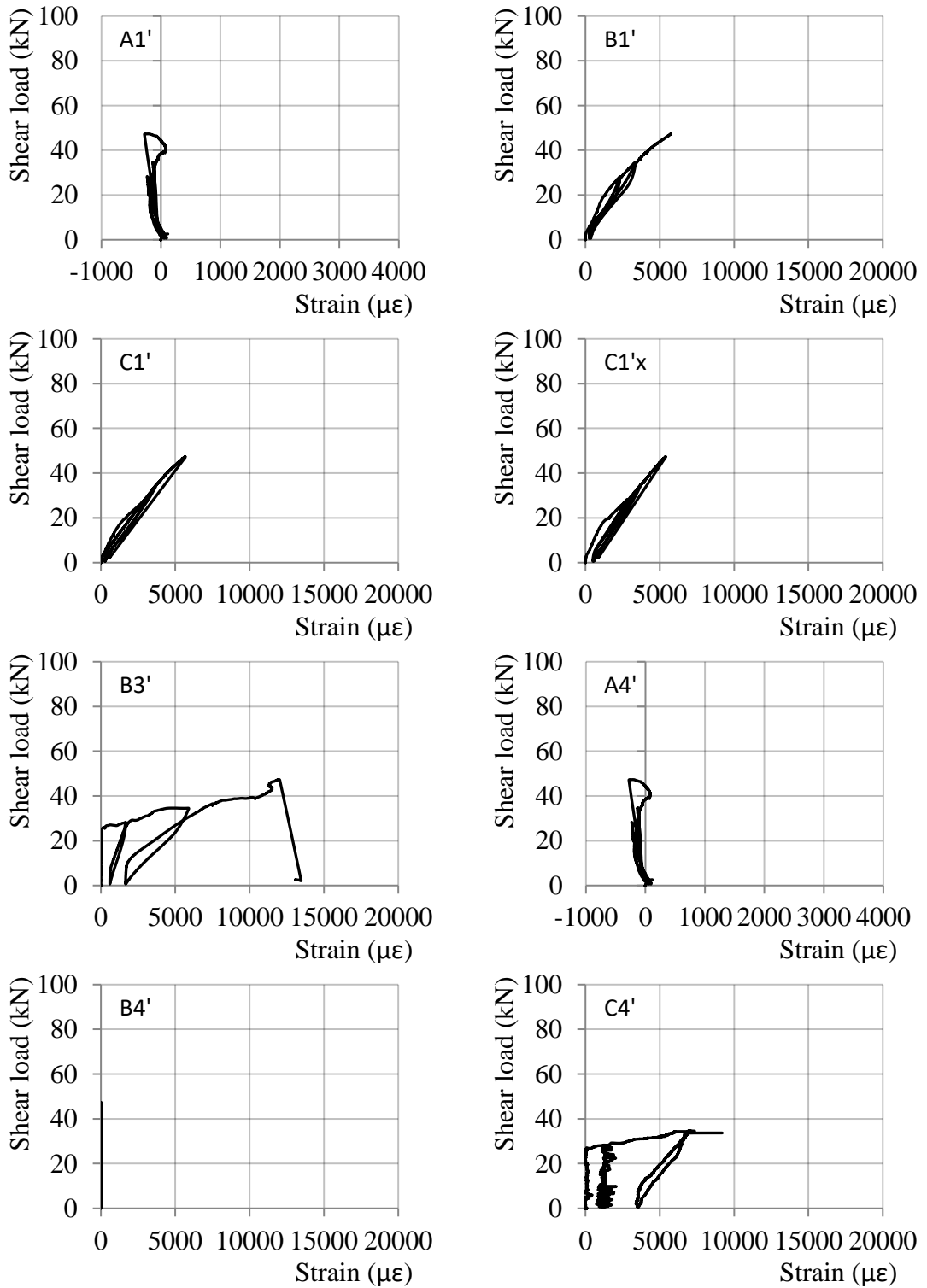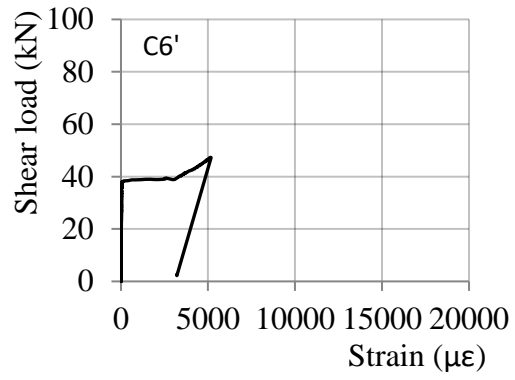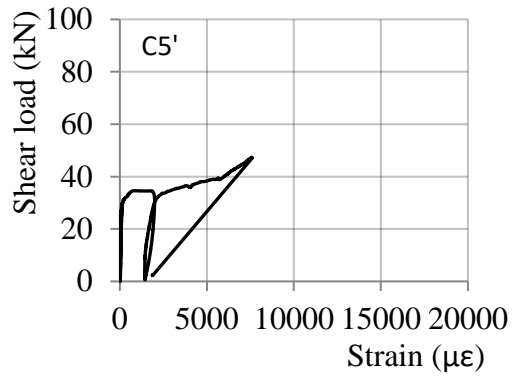
GB56

Deflections measured on top of the supports
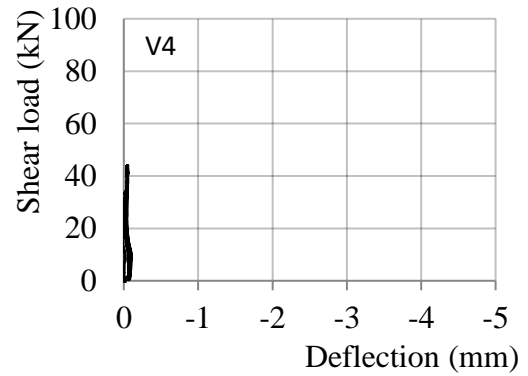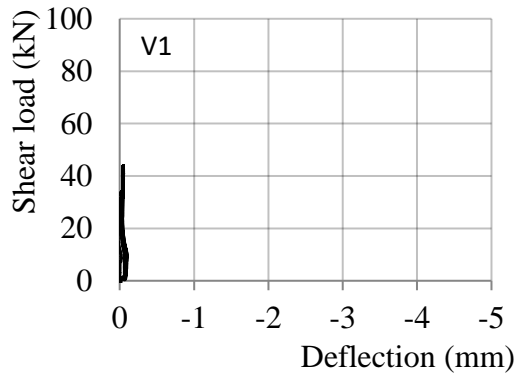
Deflections measured on the bottom of the beam
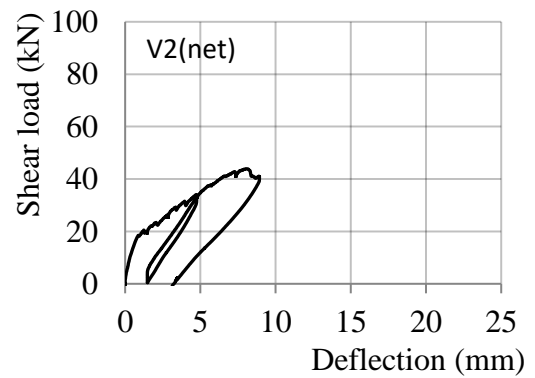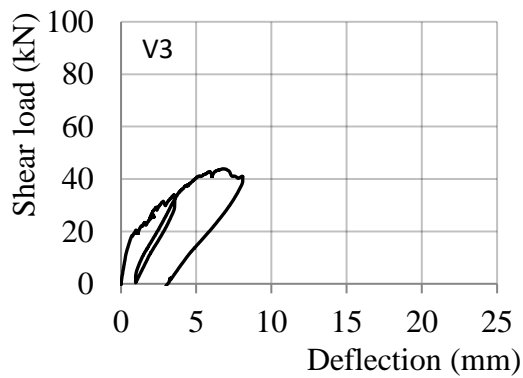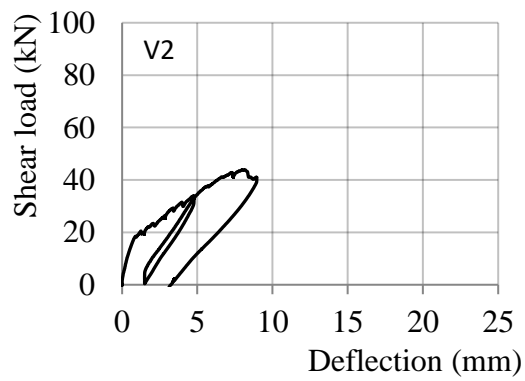
*Strain in longitudinal reinforcement –test shear span*
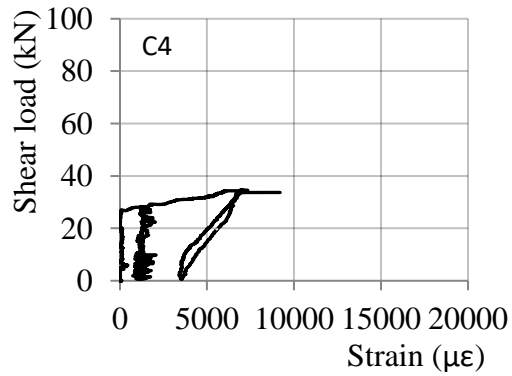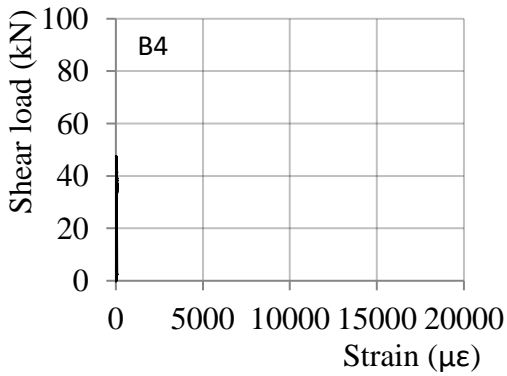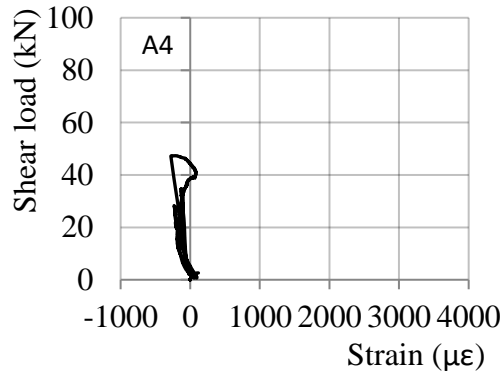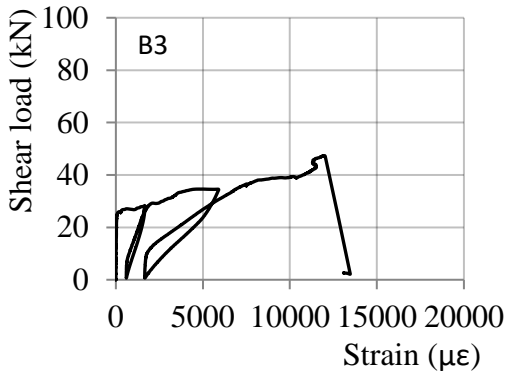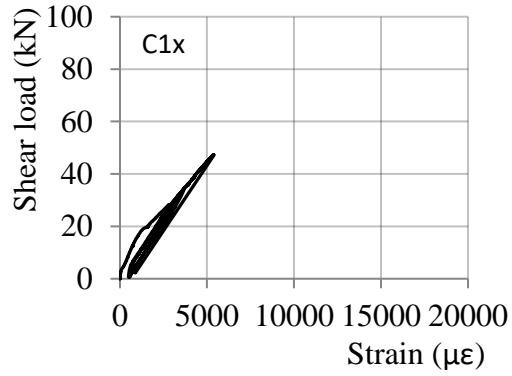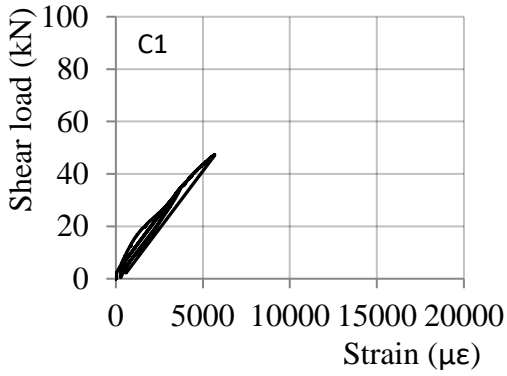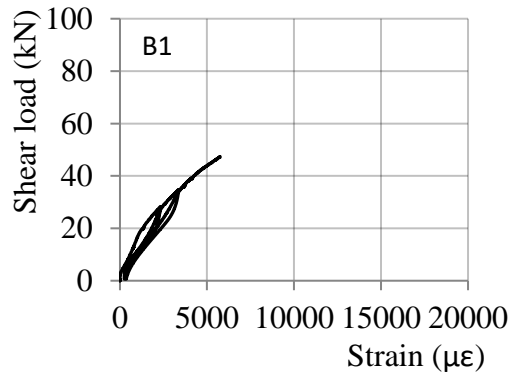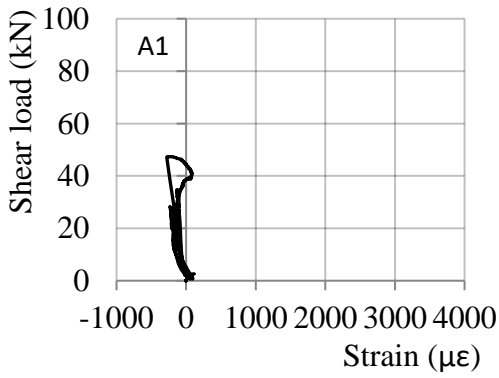
GB57

Deflections measured on top of the supports
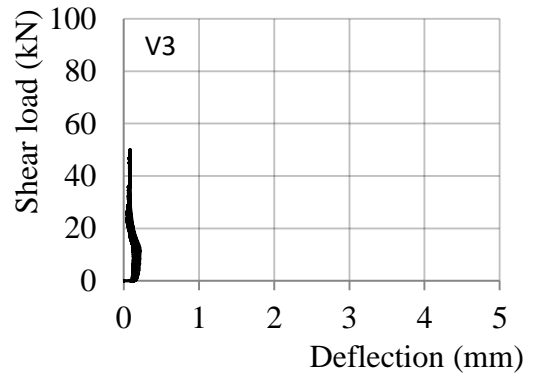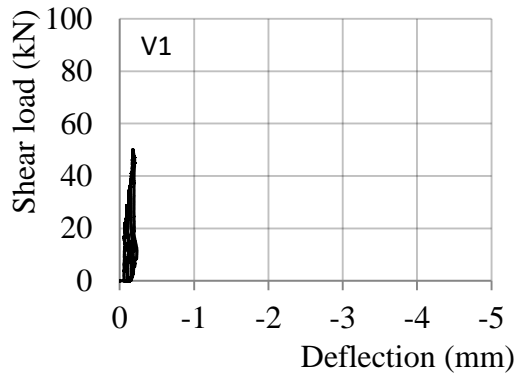
Deflections measured on the bottom of the beam
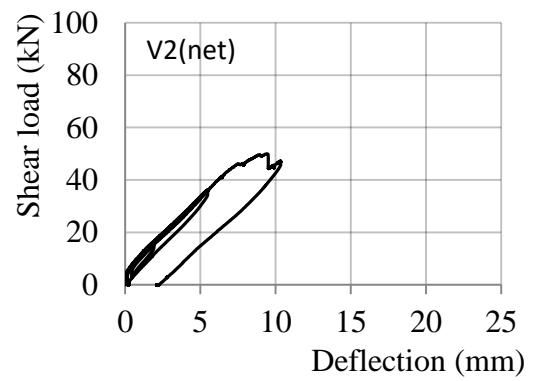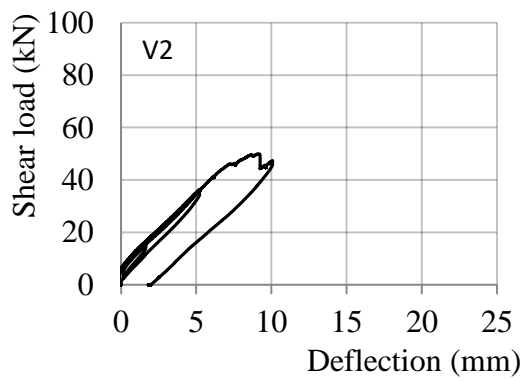
Strain in longitudinal reinforcement –test shear span
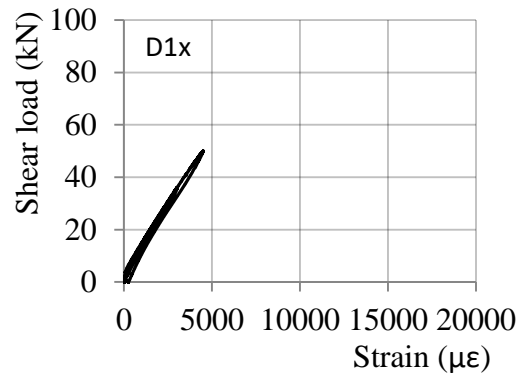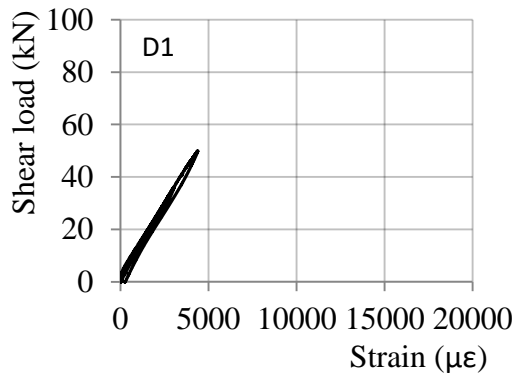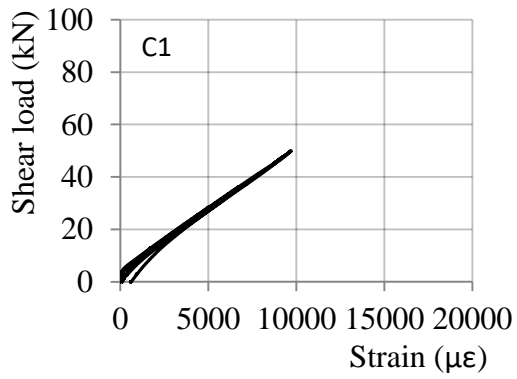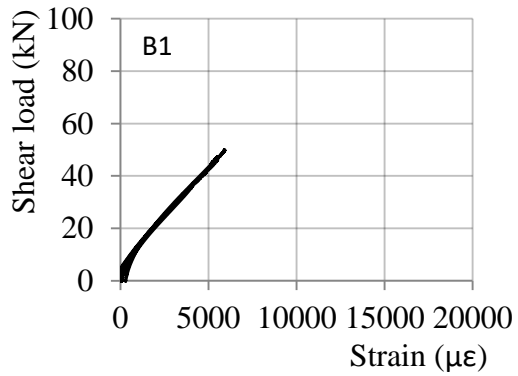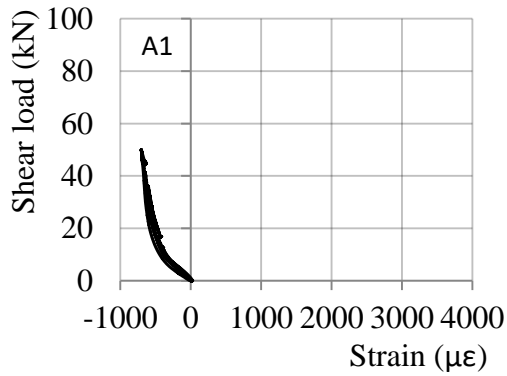
Appendix E

## Experimental Results: Beams with FRP Shear Links

GB62

Deflections measured on top of the supports
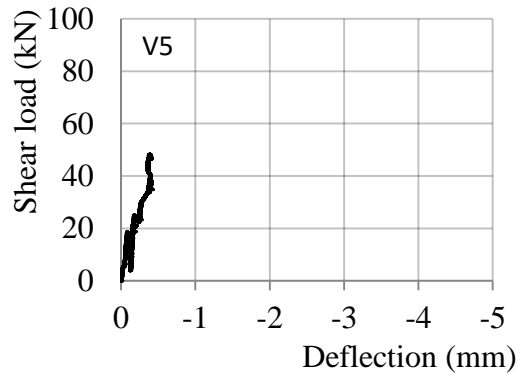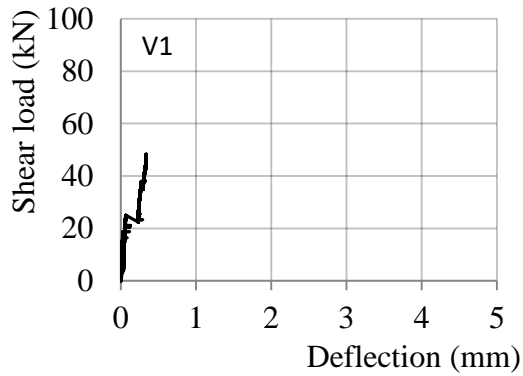
Deflections measured on the bottom of the beam
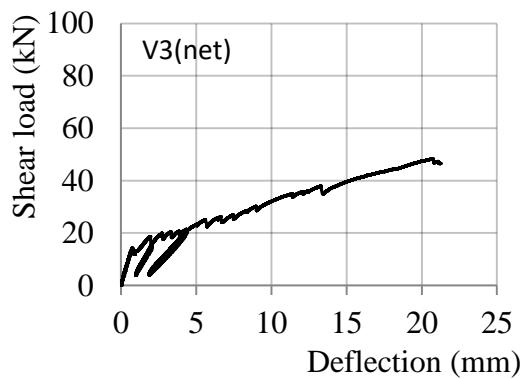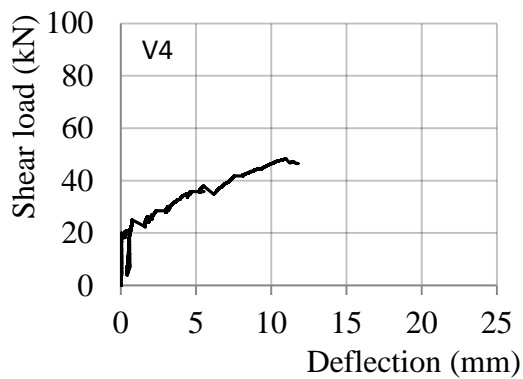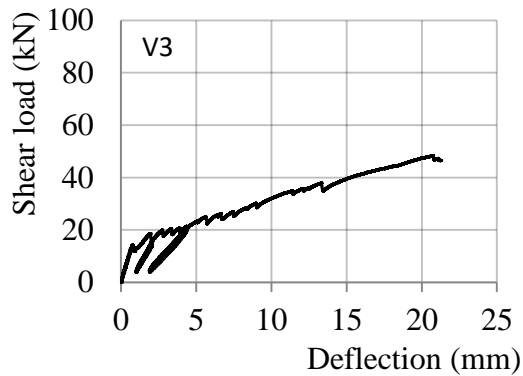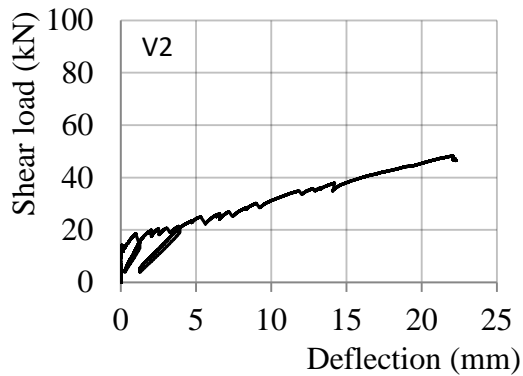
Strain in longitudinal reinforcement – non-test shear span
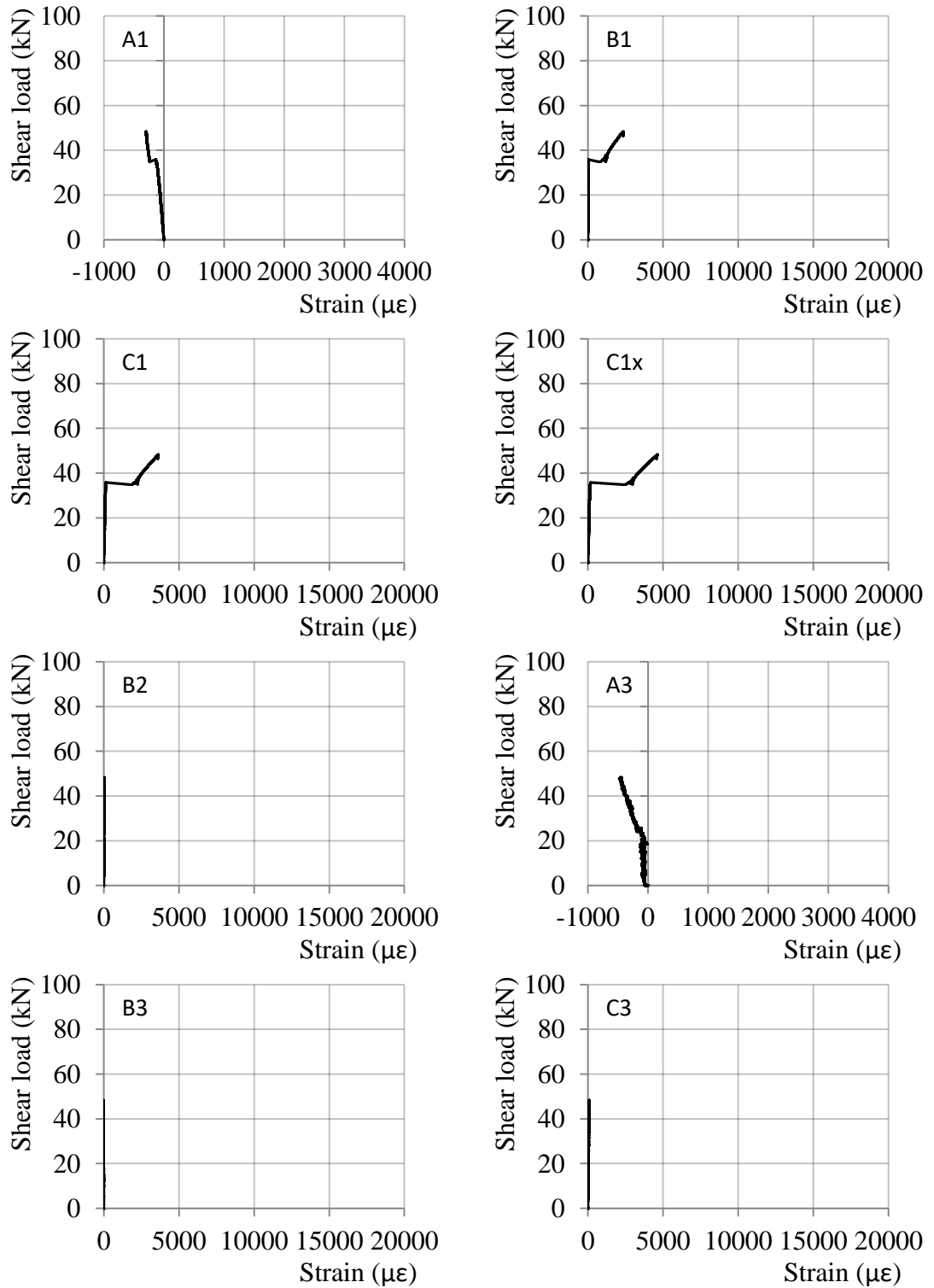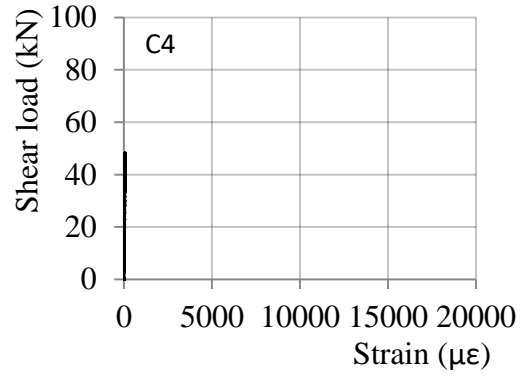
Strain in longitudinal reinforcement –test shear span
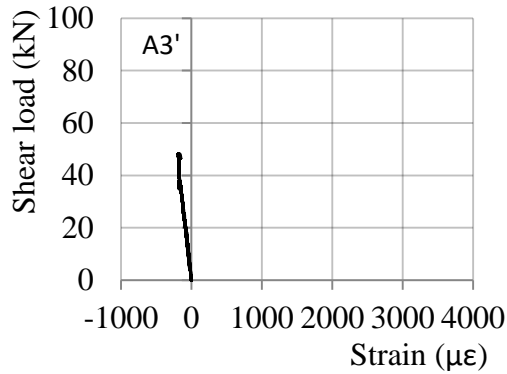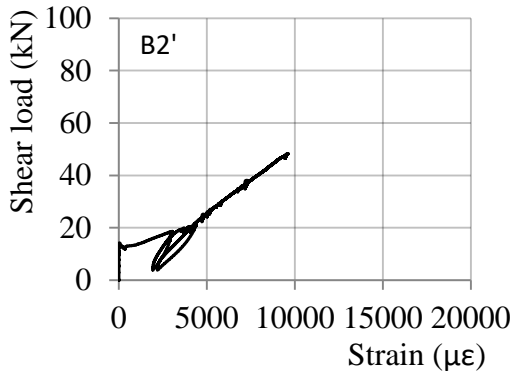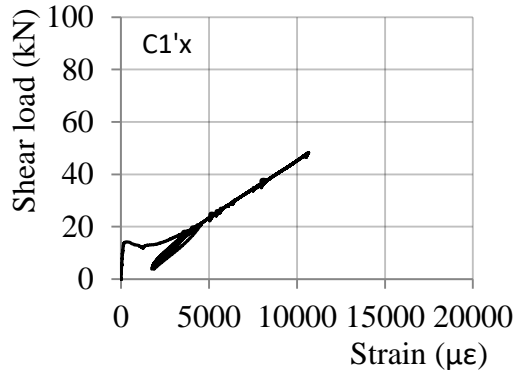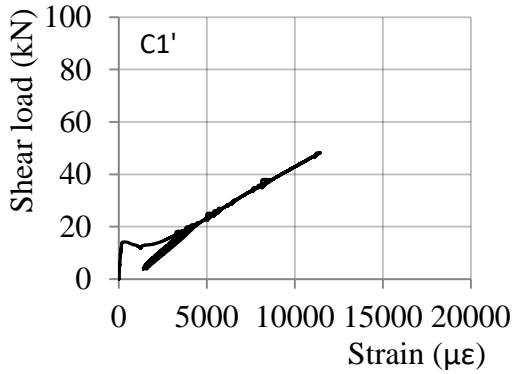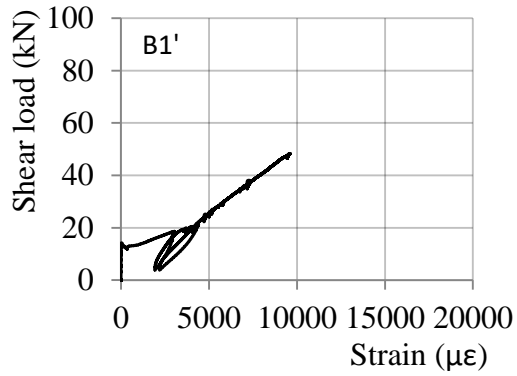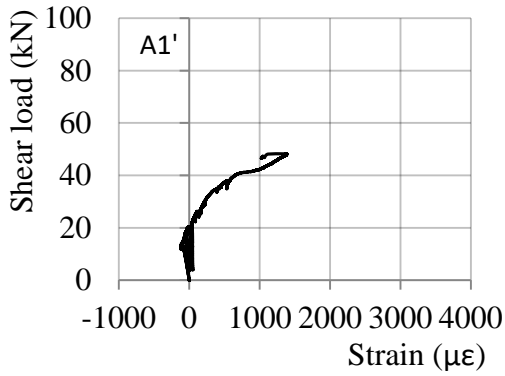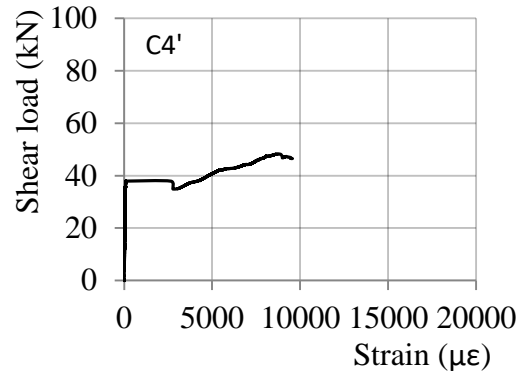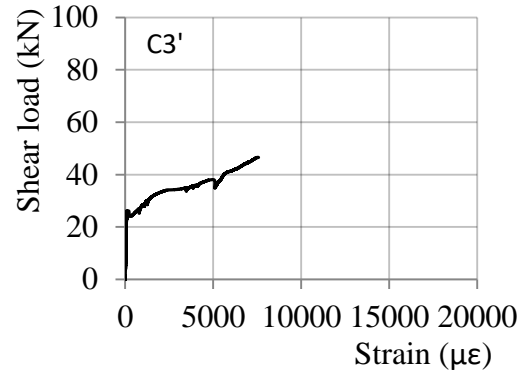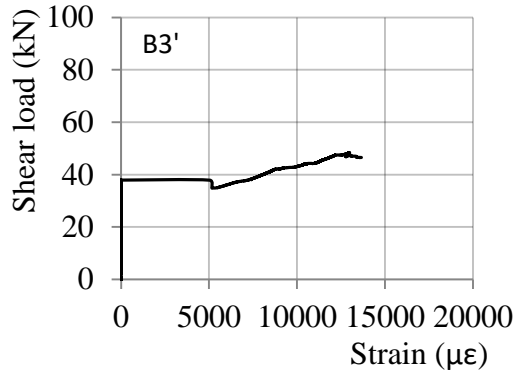
Strain in GFRP links
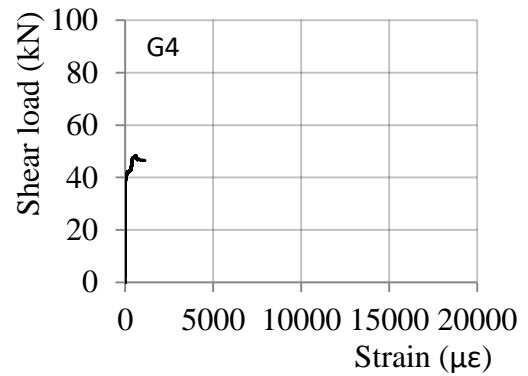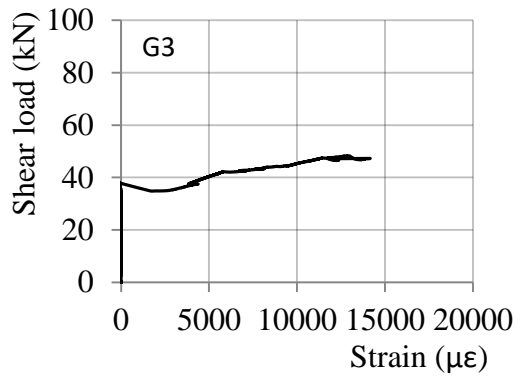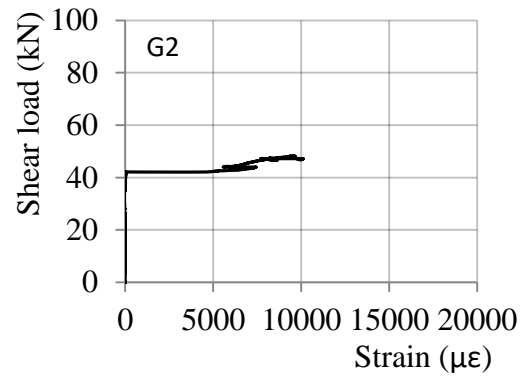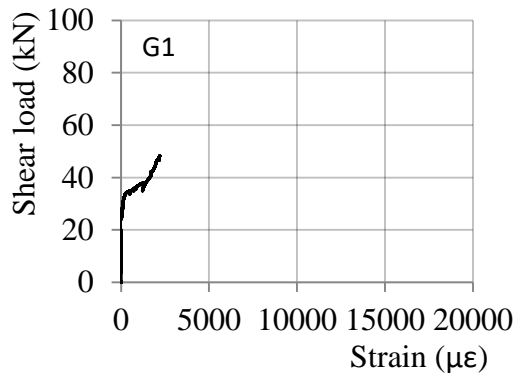
GB63

Deflections measured on top of the supports
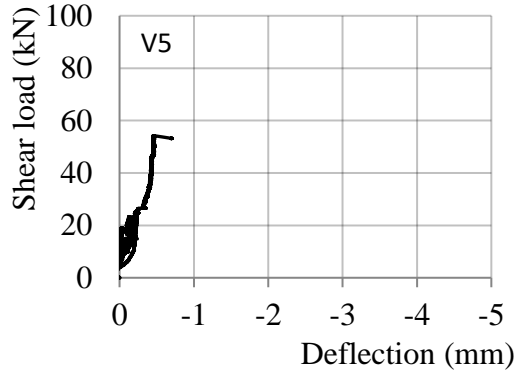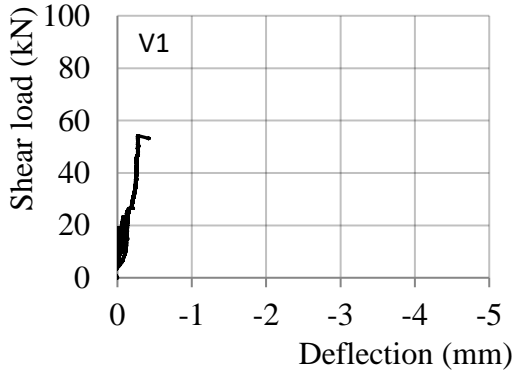
Deflections measured on the bottom of the beam
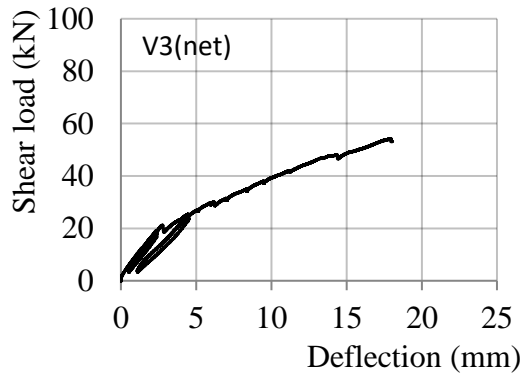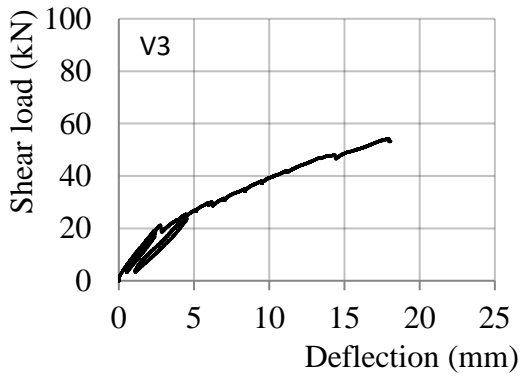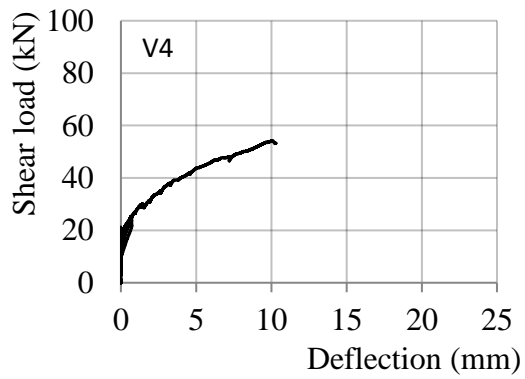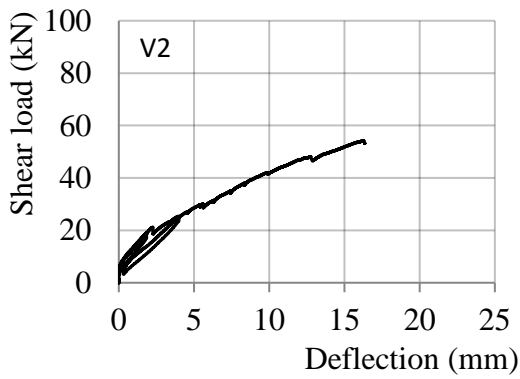
Strain in longitudinal reinforcement – non-test shear span
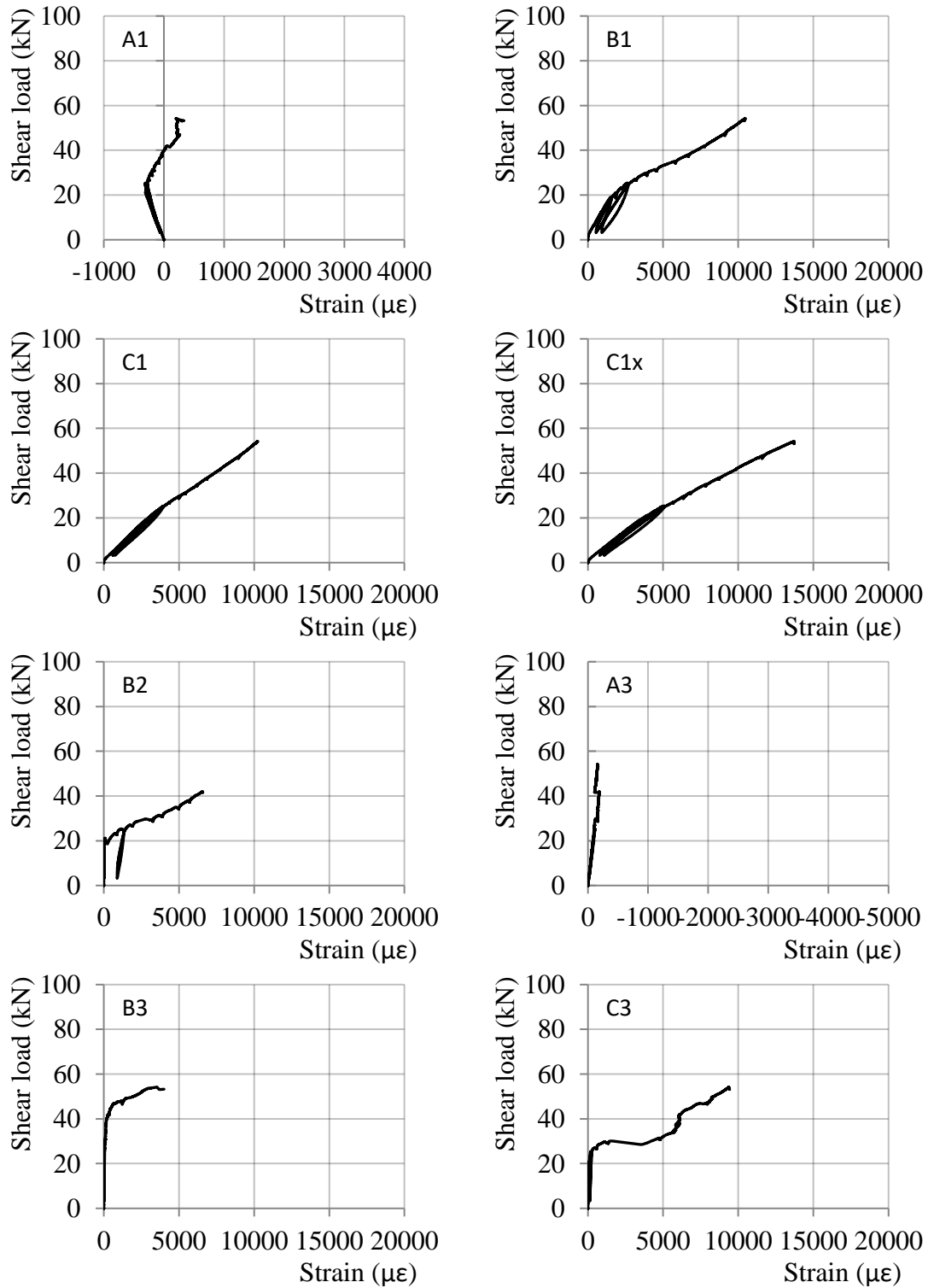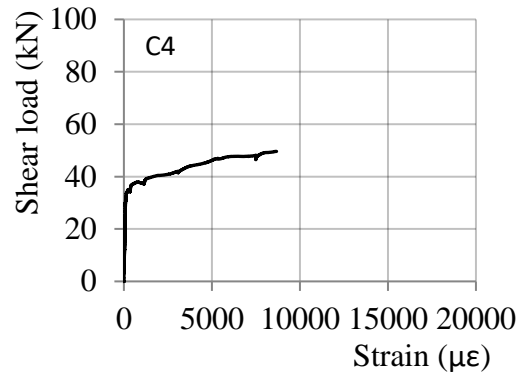
Strain in CFRP links
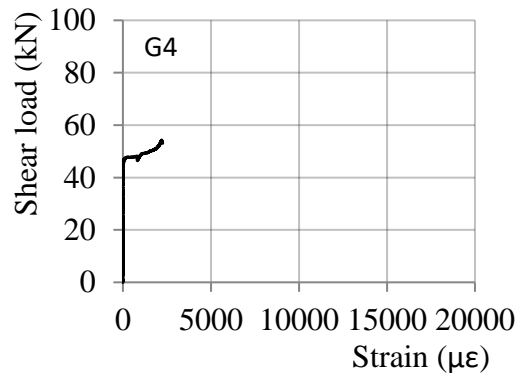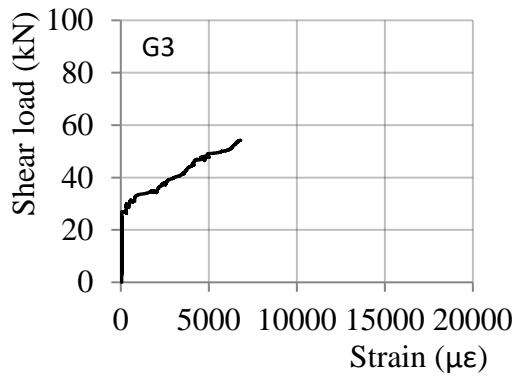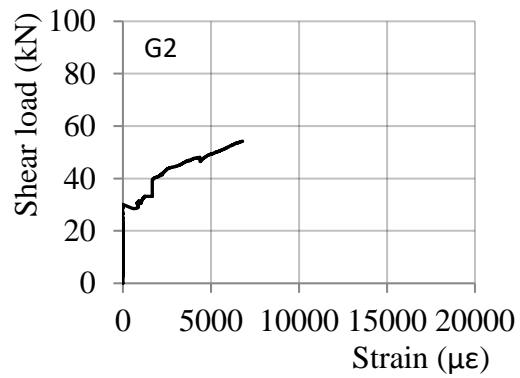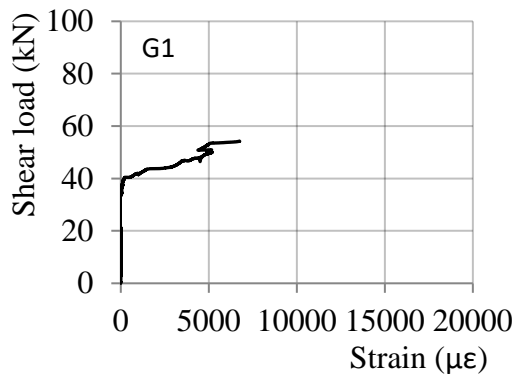
GB64

Deflections measured on top of the supports
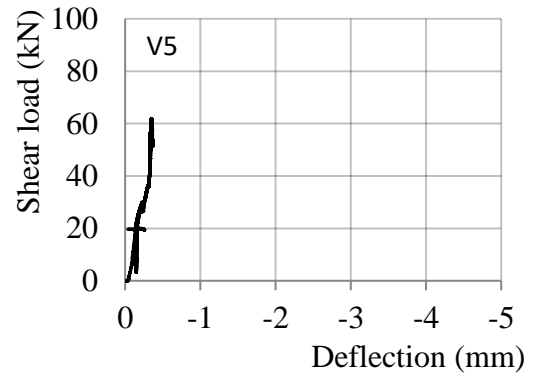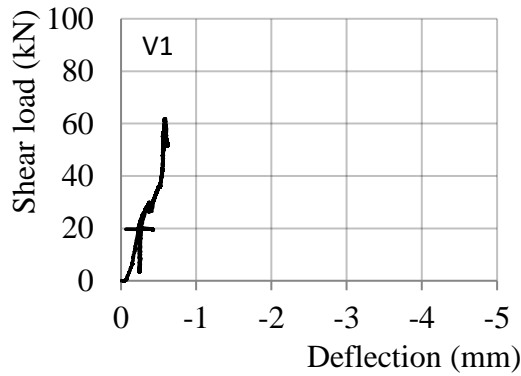
Deflections measured on the bottom of the beam
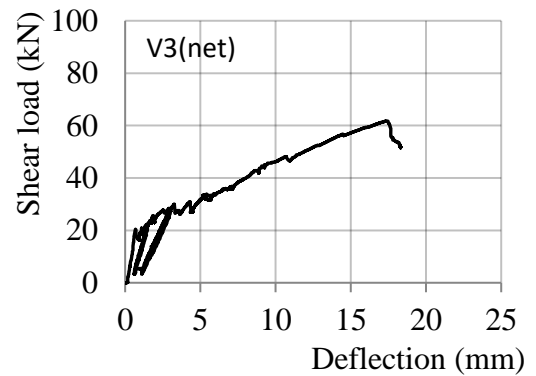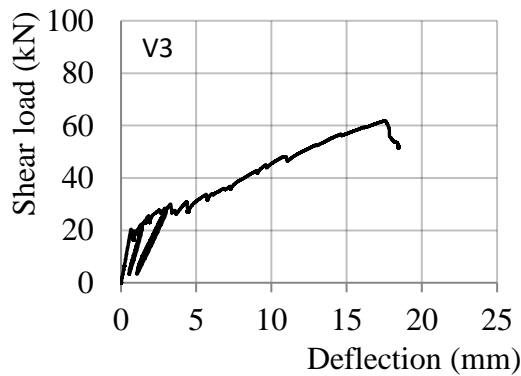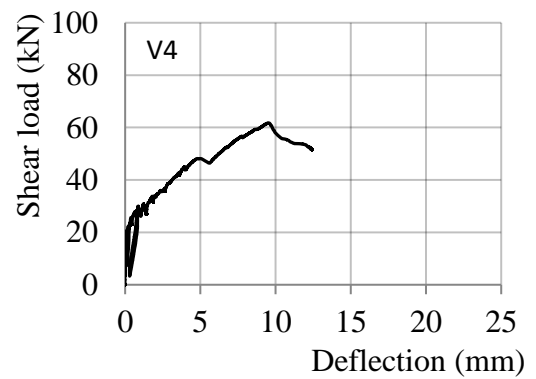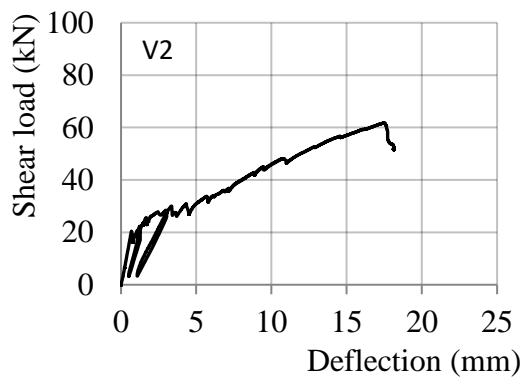
Strain in longitudinal reinforcement – non-test shear span
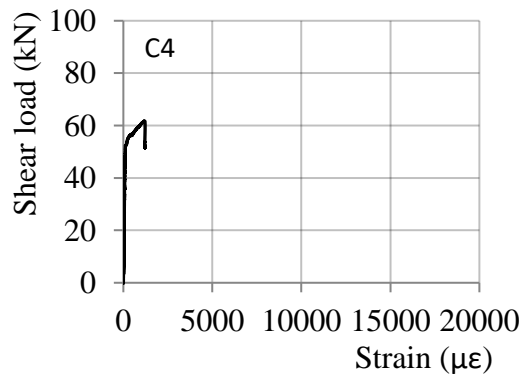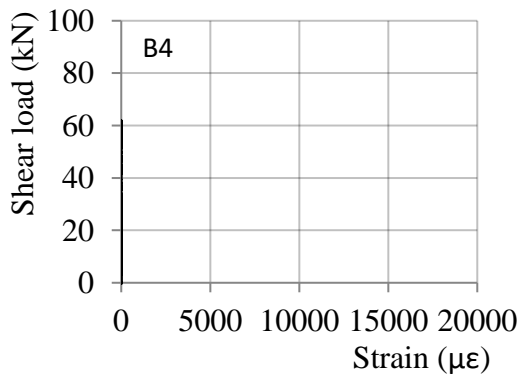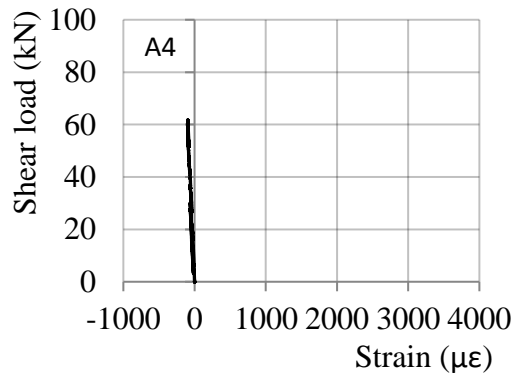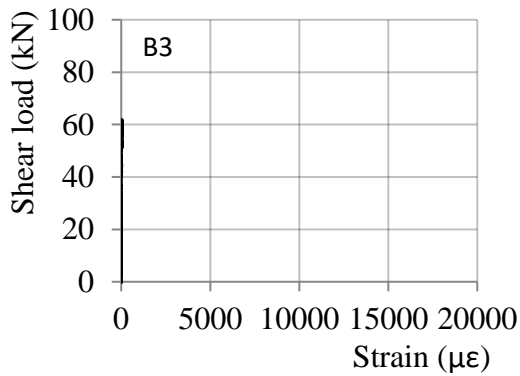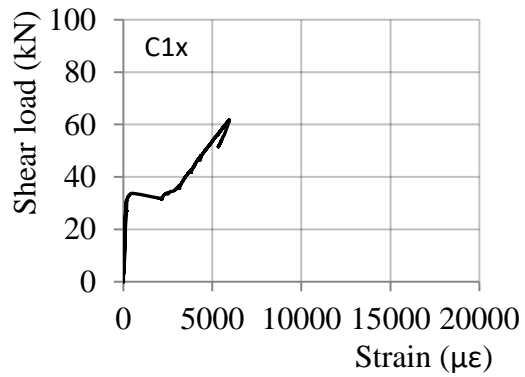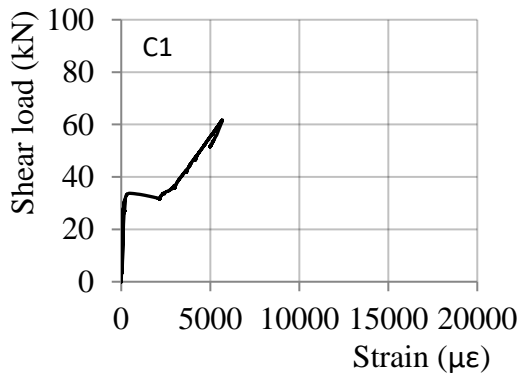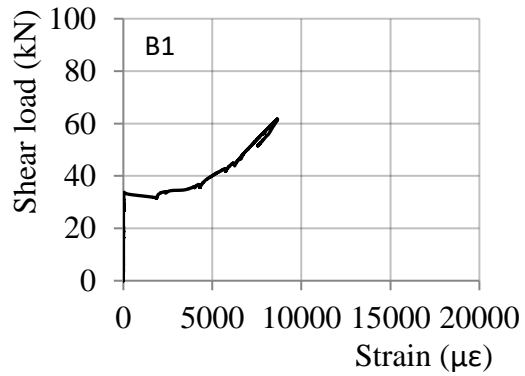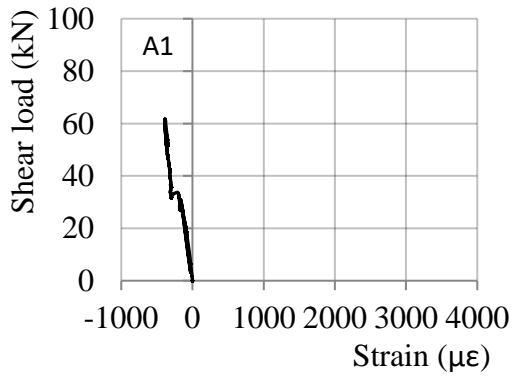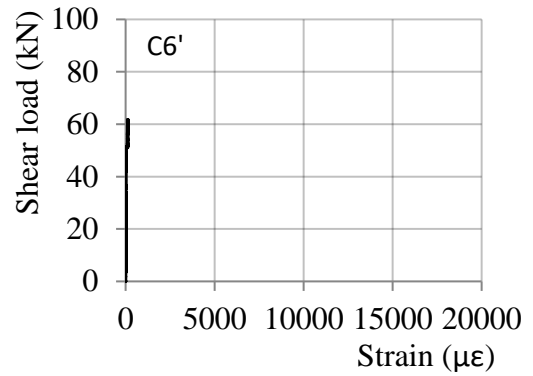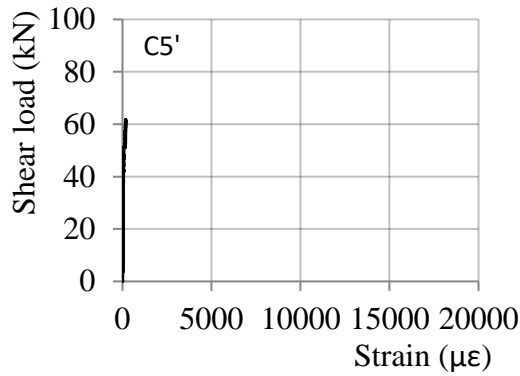
Strain in longitudinal reinforcement –test shear span
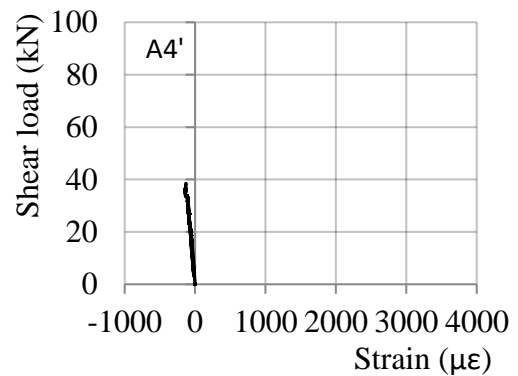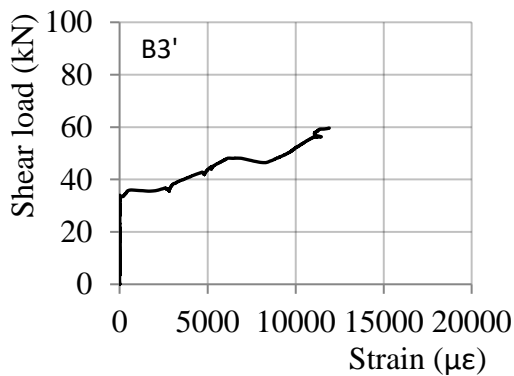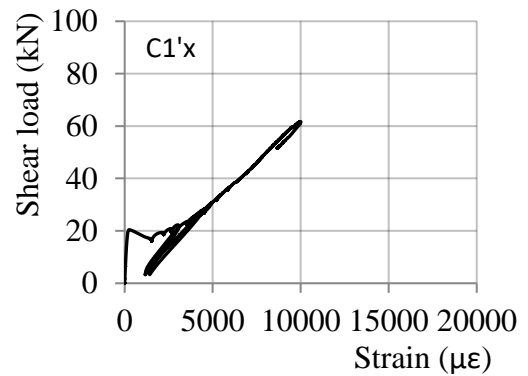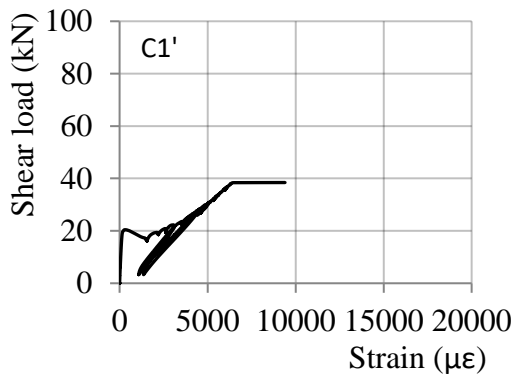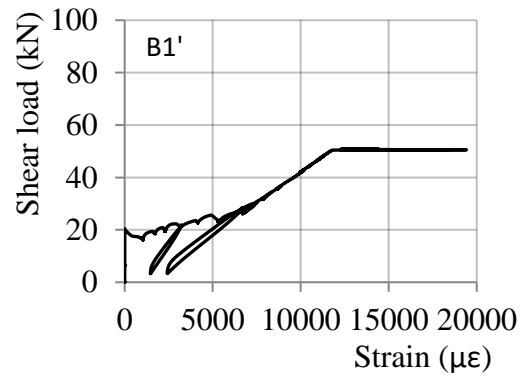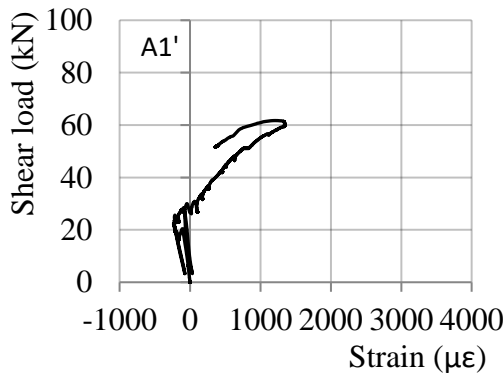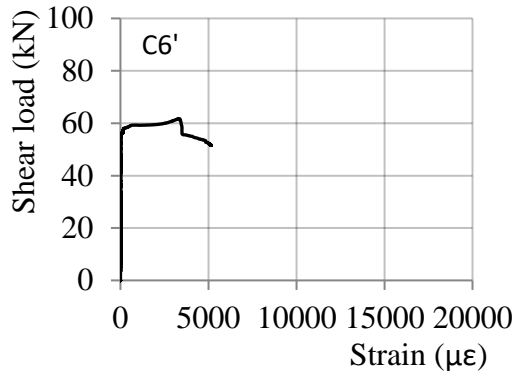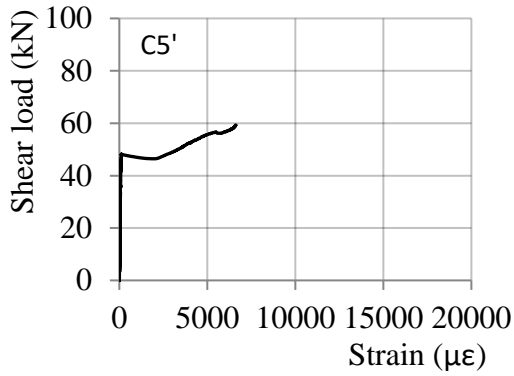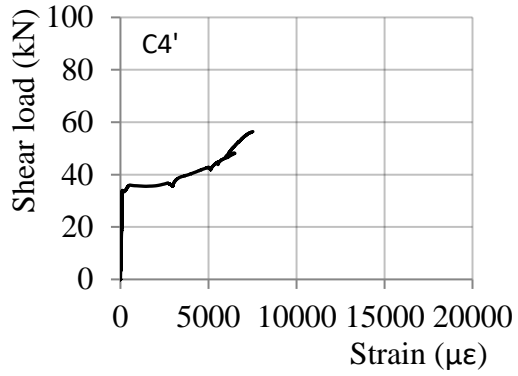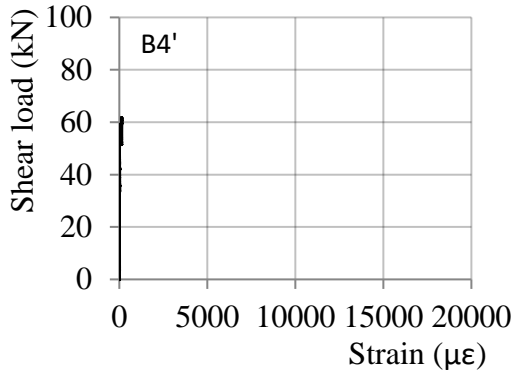
Strain in GFRP links
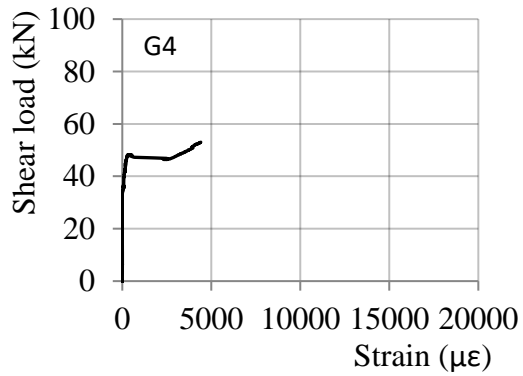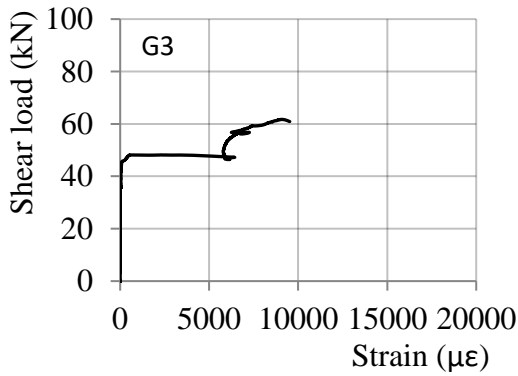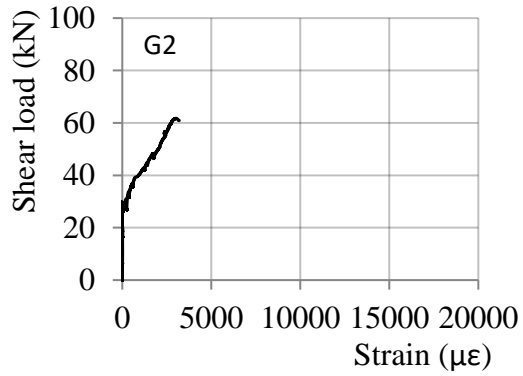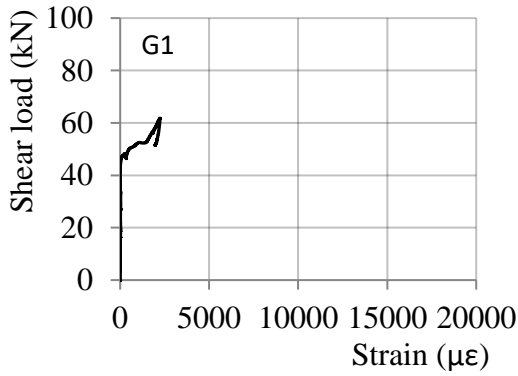
GB65

Deflections measured on top of the supports
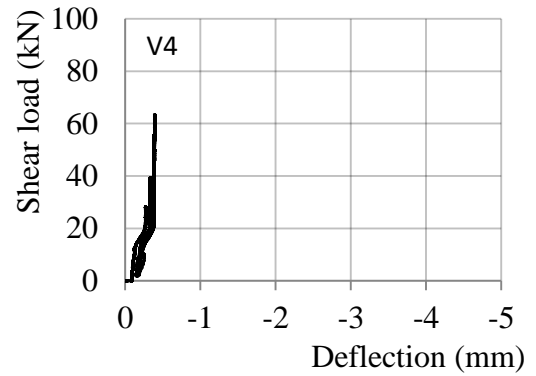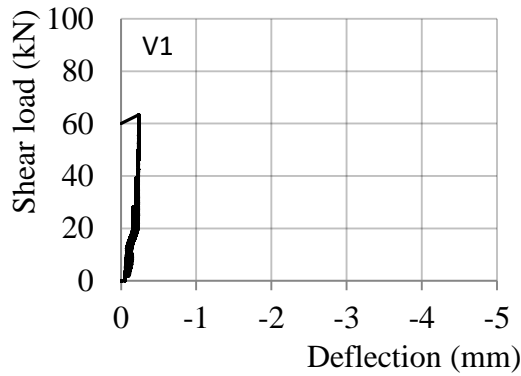
Deflections measured on the bottom of the beam
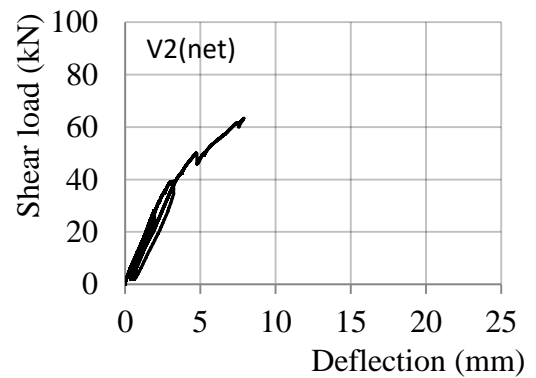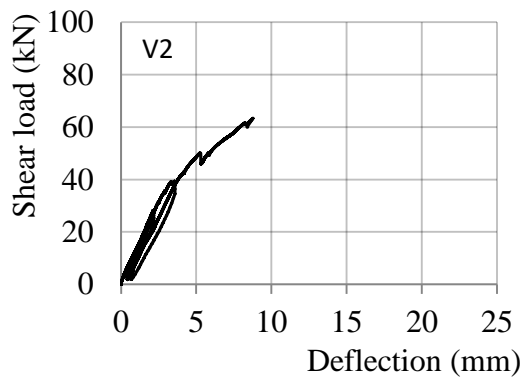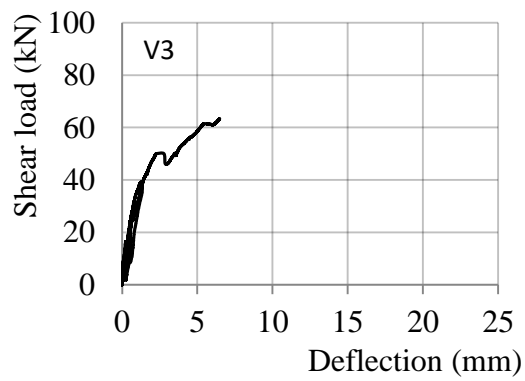
Strain in longitudinal reinforcement – test shear span
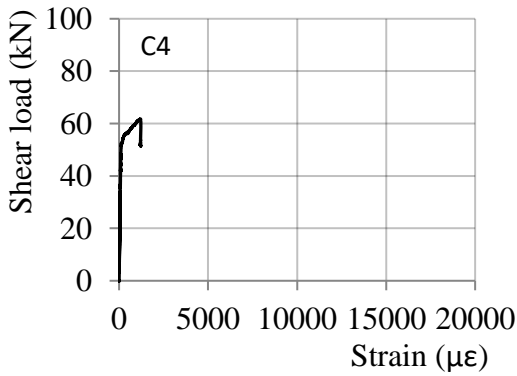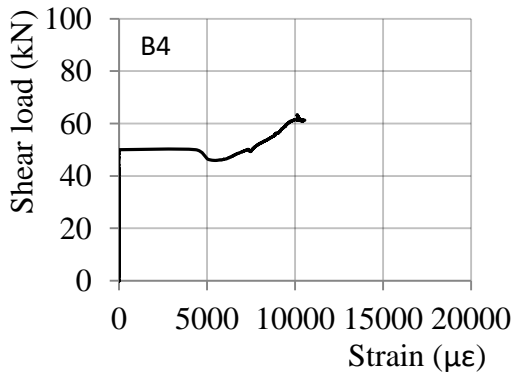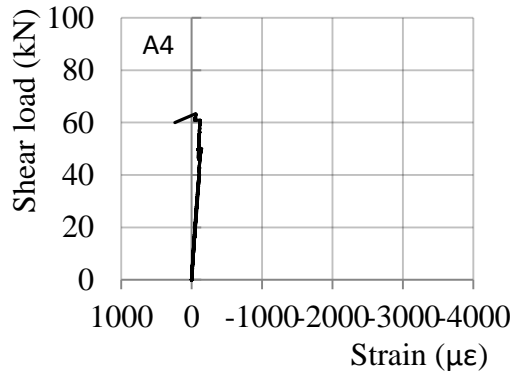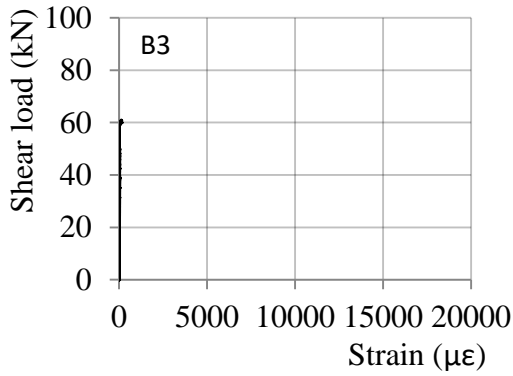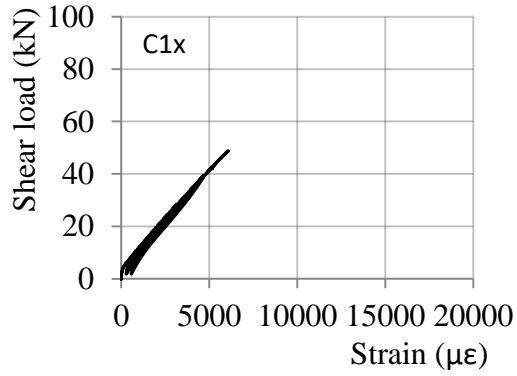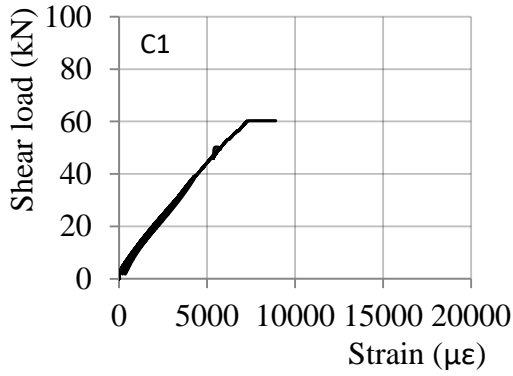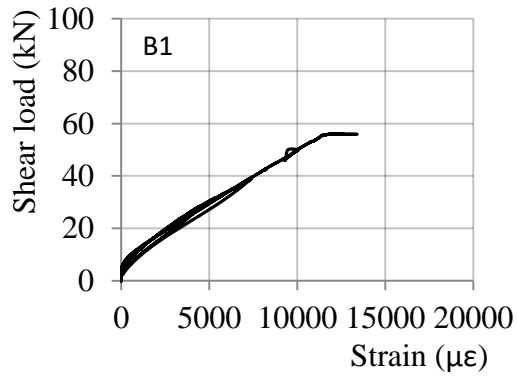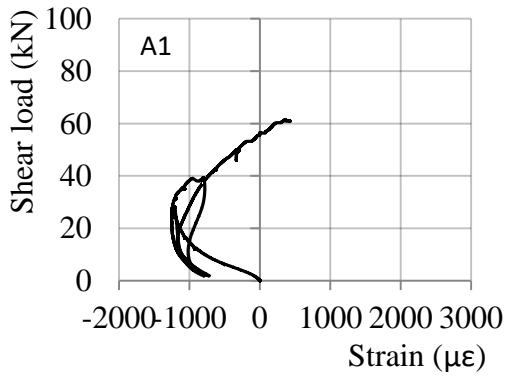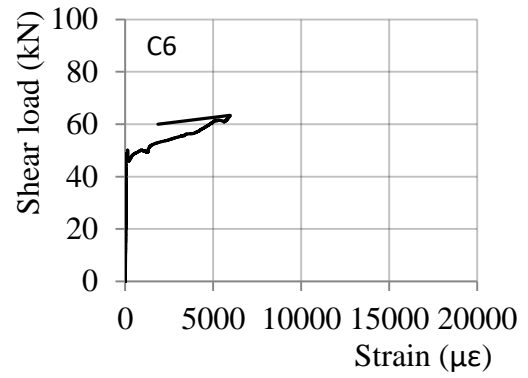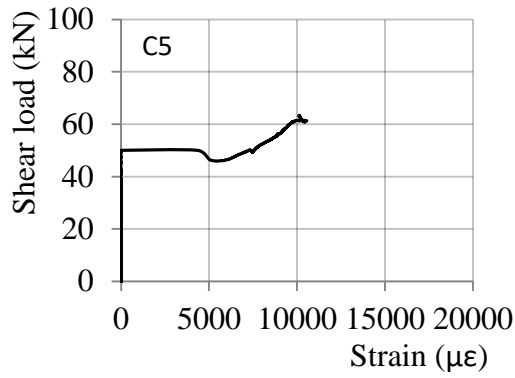
Strain in CFRP links
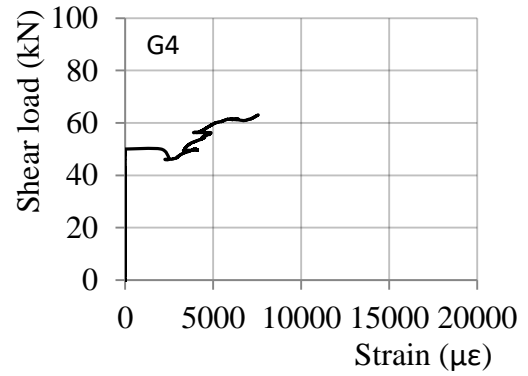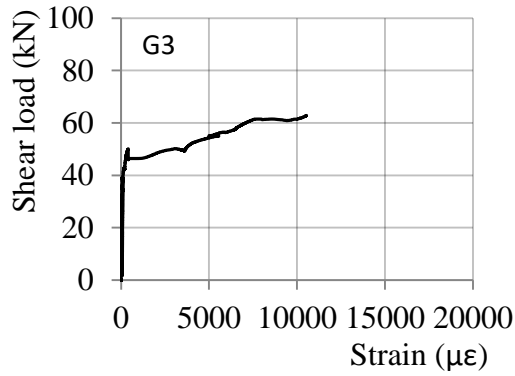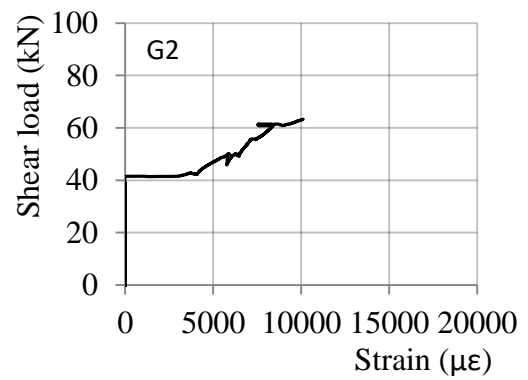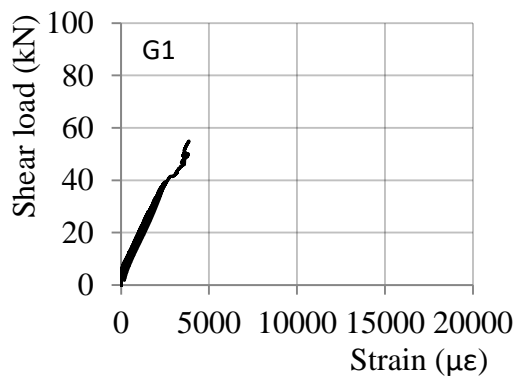
GB60

Deflections measured on top of the supports
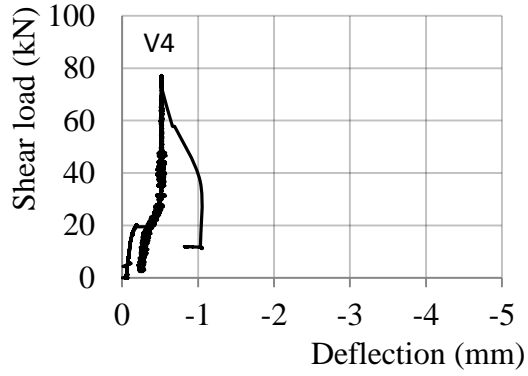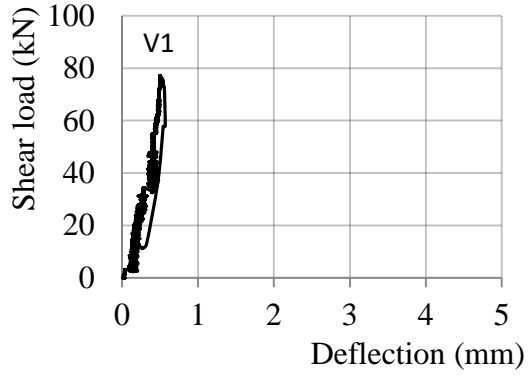
Deflections measured on the bottom of the beam

Strain in longitudinal reinforcement –-test shear span

C4

C5

D5

D6

D7

Strain in GFRP links

G1

G2
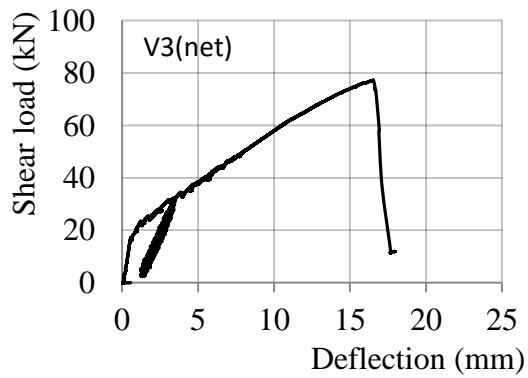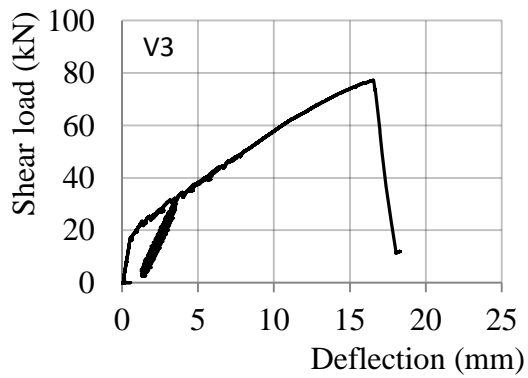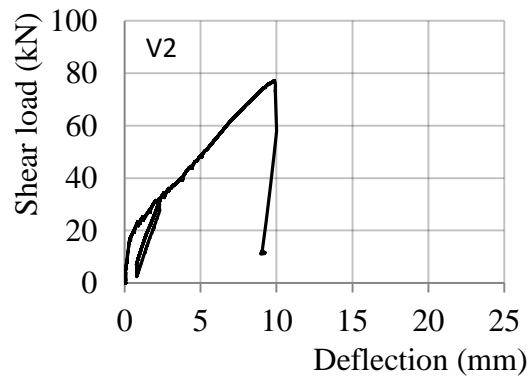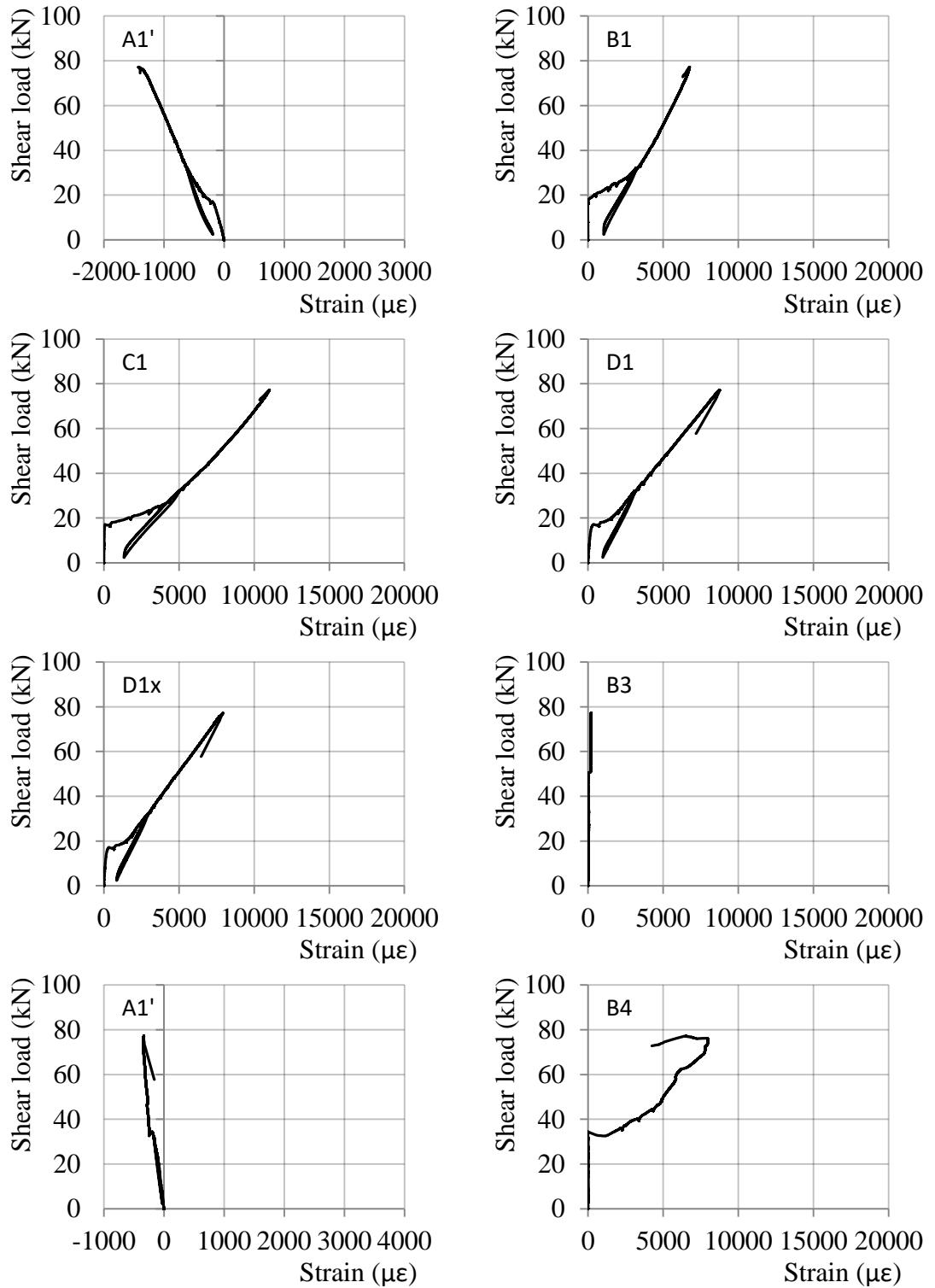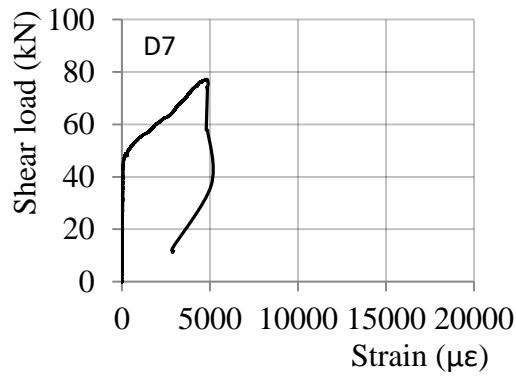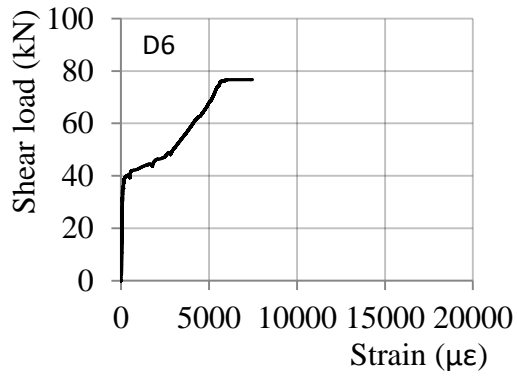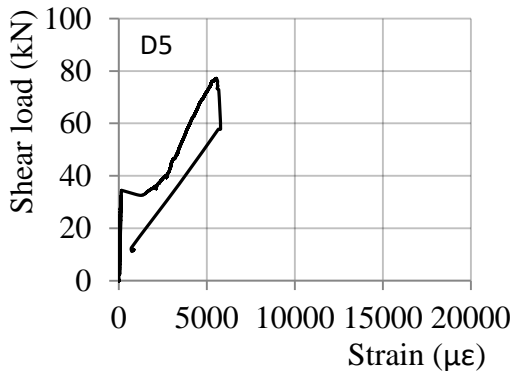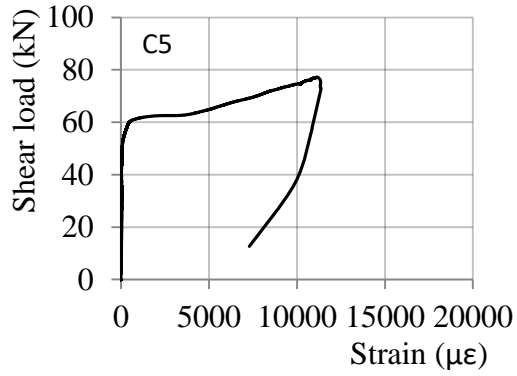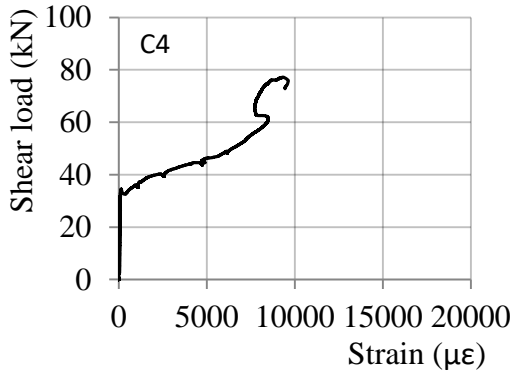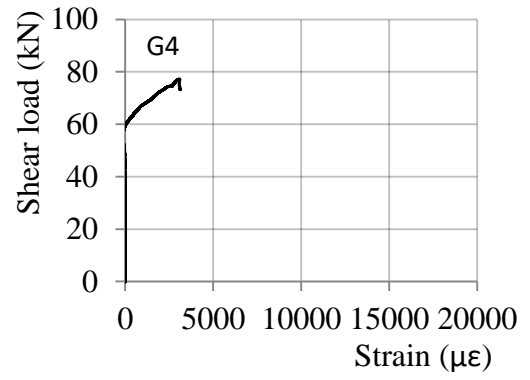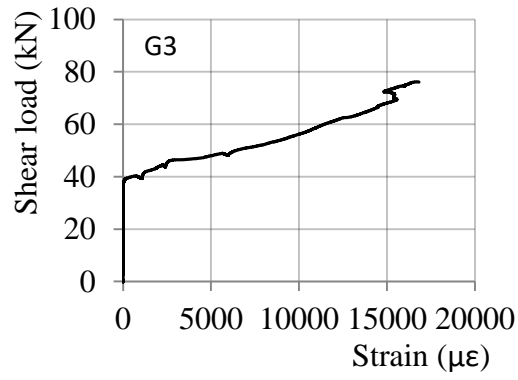
GB61

Deflections measured on top of the supports

Deflections measured on the bottom of the beam
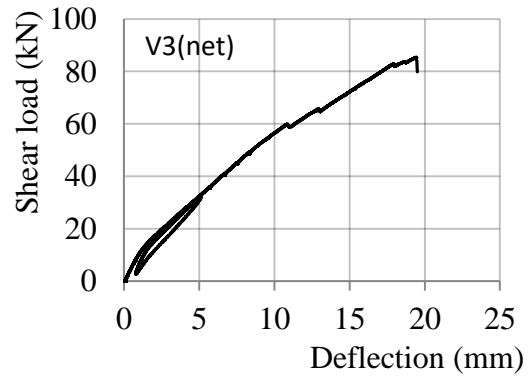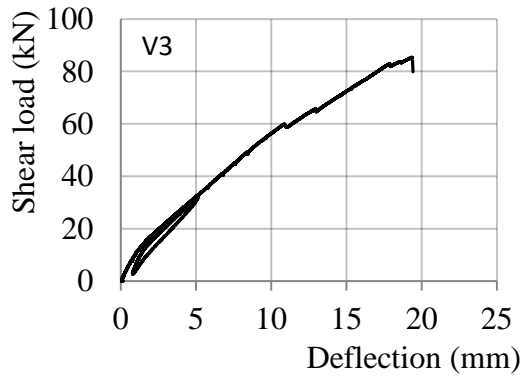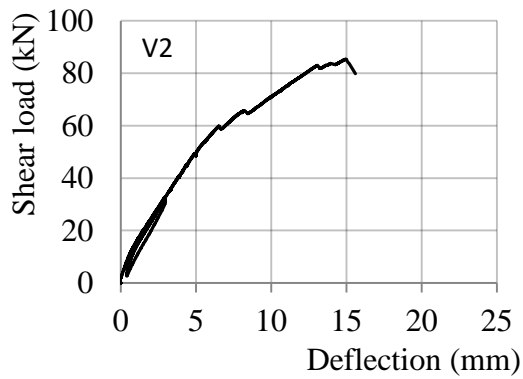
Strain in longitudinal reinforcement –-test shear span
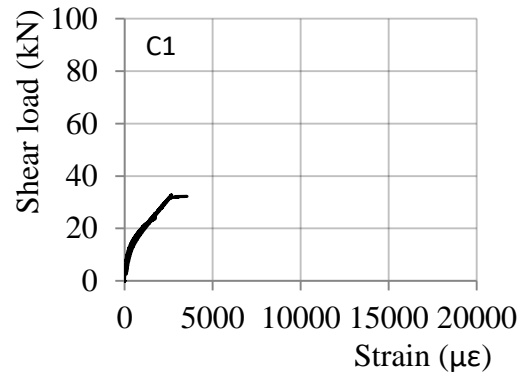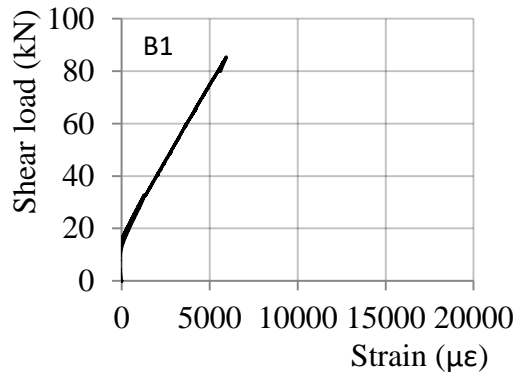
Strain in CFRP links
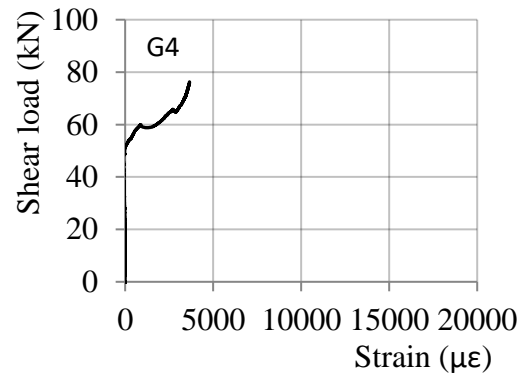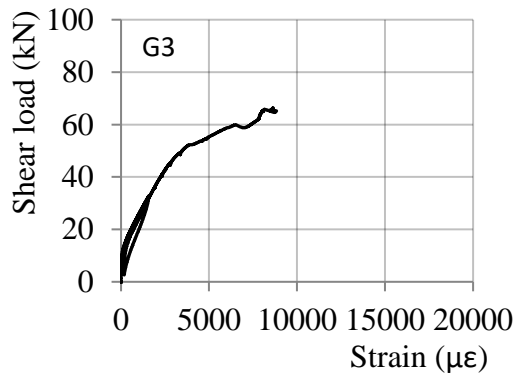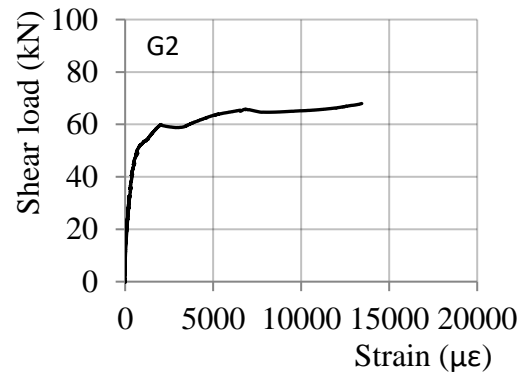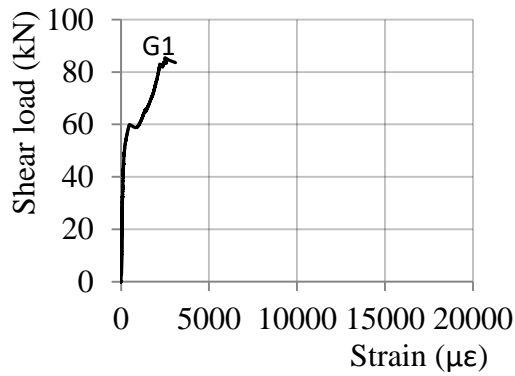
This page intentionally left blank

Appendix F

Photographs

Photo 1 Shear failure in GB58-0

Photo 2 Shear failure in GB59-0
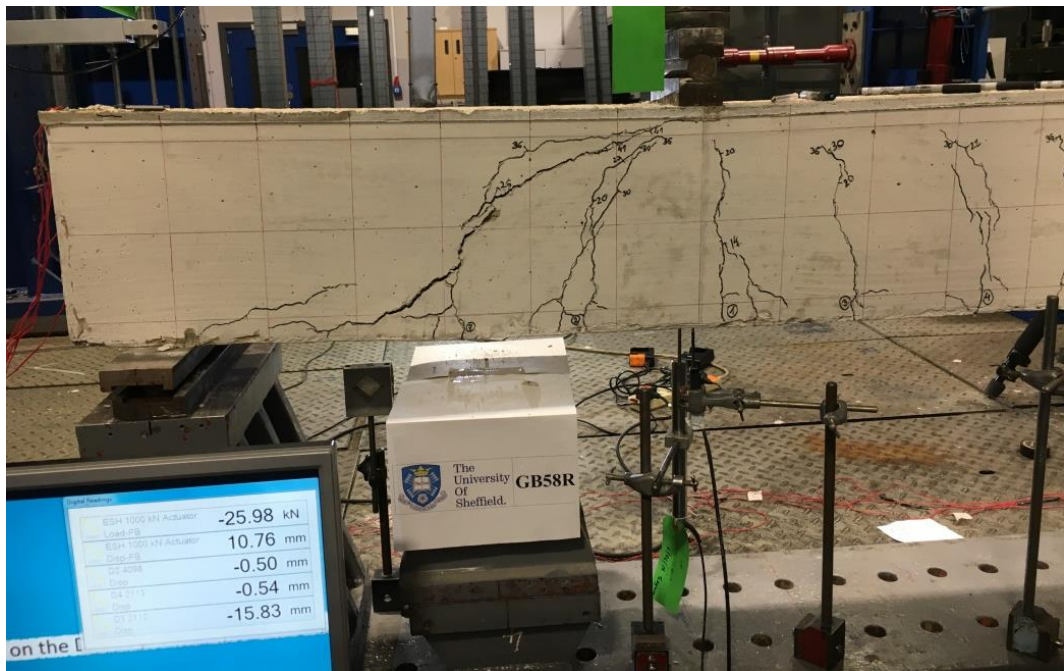
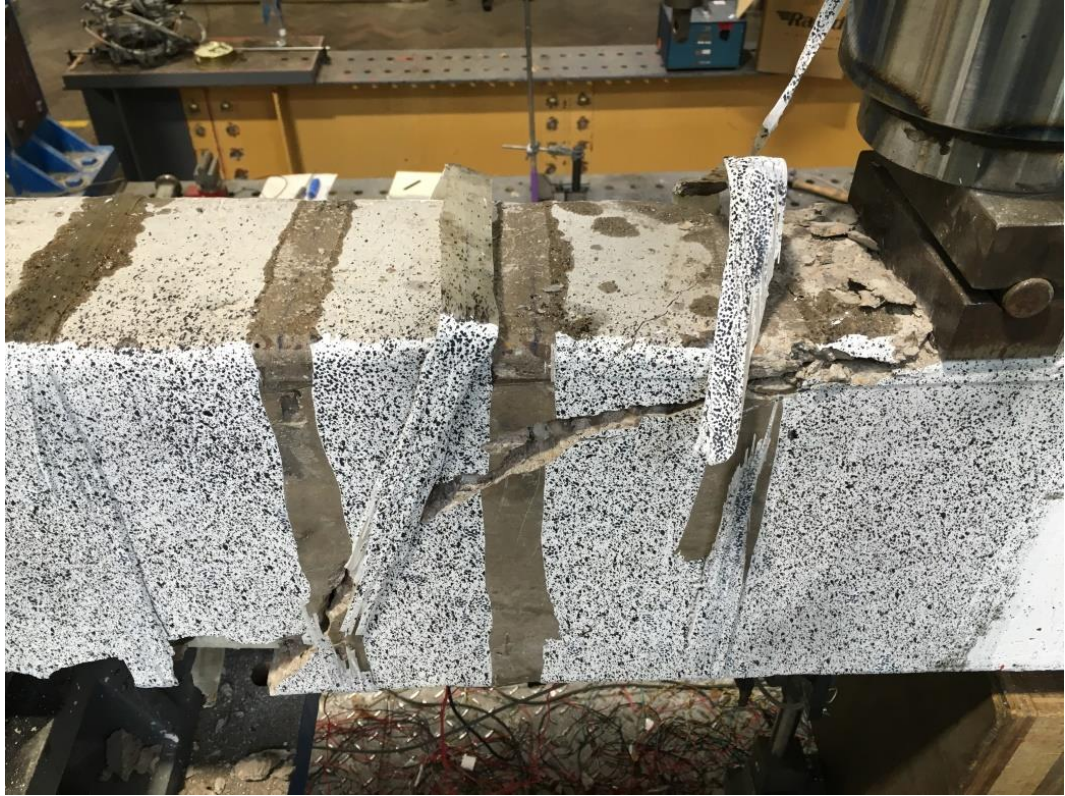**Photo 3** Shear failure in GB58R

Photo 4 Shear failure of GB59R
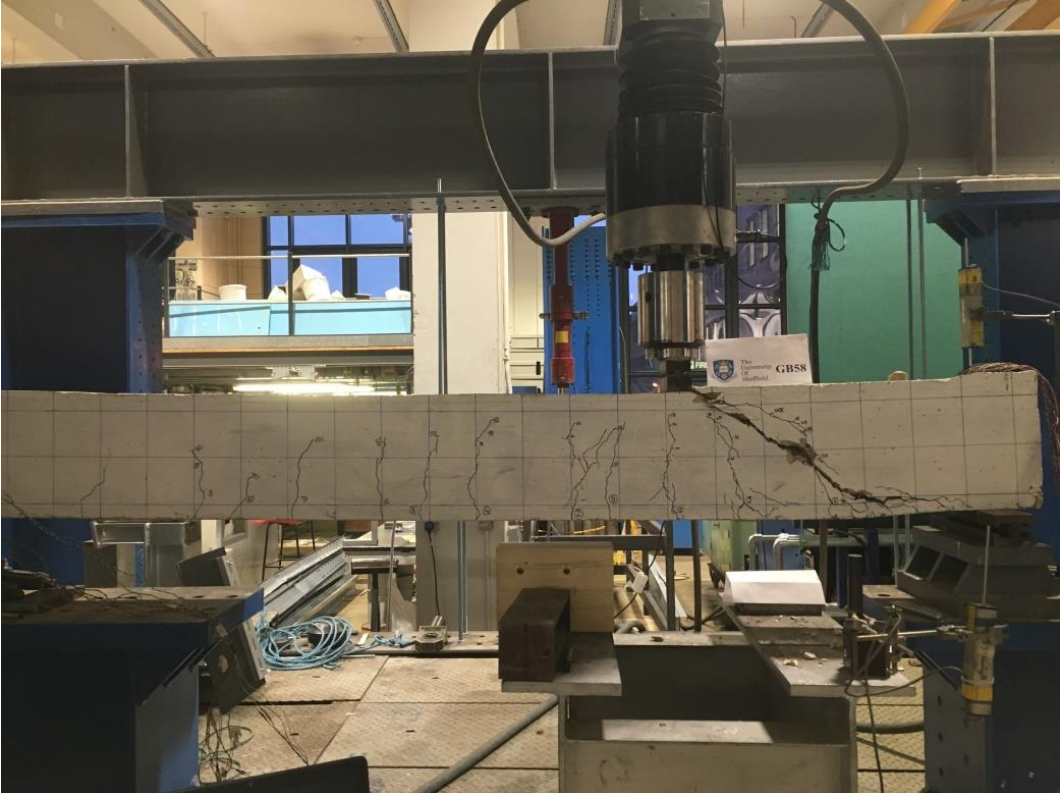
Photo 5 Shear failure of GB58
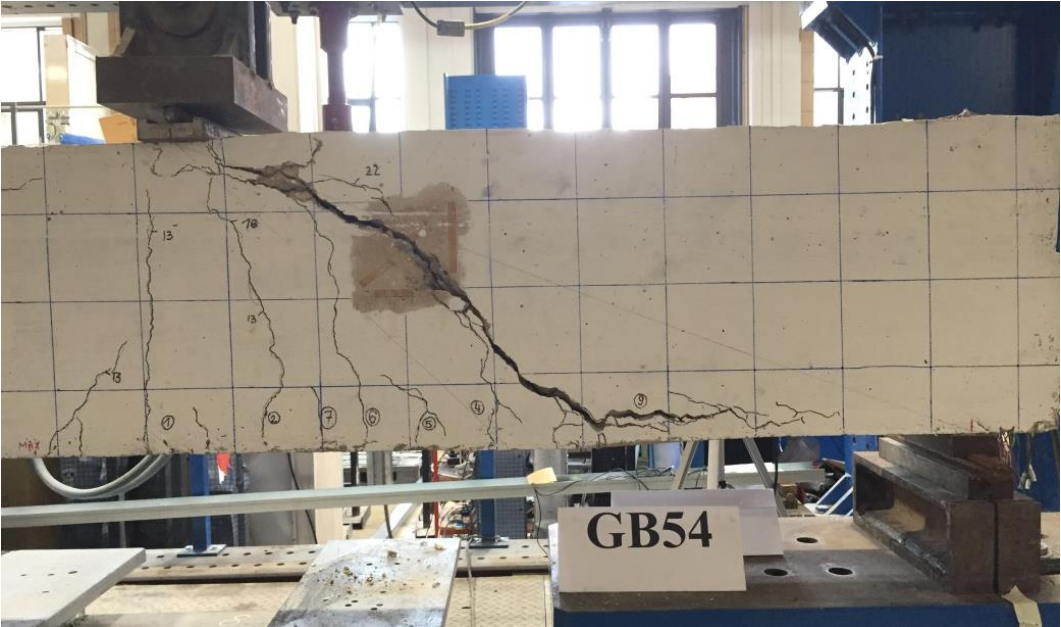
Photo 6 Shear failure of GB54
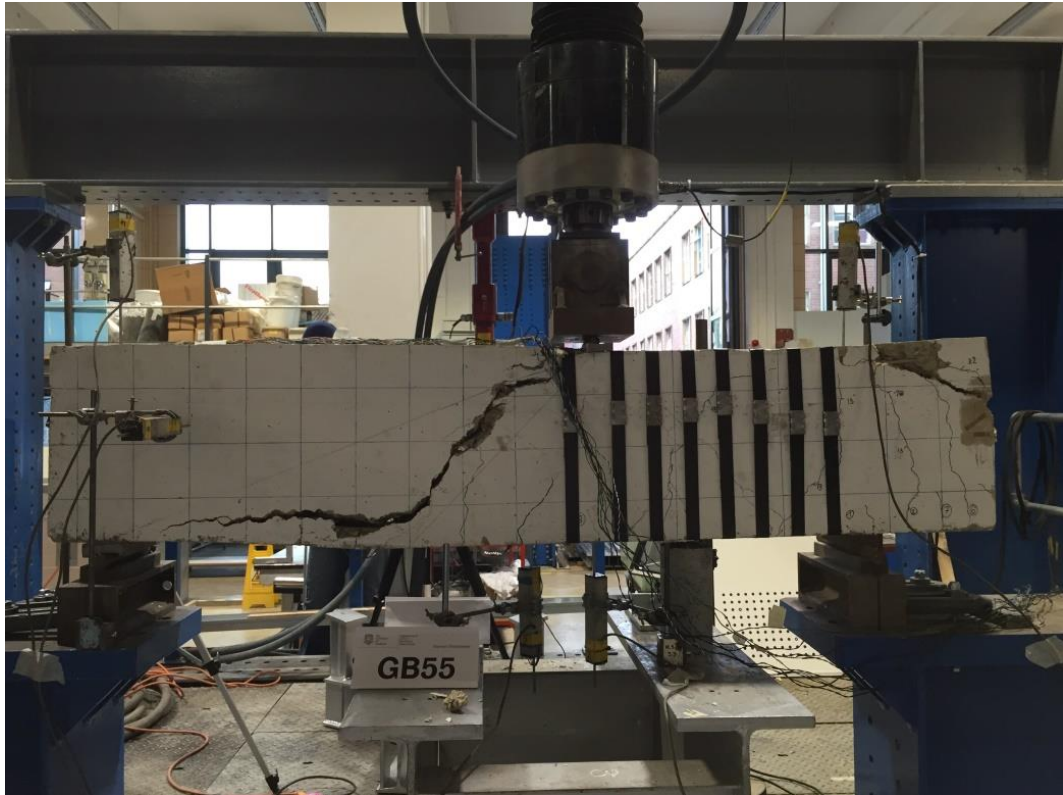
Photo 7 Shear failure of GB55
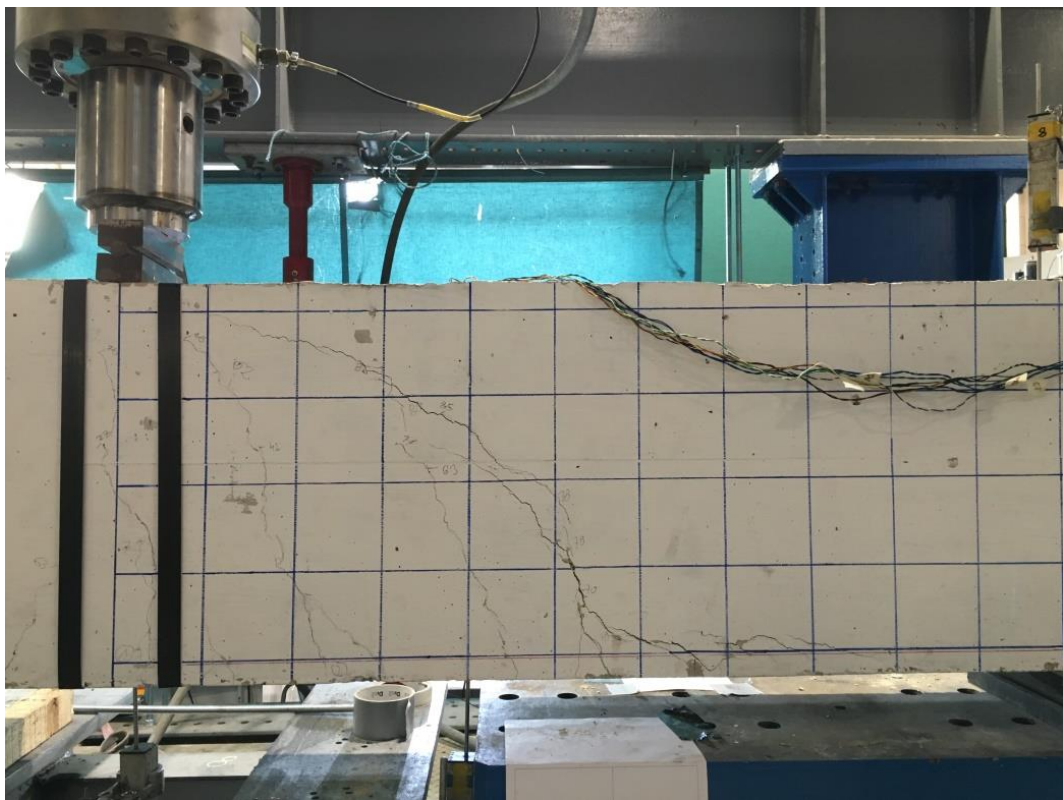
Photo 8 Shear failure of GB56

Photo 9 Shear failure of GB57
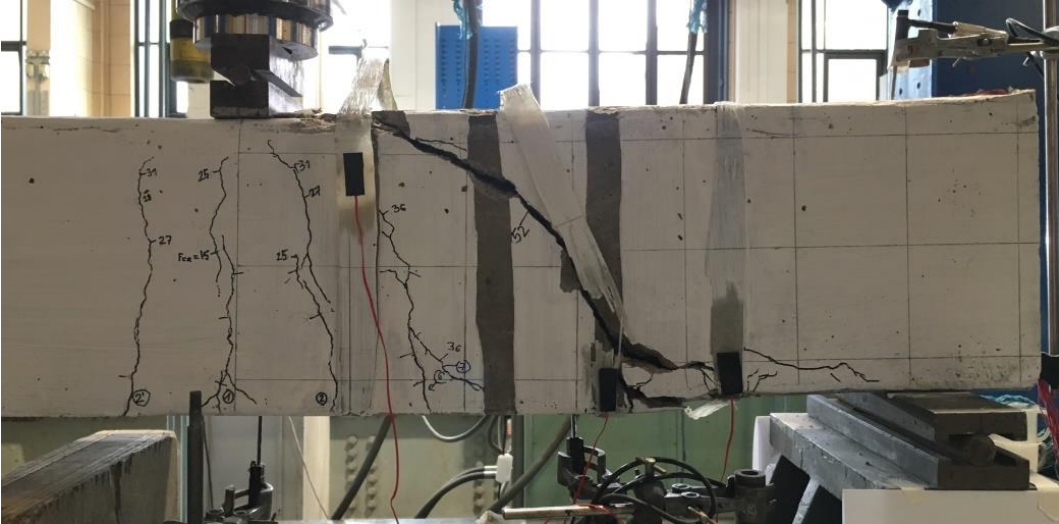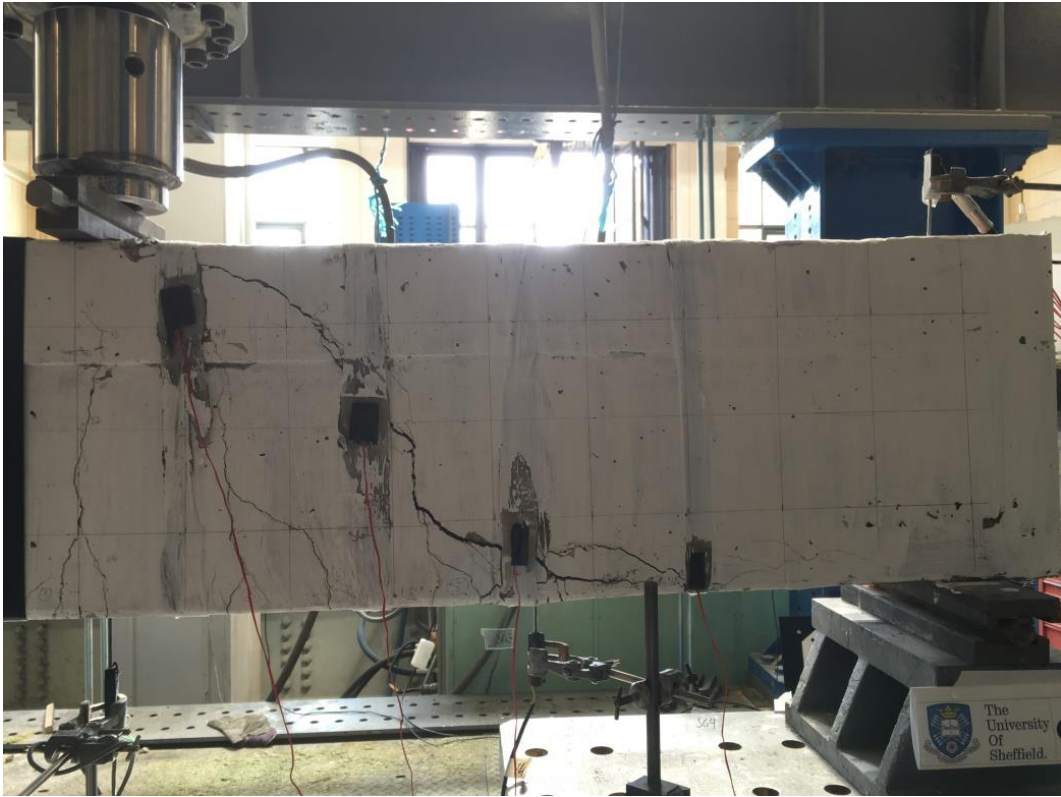

Photo 10 Shear failure of GB62

Photo 11 Shear links failure of GB62

Photo 12 Shear failure of GB63

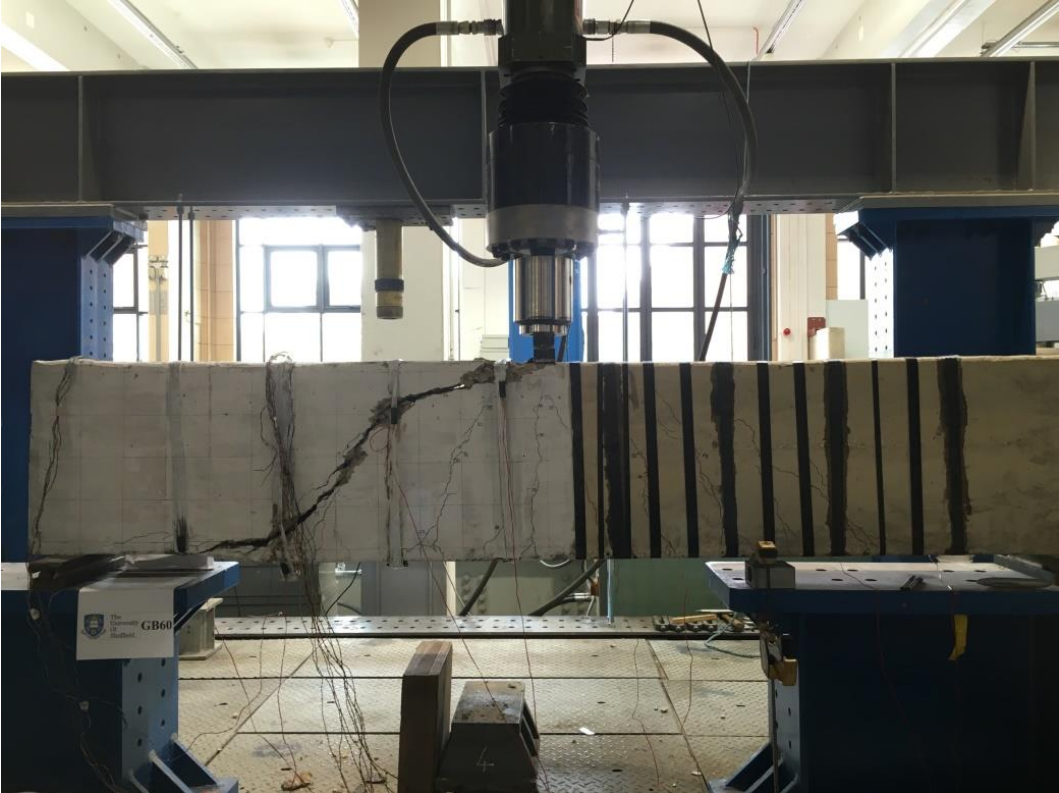**Photo 13** Shear failure of GB63

Photo 14 Shear failure of GB64

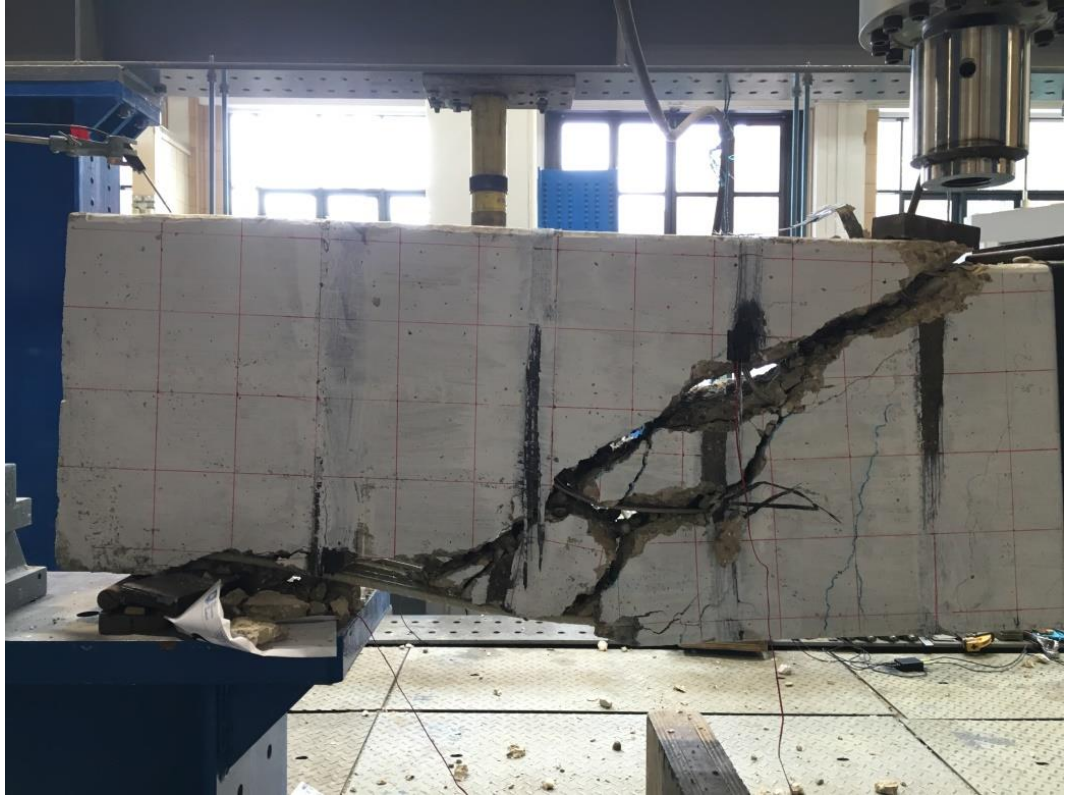**Photo 15** Shear failure of GB64

Photo 16 Shear failure GB65 (DIC side)

Photo 17 Shear failure of GB60

Photo 18 Shear link failure near shear crack (GB60)

Photo 19 Shear failure of GB61

Photo 20 Shear failure GB61 (DIC side)

Photo 21 Typical DIC test setup (GB58R)

Photo 22 Speckle pattern (GB58R)